Dissertation zur Erlangung des Doktorgrades der Fakultät fur Chemie und Pharmazie
der Ludwig-Maximilians-Universität München

Antibiotics and translation

Overcoming emerging bacterial resistance to old and new antimicrobials

Agata Lucyna Starosta

aus Rzeszow, Polen

2011

Erklärung

Diese Dissertation wurde im Sinne von § 13 Abs. 3 bzw. 4 der Promotionsordnung vom 29. Januar 1998 (in der Fassung der Sechsten Änderungssatzung von 16. August 2010) von Herrn Prof. Dr. Roland Beckmann betreut.

Ehrenwörtliche Versicherung

Diese Dissertation wurde selbstständig, ohne unerlaubte Hilfe erarbeitet.

München, am 24.11.2011

Agata Lucyna Starosta

Dissertation eingereicht am 24.11.2011

1. Gutachter: Herr Prof. Dr. Roland Beckmann

2. Gutachter: Herr Prof. Dr. Klaus Förstemann

Mündliche Prüfung am 31.01.2012

List of contents

Acknowledgements 5
List of original publications 6
Contribution report 8
Abbreviations 10
Summary 11
1 Introduction 12
1.1 Traditional antibiotics 13
1.1.1 Introduction to antibiotics 13
1.1.2 Targets for antibiotic action 14
1.1.2.1 Inhibition of cell wall synthesis 14
1.1.2.2 Inhibition of DNA replication 16
1.1.2.3 Inhibition of RNA synthesis 16
1.1.2.4 Inhibition of protein synthesis 16
1.1.3 Protein synthesis 17
1.1.3.1 Inhibitors of the small ribosomal subunit 22
1.1.3.2 Inhibitors of the large ribosomal subunit 23
1.1.3.2.1 Inhibitors of the peptidyl-transferase center 23
1.1.3.2.2 Inhibitors of the progressing nascent polypeptide chain 24
1.1.3.2.3 Inhibitors of the GTPase-associated center (GAC) 24
1.1.4 Mechanism of cell death induced by bactericidal antibiotics 25
1.2 Antibiotics used in these studies 27
1.2.1 Hygromycin A 27
1.2.2 Macrolides 29
1.2.3 Thiopeptides 31
1.2.4 Orthosomycins 34
1.2.5 Fusidic acid 35
1.3 Alternative antimicrobials targeting virulence 36
1.3.1 Definition of virulence 36
1.3.2 Colonization 36
1.3.3 Biofilm 36
1.3.4 Quorum sensing 37

1.3.5 Motility 37
1.3.6 Secretion systems 37
1.3.7 Elongation factor P 38
2 Objectives of these studies 41
3 Cumulative thesis 43
3.1 Hygromycin A 43
3.1.1 Paper 1 43
3.1.2 Paper 2 43
3.2 Macrolides 47
3.2.1 Paper 3 47
3.2.2 Paper 4 47
3.3 Thiopeptides 50
3.3.1 Paper 5 50
3.3.2 Paper 6 50
3.4 Orthosomycins 52
3.5 Fusidic acid 53
3.5.1 Paper 7 53
3.6 Elongation factor P 54
3.6.1 Paper 8 54
4 Conclusions 58
5 References 59

Acknowledgements

This would not be possible without the support of many people that I had a pleasure of meeting during my PhD studies.

First of all I would like to thank Dr. Daniel Wilson for giving me an opportunity to work in his group in the Gene Center . I am grateful for the trust and support I received from him during all those years. I appreciate each and every advice, discussion, criticism and praise I ever received from him. That was a lesson I will never forget.

I would like to thank Prof. Roland Beckmann for all the expertise, good advices and support as well as for providing us with a great scientific environment without which this work could not happen.

I am grateful to all our collaborators for having fruitful time collecting all the data: to Prof. B. Cooperman for great work on thiopeptides; Prof. A. Bogdanov for macrolide story; Prof. K. Reynolds for hygromycin A studies; Prof. C. Spahn for first and hopefuly not the last Nature paper; Prof. G. Dinos for hosting me in Greece and support in experiments; and last but not least, to Prof. J. Remme for great work on EF-P.

I would also like to thank people, whom I had a pleasure to have conducted the experiments with: Aleksandra Mikolajka, Alexandra Dönhöfer, Viktorija Karpenko, Gemma Atkinson and Vidya Dhote.

Special thanks to Lauri Peil for being my Mass Spectrometry master, for all the hours we spent discussing the most crazy ideas and then making them come true.

I would like to thank to all the former and present members of the Wilson and the Beckmann labs for the atmosphere, discussions, parties, trips and many more.

Lots of thanks to Ingegerd Walz for all the help in the emergency situations.

I would like to thank Prof. Klaus Förstemann, Prof. Mario Halic and Prof. Knud Nierhaus for being in my thesis committee.

I am very grateful to Marta Danecka and Jean-Paul Armache for surviving corrections of my thesis.

Wielki dzieki Marto i Jasiu za te wszystkie lata spedzone razem w Monachium, i w Krakowie (Marta). Bez waszego wsparcia wszystko byloby trudniejsze.

Najbardziej chcialabym podziekowac moim kochanym rodzicom i kochanej siostrze, za wychowanie i wsparcie przez te wszystkie lata, ktore spedzilam z daleka od domu, bez was to wszysko nie byloby mozliwe.

List of original publications

This thesis is based upon the following original publications
Reprints were made with permission of the publisher.

Paper 1
Palaniappan, N., Dhote, V., Ayers, S., **Starosta, A.L.**, Wilson, D.N., and Reynolds, K.A. (2009). Biosynthesis of the aminocyclitol subunit of hygromycin A in Streptomyces hygroscopicus NRRL 2388. Chem Biol *16*, 1180-1189.

Paper 2
Dhote, V., **Starosta, A.L.**, Wilson, D.N., and Reynolds, K.A. (2009). The final step of hygromycin A biosynthesis, oxidation of C-5"-dihydrohygromycin A, is linked to a putative proton gradient-dependent efflux. Antimicrob Agents Chemother *53*, 5163-5172.

Paper 3
Petropoulos, A.D., Kouvela, E.C., **Starosta, A.L.**, Wilson, D.N., Dinos, G.P., and Kalpaxis, D.L. (2009). Time-resolved binding of azithromycin to Escherichia coli ribosomes. J Mol Biol *385*, 1179-1192.

Paper 4
Starosta, A.L., Karpenko, V.V., Shishkina, A.V., Mikolajka, A., Sumbatyan, N.V., Schluenzen, F., Korshunova, G.A., Bogdanov, A.A., and Wilson, D.N. (2010). Interplay between the ribosomal tunnel, nascent chain, and macrolides influences drug inhibition. Chem Biol *17*, 504-514.

Paper 5
Starosta, A.L.*, Qin, H.*, Mikolajka, A.*, Leung, G.Y., Schwinghammer, K., Nicolaou, K.C., Chen, D.Y., Cooperman, B.S., and Wilson, D.N. (2009). Identification of distinct thiopeptide-antibiotic precursor lead compounds using translation machinery assays. Chem Biol *16*, 1087-1096.

Paper 6
Mikolajka, A., Liu, H., Chen, Y., **Starosta, A.L.**, Marquez, V., Ivanova, M., Cooperman, B.S., and Wilson, D.N. (2011). Differential effects of thiopeptide and orthosomycin antibiotics on translational GTPases. Chem Biol *18*, 589-600.

Paper 7
Ratje, A.H., Loerke, J., Mikolajka, A., Brunner, M., Hildebrand, P.W., **Starosta, A.L.**, Donhofer, A., Connell, S.R., Fucini, P., Mielke, T., Whitford, P. C., Onuchic, J. N., Yu, Y., Sanbonmatsu, K. Y., Hartmann, R. K., Penczek, P. A., Wilson, D. N., and Spahn, C. M. (2010). Head swivel on the ribosome facilitates translocation by means of intra-subunit tRNA hybrid sites. Nature *468*, 713-716.

Paper 8
Peil L.*, **Starosta, A.L.***, Virumäe, K, Aktinson, G.C., Tenson, T., Remme, J., Wilson, D.N. (2011). Formation of ε(R)-β-lysyl-hydroxylysine on translation elongation factor EF-P requires YjeK, YjeA and YfcM. Under revision at *Nature Chemical Biology*
* Equally contributed

List of publications not included in the thesis:

Paper 9
Wilson, D.N., Schluenzen, F., Harms, J.M., **Starosta, A.L.**, Connell, S.R., and Fucini, P. (2008). The oxazolidinone antibiotics perturb the ribosomal peptidyl-transferase center and effect tRNA positioning. Proc. Natl Acad. Sci USA *105*, 13339-13344.

Paper 10
Bhushan, S., Meyer, H., **Starosta, A.L.,** Becker, T., Mielke, T., Berninghausen, O., Sattler, M., Wilson, D.N., and Beckmann, R. (2010). Structural basis for translational stalling by human cytomegalovirus and fungal arginine attenuator peptide. Mol Cell *40*, 138-146.

Contribution report

Work presented in this dissertation comprises part of the results of my doctoral research conducted from October 2007 to November 2011 in cooperation with scientists from the laboratories of: Professor K. Reynolds (Portland, Oregon, US), Professor. B. Cooperman (Pennsylvania, Philadelphia,US), Professor A. Bogdanov (Moscow, Russia), Professor G. Dinos (Patras, Greece), Professor C. Spahn (Berlin, Germany) and Professor J. Remme (Tartu, Estonia).

Paper 1 (Palaniappan et al., 2009) and Paper 2 (Dhote et al., 2009)

I performed all the biochemical analysis determining the antimicrobial activities of Hygromycin A (HygA) and intermediates of HygA, using (i) *Escherichia coli* lysate *based in vitro* coupled transcription-translation assay (TT) with green fluorescence protein (GFP) as a reporter, and (ii) the AcPhe-Puromycin (AcPhe-Puro) synthesis assay. These results comprise Figure 6 (Paper 1), and Figure 4 (Paper 2), which I prepared for the papers as well as contributing to the interpretation and analysis of these results.

Paper 3 (Petropoulos et al., 2009)

I cultivated *Deinococcus radiodurans* cells and used sucrose gradient centrifugation protocol to isolated highly active 70S ribosomes, which were then used subsequently to evaluate the binding mode of azithromycin (AZI) to bacterial ribosomes in collaboration with Prof. Dinos.

Paper 4 (Starosta et al., 2010)

I carried out all the biochemical experiments to determine the inhibitory activity of tylosin (Tyl) and derivatives of Tyl using (i) TT assay using GFP and firefly luciferase (Fluc) as templates, and (ii) competition binding assay with [^{14}C]-erythromycin and *D. radiodurans* 70S ribosomes. The results are depicted in Figures 3-6 and in Supplementary Table 1 of the paper. In addition, I participated in the interpretation of the results and made Figures 1, 3-6 as well as contributing to writing of the manuscript.

Paper 5 (Starosta et al., 2009)

I measured the potency of the entire library of thiopeptide precursor compounds to inhibit synthesis of GFP in TT assay. I also measured the ability of precursors to restore translation in the presence of inhibitory concentration of parental compounds, which is

presented in Figures 4-5. I prepared Figures 1-5 and participated in the preparations of the draft of the manuscript.

Paper 6 (Mikolajka et al., 2011)

I evaluated the antimicrobial activity of thiostrepton, micrococcin and evernimicin (Evn) in TT assay using GFP as a reporter gene. These results are presented in Supplementary Figure 3, which I prepared together with Figure 5.

Paper 7 (Ratje et al., 2010)

I grew *Thermus thermophilus* cells and prepared highly pure 70S ribosomal particles using sucrose gradient centrifugation protocol. The 70S ribosomes were used for preparation of the complex of EF-G stalled with GDP and fusidic acid on the 70S ribosome.

Paper 8 (Peil et al. 2011)

I cloned and purified elongation factor P (EF-P) which was used to raise rabbit polyclonal antibodies. I established the immuno-precipitation protocol using protein A and prepared all constructs used for the rescue experiments. I identified the YfcM protein using STRING database and cloned *yfcM* gene. I purified recombinant YfcM, which I characterized using differential scanning fluorimetry (DSF). I optimized protocol for expression of EF-P modified by 128 Da and established the *in vitro* hydroxylation assay. I prepared all figures and participated in preparation of the manuscript. Additionally, I started initial characterization of phenotypes of the efp and modification enzymes deletion strains.

Abbreviations

- 30SIC – 30S initiation complex
- 70SIC – 70S initiation complex
- A/A position – both anticodon stem loop and aminoacyl arm of tRNA in A-site
- A/T position – anticodon stem loop in A site, aminoacyl arm of tRNA bound to EF-Tu
- aa-tRNA – aminoacyl-tRNA
- AB – subunits A and B of hygromycin A
- AcPhe-Puro – AcPhe-Puromycin
- AHLs – acylated homoserine lactones
- A-site – aminoacyl-tRNA binding site
- Avi – avilamycin
- AZI – azithromycin
- Cryo-EM – cryo-electron microscopy
- Des-HygA – desmethylenehygromycin A
- DGI – German Society for Infectious Diseases
- DH-HygA – 5”-dihydrohygromycin A
- DHS – deoxyhypusine synthase
- DOHH – deoxyhypusine hydroxylase
- *E. coli – Escherichia coli*
- ECDC – European Center for Disease Prevention and Control
- EF – elongation factor
- EHEC – enterohemorrhagic *E. coli*
- Ery –erythromycin
- E-site – exit site
- Evn – evernimicin
- FA – fusidic acid
- fMet-tRNA^{fMet} – initiator-tRNA
- GAC – GTPase-associated center
- GFP – green fluorescent protein
- GlcNAc – *N*-acetylglucosamine
- HygA – hygromycin A
- IC_{50} – half-inhibitory concentration
- IF – initiation factor
- *K. pneumoniae – Klebsiella pneumoniae*
- LSU – 50S large subunit
- MBL – metallo-β-lactamase
- Met-HygA – methoxyhygromycin A
- MiC – Micrococcin
- MIC – minimal inhibitory concentration
- mRNA – messenger RNA
- MurNAc – *N*-acetyl-muramic acid
- NLPH – National Laboratory of Public Health of the Ministry of Public Health and Population
- OMT – 5-O-mycaminosyl-tylonolid
- ORF – open reading frame
- P/E - anticodon stem loop in P site, aminoacyl arm bound to E-site
- PBS – penicillin-binding proteins
- P-HygA – phosphorylated hygromycin A
- Pi – Inorganic phosphate
- POST – post-translocation state
- PRE – pre-translocation state
- *Pseudomonas aeruginosa*
- P-site – peptidyl-tRNA binding site
- PTC – peptidyl-transferase center
- RF – release factor
- rRNA – ribosomal RNA
- SAM – S-adenosylmethionine
- SAXS – small-angle X-ray scattering
- SD – Shine-Dalgarno
- SRL – sarcin-ricin loop
- SS – secretion systems
- SSU – 30S small ribosomal subunits
- SubA – subunit A, dehydrofucofuranose moiety of HygA
- SubB – subunit B, α-methyl cinnamic acid moiety of HygA
- SubC – subunit C, aminocyclitol moiety of HygA
- ThS – thiostrepton
- tRNA – transfer tRNA
- TT – *E. coli* lysate-based *in vitro* coupled transcription-translation assay
- Tyl – tylosin
- UTR – untranslated region

Summary

Emerging bacterial resistance to antibiotics has led to increased interest in development of new, improved antimicrobials. In these studies we have used a number of biochemical assays in order to investigate the mechanism of action of several antibiotics inhibiting protein synthesis. We show that using biosynthetic intermediates of parental compounds we are able to evaluate the functionality of structural features of the drug (hygromycin A, thiopeptides). We revisited the mechanism of action of three classes of antibiotics (macrolides, thiopeptides and orthosomycins) and demonstrated that cryo-electron microscopy can be successfully applied to localize and visualize small molecules, such as drugs (fusidic acid). To overcome cross-resistance with clinically used antibiotics, new antimicrobial targets are needed. Bacterial virulence and pathogenicity factors have been suggested as such future targets. One such factor is elongation factor P (EF-P), a post-translationally modified protein that regulates expression of virulence determinants. Here we have investigated the discrepancies between the 144 Da and 128 Da modification states reported for EF-P *in vivo* and *in vitro*, respectively. This led us to identify a third enzyme in the EF-P modification pathway. In addition to providing fundamental insight into the role of EF-P in the cell, these studies may provide additional targets for development of novel "antivirulence" agents.

1 Introduction

Since their discovery in 1928 (Fleming, 1929), penicillins remain the most frequently prescribed antibiotics (ECDC, 2010). However, as shown in the "Annual epidemiological report on communicable diseases in Europe" published by the European Center for Disease Prevention and Control (ECDC), *Escherichia coli*, the most common Gram-negative bacteria responsible for bloodstream and urinary tract infections, showed a Europe-wide increase of resistance to all antibiotic classes under surveillance (ECDC, 2010). At this level of resistance, it eliminates aminopenicillins as a therapeutical strategy for these common infections (ECDC, 2010). Moreover, multidrug resistance among Gram-negative bacteria such as *E. coli*, *Klebsiella pneumoniae* and *Pseudomonas aeruginosa*, further increases, which limits the possibility of the antimicrobial treatment (ECDC, 2010) and raises the problem of bacterial infection to a level never seen before.

Although antibiotics have been available for the treatment of bacterial infections for over 70 years, analyses of a 30,000 years old sample show that genes encoding resistance to β-lactams, tetracycline and glycopeptides antibiotics are indeed much more ancient (D'Costa et al., 2011). This underlines the fact that bacteria are years ahead of researchers in the process of learning how to neutralize antibiotics. Furthermore, the time from the discovery of a new compound until its introduction into the market takes an average of 10-15 years (DrugDiscovery), while, as shown in experiments with *E. coli* treated with ciprofloxacin, bacteria can develop resistance within as little as 10 hours (Zhang et al., 2011). This finding, as well as recent bacterial outbreaks, emphasizes the scale of the problem of emerging antibiotic resistance among bacteria.

Cholera outbreak

Roughly 20,000 clinical cases of cholera and 1100 deaths were officially reported since the outbreak was first detected on the 21st October 2010 in the Artibonite region of Haiti (Butler, 2010). Toxigenic *Vibrio cholerae* O1, serotype Ogawa, biotype El Tor, was identified by the National Laboratory of Public Health of the Ministry of Public Health and Population in Haiti (NLPH). Identification of the isolate was confirmed by the Center for Disease Prevention and Control (CDC) in Atlanta (US). Antimicrobial susceptibility testing of selected *V. cholerae* O1 isolates conducted at the NLPH and at the CDC demonstrated susceptibility to tetracyclines, ciprofloxacin, and kanamycin; and resistance to trimethoprim, sulfamethoxazole, furazolidone, nalidixic acid, sulfisoxazole, and streptomycin (CDC, 2010).

NDM-1

The NDM-1 strain was discovered in 2008 in a Swedish patient of Indian origin who traveled to New Delhi, India, and acquired a urinary tract infection. The infection caused by a carbapenem-resistant *K. pneumoniae* strain that typed to the sequence type 14 complex. The isolate, *K. pneumoniae* 05-506, was shown to possess a metallo-β-lactamase (MBL), but was negative for previously known MBL genes (Yong et al., 2009). Gene libraries and amplification of class 1 integrons revealed three resistance-conferring regions which are (i) easily transferable to recipient strains and (ii) that confer resistance to all antibiotics, except fluoroquinolones and colistin. NDM-1 (New Delhi metallo-β-lactamase) has a molecular mass of 28 kDa, is monomeric and can hydrolyze all β-lactams, except aztreonam (Yong et al., 2009). Further investigations revealed cases of NDM-1 bacterial strains in Pakistan, India and the United Kingdom. Isolated strains were highly resistant to many antibiotics (including β-lactams, fluoroquinolones and aminoglycosides), but not to tigecycline and colistin (Kumarasamy et al., 2010).

An Escherichia coli O104:H4 outbreak

The *E. coli* bacteria outbreak begun in May 2011 in Germany. Since then, nearly 4000 cases and more than 40 deaths were reported (ECDC, 2011). A virulent *E. coli* strain O104:H4 causes haemolytic uraemic syndrome and bloody diarrhea (also known as enterohemorrhagic *E. coli,* EHEC) (Bielaszewska et al., 2011). The strain produces Shiga toxin 2 and aggregative adherences to epithelial cells (Bielaszewska et al., 2011). A Shiga-like toxin (verocytotoxin) may cause direct renal and endothelial cell damage and may adhere to the intestinal epithelium resulting in bloody diarrhea (Bae et al., 2006). Moreover, the bacteria produces extended-spectrum β-lactamases (Bielaszewska et al., 2011). According to the *German Society for Infectious Diseases* (DGI), the EHEC strain is susceptible to carbapenem, new generation macrolides and rifampicin, while being resistant, or not responding to fluoroquinolones, aminoglycosides, and fosfomycin (DGI, 2011).

1.1 Traditional antibiotics

1.1.1 Introduction to antibiotics

Traditional antibiotics, depending on their ability to either kill, or inhibit the growth of bacteria, can be classified as bactericidal, or bacteriostatic, respectively. They act by inhibiting processes essential for exponential growth, namely (i) cell wall synthesis, (ii) DNA replication, (iii) RNA transcription, and (iv) protein synthesis (Clatworthy et al., 2007). The

history of antibiotics begun in 1929 when Sir Alexander Fleming discovered penicillin (Fleming, 1929). Since that time a significant number of new antimicrobials have been discovered. Development and availability of biochemical tools have provided an understanding into the mechanism of action of new compounds, and provide a basis for development of new derivatives through the chemical modification of already existing molecules (Kohanski et al., 2010b). The dynamics of discovery of new classes of antibiotics lapsed in the 1960's following the introduction of quinolones. Nearly 40 years passed before a new class of antimicrobials was introduced, namely, the oxazolidinones with linezolid (Zyvox) as the lead compound (Walsh, 2003). However, the clinically significant resistance to each of the known classes of antimicrobials has emerged within a few years following their introduction into medical usage (**Figure 1**) (Clatworthy et al., 2007).

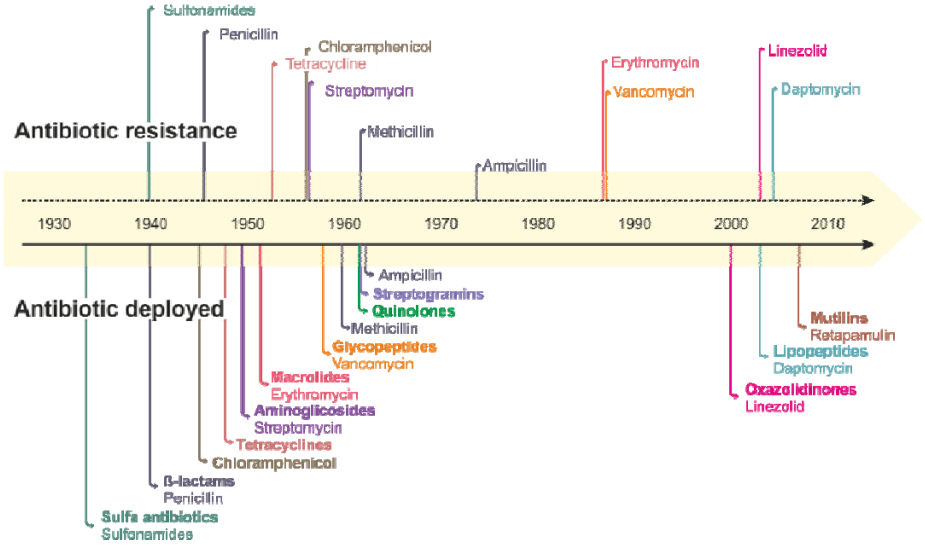

Figure 1. Timeline of antibiotic deployment and the evolution of antibiotic resistance (Fischbach and Walsh, 2009) (Clatworthy et al., 2007).

1.1.2 Targets for antibiotic action

Most commonly used classes of antibiotics target four processes essential for bacterial life: (i) cell wall biosynthesis, (ii) DNA and RNA replication, (iii) protein biosynthesis, and (iv) folate coenzyme biosynthesis, which leads to DNA biosynthesis arrest (**Figure 2**) (Walsh, 2003).

1.1.2.1 Inhibition of cell wall synthesis

The bacterial cell is surrounded by murein (also called peptydoglycan), a structure built with a number of layers assembled with *N*-acetylglucosamine (GlcNAc) and *N*-acetyl-muramic acid (MurNAc) crosslinked with β-(1-4)-glycosidic bonds (Bugg and Walsh, 1992).

The cell wall provides bacteria with the mechanical strength to allow microorganisms to survive under varying environmental conditions. Various processes allow bacteria to maintain the fitness of the cell wall. The enzymes, transglycosylases and penicillin-binding proteins (PBSs, also called transpeptidases), add disaccharide pentapeptides to extend the glycan filaments of existing peptidoglycan molecules and cross-link neighboring peptide filaments of immature peptidoglycan subunits (Park and Uehara, 2008).

Application of antibiotics inhibiting cell wall synthesis can induce changes in bacterial morphology, cell elongation, filamentation, and trigger cell stress response leading to cell lysis (Tomasz, 1979). Nearly every step of cell wall synthesis can be inhibited. β-lactams (penicillins, carbapenems and cephalosporins) penicilloylate the catalytic center of PBSs (Waxman et al., 1980), which abolishes crosslinking of peptidoglycan moieties (**Figure 2a**)

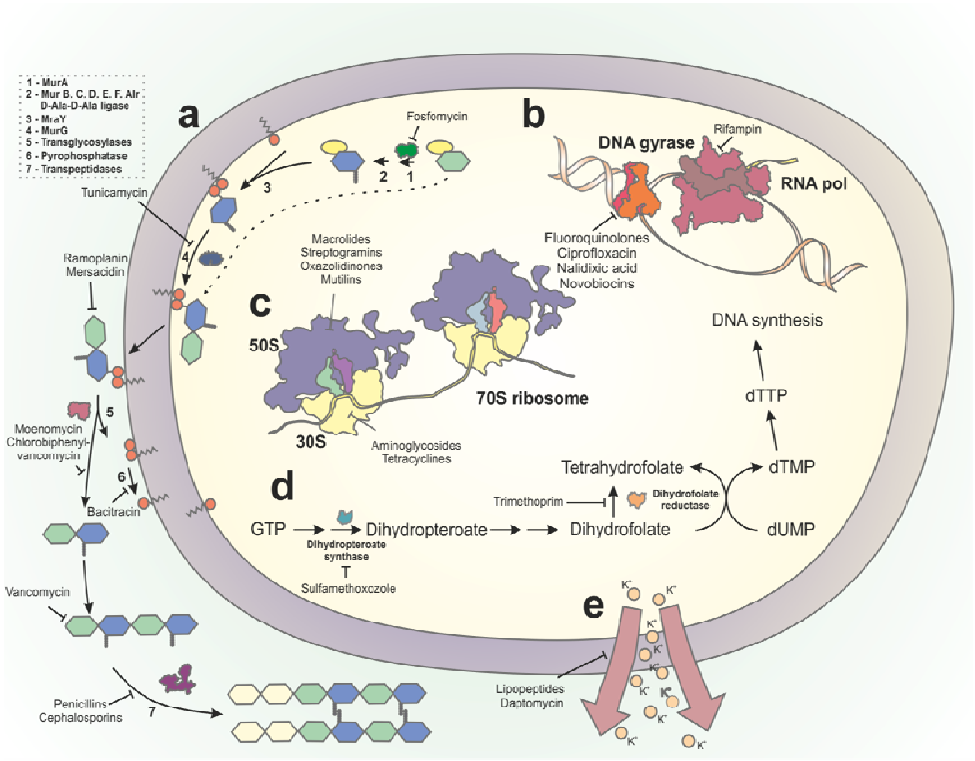

Figure 2. Major targets for antibiotics within the bacterial cell. (**a**) *Cell-wall synthesis*: Peptydoglycan is composed of two hexoses (filled hexagons) - GlcNac and MurNAc. Cytoplasmatic steps of peptydoglycan synthesis are catalyzed by the enzymes MurA-F and MurG (steps 1-4). In following step, a carrier lipid – bactoprenol phosphate (orange circle) transferrs peptidoglycan blocks across the membrane. In the next steps sugars and phosphates are added by transglycosylation and pyrophosphorylation (steps 5 and 6). Eventually, peptide chains are linked together (step 7). Inhibitors of cell-wall synthesis are marked. (**b**) *Translation*: bacterial ribosomes consist of two subunits (30S and 50S) which are targets for a number of antibiotics (**c**) *DNA synthesis and RNA replication*: rifampin binds to RNA polymerase preventing polymerase-DNA interaction, thereby inhibiting transcription. Ciprofloxacin and novobiocin inhibit DNA gyrase (**d**) *Folate metabolism*: folate is necessary for the synthesis of thymine, one of nucleotides building DNA. Antibiotics arresting thymine synthesis are depicted. Adapted from (Walsh, 2003). (**e**) *Membranes*: lipopeptides antibiotics insert into lipid bilayer inducing depolarization of membrane potential (Clatworthy et al., 2007).

(Wise and Park, 1965). Glycopeptide antibiotics (vancomycin) (**Figure 2a**) bind peptidoglycan subunits and are steric inhibitors of transglycosylases and transpeptidases (Kahne et al., 2005). Fosfomycin inhibits synthesis (Kahan et al., 1974), while bacitracin inhibits transport (Storm, 1974) of single peptidoglycan units (**Figure 2a**). Lipopeptides (daptomycin) modulate the structural integrity of bacterial cell by inserting themselves into the cell membrane and triggering membrane depolarization (**Figure 2e**) (Jung et al., 2004). Polymyxins are cyclic, positively charged peptide antibiotics, which have high affinity for lipid moiety of lipopolysaccharides. These cationic agents bind to the anionic bacterial outer membrane and disrupt their integrity (Landman et al., 2008).

1.1.2.2 Inhibition of DNA replication

DNA synthesis, messenger RNA (mRNA) transcription and cell division involve topoisomerase reactions to maintain these essential processes. Topoisomerases control the DNA winding by breaking strands, untangling the nucleic acid and then rejoining the DNA strands (Drlica and Zhao, 1997). Quinolones stall both the topoisomerase II and IV at the DNA cutting phase and prevent DNA strand ligation (**Figure 2b**) (Chen et al., 1996). Arrested DNA synthesis induces bacteriostasis leading to cell death (Kohanski et al., 2007). Sublethal dosage of quinolones, as well as β-lactams, can lead to hydroxyradical formation. This induces mutagenesis, which together with SOS-related mutagenesis and RecA-mediated processes, can stimulate evolution of mutations conferring antibiotic resistance (Kohanski et al., 2010a).

1.1.2.3 Inhibition of RNA synthesis

Rifampicin is a semi-synthetic bactericidal antibiotic, which like quinolones, can induce cell death (Kohanski et al., 2007). It binds to the β-subunit of DNA-dependent RNA polymerase leading to arrest of mRNA transcription (**Figure 2b**) (Campbell et al., 2001).

1.1.2.4 Inhibition of protein synthesis

The complexity of the structure and function of the ribosome makes it an important target for antimicrobial therapies. High-resolution crystal structures of ribosomes and ribosome-antibiotic complexes have provided detailed understanding into the mechanism of action of many classes of antibiotics (**Figure 2c**). Inhibitors of translation can bind to the functional centers on either of the subunits and inhibit nearly every step of translation (**Figure 3**). Four major binding sites for ribosomal inhibitors can be distinguished: (i) the decoding

center on the small subunit, (ii) the peptidyl-transferase center (PTC), (iii) exit tunnel and (iv) GTPase-associated center (GAC) on the large subunit.

1.1.3 Protein synthesis

Protein synthesis is an essential process in every living cell. Ribosomes are complex macromolecules which translate genetic information encoded in mRNA into the polypeptide sequence using transfer tRNAs (tRNAs) as amino acid carriers. Ribosomes consist of two distinct subunits composed of RNA and proteins, which assemble together and create three unique binding sites for tRNAs (**Figure 3**). *E. coli* small 30S ribosomal subunit (SSU) is composed of a single 16S ribosomal RNA (rRNA) and 21 ribosomal proteins, while the 50S large subunit (LSU), is composed of 5S rRNA, 23S rRNA and 33 ribosomal proteins. Both subunits join together to form a 70S ribosome (Schmeing and Ramakrishnan, 2009). mRNA is encoded by triplets of nucleotides called codons, which determine the amino acids sequence of proteins. The SSU's role is decoding of the information carried by the mRNA.

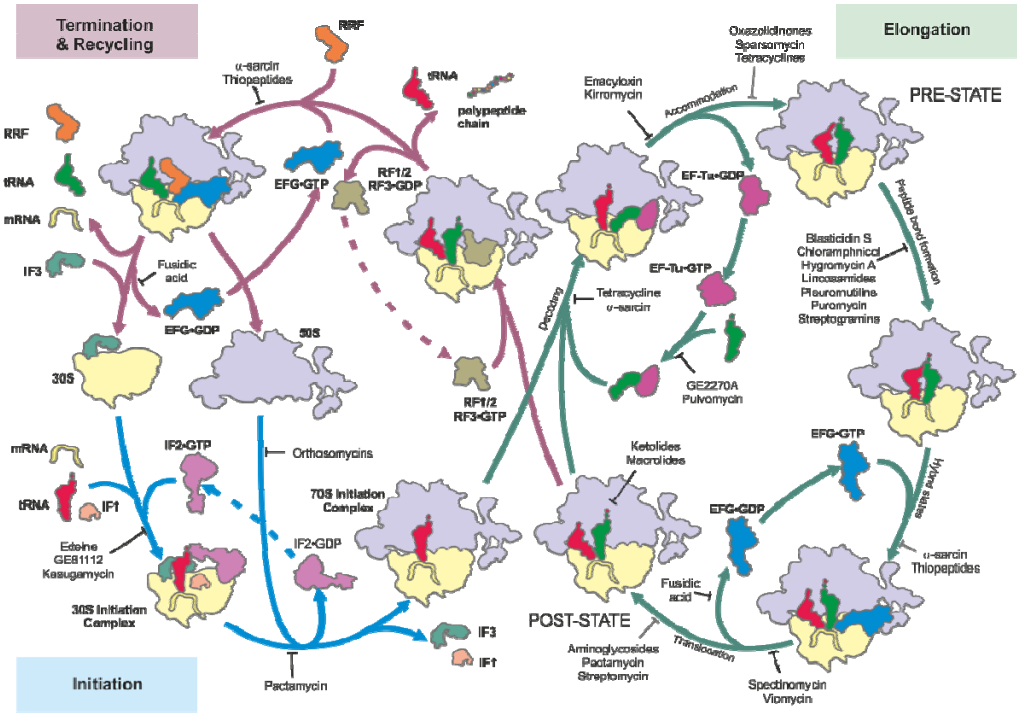

Figure 3. Four phases of translation: initiation, elongation, termination and recycling. Protein synthesis starts with 30S initiation complex formation where mRNA and initiator-tRNA positions on small ribosomal subunit, which is followed by subunit joining. 70S initiation complex can now allow EF-Tu to deliver aa-tRNA to A-site. GTP hydrolysis triggers EF-Tu to dissociate from ribosome and allows aa-tRNA to accommodate on the large subunit, which leads to peptide bond formation between peptidyl-tRNA in the P-site and aminoacyl moiety of A-tRNA. In the next step EF-G, catalyses the reaction of translocation. The cycle is repeated until a stop codon reaches the A-site. The ribosome enters into termination and recycling phases, where, with the help of release factors, RF1 and RF2, the polypeptide is released from ribosome. RRF splits ribosome into subunits which allows it to start a new cycle of translation. Almost every step is targeted by antibiotics (according to (Wilson, 2009)).

The LSU has the transferase activity and catalyses peptide bond formation between the tRNA carrying the nascent polypeptide chain, the peptidyl-tRNA, and an aminoacyl-tRNA (aa-tRNA), which carries an amino acid. Newly delivered aa-tRNAs accommodate into the A-site, peptidyl-tRNA binds in the P-site, while deacylated tRNA exits the ribosome via the E-site.

Translation is a cyclic reaction, which can be divided into four sequential steps: initiation, elongation, termination and recycling (**Figure 3**). In each step, additional factors facilitate the reaction. Translation starts with 30S initiation complex (30SIC) formation. Initiation factor 3 (IF3) binds to the SSU and prevents premature subunit joining (Karimi et al., 1999). The SSU-IF3 complex then assembles with mRNA, IF1, IF2 and initiator fMet-tRNA. The ribosomal protein S1 binds to the A/U rich 5' untranslated region (UTR) of mRNAs (Ringquist et al., 1993) and helps to position the mRNA on the SSU. The GGAGG Shine-Dalgarno (SD) sequence (Shine and Dalgarno, 1974) of canonical mRNA interacts with 3'-end of 16S rRNA (anti-SD) (Demeshkina et al., 2010; Jenner et al., 2010b; Kaminishi et al., 2007) and the start codon (AUG) is positioned in P-site. IF1 binds at a site overlapping the A-site (Carter et al., 2001; Dahlquist and Puglisi, 2000) and, together with IF2 and IF3, cooperatively promotes fMet-tRNA binding to the SSU and its positioning in a P/I site (peptidyl/initiation site) (Antoun et al., 2006; Julian et al., 2011). IF3 discriminates fMet-tRNA from other aa-tRNAs in a P-site by recognition of three unique G:C pairs in the initiator tRNA, and probably the guanosine at third position of the initiation codon (Hartz et al., 1990; Hartz et al., 1989; O'Connor et al., 2001; Risuleo et al., 1976; Sussman et al., 1996). IF binding induces head swiveling of the SSU (Julian et al., 2011). During the formation of the 70S initiation complex (70SIC), subunits join in rotated orientation and upon IF2-driven GTP hydrolysis, fMet-tRNA^{fMet} accommodates into the P-site, while subunits unratchet (Marshall et al., 2009). IFs are released from the ribosome, which then enters into the elongation cycle.

Ribosomes entering the elongation cycle have an fMet-tRNA^{fMet} bound to P-site and vacant A-site. The aa-tRNA is delivered as a ternary complex with EF-Tu and GTP (Schmeing et al., 2009; Schuette et al., 2009). tRNA within the ternary complex binds to ribosomes in a bent conformation (Blanchard et al., 2004; Schmeing et al., 2009; Voorhees et al., 2010) in an A/T position, where anticodon stem loop is bound to the A-site on the SSU and the acceptor stem carrying the amino acid is still bound to EF-Tu. Such a conformation enables direct contact with the decoding site on the SSU and discrimination of a cognate codon-anticodon interaction while remaining bound to EF-Tu. Rearrangements in the

decoding site trigger conformational changes in the ribosome, namely shoulder movement towards EF-Tu (domain closure) that increases the rate of GTPase activation of EF-Tu (Ogle et al., 2002). EF-Tu undergoes conformational changes which positions the catalytic histidine 84 (His84) in proximity with the phosphate of the nucleotide A2662 (*E. coli* numbering) of the sarcin-ricin loop (SRL) located in helix 95 (H95) of 23S rRNA (Voorhees et al., 2010). His84 places a water molecule in a position to nucleophilically attack the γ-phosphate of GTP, which leads to GTP hydrolysis (Daviter et al., 2003) and EF-Tu-GDP dissociation from the ribosome. The aa-tRNA accommodates from A/T position to A/A position, where aa-tRNA is bound to A-site on both the SSU and LSU (Blanchard et al., 2004; Douthwaite et al., 1983; Schmeing et al., 2009; Voorhees et al., 2010). Three nucleotides of the 16S rRNA, namely G530, A1492 and A1493, were shown to be crucial for tRNA binding in the decoding center (Moazed and Noller, 1990). Nucleotides A1492 and A1493 flip-out from helix 44 (h44) and together with G530 monitor Watson-Crick base-pairing geometry of the minor groove of the first two base pairs between codon and anticodon (Ogle et al., 2001). Both, rearrangements in the proteins and 23S rRNA in the LSU, accelerate interactions with the anticodon stem loop and elbow region of the tRNA, leading to positioning of the acceptor end at the PTC (Jenner et al., 2010a).

Accommodation of the aa-tRNA at the A site is followed by peptide bond formation at the PTC. The PTC is composed of nucleotides of domain V of 23S rRNA and is an active site of the ribosome. The PTC binds the CCA ends of peptidyl- and aminoacyl-tRNAs and catalyzes the nucleophilic attack of the α-amino group of the aa-tRNA on the ester carbonyl carbon of the peptidyl-tRNA, which leads to a new peptide bond (Green and Lorsch, 2002).

Crystal structures of the CCA end analogues showed that the A-site CCA end is coordinated by nucleobases G2553, U2555, U2556 of an A-loop and G2583, while the P-site CCA stacks onto nucleobases from the P-loop, including G2251, G2252, and additionally A2451 (Hansen et al., 2002b; Nissen et al., 2000), which is consistent with the CCA end positions found for entire tRNA substrates bound to ribosome (Selmer et al., 2006) and is in agreement with biochemical data (Moazed and Noller, 1991). The A-tRNA induces conformational changes in the PTC (Schmeing et al., 2005a; Schmeing et al., 2005b), which orients reactive nucleotides in the position for peptide bond formation. The 2'-OH group of A2451 positions the A76 of the P-tRNA to promote peptide bond formation (Lang et al., 2008). The 2'-OH group of the A76 of the P-tRNA mediates proton passage from attacking α-amino group of the A-tRNA to the leaving 3'-OH group (Weinger et al., 2004), while the

water molecule, coordinated by U2584 and A2602 (Schmeing et al., 2005a), acts as a proton shuttle and stabilizes the (eight-membered) transition state (Kuhlenkoetter et al., 2011). In this model, the ribosome positions substrates, but does not contribute to the catalysis of the reaction. However, recent works show that the ribosome can modulate the catalysis by changing the transition state rates (Hiller et al., 2011). Post-peptide bond formation the ribosome carries a peptidyl-tRNA at A-site and a deacylated tRNA at the P-site.

Once the peptide bond is formed, the mRNA-$tRNA_2$ complex must be moved across the ribosome in a process called translocation. In the pre-translocation state (PRE), P- and A-tRNAs move in respect to the LSU forming P/E and A/P hybrid states, where the anticodon stem loops interact with P- and A-sites on the SSU and at the same time, the acceptor arms of respective tRNAs interact with E- and P-sites on the LSU (Munro et al., 2007). The tRNA hybrid state formation is coupled with a subunit rotation (Agirrezabala et al., 2008). EF-G interacts with the ribosome (Clementi et al., 2010; Datta et al., 2005; Moazed et al., 1988; Stark et al., 2000) and stabilizes the ratcheted state of the ribosome (Munro et al., 2010a). GTP hydrolysis triggers conformational changes in EF-G (Rodnina et al., 1997). The translocation reaction, i.e. the movement of mRNA and anticodon stem-loops of P- and A-tRNAs across the SSU, is catalyzed by domain IV of EF-G (Savelsbergh et al., 2000) and is coupled with inorganic phosphate (Pi) release (Rodnina et al., 1999). In the post-translocation state (POST), the A-site becomes vacant and is ready to accept the next incoming aa-tRNA. The elongation cycle ends when a stop codon reaches the A-site, which is then recognized by release factors (RFs) (Caskey et al., 1968). Two release factors, RF1 and RF2, recognize UAA/UAG and UAA/UGA stop codons, respectively (Scolnick et al., 1968). RFs bind in the A-site spanning both subunits (Jin et al., 2010; Korostelev et al., 2008; Korostelev et al., 2010; Laurberg et al., 2008; Petry et al., 2005; Weixlbaumer et al., 2008). RFs recognize stop codons directly, and conserved nucleotides G530, A1492, A1493 of 16S rRNA do not participate in stop codon recognition (Korostelev et al., 2008). Instead, these nucleotides stabilize the open form of the RFs. Amino acids GxxE from helix 5 of both RF1 and RF2 recognize the first nucleobase, uridine in all stop codons. The second position is recognized by PVT motif of RF1 and SPF motif in RF2 located in the recognition loop of RFs, while the third position is monitored by threonine (T194), and additionally by glutamine (Q181) in the RF1 (Korostelev et al., 2008; Korostelev et al., 2010; Laurberg et al., 2008; Weixlbaumer et al., 2008). Upon recognition of the stop codon, RFs induce conformational changes in H69 of 23S rRNA. Nucleobase A1913 (H69) stacks onto A1493 (h44) and, together with A1492,

forms a pocket into which RFs accommodate (Korostelev et al., 2010; Weixlbaumer et al., 2008). Structural findings are in accordance with biochemical data showing defects in the termination of the ribosomes lacking H69 (Ali et al., 2006; Korostelev et al., 2010). Moreover, interactions between RFs and H69 help to position GGQ motif in a PTC (Korostelev et al., 2008; Laurberg et al., 2008). It should be noted that the structures of free RFs compared with RFs bound to the ribosome can differ significantly. The crystal structures of free RF1/2 showed they adopt closed conformations where GGQ and PTV/SPF motifs are approximately 23Å from each other, which is not sufficient to establish interactions with the PTC and the decoding center (Shin et al., 2004; Vestergaard et al., 2001; Zoldak et al., 2007). However, small-angle X-ray scattering (SAXS) studies showed that in the solution, RFs are present in equilibrium between open and closed forms (Vestergaard et al., 2005; Zoldak et al., 2007). Upon recognition of the stop codon, RFs undergo conformational changes from closed to active, open form where GGQ motif residing in the PTC and PTV/SPF motifs interacting with decoding center are 73 Å apart from each other (Klaholz et al., 2003; Korostelev et al., 2008; Korostelev et al., 2010; Laurberg et al., 2008; Rawat et al., 2006; Rawat et al., 2003; Weixlbaumer et al., 2008). A universally conserved GGQ motif is critical for the function of RFs, (Frolova et al., 1999; Shaw and Green, 2007). The glycines from the GGQ motif position the catalytically active glutamine (Q230) in the PTC between 23S rRNA nucleotides U2584, U2585, A2602, and A2451 (Jin et al., 2010; Korostelev et al., 2008; Korostelev et al., 2010; Weixlbaumer et al., 2008). Mutational analysis of Q230 showed that the glutamine side chain is not critical for the release reaction of the nascent polypeptide (Seit-Nebi et al., 2001; Shaw and Green, 2007), however the Q230 side chain discriminates the RF's specificity for a water molecule as the nucleophile (Shaw and Green, 2007). The amide group of Q230 backbone interacts with leaving 3'-OH group of A76 of the peptidyl-tRNA, which accounts for the catalytic activity of glutamine (Laurberg et al., 2008). The crystal structure of RF2 bound to the ribosome in a presence of non-hydrolysable analogues of Phe-tRNA^{Phe} where the ester bond was replaced by an amide bond gives inside into structural basis of catalysis of peptide release (Jin et al., 2010). Consistent with biochemical data (Brunelle et al., 2008; Zaher et al., 2011), it was suggested that 2'-OH group of A76 of the peptidyl-tRNA coordinates a water molecule for nucleophilic attack onto the ester bond, leading to hydrolysis of the newly synthesized nascent polypeptide (Jin et al., 2010). RF3 is a GTPase that destabilizes the RF1 and RF2 interaction with the ribosome (Freistroffer et al., 1997; Gao et al., 2007) by stabilization of the ratcheted form of the ribosome with tRNAs in hybrid states

(Jin et al., 2011). Moreover recent data suggest that RF3 plays a role in the fidelity of translation by detecting mis-incorporated amino acids and premature terminating protein synthesis (Zaher and Green, 2009, 2011).

Post-termination ribosomes are split into subunits with the help of the ribosome recycling factor (RRF) and EF-G, in a GTP-dependent manner (Karimi et al., 1999). RRF binds in the P-site of LSU in a fully rotated state of ribosome with deacylated tRNA in P/E position (Dunkle et al., 2011). Upon binding of EF-G, RRF promotes disruption of intersubunit bridges leading to subunit dissociation, which is stabilized by the interaction of IF3 with the SSU (Barat et al., 2007; Ito et al., 2002; Pai et al., 2008; Singh et al., 2005; Zavialov et al., 2005).

1.1.3.1 Inhibitors of the small ribosomal subunit

A number of antibiotics inhibit the delivery of tRNA to a vacant A-site and the process of decoding (**Figure 4**). Edeine interrupts binding of initiator-tRNA to the SSU (Schafer et al., 2002) and can stimulate translational misreading (Dinos et al., 2004). Pactamycin mimics mRNA (Brodersen *et al.*, 2000), and aborts the first translocation reaction (Dinos et al., 2004). Tetracyclines disable stable binding of the ternary complex aa-tRNA•EF-Tu•GTP to the A-site of the ribosome, thus impairing accommodation of aa-tRNA (Blanchard et al., 2004). Aminoglycosides have been proposed to stimulate misreading by inducing flipping-out of A1492 and A1493 and stabilizing them in the open conformation, allowing near-cognate aa-tRNA to accommodate (reviewed by (Ogle et al., 2003)). Streptomycin changes the GTPase rates of EF-Tu, thus stabilizes both cognate and near-cognate aa-tRNAs, which leads to loss of selectivity and induces high rate of misreading (Gromadski and Rodnina, 2004). Kasugamycin mimics codon nucleotides at the P- and E-site (Schluenzen et al., 2006) and inhibits translation of canonical mRNAs by destabilization of initiator tRNA binding, however translation of leaderless mRNAs remains unaffected (Moll

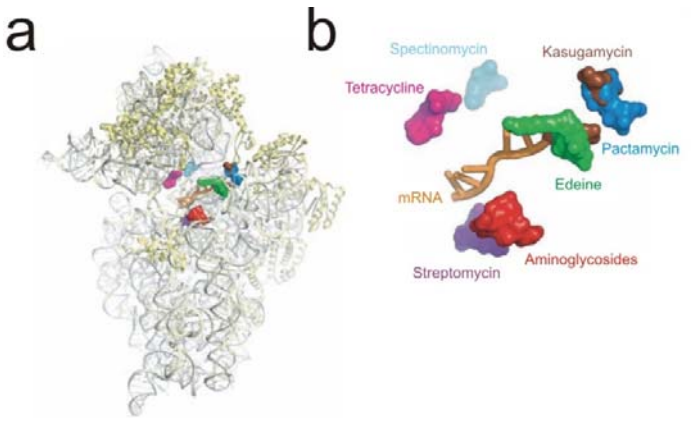

Figure 4. Inhibitors of the small ribosomal subunit. (**A-B**) Superimposition of binding sites of antibiotics (from (Wilson 2009)).

and Blasi, 2002). Moreover, kasugamycin induces the formation of 61S ribosomal particles that lack several ribosomal proteins of the SSU, including protein S1, in order to translate leaderless mRNAs (Kaberdina et al., 2009). Spectinomycin arrests the translocation reaction (Fredrick and Noller, 2003) by stabilizing an intermediate state of the translocating ribosome (Pan et al., 2007). Viomycin binds in the interface of ribosomal subunits, namely within bridge B2a (Stanley et al., 2010) and inhibits translocation by locking tRNAs in hybrid state in PRE complex and destabilizing the POST complex (Feldman et al., 2010; Ly et al., 2010).

1.1.3.2 Inhibitors of the large ribosomal subunit

The translation cycle is a target for a number of antibiotics, including inhibitors of peptide bond formation, progression of the nascent polypeptide, and the function of translational factors.

1.1.3.2.1 Inhibitors of the peptidyl-transferase center

Most of antibiotics targeting the LSU inhibit the PTC and bind in positions overlapping A- and/or P-site tRNA (**Figure 5**). Puromycin, hygromycin A, chloramphenicol, linezolid and lincosamides belong to the class of A-site inhibitors. Puromycin mimics a terminal adenosine (A76) of the CCA-end of aa-tRNA (Nissen et al., 2000) and accepts the nascent polypeptide chain from the P-tRNA (Pestka, 1969; Traut and Monro, 1964). Hygromycin A inhibits the PTC reaction and competes with chloramphenicol (Guerrero and Modolell, 1980). Chloramphenicol overlaps the aminoacyl moiety of an aa-tRNA (Bulkley et al., 2010; Dunkle et al., 2010) and inhibits peptide bond formation (Irvin and Julian, 1970). Moreover, P-tRNA enhances significantly the affinity of chloramphenicol to ribosome (Pestka, 1974). Although the binding site of the oxazolidinone (linezolid) is known (Leach et al., 2007; Wilson et al., 2008), the mechanism of inhibition remains unclear. However, it was proposed that oxazolidinones prevent accommodation of initiator fMet-tRNA on the ribosome (Wilson et al., 2008). Lincosamides (lincomycin, clindamycin) inhibit peptide bond formation

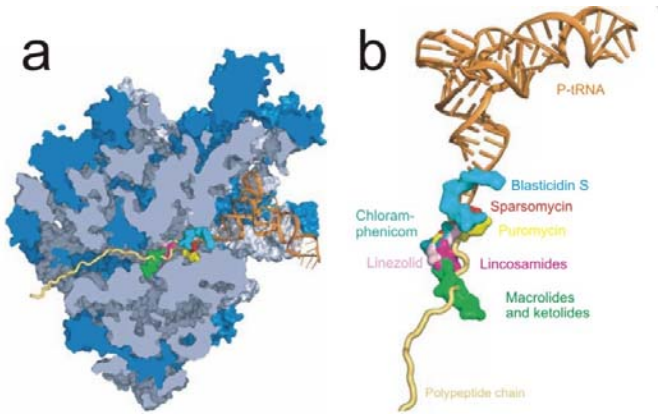

Figure 5. Inhibitors of the peptidyl transferase center. (**A-B**) superimposition of binding sites of antibiotics (from (Wilson, 2009)).

(Kallia-Raftopoulos et al., 1994) by sterically clashing with the A-site tRNA (Dunkle et al., 2010).

Blasticidin S, sparsomycin and pleuromutilins are P-site inhibitors. Blasticidin S mimics C74 and C75 of the CCA-end of P-tRNA in the interaction with P-loop (Hansen et al., 2003) and inhibits PTC reaction of both bacterial and eukaryotic ribosomes (Petropoulos et al., 2004). Sparsomycin inhibits the PTC reaction by blocking A-tRNA from binding while, at the same time, increasing the affinity of the P-tRNA (Ottenheijm et al., 1986). Pleuromutilins overlap with both A- and P-tRNA (Schlunzen et al., 2004), prevent aa-tRNA binding to the A-site and inhibit the PTC reaction (Hodgin and Hogenauer, 1974). Streptogramins are a mixture of two distinct molecules, type A (SA) and type B (SB) which act synergistically (Cocito and Chinali, 1985). SA disrupts the binding of both A- and P-tRNA (Harms et al., 2004), while SB acts analogous to macrolides by blocking progression of polypeptide (Tenson et al., 2003).

1.1.3.2.2 Inhibitors of the progressing nascent polypeptide chain

Recent studies underline the importance of the ribosomal exit tunnel in the regulation of polypeptide translation (reviewed by (Bogdanov et al., 2010; Lovett and Rogers, 1996)). The growing nascent polypeptide chain can interact with the exit tunnel (reviewed by (Wilson and Beckmann, 2011)). This interaction depends on the sequence of the emerging polypeptide and can modulate the rate of translation (Lu and Deutsch, 2008) as well as induce translational stalling of leader peptides, thus leading to an expression of downstream genes (Ramu et al., 2009; Tenson and Ehrenberg, 2002) or even induce antibiotic resistance (Lovmar et al., 2006; Ramu et al., 2009). Macrolides and ketolides bind in the upper part of ribosomal tunnel (**Figure 5**) (Hansen et al., 2002a) and induce drop-off of the peptidyl-tRNA (Mankin, 2008; Tenson et al., 2003).

1.1.3.2.3 Inhibitors of the GTPase-associated center (GAC)

Although each class of antibiotics has a distinct structure, their binding sites tend either to overlap or are in close proximity from each other, promoting the situation where resistance mutations to one class of antibiotics often leads to cross-resistance to other classes (Li et al., 2011; Long et al., 2006; Tu et al., 2005). The GAC is a functional site involved in the interaction with translational factors and stimulation of their GTPase activities. The GAC is located approximately ~50Å from the PTC and consists of helices 42-44 of 23S rRNA

(H42-44), SRL (H95) and ribosomal proteins L10, L11 and L7/L12 (Connell et al., 2007; Li et al., 2006).

Thiopeptides interfere with the binding of translational factors, such as EF-G (Harms et al., 2008), and are effective inhibitors of the translocation reaction (Munro et al., 2010b). In contrast, a subgroup of thiopeptides, including GE2270A, prevent ternary complex formation by inhibiting the binding of aa-tRNA to EF-Tu (Parmeggiani and Nissen, 2006). Orthosomycins interfere with fMet-puromycin reaction in an IF2-dependent manner (Belova et al., 2001). Fusidic acid (FA) stabilizes EF-G binding to the ribosome in the GTP conformation (Gao et al., 2009) and inhibits EF-G turnover (Ticu et al., 2009), although at low concentrations FA allows multiple GTPase cycles (Seo et al., 2006). α-sarcin and ricin are toxins targeting the conserved ribosomal region called the SRL. α-sarcin cleaves rRNA between nucleotides G2661 and A2662 (Endo and Wool, 1982) while ricin depurinates nucleotide A2660 (*E. coli* numbering) of eukaryotic ribosomes (Endo et al., 1987). Ribosomes lacking the SRL or having depurinated A2660 are not able to activate GTP hydrolysis (Benson et al., 1975; Clementi et al., 2010; Sperti et al., 1975) and thus the translocation reaction is inhibited (Gessner and Irvin, 1980; Sperti et al., 1976). Kirromycin stalls ternary complex aa-tRNA·EF-Tu·GTP on the ribosome by arresting conformational changes of EF-Tu (Parmeggiani and Nissen, 2006).

1.1.4 Mechanism of cell death induced by bactericidal antibiotics

Antibiotic-induced cell death is linked with rifampicin-induced inhibition of mRNA synthesis (Floss and Yu, 2005), fluoroquinolone-associated double-stranded DNA breaks (Drlica et al., 2008), β-lactamase-stimulated cell wall damage (Tomasz, 1979) and protein mistranslation as a result of aminoglycoside action (Vakulenko and Mobashery, 2003).

Lethal concentrations of bactericidal antibiotics induce hydroxyl radicals as a result of activation of the oxidative damage cellular death pathway, involving the tricarboxylic acid cycle, NADH deprivation, disruption of iron-sulfur clusters and induction of the Fenton reaction (Kohanski et al., 2007).

Aminoglycosides, as well as edeine and streptomycin, induce translational misreading leading to incorporation of incorrect amino acids into the polypeptide chain. Mistranslated membrane proteins can increase the permeability of the membrane to antibiotics and activate the envelope two-component stress-response system – Cpx-Arc (**Figure 6**). Cpx induces expression of the pepriplasmic protease DegP, an element of envelope stress

response, and activates the redox-responsive two-component system Arc, which leads to modulation of the metabolic and respiratory pathways, formation of hydroxyl radicals, and eventually to cell death (Kohanski et al., 2008).

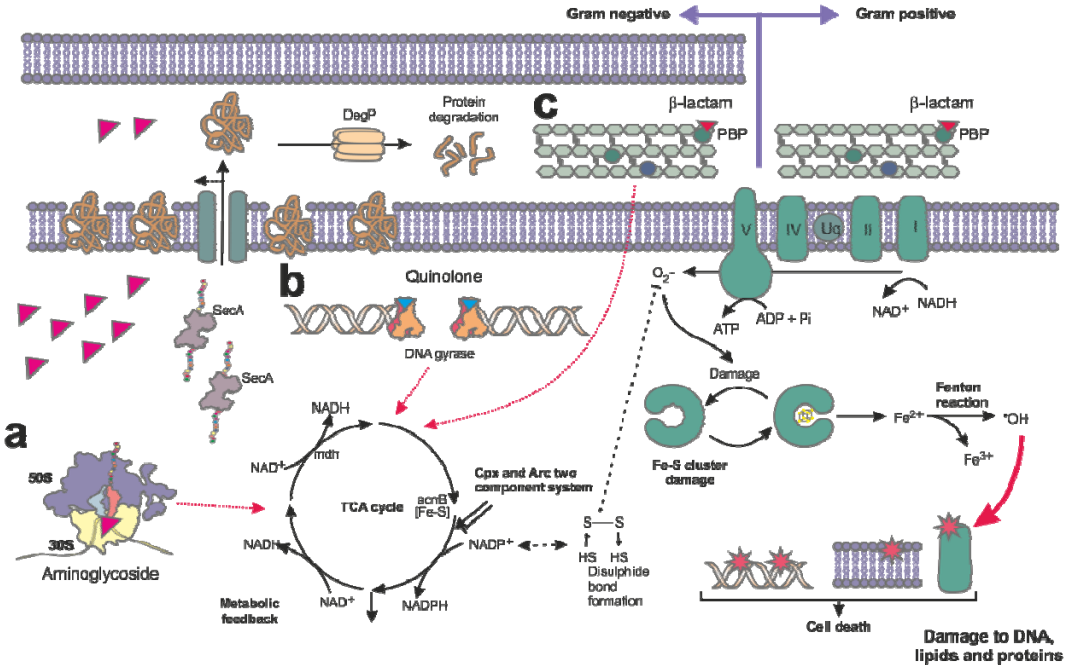

Figure 6 Mechanism of cell death induced by bactericidal antibiotics. (**a**) *Aminoglycosides*, (**b**) *quinolones* and (**c**) *β-lactams* stimulate the oxidation of NADH through the electron transport chain, which is dependent on the tricarboxylic acid (TCA) cycle. Hyperactivation of the electron transport chain stimulates superoxide (O_2-) formation. Superoxide damages Fe–S clusters, which results in release of ferrous iron and induction of the Fenton reaction. The Fenton reaction leads to the formation of hydroxyl radicals (•OH), which damage DNA, lipids and proteins. This accounts for antibiotic-induced cell death. Antibiotics also trigger hydroxyl radical formation and cell death through the envelope (Cpx) and redox-responsive (Arc) two-component systems. Redox-sensitive proteins, such as those containing disulphides (dashed lines) may also contribute to the cell death mechanism. acnb, aconitase b; mdh, malate dehydrogenase; uq, ubiquinone, according to (Kohanski et al., 2010b; Kohanski et al., 2007; Kohanski et al., 2008).

1.2 Antibiotics used in these studies

1.2.1 Hygromycin A

Hygromycin A (HygA) was discovered in the 1950's as a metabolite excreted by *Streptomyces hygroscopicus* NRRL 2388 (Pettinger and Wolfe, 1953) and does not share structural similarities with the aminoglycoside with a similar name, hygromycin B. HygA is a potent inhibitor of Gram-positive bacteria, while ineffective against Gram-negative strains due mainly to the ArcAB efflux pump mechanism (Hayashi et al., 1997). It was shown that HygA inhibits peptide bond formation and competes with chloramphenicols for binding to ribosomes (Guerrero and Modolell, 1980), suggesting that HygA is an inhibitor of the LSU. Footprinting experiments showed that HygA binding to the ribosome can be abolished by macrolides carrying two sugar moieties at the C5 position (Poulsen et al., 2000), which would extend towards the PTC (Hansen et al., 2002a). HygA protects nucleotides located in the PTC, namely U2585 (Poulsen et al., 2000), which is important for tRNA accommodation and peptidyltransferase reaction (Schmeing et al., 2005b), and U2506, from CMCT modification (Poulsen et al., 2000).

HygA is composed of the three structurally distinct moieties: subunit A – dehydrofucofuranose (SubA), B – α-methyl cinnamic acid (SubB), and C – aminocyclitol (SubC) (Habib el et al., 2003). SubA is moderately sensitive to chemical manipulation and when replaced with a hydrophobic allyl group retains antimicrobial potency (Hayashi et al., 1997; Jaynes et al., 1992). In contrast, substitution of the methyl group with propyl, allyl or hydrogen in SubB leads to decreased activity of the derivatives compared with HygA (Hayashi et al., 1997). SubC is essential for the antimicrobial activity of HygA (Hayashi et al., 1997).

The HygA biosynthesis operon consists of 29 open reading frames (ORFs) (**Figure 7**) and includes genes responsible for providing resistance to HygA, as well as regulation and synthesis of each of the HygA moieties (Palaniappan et al., 2006). The biosynthetic origin of each HygA moiety has been established using isotope-labeled precursor studies (Habib el et al., 2003): SubA is derived from glucose, SubB originates from 4-hydroxybenzoic acid and propionic acid, and SubC is synthesized from myo-inositol and methionine (Habib el et al., 2003). The glycoside bond formation between SubA and SubB, and the amide bond between SubB and SubC, follow the assembly of each of the respective moieties (Habib el et al., 2003).

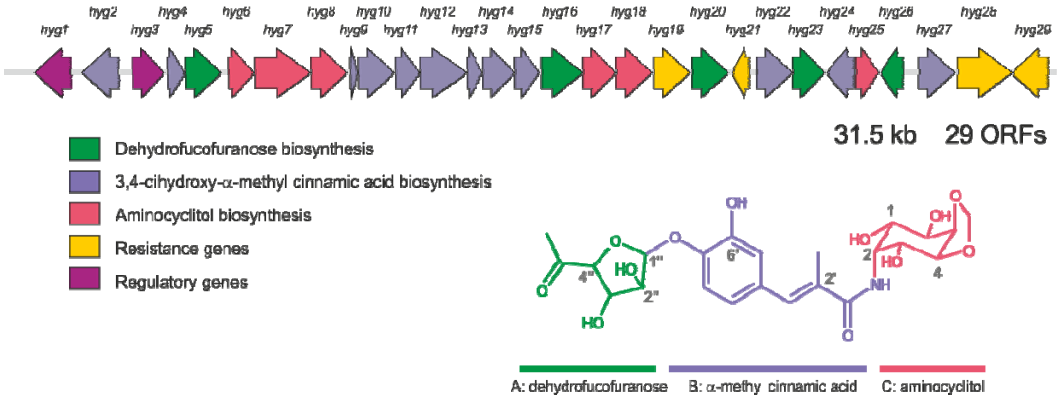

Figure 7 A HygA biosynthesis genes cluster from *Streptomyces hygroscopicus* NRRL 2388. *Subunit A* (shown in green) originates from glucose-6-phosphate via a mannose intermediate, reaction is driven by Hyg5, 23, 29, 16. The final step, oxidation of C-5"-dihydrohygromycin A is catalyzed by NAD dependent Hyg26 *Subunit B* (in purple) is derived from 4-hydroxybenzoic acid and propionic acid in a polyketide-like manner. *Subunit C* (in pink) Aminocyclitol originates from glucose-6-phosphate via myo-inositol intermediate,in a series of reactions catalyzed by Hyg 18, 25, 17, 8. The methylenedioxy bridge formation between C4 and C5 involves Hyg6 and Hyg7 (Dhote et al., 2009; Habib el et al., 2003; Palaniappan et al., 2006; Palaniappan et al., 2009)

The function of some of the gene products within the HygA operon was analysed by genetic manipulations. Knock-out of *hyg26* gene showed that its role plays crucial role in final oxidation step in biosynthesis of SubA. *S. hygroscopicus* Δ*hyg26* mutant strain was shown to produce 5"-dihydro-HygA, instead of HygA (Palaniappan et al., 2006). However, it was not possible to establish whether oxidation happened before or after moieties A and B were linked together.

Methylation at position A2503 of 23S rRNA prevents HygA from binding to the ribosome (Toh et al., 2008). Moreover, among the genes assigned as resistance genes, *hyg21* was shown to encode a 2-O-phosphotransferase, which inactivates HygA (Dhote et al., 2008). *Hyg6* and *hyg29* genes were assigned as putative methyltranferases, and *hyg19* and *hyg28*, as efflux pumps.

From the perspective of development of new antimicrobials, elucidation of the biosynthetic pathway of the aminocyclitol moiety remains an interesting and open question. Aminocyclitol, as shown in previous studies (Hayashi et al., 1997), is essential for HygA's inhibitory activity. Aminocyclitols are often found in active natural compounds, for example, the aminocyclitole-aminoglycosides (e.g. gentamycin, kanamycin or streptomycin), which are very potent antibiotics (Flatt and Mahmud, 2007).

1.2.2 Macrolides

The first members of the macrolide class of antibiotics, picromycin (Brockmann and Henkel, 1950) produced by *Streptomyces venezuelae*, and erythromycin (McGuire et al., 1952) produced by *Saccharopolyspora erythraea*, were discovered in the 1950's. The foundation of the chemical structure of macrolides is the 12-16 membered lactone ring, to which a range of sugar moieties is attached. The classic macrolide, erythromycin (Ery), belongs to the 14-membered family with C3 cladinose and C5 desosamine sugars, while azithromycin (Azi) has a 15-membered ring. Tylosin (Tyl) (**Figure 8c**) is an example of a 16-membered macrolide with a C5 mycaminose-mycarose disaccharide as well as a C14 mycinose (reviewed by (Mankin, 2008; Wilson, 2009)). Macrolides bind to non-translating ribosomes (Pestka, 1974). Chemical probing showed that macrolides universally protect nucleotide A2058 (Poulsen et al., 2000) located at the entrance of the exit tunnel, adjacent to the PTC. Macrolides with a mycarose moiety protect U2506 in the central loop of domain V 23S rRNA, while A752 (domain II), lying deeper in the exit tunnel, is protected from modifications by macrolides with a mycinose moiety (Poulsen et al., 2000). Crystal structures of macrolides bound to ribosomes confirm that the lactone ring binds to the wall of the tunnel, near the tunnel constriction formed by ribosomal proteins L4 and L22, with the C5 sugar moiety extending towards the PTC, and interacts with A2058 and A2059 (**Figure 8a, b**) (Hansen et al., 2002a; Schlunzen et al., 2001; Tu et al., 2005; Wilson et al., 2005). However, the C14 mycinose faces down the nascent polypeptide exit tunnel and interacts with A748-A752 (Hansen et al., 2002a). Tyl, carrying C6 ethyl aldehyde group, was shown to form an

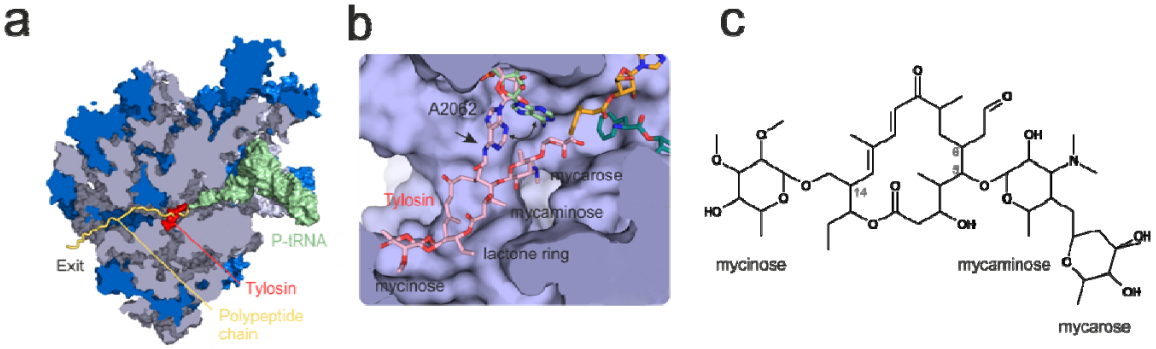

Figure 8 Binding of macrolide antibiotics within the ribosomal tunnel (**A**) The large subunit of the ribosome with visualized ribosomal exit tunnel. The position of tylosin (red), P-site tRNA (green), and a polypeptide chain (yellow) are indicated. rRNA in light blue, ribosomal proteins in dark blue. (**B**) Zoom in on the macrolide-binding site within the ribosomal tunnel. Tylosin (pink) shown with lactone ring, C14-mycinose, and C5-mycaminose-mycarose are labeled. The arrow indicates the carbinolamine bond that forms between tylosin and the N6 of 23S rRNA nucleotide A2062. The positions of A- and P-site aminoacyl-tRNAs are shown in green and orange, respectively. (**C**) Chemical structure of tylosin

unusual reversible covalent bond with the N6 of nucleobase A2062 (Hansen et al., 2002a).

Macrolides bound to the ribosome prevent the progression of most nascent polypeptide chains through the tunnel and induce peptidyl-tRNA drop-off. However, in the presence of macrolides, synthesis of short oligopeptides is still possible. The length of the peptide synthesized before peptidyl-tRNA drop-off depends on the number of sugar substituents at the position C5 and the amino acid sequence of the peptide (Tenson et al., 2003). Monosaccharides, for example as in Ery, allow synthesis of up to eight amino acid long oligopeptides, while macrolides with disaccharides (e.g., Tyl) allow translation of di- to tetrapeptides (Tenson et al., 2003). Moreover, macrolides with a mycarose moiety can directly inhibit peptide bond formation (Poulsen et al., 2000). A resistance mechanism to macrolides involving translation of pentapeptides, which leads to dissociation of the drug from the ribosome, suggests a direct interaction of the macrolide with the nascent polypeptide chain (Lovmar et al., 2006; Tenson et al., 1996; Tenson and Mankin, 2001). Furthermore, pentapeptide effects on distinct macrolides vary, which implies specific interactions between the drug and the nascent polypeptide (Vimberg et al., 2004). A number of additional resistance mechanisms are known, including (i) mono- and dimethylation of the N-6 position of A2058 by the Erm family of methyltransferases (Lai and Weisblum, 1971; Roberts et al., 1999), (ii) single substitution of A2058 to guanosine in the 23S rRNA (Vester and Douthwaite, 2001), (iii) mutations in ribosomal protein L4, such as single amino acid substitutions K63E (Chittum and Champney, 1994) and G69C as well as insertion of two amino acids, SQ, between $Q^{67}K^{68}$ (Tait-Kamradt et al., 2000), (iv) deletion of three amino acids $\Delta M^{82}R^{83}K^{84}$ in ribosomal protein L22 (Gregory and Dahlberg, 1999), (v) MefA and MsrA macrolide efflux pumps (Roberts et al., 1999; Ross et al., 1990), or (vi) inactivation of the antibiotic by modification, for example by Mph family of macrolide phosphorylases (Roberts et al., 1999).

Many macrolide resistance genes are expressed upon induction, which is driven by the presence of sublethal concentrations of the antibiotic in a mechanism called translational stalling. One of the best-characterized examples is the regulation of expression of the methyltransferase, ErmC, which is controlled by an upstream leader sequence *ermC*L (Gryczan et al., 1980; Horinouchi and Weisblum, 1980; Ramu et al., 2009). In the absence of the macrolide, *ermC* translation is attenuated, whereas the presence of the drug induces ribosome stalling during translation of *ermC*L. This, in turn, leads to a rearrangement of the mRNA secondary structure, exposure of the Shine-Dalgarno sequence and start codon, and

expression of downstream *ermC* gene. Recent results suggest that in addition to the sequence of the polypeptide, the structure of the antibiotic is also important for stalling (Vazquez-Laslop et al., 2011). The rRNA nucleotides A2062 and U1782 monitor the structure of the nascent polypeptide, while nucleotides C2610, A2503, and possibly A2058 and A2059 recognize the structure of the macrolide antibiotic (Vazquez-Laslop et al., 2011) and together transmit the signal that induces ribosomal stalling. Moreover, it was shown that the stalled peptide alters the A-site function for peptide bond formation which accounts for the translational arrest (Ramu et al., 2011).

1.2.3 Thiopeptides

Thiopeptide antibiotics are ribosomally synthesized antimicrobials. They are produced as oligopeptides which undergo a series of post-translational modifications resulting in mature, active compounds (Wieland Brown et al., 2009). Compounds belonging to the thiopeptide family have a characteristic trithiazolyl pyridine core, and a macrocyclic loop consisting of a varying number of atoms (for example, 26 in nosiheptide, thiocillin, and thiostrepton, 29 in GE2270A and 35 in berninamycin) (reviewed by (Bowers et al., 2010; Walsh et al., 2010)). Micrococcin P1 (MiC), discovered in 1948 as a metabolite of *Micrococcus* (Su, 1948) and *Bacillus cereus* (Bycroft and Gowland, 1878), was the first described member of the thiopeptide family, followed by the discovery of thiostrepton (ThS), which is produced by *Streptomyces azureus* and *S. laurentii* (Donovick et al., 1955). To date, more than 80 members of this class of antimicrobials are known. Thiopeptides due to their poor solubility, are used only in veterinary practice. However the potency of thiopeptides against multidrug resistant Gram-positive strains and recent advances in total synthesis of a number of thiopeptides (ThS (Nicolaou et al., 2005a; Nicolaou et al., 2005b), GE2270A (Muller et al., 2007) and MiC (Lefranc and Ciufolini, 2009), has renewed interest in this group of antibiotics.

The *Bacillus cereus* ATCC 14579 thiocillin biosynthesis operon has been well-characterized (**Figure 9**), revealing that thiopeptides are synthesized as pre-peptides with a leader peptide which is cleaved-off post-translationally. The C-termini derived peptide undergoes a series of modification steps, thirteen in the thiocillin maturation process, resulting in a fully active antimicrobial compound (Wieland Brown et al., 2009). *In vivo* genetic manipulations of the thiocillin structural gene has led to generation of more than 60 new

thiocillin variants (Acker et al., 2009), opening up new possibilities for generating more active compounds with improved pharmacokinetic properties.

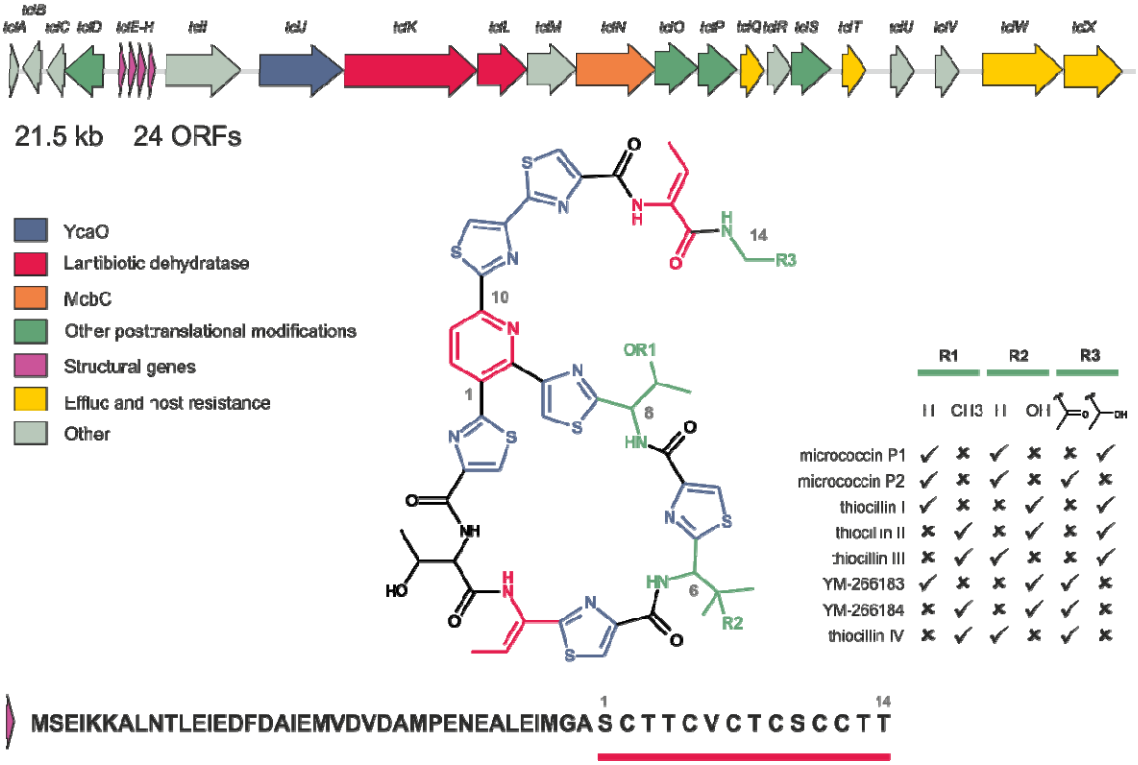

Figure 9 A thiocillin biosynthesis gene cluster from *Bacillus cereus* ATCC 14579. The C-terminal 14 residues of a 52-residue peptide precursor undergo 13 post-translational modifications to generate a set of eight related antibiotics (Wieland Brown et al., 2009)

The crystal structures of ThS and MiC bound to the LSU showed that thiopeptides bind at the GAC, spanning the N-terminal domain of ribosomal protein L11 and H43 and H44 of the 23S rRNA (**Figure 10**) (Harms et al., 2008). ThS and MiC overlap with binding positions of translation factors, such as IF2, EF-G and EF-Tu (Allen et al., 2005; Gao et al., 2009; Myasnikov et al., 2005; Schmeing et al., 2009). Biochemical data revealed that ThS inhibits IF2-dependent initiation complex formation (Brandi et al., 2004), stable binding of ternary complex EF-Tu·aa-tRNA·GTP to A-site (Gonzalez et al., 2007) and stable binding of EF-G to the ribosome (Cameron et al., 2002; Seo et al., 2006). This latter finding suggests that ThS is an inhibitor of the translocation reaction (Munro et al., 2010b; Pan et al., 2007; Pestka, 1970). Functionally, it was shown that ThS inhibits ribosome dependent EF-G's turnover (Pestka, 1970; Weisblum and Demohn, 1970). MiC, unlike ThS, stimulates *in vitro* ribosome-dependent GTPase activity of EF-G (Cundliffe and Thompson, 1981).

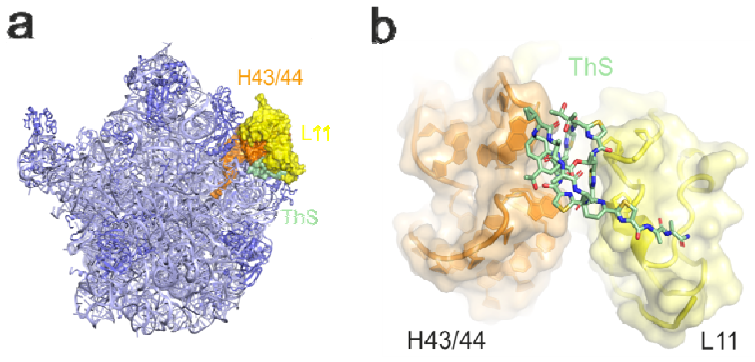

Figure 10 Thiostrepton. (**a**) An overview of thiopeptide binding site on the LSU. Interface view with helix 43 and 44 (H43/44; orange), L11 (yellow), and ThS (green) highlighted with surface representation (PDB 3CF5) (Harms et al., 2008). (**b**) The thiazole rings of ThS (green) interact with the RNA bases at the tips of H43/44 as well as the prolines in the N-terminal domain of L11 (yellow) (Starosta et al., 2009).

In contrast, GE2270A does not bind to the GAC, but instead binds to EF-Tu (**Figure 11**) and interferes with binding of the aa-tRNA, leading to inhibition of ternary complex formation (Parmeggiani and Nissen, 2006). Crystallographic data showed that GE2270A spans domain I and II of EF-Tu, and therefore prevents the aminoacyl moiety of the aa-tRNA from binding (Parmeggiani and Nissen, 2006).

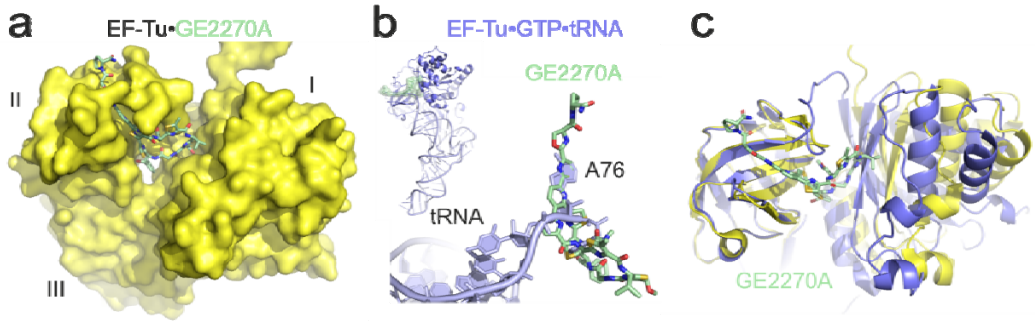

Figure 11. Binding site of GE2270A on EF-Tu. (**a**) Structure of the thiopeptide GE2270A (green) bound to EF-Tu (yellow), with domains I, II, and III indicated (PDB 2C77) (Parmeggiani et al., 2006). (**b**) GE2270A overlaps the binding position on EF-Tu of the terminal A76 and aminoacyl moiety of tRNA. Inset shows overview of EF-Tu•tRNA ternary complex (PDB 1TTT) (Nissen et al., 1995) with superimposition of GE2270A. (**c**) Superimposition of EF-Tu_GE2270A (yellow) and EF-Tu•tRNA (blue) aligned on basis of domain II. Note that GE2270A (green) clashes with domain I of EF-Tu from the ternary complex (blue) (Starosta et al., 2009).

Thiopeptides that interact with the ribosome contact nucleotides A1067 (H43) and A1095 (H44), and interact with P22 and P26 of L11. In accordance with structural data, substitutions of A1067 and A1095 (Rosendahl and Douthwaite, 1994; Thompson et al., 1988), or within the proline-rich region of L11's N-terminus (Cameron et al., 2004) lower the affinity of the drug for the ribosome and confer resistance (Baumann et al., 2010). Bacteria producing thiopeptides protect themselves from the inhibitory effects of drugs through efflux mechanisms (Wieland Brown et al., 2009). The *Streptomyces azureus* genome encodes a 2'-

O-methylase that modifies nucleotide A1067 (Thompson et al., 1982), which is used in molecular biology as ThS selection marker.

1.2.4 Orthosomycins

The evernimicin class (orthosomycins) of antibiotics were first isolated from *Micromonospora carbonaceae* in the 1960's (Weinstein et al., 1964). Orthosomycins are oligosaccharide antibiotics rich in modified L- and D-deoxysugars containing unusual orthoester and glycosyl linkages (**Figure 12c**) (Hosted et al., 2001; Weitnauer et al., 2001) and are active against Gram-positive bacteria (Nakashio et al., 1995). Evernimicin (Evn) and avilamycin (Avi) bind to the LSU and are potent protein synthesis inhibitors (McNicholas et al., 2000). Chemical probing shows that Evn and Avi protect nucleotides A2468, A2469, A2476, A2478, and A2482 in H89, and A2534 in H91 from DMS modification (Belova et al., 2001; Kofoed and Vester, 2002), which locates the orthosomycin binding site at the base of the L7/L12 ribosomal stalk (**Figure 12a, b**). Consistent with primer extension data, mutations conferring resistance to Evn are located in H89 and H91 (Belova et al., 2001). Also mutations in ribosomal protein L16 are linked to Evn resistance (Belova et al., 2001; McNicholas et al., 2001). Moreover, the modification of U2479 by AviRB, a 2'-O-methyltransferase from

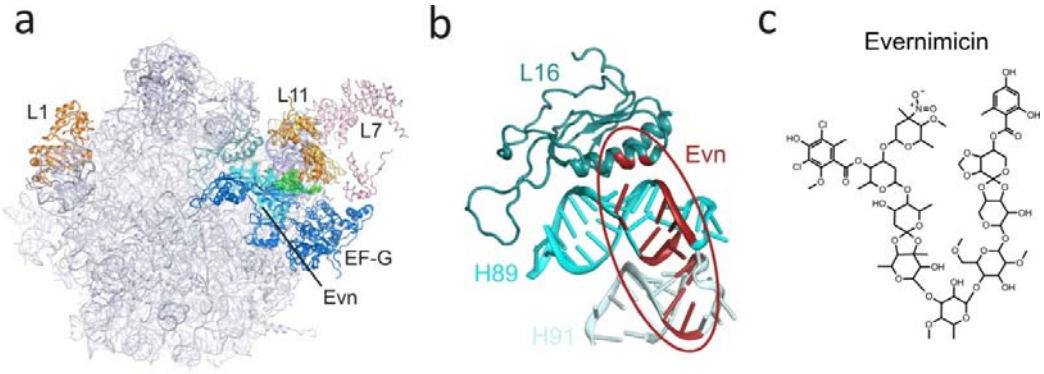

Figure 12 Orthosomycins. (**a**) An overview of the binding sites of orthosomycins on the LSU relative to EF-G. Ribosomal proteins L1, L11, and L7 are shown for reference; (**b**) Putative binding site of orthosomycins spanning from H89 and H91 of the 23S rRNA. Residues highlighted in red have been associated biochemically with Evn (review by (Wilson, 2009); (**c**) Chemical structure of Evn.

Streptomyces viridochromogenes (Mosbacher et al., 2005), and of G2470 by EmtA, a rRNA methyltransferase from *Enterococcus faecium* (Mann et al., 2001), led to an increase in the resistance to Evn. Although the exact mechanism of action of Evn remains unclear, biochemical data showed that Evn overlaps with the IF2 binding site on the LSU (La Teana et al., 2001) and inhibits fMet-puromycin synthesis on ribosome reconstituted from the 30SIC

with IF2 bound and the LSU, suggesting that Evn may inhibit IF2-dependent 70SIC formation (Belova et al., 2001).

1.2.5 Fusidic acid

Fusidic acid (FA) is a steroid antibiotic (**Figure 13c**) (Godtfredsen and Vangedal, 1962), discovered in 1960's as a metabolite of *Fusidium conccineum* (Godtfredsen et al., 1962). FA inhibits protein synthesis by impairing the function of EF-G on the ribosome. Biochemical data showed that FA does not inhibit GTP hydrolysis. Instead, FA stabilizes the ribosomal intermediate hybrid state, locks EF-G on the ribosome in the GTP conformation

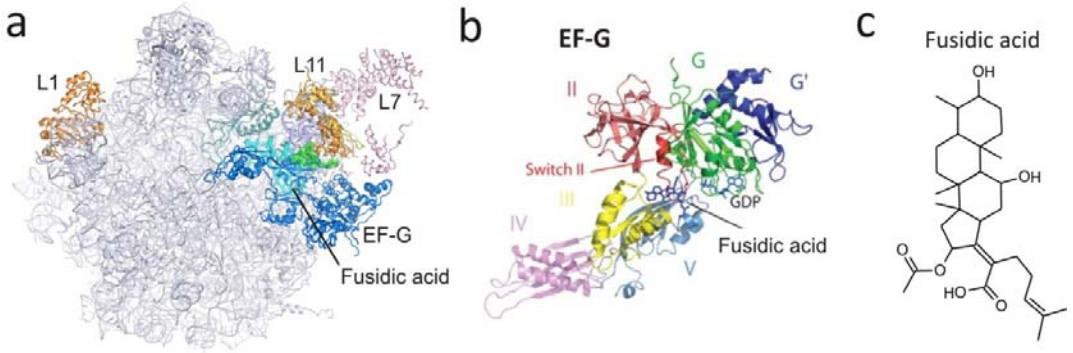

Figure 13 Fusidic acid. (**a**) An overview of the binding sites of the FA on the LSU relative to EF-G. Ribosomal proteins L1, L11, and L7 are shown for reference; (**B**) The structure of EF-G bound to the FA and GDP in the ribosome. The various domains of EF-G are colored as shown (Gao et al., 2009); (**C**) Chemical structure of FA.

even after GTP hydrolysis (Ticu et al., 2009), and does not allow EF-G's turnover (Datta et al., 2005; Spiegel et al., 2007; Ticu et al., 2009). It was shown that FA action strongly depends on the concentration, and at lower concentrations FA allows multiple GTPase turnovers (Seo et al., 2006). FA does not bind to free EF-G, but to EF-G bound to the ribosome in a GTP state (Tanaka et al., 1968), although the low resolution cryo-electron microscopy (cryo-EM) structures did not reveal the binding position of the drug (Agrawal et al., 1999; Datta et al., 2005). Nevertheless, the studies of the resistance mutations suggest that the binding site of the FA is located at the interface between domain I and III of EF-G (**Figure 13a, b**) (Laurberg et al., 2000), which is in agreement with the X-ray structure of EF-G in complex with GDP and FA bound to a pseudo-POST state 70S ribosome (Gao et al., 2009).

1.3 Alternative antimicrobials targeting virulence

Traditional antibiotics, which inhibit essential functions of bacteria, are under selective pressure that favors resistance mutations (Clatworthy et al., 2007). The need for novel antimicrobial therapies is greater than ever before. New approaches in antimicrobial development focus on bacterial virulence and interactions between bacterial and host cells (Clatworthy et al., 2007).

1.3.1 Definition of virulence

In the traditional meaning, virulence is understood as the ability of a microorganism to cause illness (Clatworthy et al., 2007). Virulence factors (toxins, cytolysines, proteases) are generally not necessary for a pathogen to survive under laboratory conditions, however their role *in vivo* is crucial for the microorganism to survive in the environment (Alksne and Projan, 2000). The analysis of genomes of many virulent bacteria has revealed diversity in their gene content, for example different *E. coli* strains, e.g. laboratory K12 strain compared with pathogenic *E. coli* 0157, differ by up to 25% of their genome, while *Salmonella enterica* differs from E.coli K12 by up to 12% (Raskin et al., 2006). The variable genes are located on so-called pathogenicity islands, clustering genes responsible for virulence and antibiotic resistance (Pallen and Wren, 2007; Raskin et al., 2006). Bacterial virulence factors are responsible for colonization, survival within host cells, modification of host cell response as well as intracellular communication (Wu et al., 2008).

1.3.2 Colonization

Pathogenic bacteria invading host cells adapt the expression of entire pathways of genes to transition from the free-living form to one that colonizes the host cell (Alksne and Projan, 2000). Colonization of host cells requires induction of expression and assembly of adhesions, fimbriae and pili, which allow bacteria to attach to the cell surface (Finlay and Cossart, 1997). Bacteria invading mammal cells must reprogram their metabolism to adapt to new living conditions. Varying pH, oxygen accessibility, osmotic pressure, nutrient availability and ion homeostasis are signals to rearrange gene expression of the pathogen (Ray et al., 2009).

1.3.3 Biofilm

Bacteria hardly ever exist as free-floating cells. They tend to live in organized colonies associated with surfaces (Jayaraman and Wood, 2008). Such colonies, called

biofilms, are highly organized structures of bacteria embedded within exopolysaccharide matrices (Lawrence et al., 1991), where nutrient and metabolite transport is regulated by bacterial communication using small messenger molecules (acylated homoserine lactones, AHLs) (Davies et al., 1998). Biofilms give bacteria a greater chance to survive in unfavourable environmental conditions, increasing their chances for successful colonization. Bacteria in biofilms show significantly decreased susceptibility to antibiotics compared to free-floating cells (Luppens et al., 2002).

1.3.4 Quorum sensing

Communication between bacteria is mostly mediated by small autoinducer molecules. Autoinducers, mostly AHLs that are secreted into the environment, can modulate transcription of genes, including virulence factors. Quorum sensing occurs when bacterial populations reach high densities, which leads to the accumulation of high concentrations of autoinducers (reviewed by (Ng and Bassler, 2009)).

1.3.5 Motility

Successful colonization of new niches requires bacteria to have the ability to migrate. Motility is a high-energy consuming process powered by rotation of flagella or movement of pili (Kearns, 2010; Verstraeten et al., 2008). Swarming and swimming motilities are flagella-dependent. While swarming is the movement of a group of bacteria over a solid surface, swimming, in contrast, is an act of a single cell moving though a viscous liquid environment (Henrichsen, 1972). Twitching motility is driven by extension and retraction of type IV pili and is important for biofilm formation (Mattick, 2002).

1.3.6 Secretion systems

Bacteria can modulate the environment or even alter the host's physiology using several secretion systems (SS) (Tseng et al., 2009). However here, only three of the major SS in bacterial pathogenicity are mentioned. The type I SS is an ABC transporter responsible for efflux of antimicrobial molecules as well as toxins, proteases and lipases (Koronakis et al., 2004). The type III SS is called the injectisome due to its ability to protrude into the host cell's surface with a needle-like structure, which allows direct release of toxins into the host's cytoplasm (Cornelis, 2010). The type IV SS is the only SS which can transport nucleic acids as well as proteins. F-plasmid based conjugation, accounts for evolution of infectious pathogens though propagation of antibiotic resistance and virulence genes (Cascales and

Christie, 2003). Moreover type IV pili have been shown to promote bacterial motility and stimulate biofilm formation (Mattick, 2002).

1.3.7 Elongation factor P

Elongation factor P (EF-P) was identified as a protein binding to the ribosome (Glick and Ganoza, 1975). Two-dimensional gel electrophoresis (2D) analysis of *E. coli* cell extract showed EF-P to be present in a ratio 1 per 10 ribosomes (An et al., 1980). EF-P was found to bind to subunits, 70S ribosomes and polysomes (Aoki et al., 2008) suggesting its role not only in translation initiation, but also in elongation steps. Although, EF-P function remains unclear, it was shown that the elongation factor stimulates formation of the first peptide bond (Ganoza and Aoki, 2000; Glick et al., 1979; Glick and Ganoza, 1975; Swaney et al., 2006). The deletion of *efp* gene leads to defects in the growth of *E. coli* (Aoki et al., 1997), virulence of *Agrobacterium tumefaciens* dependent on type IV SS (Peng et al., 2001), intestinal colonization of host cells by *Vibrio cholerae* also dependent on type IV SS (Merrell et al., 2002) and *Brucella abortus* (Iannino et al., 2011), flagella driven motility of *Bacillus subtilis* and *E. coli* (Inoue et al., 2007; Kearns et al., 2004). Moreover, it was shown that EF-P is specifically expressed in porcine lymph nodes upon *S. typhimurium* infection (Van Parys et al., 2011). The EF-P crystal structures revealed a three domain architecture that resembles a classical tRNA L-shape, suggesting possible mimicry (**Figure 14a**) (Choi and Choe, 2011; Hanawa-Suetsugu et al., 2004; Yanagisawa et al., 2010). The crystal structure of EF-P bound to 70S ribosome (Blaha et al., 2009) shows that EF-P does not bind in a canonical tRNA binding site, but rather sits between the P- and E-sites, spanning both subunits (Blaha et al., 2009). The conserved loop of domain I reaches the CCA-end of the initiator-tRNA, while domain III contacts the anticodon stem loop of tRNA (Blaha et al., 2009), supporting the hypothesis that EF-P stabilizes the initiator tRNA to promote first peptide bond reaction.

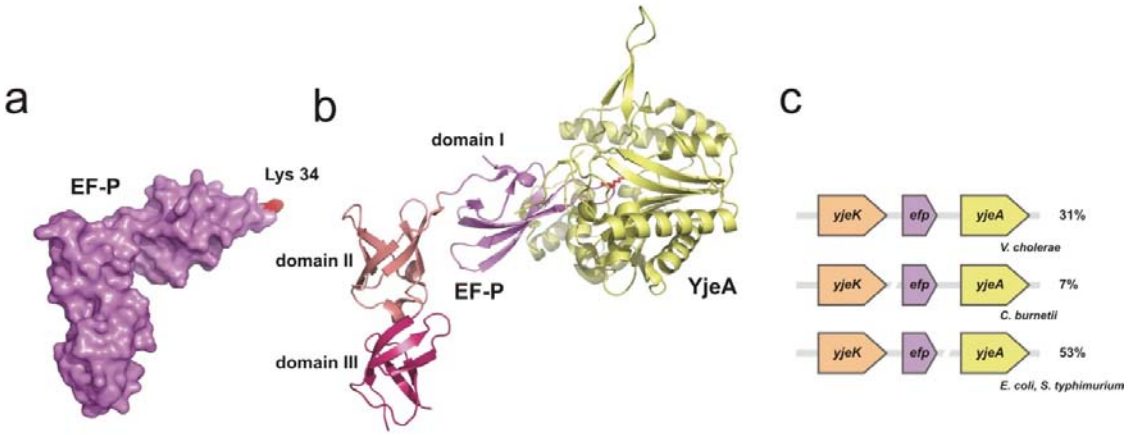

Figure 14. Elongation factor P. (**a**) EF-P crystal structure shows classical tRNA L-shape, in red - Lysine 34 undergoing modification (PDB 3A5Z); (**b**) EF-P (violet) in a complex with YjeA (yellow) (PDB 3A5Z) (Yanagisawa et al., 2010); (**c**) Physical clustering of *efp* (violet), *yjeK* (pink), and *yjeA* (yellow), according to (Bailly and de Crecy-Lagard, 2010).

EF-P is conserved among bacteria (Bailly and de Crecy-Lagard, 2010) and is homologous with eukaryotic initiation factor 5A (eIF5A) (Hanawa-Suetsugu et al., 2004). Unlike EF-P, eIF5A has only two domains, corresponding to domain I and II of EF-P (Kim et al., 1998; Peat et al., 1998). However, like eIF5A, EF-P also has a highly conserved loop in domain I (Hanawa-Suetsugu et al., 2004). A unique feature of eIF5A is the presence of a post-translational modification with hypusine, which is essential and characteristic only to eIF5A (Zanelli et al., 2006). The highly conserved lysine 50 (K50 in human eIF-5A) is modified into an unusual amino acid derived from spermidine. Hypusylation is a two-step reaction, catalyzed by two enzymes. First, the deoxyhypusine synthase (DHS) catalyzes the cleavage of the polyamine spermidine as well as the transfer of its 4-aminobutyl moiety to the ε-amino group of lysine residue of the eIF-5A precursor to form deoxyhypusine (Park, 2006). In a second step, deoxyhypusine hydroxylase (DOHH) mediates the addition of a hydroxyl group to the deoxyhypusine residue forming hypusine (Park, 2006). DHS and DOHH are not present in bacterial genomes, however, analyses of endogenous *E. coli* EF-P revealed the presence of an additional 144 Da mass (Aoki et al., 2008). Two unrelated to DHS and DOHH gene were implied to function as modification enzymes for EF-P pathway, namely, *yjeA* (a paralog of lysyl-tRNA synthetase) and *yjeK* (lysine 2,3-aminomutase) (**Figure 14c)** (Bailly and de Crecy-Lagard, 2010). Interactions between *yjeA* and *yjeK* were reported to be critical for virulence and stress resistance in *S. enterica* (Navarre et al., 2010). *Salmonella yjeA* and *yjeK* mutants share extensive phenotypic pleiotropy, including attenuated virulence in mice, a decreased ability of bacteria to colonize swine host, growth defects, susceptibility to a variety

of various growth inhibitors and altered expression of multiple proteins, including several encoded on the SPI-1 pathogenicity island (Bearson et al., 2011; Bearson et al., 2006; Kaniga et al., 1998; Navarre et al., 2010; Yanagisawa et al., 2010). YjeA mediates the post-translational modification of bacterial elongation factor P resulting in an additional 128 Da mass on EF-P (**Figure 14b**) (Navarre et al., 2010). *In vivo* experiments show that YjeK enhances the activity of YjeA (Yanagisawa et al., 2010), which is consistent with observation that (R)-β-lysine is 100-fold better substrate for YjeA than (S)-β-lysine or α-lysine (Roy et al., 2011).

2 Objectives of these studies

(I) Hygromycin A (**Paper 1 and 2**). Analysis of fermentation broth contents of several *S. hygroscopiscus* NRRL 2388 mutants revealed the presence of a mixture of HygA derivatives. Intermediates of the HygA biosynthetic pathway were investigated and affects of alterations of the aminocyclitol moiety on the antimicrobial activity of HygA were studied. Moreover how differential oxidation states of the C5" position of dehydrofucofuranose moiety affects the activity of HygA was also examined. Additionally, unpublished data is presented showing the inhibitory effect of HygA derivatives on peptide bond formation and the effect of phosphorylation of HygA by the 2-O-phosphotransferase was evaluated.

(II) Macrolides. (**Paper 3)** Structural data show that *D. radiodurans* ribosome can bind two molecules of azithromycin (AZI) (Schlunzen et al., 2003). However in the crystal structure of AZI with *Haloarcula marismortui* LSU only one molecule of AZI was bound (Hansen et al., 2002a). Here the kinetics of AZI binding to *E. coli* and *D. radiodurans* ribosomes were studied to investigate in more details the discrepancies between antibiotic binding in different species. (**Paper 4**). The C6 ethyl aldehyde group of the Tylosin (Tyl) forms a unique covalent bond with ribosomal RNA A2062 (Hansen et al., 2002a). The contribution of the covalent linkage in the binding to the ribosome and the inhibitory activity of Tyl was determined. Moreover, Tyl derivatives designed to establish interactions with ribosomal tunnel wall, and derivatives with substituents mimicking nascent polypeptide was also tested.

(III) Thiopeptides. (**Paper 5**) The complicated structure and poor solubility of thiopeptides account for their limited possibilities in terms of application for bacterial infection therapies. Therefore, a library of thiopeptide synthetic precursors was screened for their potency to inhibit protein synthesis and ribosome-dependent GTPase activity of EF-G in order to find the minimal carbon scaffold necessary for targeting the ribosome and which, in the future, could provide a basis for design of more soluble compounds. (**Paper 6**) MiC binds in a cleft between ribosomal protein L11 and H43 and H44 of the 23S rRNA (Harms et al., 2008), and stabilizes the C-terminal domain of protein L7/L12 (CTD-L7/L12) (Harms et al., 2008). Crystallographic data shows

that the G'-domain of EF-G interacts with CTD-L7/L12 (Gao et al., 2009), and was shown to be crucial for GTPase activity and Pi release (Nechifor et al., 2007; Savelsbergh et al., 2005). By comparison of different GTPases, which have reduced or absent G' domain, the hypothesis was tested that the enhanced turnover of EF-G by MiC is a result of stabilizing effects of the drug on L11- CTD-L7/L12 interaction.

(IV) Orthosomycins. (**Paper 6**). The available data suggest that Evn inhibits initiation of translation, however, the exact step at which Evn acts remains unclear. Therefore, the role of Evn in the translation cycle was dissected.

(V) Fusidic acid. (**Paper 7**) Antibiotics can trap the ribosome in distinct functional states. FA was used to visualize intermediate translocation events and ascertain whether it is possible to localize the antibiotic using Cryo-EM.

(VI) Elongation factor P. (**Paper 8**) Emerging resistance to antibiotics stresses the need for new antimicrobial targets. EF-P is linked to virulence in a number of bacterial strains. The modification of EF-P is crucial for pathogenicity. The differences between the 144 Da modifications reported for endogenous EF-P compared with the 128 Da modification observed *in vitro* was investigated. Moreover, the chemical composition of the modification was also dissected. Additionally, initial unpublished data is presented showing variability in phenotypes of wild type *E. coli* with deletion strains of the *efp* gene and genes encoding the EF-P modification enzymes.

3 Cumulative thesis

3.1 Hygromycin A

3.1.1 Paper 1

Palaniappan, N., Dhote, V., Ayers, S., **Starosta, A.L.**, Wilson, D.N., and Reynolds, K.A. (2009). Biosynthesis of the aminocyclitol subunit of hygromycin A in Streptomyces hygroscopicus NRRL 2388. Chem Biol *16*, 1180-1189.

3.1.2 Paper 2

Dhote, V., **Starosta, A.L.**, Wilson, D.N., and Reynolds, K.A. (2009). The final step of hygromycin A biosynthesis, oxidation of C-5"-dihydrohygromycin A, is linked to a putative proton gradient-dependent efflux. Antimicrob Agents Chemother *53*, 5163-5172.

The aminocyclitol subunit was shown to be essential for the antimicrobial activity of HygA (Hayashi et al., 1997). The HygA biosynthesis operon has seven genes assigned for synthesis of the aminocyclitol moiety (SubC) (**Figure 7**). Using a radiolabeled precursor approach, it was shown that the SubC of HygA is derived from glucose via a *myo*-inositol (MI) intermediate and methionine (Habib el et al., 2003). In **Paper 1**, Professor K. Reynold's group continued studies on HygA biosynthesis pathway. Gene disruption experiments and chemical complementation with MI and/or mature SubC enabled the series of steps leading to production of mature SubC to be understood. The studies demonstrated that glucose-6-phosphate is a substrate for Hyg18, assigned as myo-inositol-1 phosphate synthase. In the next step, MI-phosphate is dephosphorylated by Hyg25. MI is a substrate for inositol dehydrogenase (Hyg17). The reaction of Hyg17 is followed by transamination of the C5-oxydized MI to produce *neo*-inosamine-2 in a reaction catalyzed by Hyg8 aminotransferase. Hyg6 is a SAM-dependent methyltransferase that methylates *neo*-inosamine-2. The structure of HygA revealed a unique methylenedioxy bridge between the C4 and C5 carbons of the aminocyclitol. Therefore, it was suggested that the cyclization of the C5 methoxy group is catalyzes by Hyg7. Disruption of *hyg8* and *hyg7* genes did not lead to HygA production. However, interestingly, the intermediates of HygA were accumulated. – desmethylenehygromycin A (Des-HygA) containing a hydroxyl group at the C5 carbon, and methoxyhygromycin A (Met-HygA), with a C5-OCH_3 group instead of the methylenedioxy bridge.

The antimicrobial potency of the intermediates of HygA with altered aminocyclitol ring was examined against Δ*tolC E. coli*. The minimal inhibitory concentration (MIC) experiments for HygA and intermediates showed that, the modifications of aminocyclitol moiety lead to a significant loss (15-fold) of an *in vivo* activity of Des-HygA and Met-HygA. Moreover, the HygA-derivative lacking the aminocyclitol moiety (AB) (Palaniappan et al., 2006) displayed no detectable activity. I tested the intermediate compounds for their ability to inhibit protein synthesis in an *E. coli* lysate-based *in vitro* coupled transcription-translation assay (TT) using green fluorescent protein (GFP) as a reporter. HygA showed high *in vitro* activity with half-inhibitory concentration (IC_{50}) at 0.18 μM. Surprisingly, the intermediates of HygA displayed significant *in vitro* activity, with IC_{50} of Met-HygA at 0.32 μM and Des-HygA at a concentration of 0.5 μM, whereas the AB compound displayed no or minor inhibitory activity, even at concentrations of 75 μM. Interestingly, the order of the activity of the compound reflected the progression of methylenedioxy bridge synthesis. Additionally, in the context of a DAAD fellowship, I visited the laboratory of Professor G. Dinos (Patras, Greece) where I tested the HygA analogs for their ability to inhibit AcPhe-puromycin (AcPhe-Puro) synthesis. Interestingly, I found the same trend of the potency to inhibit peptide bond formation as I observed for the inhibition of GFP synthesis (**Figure 15a,c** vs **b,d**). These data suggest that HygA primary activity is the inhibition of the PTC. The MIC, TT and AcPhe-Puro data on the HygA intermediates confirmed that the aminocyclitol is necessary for HygA inhibitory activity *in vivo* and *in vitro*. The data showed that for the full *in vivo* activity, the aminocyclitol must be modified with an intact methylenedioxy bridge. However, alterations of the methylenedioxy ring did not lead to a loss in the *in vitro* protein synthesis inhibition activity, in particular on the peptide bond formation. Taken together, these data suggest that the aminocyclitol ring is essential for translation inhibition activity, whereas a methylenedioxy ring is crucial for full *in vivo* activity, possibly for the uptake of the drug into the cell.

Previous studies from Professor K. Reynolds's group showed that disruption of *hyg26* gene led to the accumulation of 5"-dihydro-HygA (DH-HygA) intermediate (Palaniappan et al., 2006). Hyg26 was suggested to catalyze dehydrogenation of the C5"-OH of the fucofuranose moiety (SubA). In **Paper 2**, it was shown that recombinant Hyg26 is a NAD/NADH-dependent oxidoreductase, and that the Hyg26 reaction is reversible and favors DH-HygA. Surprisingly, the disruption of the *hyg19* gene also led to the accumulation of DH-HygA. Moreover, although HygA was still detected, the level of antibiotic production was

significantly decreased. Hyg19 was predicted to be a proton gradient-dependent efflux pump. It was shown that the levels of HygA production depend on the effective export of the drug outside the cell by the Hyg19 pump. The DH-intermediates of HygA, Des-HygA and Met-HygA were tested for their antimicrobial activity. The MIC values against Δ*tolC E. coli* showed that the change of oxidation state of C5" do not alter *in vitro* activity of neither HygA nor Des-HygA and Met-HygA. Additionally, I tested DH-intermediates of HygA for their potency to inhibit protein synthesis in *E. coli* lysate based TT assay. Compared with the data for HygA the 5" oxidized analog, DH-HygA (**Figure 15a**) showed slightly reduced activity to inhibit GFP synthesis. Interestingly, DH-intermediates of Met-HygA and Des-HygA displayed significantly lower potency (8- to 15-fold decrease) to inhibit protein synthesis (**Figure 15c**) in comparison to their dehydrogenized analogs. Additionally, I analysed DH-intermediates in an AcPhe-Puro synthesis assay. As seen for inhibition of GFP synthesis, oxidized intermediates exhibited a decrease in potency to inhibit protein synthesis (**Figure 15b, d**). Although the changes in the C5" oxidation state of SubA did not have an effect *in vivo*, they significantly altered the activity of HygA and intermediates to inhibit protein synthesis, suggesting the importance of this group for the interactions with ribosome.

Additionally, the effect of phosphorylation of HygA (P-HygA) was studied. Hyg21 is a O-phosphotransferase that modifies C2" of SubA. (Dhote et al., 2008). Inactivation of HygA by phosphorylation was observed *in vivo* for Δ*tolC E. coli* and *Streptomyces lividans* (Dhote et al., 2008). I found that P-HygA significantly loses activity to inhibit protein synthesis in TT assay (>150 fold) (**Figure 15e**) and potency to inhibit AcPhe-Puro synthesis (~500 fold) (**Figure 15f**), suggesting that the modification decreases the affinity of the compound to the ribosome.

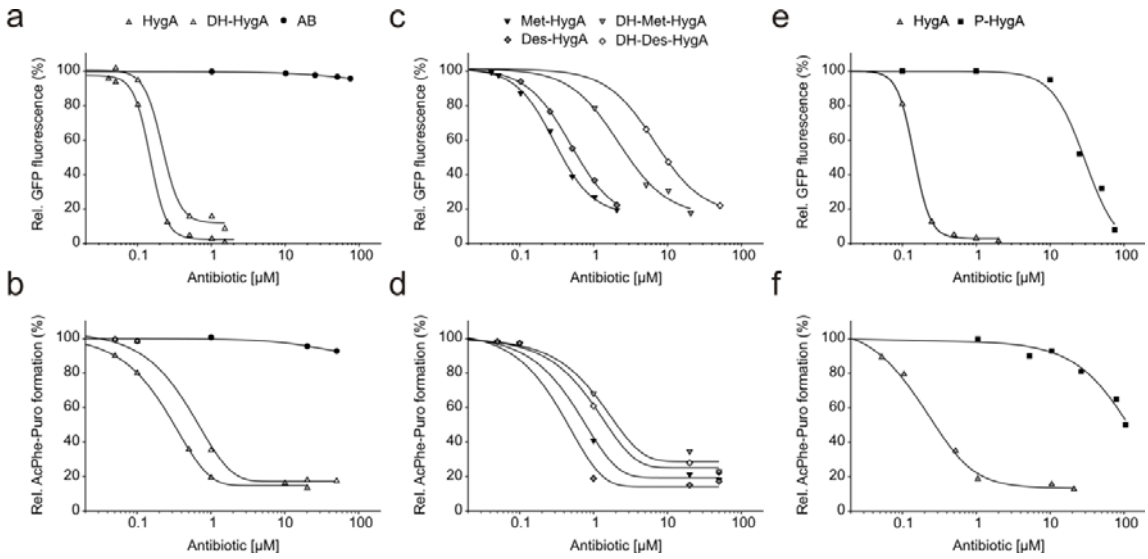

Figure 15. HygA and derivatives action (**a, c, e**) on the GFP synthesis in a TT assay and (**b, d, f**) on the AcPhe-Puro synthesis

Collectively, it was shown that gene disruption of the HygA biosynthesis pathway results in accumulation of intermediates, which enables functional studies of distinct chemical moieties of HygA to be performed. The intermediates are becoming progressively more active antimicrobials, with HygA as the most potent inhibitor. The methylene bridge was proven to be important for the *in vivo* activity of HygA, whereas it does not significantly affect translation inhibition *in vitro*. Furthermore, the C5" oxidation has no effect on *in vivo* activity, but alters the effect of HygA on the translation *in vitro*. I showed that HygA and intermediates inhibit peptide bond formation, suggesting that HygA binds in the PTC, in agreement with previous biochemical data (Guerrero and Modolell, 1980; Poulsen et al., 2000). Additionally, I demonstrated that the modification of C2" leads to the loss of inhibitory activity of HygA, possibly through sterical clashes with ribosomal components and altering the affinity to the ribosome. In conclusion, the new structurally diverse compounds may lead to design of novel antimicrobials.

3.2 Macrolides

3.2.1 Paper 3

Petropoulos, A.D., Kouvela, E.C., **Starosta, A.L.**, Wilson, D.N., Dinos, G.P., and Kalpaxis, D.L. (2009). Time-resolved binding of azithromycin to Escherichia coli ribosomes. J Mol Biol *385*, 1179-1192.

3.2.2 Paper 4

Starosta, A.L., Karpenko, V.V., Shishkina, A.V., Mikolajka, A., Sumbatyan, N.V., Schluenzen, F., Korshunova, G.A., Bogdanov, A.A., and Wilson, D.N. (2010). Interplay between the ribosomal tunnel, nascent chain, and macrolides influences drug inhibition. Chem Biol *17*, 504-514.

Azithromycin (AZI) is a 15-membered semi-synthetic derivative of erythromycin, structurally distinguished by the absence of a keto oxygen at position C9 and the insertion of a methyl-substituted nitrogen at position C10. AZI shows higher stability and improved potency against Gram-negative bacteria. AZI displayed anti-inflammatory and modulatory effects on the expression of virulence factors of *P. aeruginosa* (Bala et al., 2011). Interestingly, crystal structures of AZI bound to either the bacterial (Schlunzen et al., 2003) or archaeal (Hansen et al., 2002a) ribosome showed a different number of molecules bound per ribosome. A single molecule was found in the archaeal structure, whereas two molecules of the drug were observed in the structure of *D. radiodurans* 50S subunit.

In **Paper 3**, the group of Professor G. Dinos used kinetic and footprinting methods to characterise binding process of the AZI. It was shown that AZI binds to *E. coli* ribosomes in a two-step process. First, an initial rapid low-affinity binding state occurs where AZI inserts into a hydrophobic cleft formed by nucleotides G2057-A2059 and is also positioned by G2505. Secondly, AZI slowly accommodates into a high-affinity binding state, where interaction with hydrophobic cleft weakens and AZI moves towards U2609 and nucleotides of domain II of 23S rRNA. Moreover, U2609C substitution promotes formation of the stable complex. The low- and high-affinity AZI binding sites are unique and only one molecule of the drug binds per *E. coli* ribosome at a time. In order to to evaluate the species specific mode of AZI binding, I prepared *D. radiodurans* 70S ribosomes which were used. In contrast to previously obtained data for AZI binding to *E. coli* ribosomes, kinetic and binding data indicated that two molecules of AZI bind cooperatively to the *D. radiodurans* ribosome. This finding supported the crystallographic observations on differential binding of AZI to

ribosomes from varying species. In conclusions, in the future, our results may lead to design of compounds that preferentially target ribosomes of specific species of bacteria

The crystal structure of tylosin (Tyl) bound to *Haloarcula marismortui* LSU showed a covalent bond between the C6 ethyl aldehyde group of Tyl and the N6 of nucleobase A2062 of 23S rRNA (Hansen et al., 2002a). Nucleobase A2062 was suggested to establish interaction with nascent polypeptide (Bhushan et al., 2010; Seidelt et al., 2009; Vazquez-Laslop et al., 2011) and contribute for the stalling mechanism of ErmCL (Vazquez-Laslop et al., 2008). In **Paper 4**, the importance of ethyl aldehyde group for Tyl binding was elucidated. A series of macrolide derivatives with oligopeptide substituents was tested in order to investigate tunnel-nascent polypeptide interactions.

The group of Professor A. Bogdanov designed and synthesized several Tyl derivatives, which I have tested for their ability to establish interactions with either the ribosomal exit tunnel wall and/or the nascent polypeptide. Two sets of Tyl derivatives, with substitution at either the C6 or C14 positions were monitored for their ability to (i) compete for binding to empty *D. radiodurans* 70S ribosomes with [^{14}C]-erythromycin ([^{14}C]-Ery), or (ii) inhibit GFP synthesis in *E. coli* lysate-based TT assays.

I demonstrated that the reduced form of Tyl (Tyl-H2), where the C6 ethyl aldehyde is replaced with a hydroxyl group, is unable to compete with [^{14}C]-Ery. Moreover, in the TT assay, Tyl-H2, displayed significantly decreased potency to inhibit GFP synthesis, and was not able to inhibit protein synthesis completely. This showed that the covalent bond established between Tyl and ribosomal nucleotide A2062 is critical for drug binding and inhibitory activity. Furthermore, several C6 ethyl aldehyde oligopeptide substituents were tested. Tyl with C6-Ala-Ala dipeptide (Tyl-Ala) showed improved binding ability compared to Tyl-H2, however was still significantly worse than Tyl. The potency of Tyl-Ala to inhibit GFP synthesis was comparable with Tyl suggesting that the new analog may establish additional interactions with nascent polypeptide or ribosomal tunnel wall. The crystal structure of Tyl-Ala bound to *D. radiodurans* 50S subunits showed that Ala dipeptide stacks onto nucleotide A2062, which could account for the improved binding affinity. On this basis, a series of Tyl derivatives were designed to optimize stacking interactions with A2062. Additionally, I tested several Tyl derivatives with nucleotides and aromatic amino acids attached to C6 carbon with linkers varying in length and flexibility, including uridine, tyrosine and phenylalanine. Tyl-U with a uridine attached with a 4 atom linker was not sufficient to

significantly improve the potency of a compound in either binding to the ribosome or inhibition of a GFP synthesis. A tyrosine with either rigid or flexible 5 atom linker (Tyl=Tyr and Tyl-Tyr, respectively) showed differential effects. While Tyl=Tyr had poor properties, Tyl-Tyr was as effective as Tyl for inhibition of protein synthesis. Interestingly, a phenylalanine attached with flexible 6 atom linker showed enhanced potency to inhibit GFP synthesis compared with Tyl. Nevertheless, it has to be noted, that none of the new compounds displayed better binding properties in comparison to Tyl. This suggested that the potency of new derivatives originated not from the binding affinity but rather from the steric perturbation of growing nascent polypeptide or/and additional interactions established with nascent polypeptide.

Additionally, the activity of 5-O-mycaminosyl-tylonolid (OMT), lacking both the C5 mycarose and the C14 mycinose, was evaluated. OMT is known to be a potent antimicrobial with MIC values comparable with Tyl (Fu et al., 2006). However, little or no significant inhibitory effect of OMT on GFP synthesis was detected in our experimental set-up.

To investigate the differential effects of OMT in more detail, our collaborators synthesized a series of peptide-OMT compounds, where BocAlaAlaPhe and fMetLeuPhe peptides are attached to the C14 position. In the TT assay, only fMLF-OMT showed improved potency to inhibit GFP synthesis compared to OMT, although translation was not inhibited by more than 60%, even at a concentration 200-fold higher than the inhibitory concentration (IC_{90}) for Tyl. In contrast, the competition assay showed that OMT and OMT analogs bind to empty ribosomes. The discrepancy between the *in vivo* data, TT assay and binding experiments has led us hypothesis that OMT displays some template specificity. To address this question, the GFP reporter was substituted with firefly luciferase (Fluc). Interestingly, OMT displayed an excellent inhibitor effect of Fluc synthesis, with a potency similar to that observed for the inhibition of GFP by Tyl. The effect was remarkable for the macrolide class of antibiotics, since such differences for tetracycline (Tet) and chloramphenicol (Cam) were not observed.

In summary, for many macrolide derivatives, a lack of correlation between the binding affinities and inhibitory activity was observed. In other words, despite their potency to inhibit protein synthesis, all of the macrolide derivatives tested here were less effective at binding to the ribosome than Tyl. This suggests that the binding affinity does not exclusively determine the effectiveness of the compound and that peptide substituents of the lactone ring may contribute to the inhibitory activity. This might occur due to steric blockage of the

passage of the nascent polypeptide chain or establishment of interactions with the nascent polypeptide. Moreover, the data suggest that the sequence of the nascent chain may influence the inhibitory ability of particular macrolide antibiotics. This finding may lead to design of macrolide antibiotics exclusively inhibiting particular polypeptides.

3.3 Thiopeptides

3.3.1 Paper 5

Starosta, A.L., Qin, H., Mikolajka, A., Leung, G.Y., Schwinghammer, K., Nicolaou, K.C., Chen, D.Y., Cooperman, B.S., and Wilson, D.N. (2009). Identification of distinct thiopeptide-antibiotic precursor lead compounds using translation machinery assays. Chem Biol *16*, 1087-1096.

3.3.2 Paper 6

Mikolajka, A., Liu, H., Chen, Y., **Starosta, A.L.**, Marquez, V., Ivanova, M., Cooperman, B.S., and Wilson, D.N. (2011). Differential effects of thiopeptide and orthosomycin antibiotics on translational GTPases. Chem Biol *18*, 589-600.

Recent advances in thiopeptide total synthesis have identified synthetic fragments that can serve as lead compounds for drug development. In **Paper 5,** a library of precursors of nitrogen heterocycle core of thiopeptides synthesis provided by Professor K. C. Nicolaou was tested. Compounds were divided into four structurally distinct groups (PA-PD), which were tested for their ability to inhibit (i) 70S initiation complex formation (70SIC), monitored via fluorescence of $IF2^{Cy3}$, which increases upon LSU binding to the 30SIC; (ii) the ribosome-dependent GTPase activity of EF-G using Malachite Green assay, and (iii) *in vitro* synthesis of GFP in *E. coli* lysate based TT.

The group of Professor B. Cooperman determined that ThS and nosiheptide (NoS) are potent inhibitors of the 70SIC. However, only one compound from group A – PA1 – showed detectable inhibition of the 70SIC, but at concentrations significantly higher (60- to 400- fold) than for ThS and NoS. It should be noted that the stereochemical derivatives of PA1 showed no inhibitory activity, which emphasizes the specificity of the compound. ThS was a very effective inhibitor of the ribosome-stimulated multiple turnover GTPase activity of EF-G . However, the tested compounds showed significantly lower potency to inhibit the GTPase activity of EF-G, even at the concentrations 50- to 100-times higher than ThS. I tested ThS, NoS and GE2270A in the TT assay. All three compounds displayed high potency to inhibit GFP synthesis, whereas in contrast, none of the tested precursor compounds showed

any significant inhibitory activity, even at concentrations as high as 10-fold of ThS inhibitory concentration (IC_{90}). Surprisingly, addition of 10-fold excess of representative precursor compounds over ThS IC_{90} could reverse the inhibitory effect of ThS. Moreover, different subsets of compounds were able to restore translation inhibited by ThS, NoS or GE2270A. This finding suggests that although the active compounds in the library showed no potency to inhibit translation, they retained the ability to bind to their targets. Additionally, the ability to restore translation in the presence of GAC and EF-Tu inhibitors, suggest they may lead to design of dual inhibitors, targeting ribosomes and ternary complex formation.

Crystallographic data showed that MiC binds in a cleft spanning protein L11 and H43-44, and stabilizes CTD-L7/L12 (Harms et al., 2008). Stimulation of the GTPase activity of EF-G by MiC was suggested to be due to the stabilization of the interaction of L7-CTD with G' domain of EF-G (Harms et al., 2008). In **Paper 6,** the mode of action of MiC was elucidated. A set of translational GTPases, namely, EF-G, IF2, EF4 (LepA), BipA and TetM was tested in (i) the ribosome-dependent GTPase activity assay using the Malachite Green assay, and (ii) translocation reaction stopped flow fluorescence.

Unlike ThS that inhibited ribosome-dependent GTPase of EF-G, MiC stimulated the GTPase activity of EF-G. I confirmed that both ThS and MiC inhibit GFP synthesis in the TT assay. Therefore, the group of Professor B. Cooperman has tested the effect of ThS and MiC on EF-G dependent translocation. Despite the differential effects of MiC and ThS on the GTPase activities of EF-G, it was found that both antibiotics inhibit the translocation reaction, probably by reducing the binding affinity of EF-G to the ribosome. The MiC-dependent activation was investigated in more details. Interestingly, crystallographic data suggest that the G' domain of EF-G and ribosomal protein L7/L12 play a role in GTPase stimulation by MiC. In these study, it was found that G-proteins naturally lacking or having reduced G' domains (IF2, BipA, EF4, and TetM) were inhibited by MiC. Therefore, EF-G lacking G' domain (EF-GΔG'), as well as ribosomes lacking proteins L7/L12 (ΔL7/L12) were tested. MiC inhibited the ribosome-dependent GTPase activity of EF-GΔG'. Moreover the ΔL7/L12-ribosome dependent GTPase activity of EF-G was arrested. Collectively, these results suggest that the interaction between G'-domain of EF-G and CTD-L7/L12 is indeed necessary for Pi release. MiC, by stabilizing CTD-L7/L12, enhances turnover of EF-G.

3.4 Orthosomycins

Evn was observed to inhibit fMet-Puro synthesis in an IF2-dependent manner (Belova et al., 2001). In **Paper 6**, the step at which Evn inhibits protein synthesis was investigated. Evn was tested in (i) the ribosome-dependent GTPase activity of G-proteins using the Malachite Green assay; (ii) 70S initiation complex formation (70SIC); (iii) EF4-dependent back-translocation, and (iv) the translocation reaction using stop-flow fluorescence. Professor B. Cooperman's group demonstrated that Evn inhibits 70SIC formation by preventing the binding of the LSU to 30SIC in an IF2 dependent manner. This is in accordance with the observation that Evn inhibits ribosome-dependent GTPase activity of IF2. Thus, it was concluded that Evn sterically interferes with 30SIC-IF2 binding to the LSU.

Additionally, Evn was also tested for potency to inhibit the translocation step. Yet unlike thiopeptide antibiotics, Evn did not inhibit the EF-G catalyzed translocation reaction. This result is consistent with the observation that Evn did not affect ribosome-dependent GTPase activity of EF-G. In contrast, Evn was found to be a potent inhibitor of ribosome-dependent EF4 (LepA) GTPase activity, as well as EF4-dependent back-translocation reaction. Since EF4 is not essential for *E. coli* viability (Dibb and Wolfe, 1986), IF2-dependent initiation seems to be a major target of Evn action. Moreover, the values for inhibition of 70SIC were comparable with results I obtained for inhibition of GFP synthesis in TT assay. This observation supports the hypothesis that Evn targets predominantly the initiation phase.

3.5 Fusidic acid

3.5.1 Paper 7

Ratje, A.H., Loerke, J., Mikolajka, A., Brunner, M., Hildebrand, P.W., **Starosta, A.L.**, Donhofer, A., Connell, S.R., Fucini, P., Mielke, T., Whitford, P. C., Onuchic, J. N., Yu, Y., Sanbonmatsu, K. Y., Hartmann, R. K., Penczek, P. A., Wilson, D. N., and Spahn, C. M. (2010). Head swivel on the ribosome facilitates translocation by means of intra-subunit tRNA hybrid sites. Nature *468*, 713-716.

Despite the availability of a number of EF-G-ribosome structures, the precise mechanism of tRNA movement through the ribosome remains unclear. In **Paper 7**, Dr. A. Mikolajka, A Dönhöfer and I prepared the complex of EF-G stalled with FA on the *T. thermophilus* 70S in the presence of GDP, which was investigated by the group of Professor C.M. Spahn using cryo-EM. Two separate ribosome populations were observed, which varied in the degree of ratcheting and positioning of the L1 stalk, as well as by the degree of head swivelling of the SSU. Population I showed ~7° ratcheting with respect to the LSU, while at the same time head swivelling of ~5° was observed. On contrast, population II exhibited a 4° ratcheting but strong swiveling of the head by 18°. Examination of these two ribosomal populations revealed that the movement of tRNA with respect to the SSU is coupled with 30S head swivelling and unratcheting of the SSU. Moreover, the P-tRNA on the SSU maintains contact with P-site of the body and simultaneously establishes interaction with the exit site (E site) of the head to form previously unseen intrasubunit pe/E hybrid states.

In both populations, EF-G·GDP stalled with FA on *T. thermophilus* 70S ribosomes showed an open conformation compared to free EF-G·GDP GDP (A et al., 1994; Czworkowski et al., 1994; Laurberg et al., 2000), with domains IV and V moved relative to domains I and II. Domain III was rotated and an additional density, spanning domain I and III into which FA could be modeled, was found. The position of FA was close to the position of the switch I region in the GTP state. This suggests that FA stabilizes the rotated state of domain III, preventing the conformational change of EF-G into the GDP state and thus prevents EF-G recycling from the ribosome.

In summary, using Cryo-EM, it was possible not only to characterise translocation events, but also identify and visualize binding of a small molecule, namely the antibiotic fusidic acid.

3.6 Elongation factor P

3.6.1 Paper 8

Peil L., **Starosta, A.L.**, Virumäe, K, Aktinson, G.C., Tenson, T., Remme, J., Wilson, D.N. (2011). Formation of ε(R)-β-lysyl-hydroxylysine on translation elongation factor EF-P requires YjeK, YjeA and YfcM. *Under revision in Nature Chemical Biology.*

Elongation factor P (EF-P) and its modification are important for growth, drug resistance and virulence in pathogenic bacteria. Curiously, mass spectrometry analyses indicated that lysinylation of K34 of EF-P by YjeA results in a ~128 Da modification, leaving a difference of ~16 Da when compared with the ~144 Da reported for endogenous EF-P (Aoki et al., 2008). In collaboration with the group of Professor J. Remme, the discrepancies between *in vivo* and *in vitro* data were investigated using (i) an *E. coli* lysate-based immuno-precipitation approach, coupled with (ii) high-resolution mass spectrometry (MS) and (iii) SILAC labeling were applied in order to characterize the chemical nature of the *E. coli* EF-P modification and define the modification pathway *in vivo*.

The analyses of endogenous EF-P revealed an increase of the mass of EF-P by 144.2 ± 0.1 Da compared to expected mass of unmodified EF-P. Chymotrypsin digested EF-P showed that peptide containing lysine 34 (K34) had an additional mass of 144.09 Da (F.30VKPGK*GQAF38.A) which was in accordance with digestion of endogenous EF-P with LysC (K.32PGK*GQAFARVK42.L). Fragmentation of both the chymotrypsin and the LysC peptides confirmed K34 as the site of modification. Moreover, it was shown that modification of endogenous EF-P involves attachment of β-lysine to ε-amino group of K34 accounting for 128 Da, and that the additional 16 Da modification is associated with K34 of endogenous EF-P, rather than the added lysine.

In order to demonstrate that YjeA and YjeK were responsible for the modification of K34 of EF-P *in vivo*, endogenous EF-P was immuno-precipitated from *E. coli* AT713 strains lacking the genes for *yjeA* (Δ*yjeA*) or *yjeK* (Δ*yjeK*). Chymotrypsin proteolysis of EF-P from the Δ*yjeA* strain produced a fragment containing K34 (F.30VKPGKGQAF38.A) with no detectable modification. Similarly, an unmodified chymotrypsin fragment was also detected upon proteolysis of EF-P isolated from the Δ*yjeK* strain. Additionally, a peptide with a mass increase of +128.09 Da was found. Quantification of modified/unmodified peptide ratios revealed that the modified form is present at only ~2 % of the level of the unmodified form. These observations indicated that while YjeA can perform the lysinylation of EF-P *in vivo* in

the absence of YjeK (and therefore in the absence of (R)-β-lysine), the reaction appears to be extremely inefficient.

Given the discrepancy of 16 Da between the modification mass of the endogenous EF-P and *in vitro* lysinylated EF-P (+128 Da) (Navarre et al., 2010; Yanagisawa et al., 2010), it was concluded that a third enzyme should exist that is also involved in the modification of K34 of EF-P *in vivo*. I used STRING (Search Tool for the Retrieval of Interacting Genes/Proteins) database (http://string.embl.de) to search for proteins associated with YjeA, YjeK and EF-P. From the output, YfcM, a protein that has no reasonable homology with any protein of known structure or function, was chosen. Chymotrypsin proteolysis of EF-P from the Δ*yfcM* strain produced a fragment containing K34 (F.30VKPGKGQAF38.A) with a mass increase of 128.09 Da. Consistently, the LysC fragment of EF-P containing K34 (K.32PGK*GQAFARVK42.L) isolated from the Δ*yfcM* strain had a mass increased of 128.09 Da. The precision of the mass difference, i.e. 15.995 Da, is indicative of one atom of molecular oxygen, which has a monoisotopic mass of 15.995 Da, thus revealing YfcM as a potential hydroxylase (mono-oxygenase) that modifies K34 of lysinylated EF-P.

In order to determine the site of hydroxylation by YfcM on K34 of EF-P, the differentially deuterated lysine isoform of lysine was used. 4,4,5,5-D4-L-lysine (D4-Lys) has the hydrogen atoms (1.008 Da) of the C4-C5 positions of L-lysine substituted with deuterium (2.014 Da). LysC fragments from the wildtype were 14.993 Da larger, instead of the expected 15.995 Da. This is consistent with 14.988 Da increase expected by the mass loss of a deuterium atom (-2.014 Da) and the addition of a hydroxyl OH group. The 1 Da loss indicates that YfcM hydroxylates either the C4 (γ) or C5 (δ) position.

To screen for potential substrates of YfcM, I applied differential scanning fluorimetry (DSF), which monitors the increase in thermal stability of a protein due to the interaction with a ligand. The largest increases in thermal stability for YfcM were observed with nucleotide-based chemicals, for example, the maximum shift of ~5°C was observed in the presence of <600 μM NADP or CoA.

Dr. G. Atkinson checked genomic distribution and context of the *yfcM* gene. All bacterial species that contain the *yfcM* gene also have *efp*, *yjeA* and, with one exception (*Haemophilus influenzae* strain PittGG), *yjeK*. However, unlike *yjeA* and *yjeK* that often cluster together in the same operon as *efp*, *yfcM* is always located in a distinct region of the chromosome. The six-gene operon structure of the *prmC-aroC-mepA-yfcA-**yfcM**-yfcL* operon is highly conserved within the *Enterobacteriaceae* family.

In summary, the conserved K34 of endogenous *E. coli* EF-P was shown to bear a 144.09 Da modification, which results from two distinct reactions, namely a 128.09 Da lysinylation performed by YjeK and YjeA, followed by an additional 16 Da YfcM-dependent

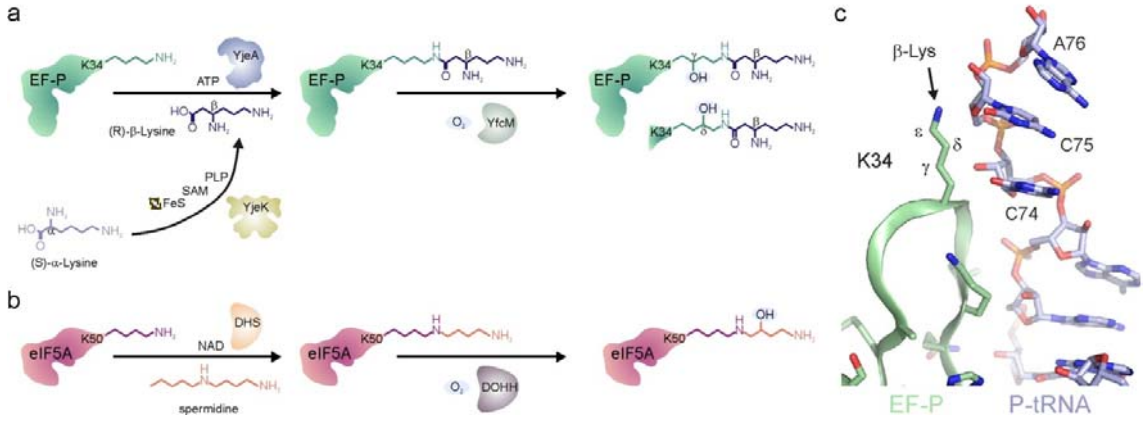

Figure 16. Modification pathway of EF-P and eIF-5A. (**A**) The FeS protein YjeK converts (S)-α-lysine to (R)-β-lysine using S-adenosyl-l-methionine (SAM) and pyridoxal-5′-phosphate (PLP). YjeA uses ATP to lysinylate EF-P by the addition of β-lysine to the ε-amino group of K34. YfcM uses molecular oxygen to hydroxylate the C4 (γ) or C5 (δ) position of K34 of EF-P. (**B**) Deoxyhypusine synthase (DHS) uses NAD to transfer the amino-butyl moiety from spermidine to the ε-amino group of K50 of human eIF5A, which is then hydroxylated by deoxyhypusine hydroxylase (DOHH). (**C**) Relative positions of K34 of EF-P (green) and the acceptor stem of the P-tRNA (blue) when bound on the ribosome. The γ, δ and ε carbon atoms of K34 and the C74, C75 and A76 positions of the tRNA are indicated. The model was built by mutation of Arg to Lys (equivalent to K34 in *E. coli*) in the *T. thermophilus* EFP·70S structure

hydroxylation. The mass spectrometry fragmentation data supports the attachment of the lysine to the ε-amino group of K34. Moreover, the low level of modified peptide observed in the absence of *yjeK*, suggests that the conversion of (S)-α-lysine to (R)-β-lysine by YjeK precedes the lysinylation of EF-P by YjeA.

Future plans

Subsequent experiments for this project will focus on establishing the functional state of EF-P, verification of the state of modification of EF-P bound to the ribosome and investigation of the mechanism of translation regulation by EF-P. Moreover, we will check how this state changes during bacterial life cycle. Initial functional data indicate that deletion strains of *efp* or modification enzymes have growth defects (smaller colonies size) (**Figure 17**). Interestingly, the size of colonies correlates with the state of modification verified by MS. We found that Δ*efp* strain had the most severe phenotype, followed by Δ*yjeA*, which, as seen in MS data, had fully unmodified EF-P. Δ*yjeK* strain (~2% modification of EF-P) showed to be less affected while Δ*yfcM* shows only minor growth effect. Motility tests showed that the lack of EF-P or complete loss of the modification leads to decreased motility (**Figure 17**).

However, Δ*yfcM* was found to swim better than wild type, suggesting that YfcM and hydroxylation may act as a negative regulator of EF-P function.

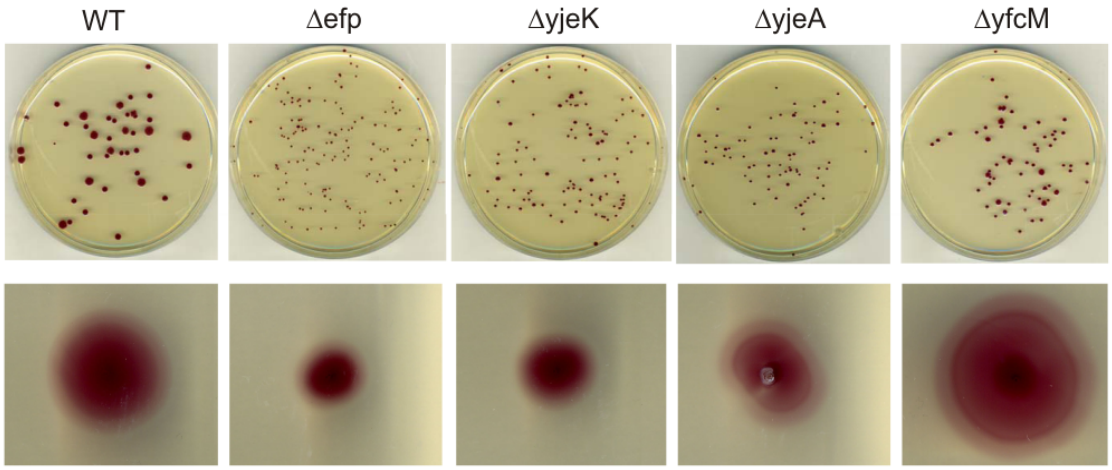

Figure 17. Upper panel – Colonies morphology of *E. coli* wild type strain and deletion strains of *efp*, *yjeK*, *yjeA* and *yfcM* genes. Cells from late logarithmic phase were plated on LB agar plates with 2,3,5-triphenyltetrazolium chloride (TTC) as a color indicator. **Lower panel** – swimming assay of *E. coli* wildtype and deletion strains of *efp*, *yjeK*, *yjeA* and *yfcM*. Cells were grown in meat extract-peptone 0.35% agar plates with TTC as color indicator

.

4 Conclusions

(I) Hygromycin A. (i) Gene disruption of HygA biosynthesis pathway leads to accumulation of intermediates; (ii) the methylene bridge is important for the *in vivo* activity of HygA, probably in terms of uptake; (iii) the C5" oxidation has a negative effect on the translation, possibly alters binding to ribosome; (iv) HygA and intermediates inhibit peptide bond formation; and (v) C2"-phosphorylation leads to loss of inhibitory activity of HygA.

(II) Macrolides. (i) Two molecules of AZI bind cooperatively to the *D. radiodurans* ribosome, while only one binds to *E. coli* ribosomes; (ii) the C6 ethyl aldehyde interaction with A2062 is crucial for binding of Tyl to ribosomes and translation inhibitory activity; (iii) the loss of ethyl aldehyde can be compensated by oligopeptides; (iv) macrolides display polypeptide chain-specific inhibition.

(III) Thiopeptides. (i) Thiopeptide synthesis precursors, despite the loss of potency to inhibit translation, display dual activity to restore translation in the presence of inhibitory concentrations of thiopeptides targeting ribosome or EF-Tu; (ii) the activation by MiC of the ribosome-dependent GTPase activity of EF-G requires the presence of ribosomal proteins L7/L12 as well as the G' domain of EF-G.

(IV) Orthosomycins. (i) Evn sterically interferes with 30SIC-IF2 binding to the LSU; (ii) Evn inhibits of EF4-dependent back-translocation.

(V) Fusidic acid. (i) FA binds in cleft between domain I and III of EF-G and stabilizes the rotated state of domain III and prevents EF-G recycling from the ribosome.

(VI) Elongation factor P. (i) endogenous EF-P is modified with a 144.09 Da modification; (ii) lysinylation of K34 is performed by YjeK and YjeA and is followed by an additional 16 Da hydroxylation by YfcM; (iii) lysine is attached to the ε-amino group of K34; (iv) conversion of (S)-α-lysine to (R)-β-lysine by YjeK precedes the lysinylation of EF-P by YjeA; (v) YfcM displays specificity for nucleotide compounds.

5 References

A, A.E., Brazhnikov, E., Garber, M., Zheltonosova, J., Chirgadze, Y., al-Karadaghi, S., Svensson, L.A., and Liljas, A. (1994). Three-dimensional structure of the ribosomal translocase: elongation factor G from Thermus thermophilus. EMBO J *13*, 3669-3677.

Acker, M.G., Bowers, A.A., and Walsh, C.T. (2009). Generation of thiocillin variants by prepeptide gene replacement and in vivo processing by Bacillus cereus. J Am Chem Soc *131*, 17563-17565.

Agirrezabala, X., Lei, J., Brunelle, J.L., Ortiz-Meoz, R.F., Green, R., and Frank, J. (2008). Visualization of the hybrid state of tRNA binding promoted by spontaneous ratcheting of the ribosome. Mol Cell *32*, 190-197.

Agrawal, R.K., Heagle, A.B., Penczek, P., Grassucci, R.A., and Frank, J. (1999). EF-G-dependent GTP hydrolysis induces translocation accompanied by large conformational changes in the 70S ribosome. Nat Struct Biol *6*, 643-647.

Ali, I.K., Lancaster, L., Feinberg, J., Joseph, S., and Noller, H.F. (2006). Deletion of a conserved, central ribosomal intersubunit RNA bridge. Mol Cell *23*, 865-874.

Alksne, L.E., and Projan, S.J. (2000). Bacterial virulence as a target for antimicrobial chemotherapy. Curr Opin Biotechnol *11*, 625-636.

Allen, G.S., Zavialov, A., Gursky, R., Ehrenberg, M., and Frank, J. (2005). The cryo-EM structure of a translation initiation complex from Escherichia coli. Cell *121*, 703-712.

An, G., Glick, B.R., Friesen, J.D., and Ganoza, M.C. (1980). Identification and quantitation of elongation factor EF-P in Escherichia coli cell-free extracts. Can J Biochem *58*, 1312-1314.

Antoun, A., Pavlov, M.Y., Lovmar, M., and Ehrenberg, M. (2006). How initiation factors maximize the accuracy of tRNA selection in initiation of bacterial protein synthesis. Mol Cell *23*, 183-193.

Aoki, H., Dekany, K., Adams, S.L., and Ganoza, M.C. (1997). The gene encoding the elongation factor P protein is essential for viability and is required for protein synthesis. J Biol Chem *272*, 32254-32259.

Aoki, H., Xu, J., Emili, A., Chosay, J.G., Golshani, A., and Ganoza, M.C. (2008). Interactions of elongation factor EF-P with the Escherichia coli ribosome. FEBS J *275*, 671-681.

Bae, W.K., Lee, Y.K., Cho, M.S., Ma, S.K., Kim, S.W., Kim, N.H., and Choi, K.C. (2006). A case of hemolytic uremic syndrome caused by Escherichia coli O104:H4. Yonsei Med J *47*, 437-439.

Bailly, M., and de Crecy-Lagard, V. (2010). Predicting the pathway involved in post-translational modification of elongation factor P in a subset of bacterial species. Biol Direct *5*, 3.

Bala, A., Kumar, R., and Harjai, K. (2011). Inhibition of quorum sensing in Pseudomonas aeruginosa by azithromycin and its effectiveness in urinary tract infections. J Med Microbiol *60*, 300-306.

Barat, C., Datta, P.P., Raj, V.S., Sharma, M.R., Kaji, H., Kaji, A., and Agrawal, R.K. (2007). Progression of the ribosome recycling factor through the ribosome dissociates the two ribosomal subunits. Mol Cell *27*, 250-261.

Baumann, S., Schoof, S., Bolten, M., Haering, C., Takagi, M., Shin-ya, K., and Arndt, H.D. (2010). Molecular determinants of microbial resistance to thiopeptide antibiotics. J Am Chem Soc *132*, 6973-6981.

Bearson, S.M., Bearson, B.L., Brunelle, B.W., Sharma, V.K., and Lee, I.S. (2011). A mutation in the poxA gene of Salmonella enterica serovar Typhimurium alters protein production, elevates susceptibility to environmental challenges, and decreases swine colonization. Foodborne Pathog Dis *8*, 725-732.

Bearson, S.M., Bearson, B.L., and Rasmussen, M.A. (2006). Identification of Salmonella enterica serovar Typhimurium genes important for survival in the swine gastric environment. Appl Environ Microbiol *72*, 2829-2836.

Belova, L., Tenson, T., Xiong, L., McNicholas, P.M., and Mankin, A.S. (2001). A novel site of antibiotic action in the ribosome: interaction of evernimicin with the large ribosomal subunit. Proc Natl Acad Sci U S A *98*, 3726-3731.

Benson, S., Olsnes, S., Pihl, A., Skorve, J., and Abraham, A.K. (1975). On the mechanism of protein-synthesis inhibition by abrin and ricin. Inhibition of the GTP-hydrolysis site on the 60-S ribosomal subunit. Eur J Biochem *59*, 573-580.

Bhushan, S., Gartmann, M., Halic, M., Armache, J.P., Jarasch, A., Mielke, T., Berninghausen, O., Wilson, D.N., and Beckmann, R. (2010). alpha-Helical nascent polypeptide chains visualized within distinct regions of the ribosomal exit tunnel. Nat Struct Mol Biol *17*, 313-317.

Bielaszewska, M., Mellmann, A., Zhang, W., Kock, R., Fruth, A., Bauwens, A., Peters, G., and Karch, H. (2011). Characterisation of the Escherichia coli strain associated with an outbreak of haemolytic uraemic syndrome in Germany, 2011: a microbiological study. Lancet Infect Dis.

Blaha, G., Stanley, R.E., and Steitz, T.A. (2009). Formation of the first peptide bond: the structure of EF-P bound to the 70S ribosome. Science *325*, 966-970.

Blanchard, S.C., Gonzalez, R.L., Kim, H.D., Chu, S., and Puglisi, J.D. (2004). tRNA selection and kinetic proofreading in translation. Nat Struct Mol Biol *11*, 1008-1014.

Bogdanov, A.A., Sumbatyan, N.V., Shishkina, A.V., Karpenko, V.V., and Korshunova, G.A. (2010). Ribosomal tunnel and translation regulation. Biochemistry (Mosc) *75*, 1501-1516.

Bowers, A.A., Acker, M.G., Koglin, A., and Walsh, C.T. (2010). Manipulation of thiocillin variants by prepeptide gene replacement: structure, conformation, and activity of heterocycle substitution mutants. J Am Chem Soc *132*, 7519-7527.

Brandi, L., Marzi, S., Fabbretti, A., Fleischer, C., Hill, W.E., Gualerzi, C.O., and Stephen Lodmell, J. (2004). The translation initiation functions of IF2: targets for thiostrepton inhibition. J Mol Biol *335*, 881-894.

Brockmann, H., and Henkel, W. (1950). Pikromycin, ein neues Antibioticum aus Actinomyceten. Naturwissensch *37*, 138-139.

Brunelle, J.L., Shaw, J.J., Youngman, E.M., and Green, R. (2008). Peptide release on the ribosome depends critically on the 2' OH of the peptidyl-tRNA substrate. RNA *14*, 1526-1531.

Bugg, T.D., and Walsh, C.T. (1992). Intracellular steps of bacterial cell wall peptidoglycan biosynthesis: enzymology, antibiotics, and antibiotic resistance. Nat Prod Rep *9*, 199-215.

Bulkley, D., Innis, C.A., Blaha, G., and Steitz, T.A. (2010). Revisiting the structures of several antibiotics bound to the bacterial ribosome. Proc Natl Acad Sci U S A *107*, 17158-17163.

Butler, D. (2010). Cholera tightens grip on Haiti. Nature *468*, 483-484.

Bycroft, B.W., and Gowland, M.S. (1878). The structures of the highly modified peptide antibiotics micrococcin P1 and P2. J Chem Soc, Chem Commun, 256-258.

Cameron, D.M., Thompson, J., Gregory, S.T., March, P.E., and Dahlberg, A.E. (2004). Thiostrepton-resistant mutants of Thermus thermophilus. Nucleic Acids Res *32*, 3220-3227.

Cameron, D.M., Thompson, J., March, P.E., and Dahlberg, A.E. (2002). Initiation factor IF2, thiostrepton and micrococcin prevent the binding of elongation factor G to the Escherichia coli ribosome. J Mol Biol *319*, 27-35.

Campbell, E.A., Korzheva, N., Mustaev, A., Murakami, K., Nair, S., Goldfarb, A., and Darst, S.A. (2001). Structural mechanism for rifampicin inhibition of bacterial rna polymerase. Cell *104*, 901-912.

Carter, A.P., Clemons, W.M., Jr., Brodersen, D.E., Morgan-Warren, R.J., Hartsch, T., Wimberly, B.T., and Ramakrishnan, V. (2001). Crystal structure of an initiation factor bound to the 30S ribosomal subunit. Science *291*, 498-501.

Cascales, E., and Christie, P.J. (2003). The versatile bacterial type IV secretion systems. Nat Rev Microbiol *1*, 137-149.

Caskey, C.T., Tompkins, R., Scolnick, E., Caryk, T., and Nirenberg, M. (1968). Sequential translation of trinucleotide codons for the initiation and termination of protein synthesis. Science *162*, 135-138.

CDC (2010). Cholera outbreak --- Haiti, October 2010. MMWR Morb Mortal Wkly Rep *59*, 1411.

Chen, C.R., Malik, M., Snyder, M., and Drlica, K. (1996). DNA gyrase and topoisomerase IV on the bacterial chromosome: quinolone-induced DNA cleavage. J Mol Biol *258*, 627-637.

Chittum, H.S., and Champney, W.S. (1994). Ribosomal protein gene sequence changes in erythromycin-resistant mutants of Escherichia coli. J Bacteriol *176*, 6192-6198.

Choi, S., and Choe, J. (2011). Crystal structure of elongation factor P from Pseudomonas aeruginosa at 1.75 A resolution. Proteins *79*, 1688-1693.

Clatworthy, A.E., Pierson, E., and Hung, D.T. (2007). Targeting virulence: a new paradigm for antimicrobial therapy. Nat Chem Biol *3*, 541-548.

Clementi, N., Chirkova, A., Puffer, B., Micura, R., and Polacek, N. (2010). Atomic mutagenesis reveals A2660 of 23S ribosomal RNA as key to EF-G GTPase activation. Nat Chem Biol *6*, 344-351.

Cocito, C., and Chinali, G. (1985). Molecular mechanism of action of virginiamycin-like antibiotics (synergimycins) on protein synthesis in bacterial cell-free systems. J Antimicrob Chemother *16 Suppl A*, 35-52.

Connell, S.R., Takemoto, C., Wilson, D.N., Wang, H., Murayama, K., Terada, T., Shirouzu, M., Rost, M., Schuler, M., Giesebrecht, J.*, et al.* (2007). Structural basis for interaction of the ribosome with the switch regions of GTP-bound elongation factors. Mol Cell *25*, 751-764.

Cornelis, G.R. (2010). The type III secretion injectisome, a complex nanomachine for intracellular 'toxin' delivery. Biol Chem *391*, 745-751.

Cundliffe, E., and Thompson, J. (1981). Concerning the mode of action of micrococcin upon bacterial protein synthesis. Eur J Biochem *118*, 47-52.

Czworkowski, J., Wang, J., Steitz, T.A., and Moore, P.B. (1994). The crystal structure of elongation factor G complexed with GDP, at 2.7 A resolution. EMBO J *13*, 3661-3668.

D'Costa, V.M., King, C.E., Kalan, L., Morar, M., Sung, W.W., Schwarz, C., Froese, D., Zazula, G., Calmels, F., Debruyne, R.*, et al.* (2011). Antibiotic resistance is ancient. Nature *477*, 457-461.

Dahlquist, K.D., and Puglisi, J.D. (2000). Interaction of translation initiation factor IF1 with the E. coli ribosomal A site. J Mol Biol *299*, 1-15.

Datta, P.P., Sharma, M.R., Qi, L., Frank, J., and Agrawal, R.K. (2005). Interaction of the G' domain of elongation factor G and the C-terminal domain of ribosomal protein L7/L12 during translocation as revealed by cryo-EM. Mol Cell *20*, 723-731.

Davies, D.G., Parsek, M.R., Pearson, J.P., Iglewski, B.H., Costerton, J.W., and Greenberg, E.P. (1998). The involvement of cell-to-cell signals in the development of a bacterial biofilm. Science *280*, 295-298.

Daviter, T., Wieden, H.J., and Rodnina, M.V. (2003). Essential role of histidine 84 in elongation factor Tu for the chemical step of GTP hydrolysis on the ribosome. J Mol Biol *332*, 689-699.

Demeshkina, N., Jenner, L., Yusupova, G., and Yusupov, M. (2010). Interactions of the ribosome with mRNA and tRNA. Curr Opin Struct Biol *20*, 325-332.

DGI (2011). EHEC infection and antibiotic therapy. Deutsche Gesellschaft für Infectiologie eV.

Dhote, V., Gupta, S., and Reynolds, K.A. (2008). An O-phosphotransferase catalyzes phosphorylation of hygromycin A in the antibiotic-producing organism Streptomyces hygroscopicus. Antimicrob Agents Chemother *52*, 3580-3588.

Dhote, V., Starosta, A.L., Wilson, D.N., and Reynolds, K.A. (2009). The final step of hygromycin A biosynthesis, oxidation of C-5"-dihydrohygromycin A, is linked to a putative proton gradient-dependent efflux. Antimicrob Agents Chemother *53*, 5163-5172.

Dibb, N.J., and Wolfe, P.B. (1986). lep operon proximal gene is not required for growth or secretion by Escherichia coli. J Bacteriol *166*, 83-87.

Dinos, G., Wilson, D.N., Teraoka, Y., Szaflarski, W., Fucini, P., Kalpaxis, D., and Nierhaus, K.H. (2004). Dissecting the ribosomal inhibition mechanisms of edeine and pactamycin: the universally conserved residues G693 and C795 regulate P-site RNA binding. Mol Cell *13*, 113-124.

Donovick, R., Pagano, J.F., Stout, H.A., and Weinstein, M.J. (1955). Thiostrepton, a new antibiotic. I. In vitro studies. Antibiot Annu *3*, 554-559.

Douthwaite, S., Garrett, R.A., and Wagner, R. (1983). Comparison of Escherichia coli tRNAPhe in the free state, in the ternary complex and in the ribosomal A and P sites by chemical probing. Eur J Biochem *131*, 261-269.

Drlica, K., Malik, M., Kerns, R.J., and Zhao, X. (2008). Quinolone-mediated bacterial death. Antimicrob Agents Chemother *52*, 385-392.

Drlica, K., and Zhao, X. (1997). DNA gyrase, topoisomerase IV, and the 4-quinolones. Microbiol Mol Biol Rev *61*, 377-392.

DrugDiscovery Drug Discovery and Development.
http://wwwphrmaorg/sites/default/files/159/rd_brochure_022307pdf

Dunkle, J.A., Wang, L., Feldman, M.B., Pulk, A., Chen, V.B., Kapral, G.J., Noeske, J., Richardson, J.S., Blanchard, S.C., and Cate, J.H. (2011). Structures of the bacterial ribosome in classical and hybrid states of tRNA binding. Science *332*, 981-984.

Dunkle, J.A., Xiong, L., Mankin, A.S., and Cate, J.H. (2010). Structures of the Escherichia coli ribosome with antibiotics bound near the peptidyl transferase center explain spectra of drug action. Proc Natl Acad Sci U S A *107*, 17152-17157.

ECDC (2010). Annual epidemiological report on communicable diseases in Europe. European Centre for Disease Prevention and Control, Surveillance report.

ECDC (2011). Shiga toxin-producing E. coli (STEC): Update on outbreak in the EU (27 July 2011, 11:00).

Endo, Y., Mitsui, K., Motizuki, M., and Tsurugi, K. (1987). The mechanism of action of ricin and related toxic lectins on eukaryotic ribosomes. The site and the characteristics of the modification in 28 S ribosomal RNA caused by the toxins. J Biol Chem *262*, 5908-5912.

Endo, Y., and Wool, I.G. (1982). The site of action of alpha-sarcin on eukaryotic ribosomes. The sequence at the alpha-sarcin cleavage site in 28 S ribosomal ribonucleic acid. J Biol Chem *257*, 9054-9060.

Feldman, M.B., Terry, D.S., Altman, R.B., and Blanchard, S.C. (2010). Aminoglycoside activity observed on single pre-translocation ribosome complexes. Nat Chem Biol *6*, 54-62.

Finlay, B.B., and Cossart, P. (1997). Exploitation of mammalian host cell functions by bacterial pathogens. Science *276*, 718-725.

Fischbach, M.A., and Walsh, C.T. (2009). Antibiotics for emerging pathogens. Science *325*, 1089-1093.

Flatt, P.M., and Mahmud, T. (2007). Biosynthesis of aminocyclitol-aminoglycoside antibiotics and related compounds. Nat Prod Rep *24*, 358-392.

Fleming, A. (1929). On the antibacterial action of cultures of a penicillium, with special reference to their use in the isolation of B. influenzae. Br J Exp Pathol *10*, 226–236.

Floss, H.G., and Yu, T.W. (2005). Rifamycin-mode of action, resistance, and biosynthesis. Chem Rev *105*, 621-632.

Fredrick, K., and Noller, H.F. (2003). Catalysis of ribosomal translocation by sparsomycin. Science *300*, 1159-1162.

Freistroffer, D.V., Pavlov, M.Y., MacDougall, J., Buckingham, R.H., and Ehrenberg, M. (1997). Release factor RF3 in E.coli accelerates the dissociation of release factors RF1 and RF2 from the ribosome in a GTP-dependent manner. EMBO J *16*, 4126-4133.

Frolova, L.Y., Tsivkovskii, R.Y., Sivolobova, G.F., Oparina, N.Y., Serpinsky, O.I., Blinov, V.M., Tatkov, S.I., and Kisselev, L.L. (1999). Mutations in the highly conserved GGQ motif of class 1 polypeptide release factors abolish ability of human eRF1 to trigger peptidyl-tRNA hydrolysis. RNA *5*, 1014-1020.

Fu, H., Marquez, S., Gu, X., Katz, L., and Myles, D.C. (2006). Synthesis and in vitro antibiotic activity of 16-membered 9-O-arylalkyloxime macrolides. Bioorg Med Chem Lett *16*, 1259-1266.

Ganoza, M.C., and Aoki, H. (2000). Peptide bond synthesis: function of the efp gene product. Biol Chem *381*, 553-559.

Gao, H., Zhou, Z., Rawat, U., Huang, C., Bouakaz, L., Wang, C., Cheng, Z., Liu, Y., Zavialov, A., Gursky, R.*, et al.* (2007). RF3 induces ribosomal conformational changes responsible for dissociation of class I release factors. Cell *129*, 929-941.

Gao, Y.G., Selmer, M., Dunham, C.M., Weixlbaumer, A., Kelley, A.C., and Ramakrishnan, V. (2009). The structure of the ribosome with elongation factor G trapped in the posttranslocational state. Science *326*, 694-699.

Gessner, S.L., and Irvin, J.D. (1980). Inhibition of elongation factor 2-dependent translocation by the pokeweed antiviral protein and ricin. J Biol Chem *255*, 3251-3253.

Glick, B.R., Chladek, S., and Ganoza, M.C. (1979). Peptide bond formation stimulated by protein synthesis factor EF-P depends on the aminoacyl moiety of the acceptor. Eur J Biochem *97*, 23-28.

Glick, B.R., and Ganoza, M.C. (1975). Identification of a soluble protein that stimulates peptide bond synthesis. Proc Natl Acad Sci U S A *72*, 4257-4260.

Godtfredsen, W.O., Jahnsen, S., Lorck, H., Roholt, K., and Tybring, L. (1962). Fusidic acid: a new antibiotic. Nature *193*, 987.

Godtfredsen, W.O., and Vangedal, S. (1962). The structure of fusidic acid. Tetrahedron *18*, 1029-1048.

Gonzalez, R.L., Jr., Chu, S., and Puglisi, J.D. (2007). Thiostrepton inhibition of tRNA delivery to the ribosome. RNA *13*, 2091-2097.

Green, R., and Lorsch, J.R. (2002). The path to perdition is paved with protons. Cell *110*, 665-668.

Gregory, S.T., and Dahlberg, A.E. (1999). Erythromycin resistance mutations in ribosomal proteins L22 and L4 perturb the higher order structure of 23 S ribosomal RNA. J Mol Biol *289*, 827-834.

Gromadski, K.B., and Rodnina, M.V. (2004). Streptomycin interferes with conformational coupling between codon recognition and GTPase activation on the ribosome. Nat Struct Mol Biol *11*, 316-322.

Gryczan, T.J., Grandi, G., Hahn, J., Grandi, R., and Dubnau, D. (1980). Conformational alteration of mRNA structure and the posttranscriptional regulation of erythromycin-induced drug resistance. Nucleic Acids Res *8*, 6081-6097.

Guerrero, M.D., and Modolell, J. (1980). Hygromycin A, a novel inhibitor of ribosomal peptidyltransferase. Eur J Biochem *107*, 409-414.

Habib el, S.E., Scarsdale, J.N., and Reynolds, K.A. (2003). Biosynthetic origin of hygromycin A. Antimicrob Agents Chemother *47*, 2065-2071.

Hanawa-Suetsugu, K., Sekine, S., Sakai, H., Hori-Takemoto, C., Terada, T., Unzai, S., Tame, J.R., Kuramitsu, S., Shirouzu, M., and Yokoyama, S. (2004). Crystal structure of

elongation factor P from Thermus thermophilus HB8. Proc Natl Acad Sci U S A *101*, 9595-9600.

Hansen, J.L., Ippolito, J.A., Ban, N., Nissen, P., Moore, P.B., and Steitz, T.A. (2002a). The structures of four macrolide antibiotics bound to the large ribosomal subunit. Mol Cell *10*, 117-128.

Hansen, J.L., Moore, P.B., and Steitz, T.A. (2003). Structures of five antibiotics bound at the peptidyl transferase center of the large ribosomal subunit. J Mol Biol *330*, 1061-1075.

Hansen, J.L., Schmeing, T.M., Moore, P.B., and Steitz, T.A. (2002b). Structural insights into peptide bond formation. Proc Natl Acad Sci U S A *99*, 11670-11675.

Harms, J.M., Schlunzen, F., Fucini, P., Bartels, H., and Yonath, A. (2004). Alterations at the peptidyl transferase centre of the ribosome induced by the synergistic action of the streptogramins dalfopristin and quinupristin. BMC Biol *2*, 4.

Harms, J.M., Wilson, D.N., Schluenzen, F., Connell, S.R., Stachelhaus, T., Zaborowska, Z., Spahn, C.M., and Fucini, P. (2008). Translational regulation via L11: molecular switches on the ribosome turned on and off by thiostrepton and micrococcin. Mol Cell *30*, 26-38.

Hartz, D., Binkley, J., Hollingsworth, T., and Gold, L. (1990). Domains of initiator tRNA and initiation codon crucial for initiator tRNA selection by Escherichia coli IF3. Genes Dev *4*, 1790-1800.

Hartz, D., McPheeters, D.S., and Gold, L. (1989). Selection of the initiator tRNA by Escherichia coli initiation factors. Genes Dev *3*, 1899-1912.

Hayashi, S.F., Norcia, L.J., Seibel, S.B., and Silvia, A.M. (1997). Structure-activity relationships of hygromycin A and its analogs: protein synthesis inhibition activity in a cell free system. J Antibiot (Tokyo) *50*, 514-521.

Henrichsen, J. (1972). Bacterial surface translocation: a survey and a classification. Bacteriol Rev *36*, 478-503.

Hiller, D.A., Singh, V., Zhong, M., and Strobel, S.A. (2011). A two-step chemical mechanism for ribosome-catalysed peptide bond formation. Nature *476*, 236-239.

Hodgin, L.A., and Hogenauer, G. (1974). The mode of action of pleuromutilin derivatives. Effect on cell-free polypeptide synthesis. Eur J Biochem *47*, 527-533.

Horinouchi, S., and Weisblum, B. (1980). Posttranscriptional modification of mRNA conformation: mechanism that regulates erythromycin-induced resistance. Proc Natl Acad Sci U S A *77*, 7079-7083.

Hosted, T.J., Wang, T.X., Alexander, D.C., and Horan, A.C. (2001). Characterization of the biosynthetic gene cluster for the oligosaccharide antibiotic, Evernimicin, in Micromonospora carbonacea var. africana ATCC39149. J Ind Microbiol Biotechnol *27*, 386-392.

Iannino, F., Ugalde, J.E., and Inon de Iannino, N. (2011). Brucella abortus efp gene is required for an efficient internalization in HeLa cells. Microb Pathog.

Inoue, T., Shingaki, R., Hirose, S., Waki, K., Mori, H., and Fukui, K. (2007). Genome-wide screening of genes required for swarming motility in Escherichia coli K-12. J Bacteriol *189*, 950-957.

Irvin, J.D., and Julian, G.R. (1970). The distribution of 14C-proline peptides synthesized in vitro directed by polycytidylic acid; the effect of chloramphenicol. FEBS Lett *8*, 129-132.

Ito, K., Fujiwara, T., Toyoda, T., and Nakamura, Y. (2002). Elongation factor G participates in ribosome disassembly by interacting with ribosome recycling factor at their tRNA-mimicry domains. Mol Cell *9*, 1263-1272.

Jayaraman, A., and Wood, T.K. (2008). Bacterial quorum sensing: signals, circuits, and implications for biofilms and disease. Annu Rev Biomed Eng *10*, 145-167.

Jaynes, B.H., Elliott, N.C., and Schicho, D.L. (1992). Semisynthetic hygromycin A analogs: synthesis and anti-bacterial activity of derivatives lacking the furanose moiety. J Antibiot (Tokyo) *45*, 1705-1707.

Jenner, L., Demeshkina, N., Yusupova, G., and Yusupov, M. (2010a). Structural rearrangements of the ribosome at the tRNA proofreading step. Nat Struct Mol Biol *17*, 1072-1078.

Jenner, L.B., Demeshkina, N., Yusupova, G., and Yusupov, M. (2010b). Structural aspects of messenger RNA reading frame maintenance by the ribosome. Nat Struct Mol Biol *17*, 555-560.

Jin, H., Kelley, A.C., Loakes, D., and Ramakrishnan, V. (2010). Structure of the 70S ribosome bound to release factor 2 and a substrate analog provides insights into catalysis of peptide release. Proc Natl Acad Sci U S A *107*, 8593-8598.

Jin, H., Kelley, A.C., and Ramakrishnan, V. (2011). Crystal structure of the hybrid state of ribosome in complex with the guanosine triphosphatase release factor 3. Proc Natl Acad Sci U S A.

Julian, P., Milon, P., Agirrezabala, X., Lasso, G., Gil, D., Rodnina, M.V., and Valle, M. (2011). The Cryo-EM structure of a complete 30S translation initiation complex from Escherichia coli. PLoS Biol *9*, e1001095.

Jung, D., Rozek, A., Okon, M., and Hancock, R.E. (2004). Structural transitions as determinants of the action of the calcium-dependent antibiotic daptomycin. Chem Biol *11*, 949-957.

Kaberdina, A.C., Szaflarski, W., Nierhaus, K.H., and Moll, I. (2009). An unexpected type of ribosomes induced by kasugamycin: a look into ancestral times of protein synthesis? Mol Cell *33*, 227-236.

Kahan, F.M., Kahan, J.S., Cassidy, P.J., and Kropp, H. (1974). The mechanism of action of fosfomycin (phosphonomycin). Ann N Y Acad Sci *235*, 364-386.

Kahne, D., Leimkuhler, C., Lu, W., and Walsh, C. (2005). Glycopeptide and lipoglycopeptide antibiotics. Chem Rev *105*, 425-448.

Kallia-Raftopoulos, S., Kalpaxis, D.L., and Coutsogeorgopoulos, C. (1994). New aspects of the kinetics of inhibition by lincomycin of peptide bond formation. Mol Pharmacol *46*, 1009-1014.

Kaminishi, T., Wilson, D.N., Takemoto, C., Harms, J.M., Kawazoe, M., Schluenzen, F., Hanawa-Suetsugu, K., Shirouzu, M., Fucini, P., and Yokoyama, S. (2007). A snapshot of the 30S ribosomal subunit capturing mRNA via the Shine-Dalgarno interaction. Structure *15*, 289-297.

Kaniga, K., Compton, M.S., Curtiss, R., 3rd, and Sundaram, P. (1998). Molecular and functional characterization of Salmonella enterica serovar typhimurium poxA gene: effect on attenuation of virulence and protection. Infect Immun *66*, 5599-5606.

Karimi, R., Pavlov, M.Y., Buckingham, R.H., and Ehrenberg, M. (1999). Novel roles for classical factors at the interface between translation termination and initiation. Mol Cell *3*, 601-609.

Kearns, D.B. (2010). A field guide to bacterial swarming motility. Nat Rev Microbiol *8*, 634-644.

Kearns, D.B., Chu, F., Rudner, R., and Losick, R. (2004). Genes governing swarming in Bacillus subtilis and evidence for a phase variation mechanism controlling surface motility. Mol Microbiol *52*, 357-369.

Kim, K.K., Hung, L.W., Yokota, H., Kim, R., and Kim, S.H. (1998). Crystal structures of eukaryotic translation initiation factor 5A from Methanococcus jannaschii at 1.8 A resolution. Proc Natl Acad Sci U S A *95*, 10419-10424.

Klaholz, B.P., Pape, T., Zavialov, A.V., Myasnikov, A.G., Orlova, E.V., Vestergaard, B., Ehrenberg, M., and van Heel, M. (2003). Structure of the Escherichia coli ribosomal termination complex with release factor 2. Nature *421*, 90-94.

Kofoed, C.B., and Vester, B. (2002). Interaction of avilamycin with ribosomes and resistance caused by mutations in 23S rRNA. Antimicrob Agents Chemother *46*, 3339-3342.

Kohanski, M.A., DePristo, M.A., and Collins, J.J. (2010a). Sublethal antibiotic treatment leads to multidrug resistance via radical-induced mutagenesis. Mol Cell *37*, 311-320.

Kohanski, M.A., Dwyer, D.J., and Collins, J.J. (2010b). How antibiotics kill bacteria: from targets to networks. Nat Rev Microbiol *8*, 423-435.

Kohanski, M.A., Dwyer, D.J., Hayete, B., Lawrence, C.A., and Collins, J.J. (2007). A common mechanism of cellular death induced by bactericidal antibiotics. Cell *130*, 797-810.

Kohanski, M.A., Dwyer, D.J., Wierzbowski, J., Cottarel, G., and Collins, J.J. (2008). Mistranslation of membrane proteins and two-component system activation trigger antibiotic-mediated cell death. Cell *135*, 679-690.

Koronakis, V., Eswaran, J., and Hughes, C. (2004). Structure and function of TolC: the bacterial exit duct for proteins and drugs. Annu Rev Biochem *73*, 467-489.

Korostelev, A., Asahara, H., Lancaster, L., Laurberg, M., Hirschi, A., Zhu, J., Trakhanov, S., Scott, W.G., and Noller, H.F. (2008). Crystal structure of a translation termination complex formed with release factor RF2. Proc Natl Acad Sci U S A *105*, 19684-19689.

Korostelev, A., Zhu, J., Asahara, H., and Noller, H.F. (2010). Recognition of the amber UAG stop codon by release factor RF1. EMBO J *29*, 2577-2585.

Kuhlenkoetter, S., Wintermeyer, W., and Rodnina, M.V. (2011). Different substrate-dependent transition states in the active site of the ribosome. Nature *476*, 351-354.

Kumarasamy, K.K., Toleman, M.A., Walsh, T.R., Bagaria, J., Butt, F., Balakrishnan, R., Chaudhary, U., Doumith, M., Giske, C.G., Irfan, S.*, et al.* (2010). Emergence of a new antibiotic resistance mechanism in India, Pakistan, and the UK: a molecular, biological, and epidemiological study. Lancet Infect Dis *10*, 597-602.

La Teana, A., Gualerzi, C.O., and Dahlberg, A.E. (2001). Initiation factor IF 2 binds to the alpha-sarcin loop and helix 89 of Escherichia coli 23S ribosomal RNA. RNA *7*, 1173-1179.

Lai, C.J., and Weisblum, B. (1971). Altered methylation of ribosomal RNA in an erythromycin-resistant strain of Staphylococcus aureus. Proc Natl Acad Sci U S A *68*, 856-860.

Landman, D., Georgescu, C., Martin, D.A., and Quale, J. (2008). Polymyxins revisited. Clin Microbiol Rev *21*, 449-465.

Lang, K., Erlacher, M., Wilson, D.N., Micura, R., and Polacek, N. (2008). The role of 23S ribosomal RNA residue A2451 in peptide bond synthesis revealed by atomic mutagenesis. Chem Biol *15*, 485-492.

Laurberg, M., Asahara, H., Korostelev, A., Zhu, J., Trakhanov, S., and Noller, H.F. (2008). Structural basis for translation termination on the 70S ribosome. Nature *454*, 852-857.

Laurberg, M., Kristensen, O., Martemyanov, K., Gudkov, A.T., Nagaev, I., Hughes, D., and Liljas, A. (2000). Structure of a mutant EF-G reveals domain III and possibly the fusidic acid binding site. J Mol Biol *303*, 593-603.

Lawrence, J.R., Korber, D.R., Hoyle, B.D., Costerton, J.W., and Caldwell, D.E. (1991). Optical sectioning of microbial biofilms. J Bacteriol *173*, 6558-6567.

Leach, K.L., Swaney, S.M., Colca, J.R., McDonald, W.G., Blinn, J.R., Thomasco, L.M., Gadwood, R.C., Shinabarger, D., Xiong, L., and Mankin, A.S. (2007). The site of action of oxazolidinone antibiotics in living bacteria and in human mitochondria. Mol Cell *26*, 393-402.

Lefranc, D., and Ciufolini, M.A. (2009). Total synthesis and stereochemical assignment of micrococcin P1. Angew Chem Int Ed Engl *48*, 4198-4201.

Li, B.B., Wu, C.M., Wang, Y., and Shen, J.Z. (2011). Single and dual mutations at positions 2058, 2503 and 2504 of 23S rRNA and their relationship to resistance to antibiotics that target the large ribosomal subunit. J Antimicrob Chemother *66*, 1983-1986.

Li, W., Sengupta, J., Rath, B.K., and Frank, J. (2006). Functional conformations of the L11-ribosomal RNA complex revealed by correlative analysis of cryo-EM and molecular dynamics simulations. RNA *12*, 1240-1253.

Long, K.S., Poehlsgaard, J., Kehrenberg, C., Schwarz, S., and Vester, B. (2006). The Cfr rRNA methyltransferase confers resistance to Phenicols, Lincosamides,

Oxazolidinones, Pleuromutilins, and Streptogramin A antibiotics. Antimicrob Agents Chemother *50*, 2500-2505.

Lovett, P.S., and Rogers, E.J. (1996). Ribosome regulation by the nascent peptide. Microbiol Rev *60*, 366-385.

Lovmar, M., Nilsson, K., Vimberg, V., Tenson, T., Nervall, M., and Ehrenberg, M. (2006). The molecular mechanism of peptide-mediated erythromycin resistance. J Biol Chem *281*, 6742-6750.

Lu, J., and Deutsch, C. (2008). Electrostatics in the ribosomal tunnel modulate chain elongation rates. J Mol Biol *384*, 73-86.

Luppens, S.B., Reij, M.W., van der Heijden, R.W., Rombouts, F.M., and Abee, T. (2002). Development of a standard test to assess the resistance of Staphylococcus aureus biofilm cells to disinfectants. Appl Environ Microbiol *68*, 4194-4200.

Ly, C.T., Altuntop, M.E., and Wang, Y. (2010). Single-molecule study of viomycin's inhibition mechanism on ribosome translocation. Biochemistry *49*, 9732-9738.

Mankin, A.S. (2008). Macrolide myths. Curr Opin Microbiol *11*, 414-421.

Mann, P.A., Xiong, L., Mankin, A.S., Chau, A.S., Mendrick, C.A., Najarian, D.J., Cramer, C.A., Loebenberg, D., Coates, E., Murgolo, N.J.*, et al.* (2001). EmtA, a rRNA methyltransferase conferring high-level evernimicin resistance. Mol Microbiol *41*, 1349-1356.

Marshall, R.A., Aitken, C.E., and Puglisi, J.D. (2009). GTP hydrolysis by IF2 guides progression of the ribosome into elongation. Mol Cell *35*, 37-47.

Mattick, J.S. (2002). Type IV pili and twitching motility. Annu Rev Microbiol *56*, 289-314.

McGuire, J.M., Bunch, R.L., Anderson, R.C., Boaz, H.E., Flynn, E.H., Powell, H.M., and Smith, J.W. (1952). Ilotycin, a new antibiotic. Antibiot Chemother *2*, 281-283.

McNicholas, P.M., Mann, P.A., Najarian, D.J., Miesel, L., Hare, R.S., and Black, T.A. (2001). Effects of mutations in ribosomal protein L16 on susceptibility and accumulation of evernimicin. Antimicrob Agents Chemother *45*, 79-83.

McNicholas, P.M., Najarian, D.J., Mann, P.A., Hesk, D., Hare, R.S., Shaw, K.J., and Black, T.A. (2000). Evernimicin binds exclusively to the 50S ribosomal subunit and inhibits translation in cell-free systems derived from both gram-positive and gram-negative bacteria. Antimicrob Agents Chemother *44*, 1121-1126.

Merrell, D.S., Hava, D.L., and Camilli, A. (2002). Identification of novel factors involved in colonization and acid tolerance of Vibrio cholerae. Mol Microbiol *43*, 1471-1491.

Mikolajka, A., Liu, H., Chen, Y., Starosta, A.L., Marquez, V., Ivanova, M., Cooperman, B.S., and Wilson, D.N. (2011). Differential effects of thiopeptide and orthosomycin antibiotics on translational GTPases. Chem Biol *18*, 589-600.

Moazed, D., and Noller, H.F. (1990). Binding of tRNA to the ribosomal A and P sites protects two distinct sets of nucleotides in 16 S rRNA. J Mol Biol *211*, 135-145.

Moazed, D., and Noller, H.F. (1991). Sites of interaction of the CCA end of peptidyl-tRNA with 23S rRNA. Proc Natl Acad Sci U S A *88*, 3725-3728.

Moazed, D., Robertson, J.M., and Noller, H.F. (1988). Interaction of elongation factors EF-G and EF-Tu with a conserved loop in 23S RNA. Nature *334*, 362-364.

Moll, I., and Blasi, U. (2002). Differential inhibition of 30S and 70S translation initiation complexes on leaderless mRNA by kasugamycin. Biochem Biophys Res Commun *297*, 1021-1026.

Mosbacher, T.G., Bechthold, A., and Schulz, G.E. (2005). Structure and function of the antibiotic resistance-mediating methyltransferase AviRb from Streptomyces viridochromogenes. J Mol Biol *345*, 535-545.

Muller, H.M., Delgado, O., and Bach, T. (2007). Total synthesis of the thiazolyl peptide GE2270 A. Angew Chem Int Ed Engl *46*, 4771-4774.

Munro, J.B., Altman, R.B., O'Connor, N., and Blanchard, S.C. (2007). Identification of two distinct hybrid state intermediates on the ribosome. Mol Cell *25*, 505-517.

Munro, J.B., Altman, R.B., Tung, C.S., Sanbonmatsu, K.Y., and Blanchard, S.C. (2010a). A fast dynamic mode of the EF-G-bound ribosome. EMBO J *29*, 770-781.

Munro, J.B., Wasserman, M.R., Altman, R.B., Wang, L., and Blanchard, S.C. (2010b). Correlated conformational events in EF-G and the ribosome regulate translocation. Nat Struct Mol Biol *17*, 1470-1477.

Myasnikov, A.G., Marzi, S., Simonetti, A., Giuliodori, A.M., Gualerzi, C.O., Yusupova, G., Yusupov, M., and Klaholz, B.P. (2005). Conformational transition of initiation factor 2 from the GTP- to GDP-bound state visualized on the ribosome. Nat Struct Mol Biol *12*, 1145-1149.

Nakashio, S., Iwasawa, H., Dun, F.Y., Kanemitsu, K., and Shimada, J. (1995). Everninomicin, a new oligosaccharide antibiotic: its antimicrobial activity, post-antibiotic effect and synergistic bactericidal activity. Drugs Exp Clin Res *21*, 7-16.

Navarre, W.W., Zou, S.B., Roy, H., Xie, J.L., Savchenko, A., Singer, A., Edvokimova, E., Prost, L.R., Kumar, R., Ibba, M.*, et al.* (2010). PoxA, yjeK, and elongation factor P

coordinately modulate virulence and drug resistance in Salmonella enterica. Mol Cell *39*, 209-221.

Nechifor, R., Murataliev, M., and Wilson, K.S. (2007). Functional interactions between the G' subdomain of bacterial translation factor EF-G and ribosomal protein L7/L12. J Biol Chem *282*, 36998-37005.

Ng, W.L., and Bassler, B.L. (2009). Bacterial quorum-sensing network architectures. Annu Rev Genet *43*, 197-222.

Nicolaou, K.C., Safina, B.S., Zak, M., Lee, S.H., Nevalainen, M., Bella, M., Estrada, A.A., Funke, C., Zecri, F.J., and Bulat, S. (2005a). Total synthesis of thiostrepton. Retrosynthetic analysis and construction of key building blocks. J Am Chem Soc *127*, 11159-11175.

Nicolaou, K.C., Zak, M., Safina, B.S., Estrada, A.A., Lee, S.H., and Nevalainen, M. (2005b). Total synthesis of thiostrepton. Assembly of key building blocks and completion of the synthesis. J Am Chem Soc *127*, 11176-11183.

Nissen, P., Hansen, J., Ban, N., Moore, P.B., and Steitz, T.A. (2000). The structural basis of ribosome activity in peptide bond synthesis. Science *289*, 920-930.

O'Connor, M., Gregory, S.T., Rajbhandary, U.L., and Dahlberg, A.E. (2001). Altered discrimination of start codons and initiator tRNAs by mutant initiation factor 3. RNA *7*, 969-978.

Ogle, J.M., Brodersen, D.E., Clemons, W.M., Jr., Tarry, M.J., Carter, A.P., and Ramakrishnan, V. (2001). Recognition of cognate transfer RNA by the 30S ribosomal subunit. Science *292*, 897-902.

Ogle, J.M., Carter, A.P., and Ramakrishnan, V. (2003). Insights into the decoding mechanism from recent ribosome structures. Trends Biochem Sci *28*, 259-266.

Ogle, J.M., Murphy, F.V., Tarry, M.J., and Ramakrishnan, V. (2002). Selection of tRNA by the ribosome requires a transition from an open to a closed form. Cell *111*, 721-732.

Ottenheijm, H.C., van den Broek, L.A., Ballesta, J.P., and Zylicz, Z. (1986). Chemical and biological aspects of sparsomycin, an antibiotic from Streptomyces. Prog Med Chem *23*, 219-268.

Pai, R.D., Zhang, W., Schuwirth, B.S., Hirokawa, G., Kaji, H., Kaji, A., and Cate, J.H. (2008). Structural Insights into ribosome recycling factor interactions with the 70S ribosome. J Mol Biol *376*, 1334-1347.

Palaniappan, N., Ayers, S., Gupta, S., Habib el, S., and Reynolds, K.A. (2006). Production of hygromycin A analogs in Streptomyces hygroscopicus NRRL 2388 through identification and manipulation of the biosynthetic gene cluster. Chem Biol *13*, 753-764.

Palaniappan, N., Dhote, V., Ayers, S., Starosta, A.L., Wilson, D.N., and Reynolds, K.A. (2009). Biosynthesis of the aminocyclitol subunit of hygromycin A in Streptomyces hygroscopicus NRRL 2388. Chem Biol *16*, 1180-1189.

Pallen, M.J., and Wren, B.W. (2007). Bacterial pathogenomics. Nature *449*, 835-842.

Pan, D., Kirillov, S.V., and Cooperman, B.S. (2007). Kinetically competent intermediates in the translocation step of protein synthesis. Mol Cell *25*, 519-529.

Park, J.T., and Uehara, T. (2008). How bacteria consume their own exoskeletons (turnover and recycling of cell wall peptidoglycan). Microbiol Mol Biol Rev *72*, 211-227, table of contents.

Park, M.H. (2006). The post-translational synthesis of a polyamine-derived amino acid, hypusine, in the eukaryotic translation initiation factor 5A (eIF5A). J Biochem *139*, 161-169.

Parmeggiani, A., and Nissen, P. (2006). Elongation factor Tu-targeted antibiotics: four different structures, two mechanisms of action. FEBS Lett *580*, 4576-4581.

Peat, T.S., Newman, J., Waldo, G.S., Berendzen, J., and Terwilliger, T.C. (1998). Structure of translation initiation factor 5A from Pyrobaculum aerophilum at 1.75 A resolution. Structure *6*, 1207-1214.

Peng, W.T., Banta, L.M., Charles, T.C., and Nester, E.W. (2001). The chvH locus of Agrobacterium encodes a homologue of an elongation factor involved in protein synthesis. J Bacteriol *183*, 36-45.

Pestka, S. (1969). Studies on the formation of transfer ribonucleic acid-ribosome complexes. XI. Antibiotic effects on phenylalanyl-oligonucleotide binding to ribosomes. Proc Natl Acad Sci U S A *64*, 709-714.

Pestka, S. (1970). Thiostrepton: a ribosomal inhibitor of translocation. Biochem Biophys Res Commun *40*, 667-674.

Pestka, S. (1974). Antibiotics as probes of ribosome structure: binding of chloramphenicol and erythromycin to polyribosomes; effect of other antibiotics. Antimicrob Agents Chemother *5*, 255-267.

Petropoulos, A.D., Kouvela, E.C., Starosta, A.L., Wilson, D.N., Dinos, G.P., and Kalpaxis, D.L. (2009). Time-resolved binding of azithromycin to Escherichia coli ribosomes. J Mol Biol *385*, 1179-1192.

Petropoulos, A.D., Xaplanteri, M.A., Dinos, G.P., Wilson, D.N., and Kalpaxis, D.L. (2004). Polyamines affect diversely the antibiotic potency: insight gained from kinetic studies of the blasticidin S AND spiramycin interactions with functional ribosomes. J Biol Chem *279*, 26518-26525.

Petry, S., Brodersen, D.E., Murphy, F.V.t., Dunham, C.M., Selmer, M., Tarry, M.J., Kelley, A.C., and Ramakrishnan, V. (2005). Crystal structures of the ribosome in complex with release factors RF1 and RF2 bound to a cognate stop codon. Cell *123*, 1255-1266.

Pettinger, R.C., and Wolfe, R.N. (1953). Hygromycin I. Preliminary studies on the production and biological activity of a new antibiotic. Antibiot Chemother *3*, 1268-1278.

Poulsen, S.M., Kofoed, C., and Vester, B. (2000). Inhibition of the ribosomal peptidyl transferase reaction by the mycarose moiety of the antibiotics carbomycin, spiramycin and tylosin. J Mol Biol *304*, 471-481.

Ramu, H., Mankin, A., and Vazquez-Laslop, N. (2009). Programmed drug-dependent ribosome stalling. Mol Microbiol *71*, 811-824.

Ramu, H., Vazquez-Laslop, N., Klepacki, D., Dai, Q., Piccirilli, J., Micura, R., and Mankin, A.S. (2011). Nascent peptide in the ribosome exit tunnel affects functional properties of the A-site of the peptidyl transferase center. Mol Cell *41*, 321-330.

Raskin, D.M., Seshadri, R., Pukatzki, S.U., and Mekalanos, J.J. (2006). Bacterial genomics and pathogen evolution. Cell *124*, 703-714.

Ratje, A.H., Loerke, J., Mikolajka, A., Brunner, M., Hildebrand, P.W., Starosta, A.L., Donhofer, A., Connell, S.R., Fucini, P., Mielke, T.*, et al.* (2010). Head swivel on the ribosome facilitates translocation by means of intra-subunit tRNA hybrid sites. Nature *468*, 713-716.

Rawat, U., Gao, H., Zavialov, A., Gursky, R., Ehrenberg, M., and Frank, J. (2006). Interactions of the release factor RF1 with the ribosome as revealed by cryo-EM. J Mol Biol *357*, 1144-1153.

Rawat, U.B., Zavialov, A.V., Sengupta, J., Valle, M., Grassucci, R.A., Linde, J., Vestergaard, B., Ehrenberg, M., and Frank, J. (2003). A cryo-electron microscopic study of ribosome-bound termination factor RF2. Nature *421*, 87-90.

Ray, K., Marteyn, B., Sansonetti, P.J., and Tang, C.M. (2009). Life on the inside: the intracellular lifestyle of cytosolic bacteria. Nat Rev Microbiol *7*, 333-340.

Ringquist, S., MacDonald, M., Gibson, T., and Gold, L. (1993). Nature of the ribosomal mRNA track: analysis of ribosome-binding sites containing different sequences and secondary structures. Biochemistry *32*, 10254-10262.

Risuleo, G., Gualerzi, C., and Pon, C. (1976). Specificity and properties of the destabilization, induced by initiation factor IF-3, of ternary complexes of the 30-S ribosomal subunit, aminoacyl-tRNA and polynucleotides. Eur J Biochem *67*, 603-613.

Roberts, M.C., Sutcliffe, J., Courvalin, P., Jensen, L.B., Rood, J., and Seppala, H. (1999). Nomenclature for macrolide and macrolide-lincosamide-streptogramin B resistance determinants. Antimicrob Agents Chemother *43*, 2823-2830.

Rodnina, M.V., Savelsbergh, A., Katunin, V.I., and Wintermeyer, W. (1997). Hydrolysis of GTP by elongation factor G drives tRNA movement on the ribosome. Nature *385*, 37-41.

Rodnina, M.V., Savelsbergh, A., Matassova, N.B., Katunin, V.I., Semenkov, Y.P., and Wintermeyer, W. (1999). Thiostrepton inhibits the turnover but not the GTPase of elongation factor G on the ribosome. Proc Natl Acad Sci U S A *96*, 9586-9590.

Rosendahl, G., and Douthwaite, S. (1994). The antibiotics micrococcin and thiostrepton interact directly with 23S rRNA nucleotides 1067A and 1095A. Nucleic Acids Res *22*, 357-363.

Ross, J.I., Eady, E.A., Cove, J.H., Cunliffe, W.J., Baumberg, S., and Wootton, J.C. (1990). Inducible erythromycin resistance in staphylococci is encoded by a member of the ATP-binding transport super-gene family. Mol Microbiol *4*, 1207-1214.

Roy, H., Zou, S.B., Bullwinkle, T.J., Wolfe, B.S., Gilreath, M.S., Forsyth, C.J., Navarre, W.W., and Ibba, M. (2011). The tRNA synthetase paralog PoxA modifies elongation factor-P with (R)-beta-lysine. Nat Chem Biol *7*, 667-669.

Savelsbergh, A., Matassova, N.B., Rodnina, M.V., and Wintermeyer, W. (2000). Role of domains 4 and 5 in elongation factor G functions on the ribosome. J Mol Biol *300*, 951-961.

Savelsbergh, A., Mohr, D., Kothe, U., Wintermeyer, W., and Rodnina, M.V. (2005). Control of phosphate release from elongation factor G by ribosomal protein L7/12. EMBO J *24*, 4316-4323.

Schafer, M.A., Tastan, A.O., Patzke, S., Blaha, G., Spahn, C.M., Wilson, D.N., and Nierhaus, K.H. (2002). Codon-anticodon interaction at the P site is a prerequisite for tRNA interaction with the small ribosomal subunit. J Biol Chem *277*, 19095-19105.

Schluenzen, F., Takemoto, C., Wilson, D.N., Kaminishi, T., Harms, J.M., Hanawa-Suetsugu, K., Szaflarski, W., Kawazoe, M., Shirouzu, M., Nierhaus, K.H.*, et al.* (2006). The antibiotic kasugamycin mimics mRNA nucleotides to destabilize tRNA binding and inhibit canonical translation initiation. Nat Struct Mol Biol *13*, 871-878.

Schlunzen, F., Harms, J.M., Franceschi, F., Hansen, H.A., Bartels, H., Zarivach, R., and Yonath, A. (2003). Structural basis for the antibiotic activity of ketolides and azalides. Structure *11*, 329-338.

Schlunzen, F., Pyetan, E., Fucini, P., Yonath, A., and Harms, J.M. (2004). Inhibition of peptide bond formation by pleuromutilins: the structure of the 50S ribosomal subunit from Deinococcus radiodurans in complex with tiamulin. Mol Microbiol *54*, 1287-1294.

Schlunzen, F., Zarivach, R., Harms, J., Bashan, A., Tocilj, A., Albrecht, R., Yonath, A., and Franceschi, F. (2001). Structural basis for the interaction of antibiotics with the peptidyl transferase centre in eubacteria. Nature *413*, 814-821.

Schmeing, T.M., Huang, K.S., Kitchen, D.E., Strobel, S.A., and Steitz, T.A. (2005a). Structural insights into the roles of water and the 2' hydroxyl of the P site tRNA in the peptidyl transferase reaction. Mol Cell *20*, 437-448.

Schmeing, T.M., Huang, K.S., Strobel, S.A., and Steitz, T.A. (2005b). An induced-fit mechanism to promote peptide bond formation and exclude hydrolysis of peptidyl-tRNA. Nature *438*, 520-524.

Schmeing, T.M., and Ramakrishnan, V. (2009). What recent ribosome structures have revealed about the mechanism of translation. Nature *461*, 1234-1242.

Schmeing, T.M., Voorhees, R.M., Kelley, A.C., Gao, Y.G., Murphy, F.V.t., Weir, J.R., and Ramakrishnan, V. (2009). The crystal structure of the ribosome bound to EF-Tu and aminoacyl-tRNA. Science *326*, 688-694.

Schuette, J.C., Murphy, F.V.t., Kelley, A.C., Weir, J.R., Giesebrecht, J., Connell, S.R., Loerke, J., Mielke, T., Zhang, W., Penczek, P.A.*, et al.* (2009). GTPase activation of elongation factor EF-Tu by the ribosome during decoding. EMBO J *28*, 755-765.

Scolnick, E., Tompkins, R., Caskey, T., and Nirenberg, M. (1968). Release factors differing in specificity for terminator codons. Proc Natl Acad Sci U S A *61*, 768-774.

Seidelt, B., Innis, C.A., Wilson, D.N., Gartmann, M., Armache, J.P., Villa, E., Trabuco, L.G., Becker, T., Mielke, T., Schulten, K.*, et al.* (2009). Structural insight into nascent polypeptide chain-mediated translational stalling. Science *326*, 1412-1415.

Seit-Nebi, A., Frolova, L., Justesen, J., and Kisselev, L. (2001). Class-1 translation termination factors: invariant GGQ minidomain is essential for release activity and ribosome binding but not for stop codon recognition. Nucleic Acids Res *29*, 3982-3987.

Selmer, M., Dunham, C.M., Murphy, F.V.t., Weixlbaumer, A., Petry, S., Kelley, A.C., Weir, J.R., and Ramakrishnan, V. (2006). Structure of the 70S ribosome complexed with mRNA and tRNA. Science *313*, 1935-1942.

Seo, H.S., Abedin, S., Kamp, D., Wilson, D.N., Nierhaus, K.H., and Cooperman, B.S. (2006). EF-G-dependent GTPase on the ribosome. conformational change and fusidic acid inhibition. Biochemistry *45*, 2504-2514.

Shaw, J.J., and Green, R. (2007). Two distinct components of release factor function uncovered by nucleophile partitioning analysis. Mol Cell *28*, 458-467.

Shin, D.H., Brandsen, J., Jancarik, J., Yokota, H., Kim, R., and Kim, S.H. (2004). Structural analyses of peptide release factor 1 from Thermotoga maritima reveal domain flexibility required for its interaction with the ribosome. J Mol Biol *341*, 227-239.

Shine, J., and Dalgarno, L. (1974). The 3'-terminal sequence of Escherichia coli 16S ribosomal RNA: complementarity to nonsense triplets and ribosome binding sites. Proc Natl Acad Sci U S A *71*, 1342-1346.

Singh, N.S., Das, G., Seshadri, A., Sangeetha, R., and Varshney, U. (2005). Evidence for a role of initiation factor 3 in recycling of ribosomal complexes stalled on mRNAs in Escherichia coli. Nucleic Acids Res *33*, 5591-5601.

Sperti, S., Montanaro, L., Mattioli, A., and Testoni, G. (1975). Relationship between elongation factor I- and elongation factor II- dependent guanosine triphosphatase activities of ribosomes. Inhibition of both activities by ricin. Biochem J *148*, 447-451.

Sperti, S., Montanaro, L., Mattioli, A., Testoni, G., and Stirpe, F. (1976). Inhibition of protein synthesis in vitro by crotins and ricin. Effect on the steps of peptide chain elongation. Biochem J *156*, 7-13.

Spiegel, P.C., Ermolenko, D.N., and Noller, H.F. (2007). Elongation factor G stabilizes the hybrid-state conformation of the 70S ribosome. RNA *13*, 1473-1482.

Stanley, R.E., Blaha, G., Grodzicki, R.L., Strickler, M.D., and Steitz, T.A. (2010). The structures of the anti-tuberculosis antibiotics viomycin and capreomycin bound to the 70S ribosome. Nat Struct Mol Biol *17*, 289-293.

Stark, H., Rodnina, M.V., Wieden, H.J., van Heel, M., and Wintermeyer, W. (2000). Large-scale movement of elongation factor G and extensive conformational change of the ribosome during translocation. Cell *100*, 301-309.

Starosta, A.L., Karpenko, V.V., Shishkina, A.V., Mikolajka, A., Sumbatyan, N.V., Schluenzen, F., Korshunova, G.A., Bogdanov, A.A., and Wilson, D.N. (2010). Interplay between the ribosomal tunnel, nascent chain, and macrolides influences drug inhibition. Chem Biol *17*, 504-514.

Starosta, A.L., Qin, H., Mikolajka, A., Leung, G.Y., Schwinghammer, K., Nicolaou, K.C., Chen, D.Y., Cooperman, B.S., and Wilson, D.N. (2009). Identification of distinct thiopeptide-antibiotic precursor lead compounds using translation machinery assays. Chem Biol *16*, 1087-1096.

Storm, D.R. (1974). Mechanism of bacitracin action: a specific lipid-peptide interaction. Ann N Y Acad Sci *235*, 387-398.

Su, T.L. (1948). Micrococcin, an antibacterial substance formed by a strain of Micrococcus. Br J Exp Pathol *29*, 473-481.

Sussman, J.K., Simons, E.L., and Simons, R.W. (1996). Escherichia coli translation initiation factor 3 discriminates the initiation codon in vivo. Mol Microbiol *21*, 347-360.

Swaney, S., McCroskey, M., Shinabarger, D., Wang, Z., Turner, B.A., and Parker, C.N. (2006). Characterization of a high-throughput screening assay for inhibitors of elongation factor p and ribosomal peptidyl transferase activity. J Biomol Screen *11*, 736-742.

Tait-Kamradt, A., Davies, T., Cronan, M., Jacobs, M.R., Appelbaum, P.C., and Sutcliffe, J. (2000). Mutations in 23S rRNA and ribosomal protein L4 account for resistance in pneumococcal strains selected in vitro by macrolide passage. Antimicrob Agents Chemother *44*, 2118-2125.

Tanaka, N., Kinoshita, T., and Masukawa, H. (1968). Mechanism of protein synthesis inhibition by fusidic acid and related antibiotics. Biochem Biophys Res Commun *30*, 278-283.

Tenson, T., DeBlasio, A., and Mankin, A. (1996). A functional peptide encoded in the Escherichia coli 23S rRNA. Proc Natl Acad Sci U S A *93*, 5641-5646.

Tenson, T., and Ehrenberg, M. (2002). Regulatory nascent peptides in the ribosomal tunnel. Cell *108*, 591-594.

Tenson, T., Lovmar, M., and Ehrenberg, M. (2003). The mechanism of action of macrolides, lincosamides and streptogramin B reveals the nascent peptide exit path in the ribosome. J Mol Biol *330*, 1005-1014.

Tenson, T., and Mankin, A.S. (2001). Short peptides conferring resistance to macrolide antibiotics. Peptides *22*, 1661-1668.

Thompson, C.J., Skinner, R.H., Thompson, J., Ward, J.M., Hopwood, D.A., and Cundliffe, E. (1982). Biochemical characterization of resistance determinants cloned from antibiotic-producing streptomycetes. J Bacteriol *151*, 678-685.

Thompson, J., Cundliffe, E., and Dahlberg, A.E. (1988). Site-directed mutagenesis of Escherichia coli 23 S ribosomal RNA at position 1067 within the GTP hydrolysis centre. J Mol Biol *203*, 457-465.

Ticu, C., Nechifor, R., Nguyen, B., Desrosiers, M., and Wilson, K.S. (2009). Conformational changes in switch I of EF-G drive its directional cycling on and off the ribosome. EMBO J *28*, 2053-2065.

Toh, S.M., Xiong, L., Bae, T., and Mankin, A.S. (2008). The methyltransferase YfgB/RlmN is responsible for modification of adenosine 2503 in 23S rRNA. RNA *14*, 98-106.

Tomasz, A. (1979). The mechanism of the irreversible antimicrobial effects of penicillins: how the beta-lactam antibiotics kill and lyse bacteria. Annu Rev Microbiol *33*, 113-137.

Traut, R.R., and Monro, R.E. (1964). The Puromycin Reaction and Its Relation to Protein Synthesis. J Mol Biol *10*, 63-72.

Tseng, T.T., Tyler, B.M., and Setubal, J.C. (2009). Protein secretion systems in bacterial-host associations, and their description in the Gene Ontology. BMC Microbiol *9 Suppl 1*, S2.

Tu, D., Blaha, G., Moore, P.B., and Steitz, T.A. (2005). Structures of MLSBK antibiotics bound to mutated large ribosomal subunits provide a structural explanation for resistance. Cell *121*, 257-270.

Vakulenko, S.B., and Mobashery, S. (2003). Versatility of aminoglycosides and prospects for their future. Clin Microbiol Rev *16*, 430-450.

Van Parys, A., Boyen, F., Leyman, B., Verbrugghe, E., Haesebrouck, F., and Pasmans, F. (2011). Tissue-Specific Salmonella Typhimurium Gene Expression during Persistence in Pigs. PLoS One *6*, e24120.

Vazquez-Laslop, N., Klepacki, D., Mulhearn, D.C., Ramu, H., Krasnykh, O., Franzblau, S., and Mankin, A.S. (2011). Role of antibiotic ligand in nascent peptide-dependent ribosome stalling. Proc Natl Acad Sci U S A *108*, 10496-10501.

Vazquez-Laslop, N., Thum, C., and Mankin, A.S. (2008). Molecular mechanism of drug-dependent ribosome stalling. Mol Cell *30*, 190-202.

Verstraeten, N., Braeken, K., Debkumari, B., Fauvart, M., Fransaer, J., Vermant, J., and Michiels, J. (2008). Living on a surface: swarming and biofilm formation. Trends Microbiol *16*, 496-506.

Vester, B., and Douthwaite, S. (2001). Macrolide resistance conferred by base substitutions in 23S rRNA. Antimicrob Agents Chemother *45*, 1-12.

Vestergaard, B., Sanyal, S., Roessle, M., Mora, L., Buckingham, R.H., Kastrup, J.S., Gajhede, M., Svergun, D.I., and Ehrenberg, M. (2005). The SAXS solution structure of RF1 differs from its crystal structure and is similar to its ribosome bound cryo-EM structure. Mol Cell *20*, 929-938.

Vestergaard, B., Van, L.B., Andersen, G.R., Nyborg, J., Buckingham, R.H., and Kjeldgaard, M. (2001). Bacterial polypeptide release factor RF2 is structurally distinct from eukaryotic eRF1. Mol Cell *8*, 1375-1382.

Vimberg, V., Xiong, L., Bailey, M., Tenson, T., and Mankin, A. (2004). Peptide-mediated macrolide resistance reveals possible specific interactions in the nascent peptide exit tunnel. Mol Microbiol *54*, 376-385.

Voorhees, R.M., Schmeing, T.M., Kelley, A.C., and Ramakrishnan, V. (2010). The mechanism for activation of GTP hydrolysis on the ribosome. Science *330*, 835-838.

Walsh, C. (2003). Where will new antibiotics come from? Nat Rev Microbiol *1*, 65-70.

Walsh, C.T., Acker, M.G., and Bowers, A.A. (2010). Thiazolyl peptide antibiotic biosynthesis: a cascade of post-translational modifications on ribosomal nascent proteins. J Biol Chem *285*, 27525-27531.

Waxman, D.J., Yocum, R.R., and Strominger, J.L. (1980). Penicillins and cephalosporins are active site-directed acylating agents: evidence in support of the substrate analogue hypothesis. Philos Trans R Soc Lond B Biol Sci *289*, 257-271.

Weinger, J.S., Parnell, K.M., Dorner, S., Green, R., and Strobel, S.A. (2004). Substrate-assisted catalysis of peptide bond formation by the ribosome. Nat Struct Mol Biol *11*, 1101-1106.

Weinstein, M.J., Luedemann, G.M., Oden, E.M., and Wagman, G.H. (1964). Everninomicin, a New Antibiotic Complex from Micromonospora Carbonacea. Antimicrob Agents Chemother (Bethesda) *10*, 24-32.

Weisblum, B., and Demohn, V. (1970). Inhibition by thiostrepton of the formation of a ribosome-bound guanine nucleotide complex. FEBS Lett *11*, 149-152.

Weitnauer, G., Muhlenweg, A., Trefzer, A., Hoffmeister, D., Sussmuth, R.D., Jung, G., Welzel, K., Vente, A., Girreser, U., and Bechthold, A. (2001). Biosynthesis of the orthosomycin antibiotic avilamycin A: deductions from the molecular analysis of the avi biosynthetic gene cluster of Streptomyces viridochromogenes Tu57 and production of new antibiotics. Chem Biol *8*, 569-581.

Weixlbaumer, A., Jin, H., Neubauer, C., Voorhees, R.M., Petry, S., Kelley, A.C., and Ramakrishnan, V. (2008). Insights into translational termination from the structure of RF2 bound to the ribosome. Science *322*, 953-956.

Wieland Brown, L.C., Acker, M.G., Clardy, J., Walsh, C.T., and Fischbach, M.A. (2009). Thirteen posttranslational modifications convert a 14-residue peptide into the antibiotic thiocillin. Proc Natl Acad Sci U S A *106*, 2549-2553.

Wilson, D.N. (2009). The A-Z of bacterial translation inhibitors. Crit Rev Biochem Mol Biol *44*, 393-433.

Wilson, D.N., and Beckmann, R. (2011). The ribosomal tunnel as a functional environment for nascent polypeptide folding and translational stalling. Curr Opin Struct Biol *21*, 274-282.

Wilson, D.N., Harms, J.M., Nierhaus, K.H., Schlunzen, F., and Fucini, P. (2005). Species-specific antibiotic-ribosome interactions: implications for drug development. Biol Chem *386*, 1239-1252.

Wilson, D.N., Schluenzen, F., Harms, J.M., Starosta, A.L., Connell, S.R., and Fucini, P. (2008). The oxazolidinone antibiotics perturb the ribosomal peptidyl-transferase center and effect tRNA positioning. Proc Natl Acad Sci U S A *105*, 13339-13344.

Wise, E.M., Jr., and Park, J.T. (1965). Penicillin: its basic site of action as an inhibitor of a peptide cross-linking reaction in cell wall mucopeptide synthesis. Proc Natl Acad Sci U S A *54*, 75-81.

Wu, H.J., Wang, A.H., and Jennings, M.P. (2008). Discovery of virulence factors of pathogenic bacteria. Curr Opin Chem Biol *12*, 93-101.

Yanagisawa, T., Sumida, T., Ishii, R., Takemoto, C., and Yokoyama, S. (2010). A paralog of lysyl-tRNA synthetase aminoacylates a conserved lysine residue in translation elongation factor P. Nat Struct Mol Biol *17*, 1136-1143.

Yong, D., Toleman, M.A., Giske, C.G., Cho, H.S., Sundman, K., Lee, K., and Walsh, T.R. (2009). Characterization of a new metallo-beta-lactamase gene, bla(NDM-1), and a novel erythromycin esterase gene carried on a unique genetic structure in Klebsiella pneumoniae sequence type 14 from India. Antimicrob Agents Chemother *53*, 5046-5054.

Zaher, H.S., and Green, R. (2009). Quality control by the ribosome following peptide bond formation. Nature *457*, 161-166.

Zaher, H.S., and Green, R. (2011). A Primary Role for Release Factor 3 in Quality Control during Translation Elongation in Escherichia coli. Cell *147*, 396-408.

Zaher, H.S., Shaw, J.J., Strobel, S.A., and Green, R. (2011). The 2'-OH group of the peptidyl-tRNA stabilizes an active conformation of the ribosomal PTC. EMBO J *30*, 2445-2453.

Zanelli, C.F., Maragno, A.L., Gregio, A.P., Komili, S., Pandolfi, J.R., Mestriner, C.A., Lustri, W.R., and Valentini, S.R. (2006). eIF5A binds to translational machinery components and affects translation in yeast. Biochem Biophys Res Commun *348*, 1358-1366.

Zavialov, A.V., Hauryliuk, V.V., and Ehrenberg, M. (2005). Splitting of the posttermination ribosome into subunits by the concerted action of RRF and EF-G. Mol Cell *18*, 675-686.

Zhang, Q., Lambert, G., Liao, D., Kim, H., Robin, K., Tung, C.K., Pourmand, N., and Austin, R.H. (2011). Acceleration of emergence of bacterial antibiotic resistance in connected microenvironments. Science *333*, 1764-1767.

Zoldak, G., Redecke, L., Svergun, D.I., Konarev, P.V., Voertler, C.S., Dobbek, H., Sedlak, E., and Sprinzl, M. (2007). Release factors 2 from Escherichia coli and Thermus thermophilus: structural, spectroscopic and microcalorimetric studies. Nucleic Acids Res *35*, 1343-1353.

Paper 1

Please cite this article in press as: Palaniappan et al., Biosynthesis of the Aminocyclitol Subunit of Hygromycin A in *Streptomyces hygroscopicus* NRRL 2388, Chemistry & Biology (2009), doi:10.1016/j.chembiol.2009.10.013

Chemistry & Biology
Article

Biosynthesis of the Aminocyclitol Subunit of Hygromycin A in *Streptomyces hygroscopicus* NRRL 2388

Nadaraj Palaniappan,[1] Vidya Dhote,[1] Sloan Ayers,[1] Agata L. Starosta,[2,3] Daniel N. Wilson,[2,3] and Kevin A. Reynolds[1,*]
[1]Department of Chemistry, Portland State University, P.O. Box 751, Portland, OR 97207-0751, USA
[2]Center for Integrated Protein Science Munich (CiPS-M)
[3]Gene Center and Department of Chemistry and Biochemistry
Ludwig-Maximilians-Universität Munchen, Feodor-Lynen-Strasse 25, D-81377 Munich, Germany
*Correspondence: reynoldsk@pdx.edu
DOI 10.1016/j.chembiol.2009.10.013

SUMMARY

The antibacterial activity of hygromycin A (HA) arises from protein synthesis inhibition and is dependent upon a methylenedioxy bridged-aminocyclitol moiety. Selective gene deletions and chemical complementation in *Streptomyces hygroscopicus* NRRL 2388 showed that the *hyg18* and *hyg25* gene products, proposed to generate a *myo*-inositol intermediate, are dispensable for HA biosynthesis but contribute to antibiotic yields. Hyg8 and Hyg17, proposed to introduce the amine functionality, are essential for HA biosynthesis. Hyg6 is a methyltransferase acting on the aminocyclitol, and a Δ*hyg6* mutant produces desmethylenehygromycin A. Deletion of *hyg7*, a metallo-dependant hydrolase homolog gene, resulted in methoxyhygromycin A production, demonstrating that the corresponding gene product is responsible for the proposed oxidative cyclization step of methylenedioxy bridge formation. The methyl/methylene group is not required for in vitro protein synthesis inhibition but is essential for activity against *Escherichia coli*.

INTRODUCTION

Aminocyclitols, which are characterized by the presence of a cyclohexane moiety with hydroxyl and amino or guanidino substituents, are found in a large class of natural products with broad-ranging biological properties. The aminocyclitol-aminoglycosides have long been known for their antibacterial activities and have found applications as antibiotics in clinical use (streptomycin, gentamicin, and kanamycin), veterinary medicine (spectinomycin), and agriculture (kasugamycin and validamycin A) (Flatt and Mahmud, 2007; Mahmud, 2009). The C_7N aminocyclitol-containing compound, acarbose, has α-glucosidase inhibitory activity, potentially useful in the treatment of type II insulin-independent diabetes mellitus (Mahmud, 2003). Structure-activity relationship studies have established the importance of the aminocyclitol moiety for the biological activity of many of these natural products. Genetic and biochemical studies have also revealed the complexity and diversity of the biosynthetic pathways that produce these critical aminocyclitol moieties (Flatt and Mahmud, 2007; Mahmud, 2009).

Hygromycin A (HA, compound **1**) (Figure 1) is a secondary metabolite produced by the soil bacterium *Streptomyces hygroscopicus* NRRL 2388 (Mann et al., 1953; Pittenger et al., 1953). HA is structurally distinguished by the presence of three distinct moieties, 5-dehydro-α-L-fucofuranose (subunit A), (*E*)-3-(3,4-dihydroxyphenyl)-2-methylacrylic acid (subunit B), and the aminocyclitol, 2L-2-amino-2-deoxy-4,5-*O*-methylene-*neo*-inositol (subunit C). The mechanism of action of HA as a bacterial ribosomal peptidyl transferase inhibitor, and also its hemagglutination inactivation, antitreponemal, and immunosuppressant properties have been well-elucidated (Guerrero and Modolell, 1980; Nakagawa et al., 1987; Omura et al., 1987; Uyeda et al., 2001; Yoshida et al., 1986). Herbicidal properties have been identified for HA and methoxyhygromycin A (**2**) (Figure 1), a shunt product or pathway intermediate obtained in the course of HA biosynthesis (Kim et al., 1990; Lee et al., 2003). Structure-activity relationship studies have revealed that subunit C is indispensable for HA's antibacterial activity (Hayashi et al., 1997).

A plausible pathway for HA biosynthesis has been proposed, based on isotope-labeled precursor incorporation studies (Habib et al., 2003). Analyses of labeling patterns of the resulting HA have shown that (1) subunit A originates from glucose-6-phosphate via a mannose intermediate, (2) the central subunit B is derived from 4-hydroxybenzoic acid and propionic acid in a polyketide-like manner, and (3) *myo*-inositol and methionine are the precursors for subunit C. It has further been suggested that the glycoside bond (which links subunits A and B) and the amide bond (linking subunits B and C) are formed after each of the subunits is assembled. The results from the biosynthetic incorporation studies provided a strategy for identification, and subsequent cloning and sequencing of the HA biosynthetic gene cluster of *S. hygroscopicus* (GenBank DQ314862) (Palaniappan et al., 2006). Analysis of this 31.5 kb gene cluster led to the identification of 29 open reading frames (ORFs).

Several of the gene products were assigned putative roles in biosynthesis of the aminocyclitol subunit of HA. In the proposed pathway, glucose-6-phosphate is first converted to *myo*-inositol-1-phosphate (MIP) by a *myo*-inositol-1-phosphate synthase encoded by *hyg18*. MIP is then dephosphorylated to form *myo*-inositol by the *hyg25* gene product, a putative *myo*-inositol phosphatase. Analogous steps are also encountered in the biosynthesis of the aminocyclitol moiety of

Please cite this article in press as: Palaniappan et al., Biosynthesis of the Aminocyclitol Subunit of Hygromycin A in *Streptomyces hygroscopicus* NRRL 2388, Chemistry & Biology (2009), doi:10.1016/j.chembiol.2009.10.013

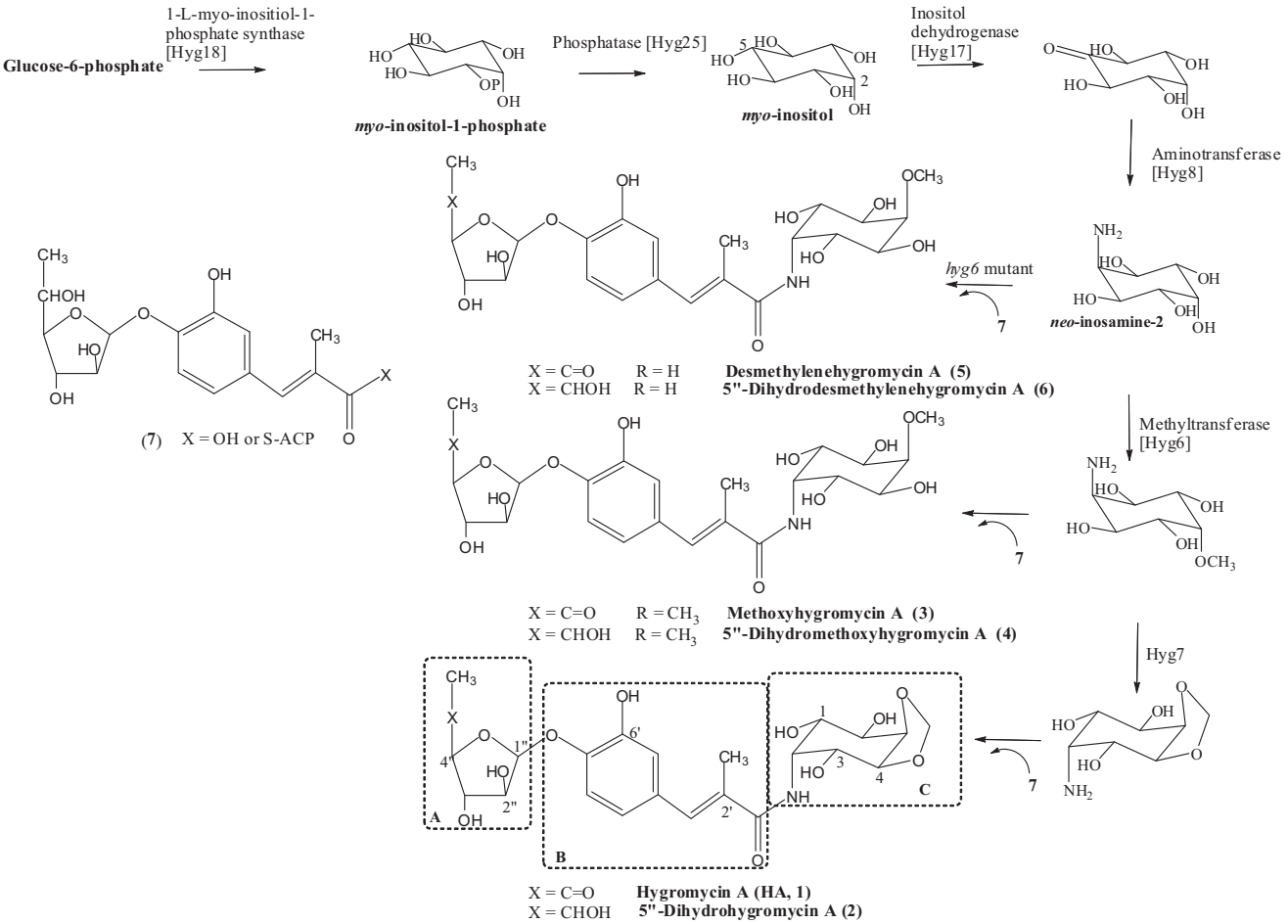

Figure 1. Relationship between Hygromycin A Analogs and the Biosynthetic Pathway Leading to the Aminocyclitol Moiety

The three structural moieties, 5-dehydro-α-L-fucofuranose (subunit A), (*E*)-3-(3,4-dihydroxyphenyl)-2-methylacrylic acid (subunit B), and 2L-2-amino-2-deoxy-4,5-*O*-methylene-*neo*-inositol (subunit C) are indicated.

streptomycin, bluensomycin, spectinomycin, fortimicin, and the D-inositol of kasugamycin (Flatt and Mahmud, 2007). The subsequent oxidation and transamination reactions in the above compounds occur at the C2 hydroxyl of *myo*-inositol to form *scyllo*-inosamine, whereas in the case of HA biosynthesis the labeling studies are consistent with them occurring at the C5 hydroxyl, leading to the unique *neo*-inosamine-2 product. An inositol dehydrogenase (encoded by *hyg17*) and a putative aminotransferase (encoded by *hyg8*) were proposed to catalyze these steps, respectively. A distinct structural feature of HA is the methylenedioxy bridge between C4 and C5 of the C subunit, shown to be derived from *S*-adenosylmethionine (SAM). It has been proposed that the bridge formation involves methylation of the C5 hydroxyl group of *neo*-inosamine-2 (which is equivalent to C1 of *myo*-inositol) by a SAM-dependent methyltransferase, followed by cyclization. The *hyg6* and *hyg29* genes in the HA gene cluster are methyltransferase homologs, and it was not possible to determine from sequence analysis which of the two encodes the putative *O*-methyltransferase acting on *neo*-inosamine-2. No candidate gene for the subsequent cyclization step was identified and sequence analysis gave no insight into the timing of the various steps.

We report herein a verification of the proposed roles of these *hyg* genes in biosynthesis of the aminocyclitol subunit through a series of targeted gene disruption experiments and chemical complementation studies. A biologically active new desmethylene analog of HA has been purified and characterized from a Δ*hyg6* mutant, demonstrating that Hyg6 is the C5 *O*-methyltransferase that introduces the methyl group on the aminocyclitol and that introduction of the amine group can occur without this step. The analyses have also shown that the *hyg7* gene product is required for the cyclization step that generates the methylenedioxy bridge. The selective production of hygromycin analogs by the Δ*hyg6* and Δ*hyg7* mutants has provided an opportunity to probe the importance of a methyl or methylene group on the aminocylitol ring for both in vitro protein synthesis inhibitory activity and antibacterial activity.

RESULTS

Hygromycin Production by Mutant Strains

The HA biosynthetic gene cluster harbors seven genes that are predicted to be functional in the biosynthesis of the 2L-2-amino-2-deoxy-4,5-*O*-methylene-*neo*-inositol moiety (subunit C)

Table 1. Results of Feeding Antibiotic Precursors to Different *hyg* Mutant Strains

	Antibiotic Production			Production with *myo*-inositol Supplementation			Production with Subunit C Supplementation		
Strain	HA (mg/l)	3 (mg/l)	5 (mg/l)	HA (mg/l)	3 (mg/l)	5 (mg/l)	HA (mg/l)	3 (mg/l)	5 (mg/l)
Wild type	1190 ± 120			1090 ± 40					
Δ*hyg18* (*myo*-inositol-1-phosphate synthase)	588 ± 21			1090 ± 15					
Δ*hyg25* (*myo*-inositol-1-phosphatase)	961 ± 84			956 ± 74					
Δ*hyg17* (*myo*-inositol dehydrogenase)	147 ± 20			204 ± 41			630 ± 12		
Δ*hyg8* (Aminotransferase)	—	—					N/D		
Δ*hyg8*+Δ*hyg7*							3 ± 1		
Δ*hyg6* (Methyltransferase)	—	—	530 ± 60			435 ± 30	180 ± 90		690 ± 270
Δ*hyg29* (Methyltransferase)	485 ± 21								
Δ*hyg7*		287 ± 19			411 ± 19		671 ± 40	386 ± 33	

N/D, not detectable.

(Palaniappan et al., 2006). A polymerase chain reaction (PCR)-targeted gene replacement strategy for in vivo functional analyses of these genes was used (Gust et al., 2003) and the fermentation broths of the corresponding mutants were examined for the presence of HA or its analogs. The mutants were also chemically complemented with either subunit C (the putative final product of the aminocyclitol pathway) or the putative *myo*-inositol intermediate, and the effect on product ratios and yields were determined (Table 1).

The involvement of *myo*-inositol-1-phosphate synthase and *myo*-inositol phosphatase to generate *myo*-inositol from glucose-6-phosphate has been reported from a host of diverse sources such as higher plants and animals, parasites, fungi, green algae, bacteria, and archaea (Majumder et al., 2003). The *hyg18* gene product is proposed to be a *myo*-inositol-1-phosphate synthase and the Δ*hyg18* mutant produced HA, **3,** and their corresponding C5″-reduced analogs **2** and **4** (Figure 1) at approximately 50% of the levels observed for the wild-type strain (Table 1). A small amount (~23 mg/l) of (E)-3-(3-hydroxy-4-O-α-fucofuranosylphenyl)-2-methylacrylic acid (**7**) (Figure 1) was also observed. This shunt product is not observed in the wild-type but has been identified previously in the SCH30 (short-chain dehydrogenase, Δ*hyg26*) mutant (Palaniappan et al., 2006). Chemical complementation of the Δ*hyg18* mutant with *myo*-inositol led to almost complete restoration of HA and loss of production of the **7** shunt product. In contrast, no increase in HA yields was observed with addition of *myo*-inositol to the wild-type strain (suggesting that *myo*-inositol is limiting in the Δ*hyg18* mutant but not in the wild-type). The *hyg25* gene product is predicted to be a *myo*-inositol phosphatase, and a Δ*hyg25* mutant was observed to produce HA in amounts comparable to that in the wild-type, both in the absence and presence of *myo*-inositol.

Blocking the aminocyclitol pathway at steps subsequent to the proposed *myo*-inositol intermediate had more pronounced effects on antibiotic production. Disruption of *hyg17*, which presumably encodes a *myo*-inositol dehydrogenase for C5 oxidation of *myo*-inositol, resulted in an 8-fold decrease in HA production (Table 1). Consistent with predictions, chemical complementation of the Δ*hyg17* mutant with *myo*-inositol did not lead to restoration of HA production. Chemical complementation of this mutant with subunit C led to a 4-fold increase in HA production levels, to approximately 50% of that seen in the wild-type. This experiment provided clear evidence that Hyg17 operates at a step in the aminocyclitol pathway after formation of the *myo*-inositol and that the final subunit C can be incorporated intact into HA. The Δ*hyg17* strain was also grown in the presence of valienamine, the C_7N aminocyclitol moiety used in biosynthesis of the antifungal antibiotic validamycin A (Mahmud et al., 2007). Liquid chromatography mass spectrometry (LC-MS) analyses of the fermentation broth showed the presence of an ionic species with a $[M+H]^+$ of 496 amu, the expected mass resulting from valienamine incorporation in place of the normal biosynthetic aminocyclitol moiety. A limited supply of valienamine precluded efforts to purify the proposed new HA analog for either structural elucidation or bioactivity assays. Further mutasynthesis experiments in Δ*hyg17* using amino sugars such as glucosamine, galactosamine, and mannosamine did not result in production of any detectable new HA products.

The *hyg8* gene is proposed to encode a putative class III pyridoxal-phosphate-dependent aminotransferase, catalyzing transamination of C5-oxidized *myo*-inositol to produce *neo*-inosamine-2 (Palaniappan et al., 2006). A complete loss of HA production was observed in the Δ*hyg8* mutant and could not be restored by chemical complementation with subunit C. An additional mutation, where *hyg7* and *hyg8* were both deleted, also abolished HA production completely. In this case, however, very low levels of HA production were observed with subunit C addition. As described below, a Δ*hyg7* mutant gives dramatically different results, and the loss of HA production and poor chemical complementation with subunit C appear to be linked to loss of *hyg8*.

The *hyg6* and *hyg29* genes show homology to methyltransferases and analysis of their predicted amino acid sequences did not indicate which of them was likely required for the proposed SAM-dependant methylation of *neo*-inosamine-2. A Δ*hyg29* mutant was generated, and high-performance liquid

Please cite this article in press as: Palaniappan et al., Biosynthesis of the Aminocyclitol Subunit of Hygromycin A in *Streptomyces hygroscopicus* NRRL 2388, Chemistry & Biology (2009), doi:10.1016/j.chembiol.2009.10.013

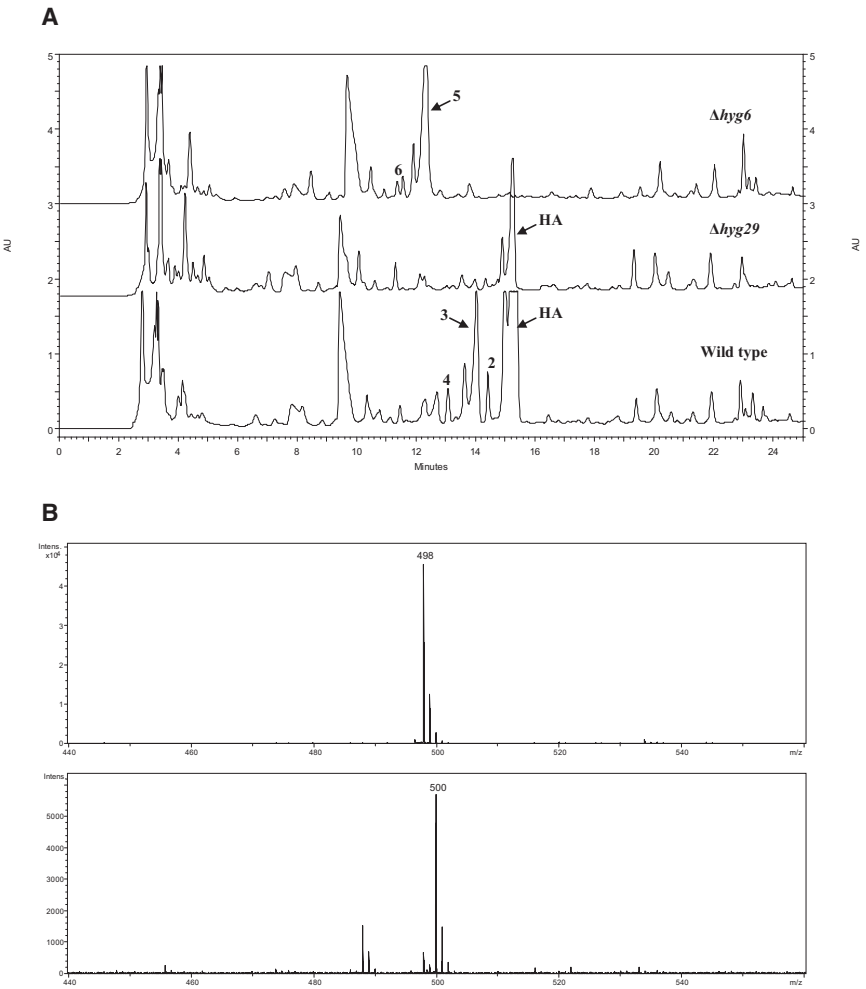

Figure 2. Effect of Methyltransferase gene (*hyg6*, *hyg29*) Disruptions on Hygromycin A Production

(A) Reverse-phase HPLC analysis of fermentation broths of wild-type, Δ*hyg29*, and Δ*hyg6* strains. Disruption of *hyg29* caused a decrease in hygromycin A production. Disruption of *hyg6* resulted in the generation of new metabolites with shorter retention times than hygromycin A.

(B) Mass spectrometric analysis (negative mode) of Δ*hyg6* fermentation broth. Two new species were identified with $[M-H]^-$ values of 498 and 500 corresponding to desmethylenehygromycin A (**5**) and 5″-dihydrodesmethylenehygromycin A (**6**), respectively.

chromatography (HPLC) and MS analyses of the fermentation broth of this strain revealed the same products (HA and **3**) at approximately 60% of those seen in the wild-type. In contrast, the production of HA was completely abolished in a Δ*hyg6* strain, and HPLC analysis of the fermentation broth of this mutant revealed a dominant new peak and an additional minor peak with shorter retention times than HA under the standard reverse-phase HPLC conditions (Figure 2). The major peak showed a mass in negative mode of m/z = 498 $[M - H]^-$ and the minor peak showed a mass of m/z = 500 $[M - H]^-$. An m/z of 499 is consistent with the mass of HA that is missing the methylene group bridging *O*-4 and *O*-5. An m/z of 501 observed for the smaller peak corresponds to a reduced derivative of the major peak. The MS analyses were thus consistent with production of desmethylene HA analogs (**5, 6**) (Figure 1) by the Δ*hyg6* strain. The production titers of **5** were ~400 mg/l. When subunit C was provided to this strain, low levels of HA could be observed although the levels of **5** were not significantly altered.

A unique feature of the aminocyclitol moiety of HA is the C4-C5 methylenedioxy bridge, which is essential for optimal biological activity (Hecker et al., 1992). Sequence analyses of the 29 ORFs of the HA gene cluster did not reveal a putative candidate gene product for the cyclization step of bridge formation. We had hypothesized that the *hyg7* gene product, which is homologous to D-aminoacylases/amidohydrolases, mediates formation of the amide bond between subunits B and C, and that a Δ*hyg7* mutant would accumulate **7.** However, as shown in Figure 3A, the Δ*hyg7* strain produced **3** and trace levels of **4**. Chemical complementation with subunit C, but not *myo*-inositol, led to a restoration of HA production (55% of that seen in the wild-type strain) (Figure 3A). A series of chemical complementation experiments of this strain with subunit C in the presence of either radiolabeled [2-^{3}H] *myo*-inositol or [carboxyl-^{14}C] 4-hydroxybenzoic acid was also carried out (Figure 3B). These analyses demonstrated that while HA production was restored by supplementation with subunit C, radiolabeled *myo*-inositol incorporation was only observed into **3**. A similar study with radiolabeled 4-hydroxybenzoic acid resulted, predictably, in its incorporation into both HA and **3**. Taken together, these observations clearly indicate that cyclization of the C5 methoxy group, resulting in formation of the methylenedioxy bridge, is dependant upon the *hyg7* gene product.

Structural Elucidation of Desmethylene HA Analogs

The two new compounds isolated from the Δ*hyg6* strain were purified by semipreparative HPLC and their structures were elucidated by nuclear magnetic resonance (NMR). The most obvious change observed in the ^{1}H-NMR spectra of **5** and **6** was the absence of either the three-proton singlet at ~3.5 ppm (for the *O*-5 methyl group of **3**), or two one-proton singlets at ~5.18 ppm and 4.83 ppm (for the methylene group bridging O-4 and O-5 of HA).

The differences in the ^{1}H-NMR spectra between **5** and **6** involve the fucofuranose moiety. The H-6″ signal for **5** is a singlet at 1.99 ppm (overlapping with protons from α–CH_3), whereas the H-6″ signal for **6** is a doublet at 1.20 ppm. The H-4″ signal is also shifted from ~4.4 ppm in **5** to 3.74 ppm in **6** (shifts are approximate for H-4″ in **5** because this signal is obscured by other signals at the same chemical shift). There is also a new signal

CHBIOL 1595

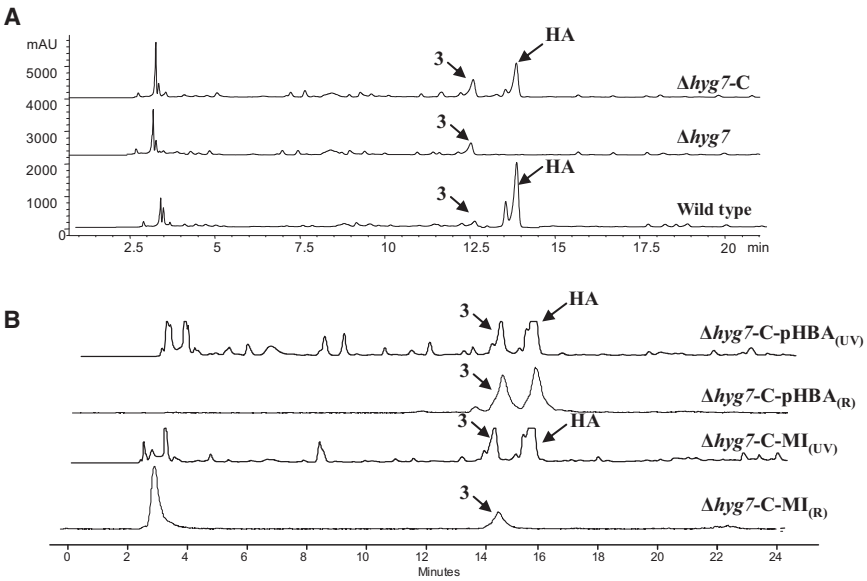

Figure 3. Effect of *hyg7* Gene Disruption on Hygromycin A Production

(A) Reverse-phase HPLC analysis of Δ*hyg7* fermentation broth. The Δ*hyg7* strain produced only compound **3**. Restoration of HA production was observed upon subunit C supplementation as seen in the HPLC chromatogram "Δ*hyg7*-C."

(B) HPLC analysis of Δ*hyg7* fermentation supplemented with C subunit in the presence of [2-^{3}H] *myo*-inositol or [carboxyl-^{14}C] 4-hydroxybenzoic acid. Δ*hyg7*-C-MI$_{(UV)}$ and Δ*hyg7*-C-pHBA$_{(UV)}$ are UV traces of fermentation broth of Δ*hyg7* supplemented with subunit C in the presence of [2-^{3}H] *myo*-inositol and [carboxyl-^{14}C] 4-hydroxybenzoic acid, respectively. Δ*hyg7*-C-MI$_{(R)}$ and Δ*hyg7*-C-pHBA$_{(R)}$ represent the radiolabeled traces recorded by Beta-Ram (R) radioactivity quantization system for their respective UV traces. This analysis clearly indicated the role of *hyg7* in the cyclization step of methylenedioxy bridge formation.

for H-5″ of **6** that appears at approximately 3.79 ppm, which is obscured by other signals.

Activity of Desmethylenehygromycin A

The antibacterial activity of **5** was determined using Δ*tolC E. coli* as test organism and compared with that of HA, **3**, and **7** to determine the importance of the methyl/methylene group on the cyclitol. The MIC$_{90}$ of HA for Δ*tolC E. coli* was determined to be 10 μg/ml (Table 2). Compounds **3** and **5** had much less activity, with the MIC$_{90}$ for both being 150 μg/ml. Compound **7** lacked inhibitory activity even at a concentration of 250 μg/ml. The compounds were also assessed for their ability to inhibit the synthesis of green fluorescent protein (GFP) using an *E. coli* in vitro coupled transcription-translation system (Dinos et al., 2004; Szaflarski et al., 2008). HA was shown to be highly active in vitro, having an IC$_{50}$ and IC$_{90}$ of 0.18 μM and 0.25 μM, respectively, whereas compound **7** was inactive exhibiting no effect on translation at 75 μM. In contrast to their poor MIC values, both **3** and **5** displayed significant activity as in vitro transcription-translation inhibitors, although their IC$_{50/90}$ values were higher than those of HA (Table 2, Figure 4).

Resistance of Δ*hyg29* Mutant Strain to HA

In order to verify whether the *hyg29* gene contributed to self-resistance of *S. hygroscopicus*, spores of the wild-type and Δ*hyg29* strains were grown on agar plates with different HA concentrations. The MIC$_{95}$ of HA for the wild-type was found to be 400 μg/ml. The mutant also showed high level of self-resistance, with an MIC$_{95}$ value of 300 μg/ml.

Table 2. Comparison of MIC$_{90}$ and IC$_{50/90}$ Data for Hygromycin A and Analogs

	HA	3	5	7
MIC$_{90}$ (μg/ml)	10	150	150	>250
IC$_{50}$ (μM)	0.18	0.5	0.32	>75
IC$_{90}$ (μM)	0.25	2	1	>75

DISCUSSION

Myo-inositol represents a common intermediate in the majority of pathways that generate aminocyclitol components of aminoglycoside antibiotics (Flatt and Mahmud, 2007; Mahmud, 2009). Branch points from this intermediate then give rise to the various products. In the proposed biosynthetic pathway (Figure 1B) that generates the aminocyclitol moiety of hygromycin A, this branching step is oxidation of the C5 hydroxyl of myo-inositol to form *neo*-inosose (Habib et al., 2003). The steps that precede *myo*-inositol are well known, reasonably widespread in organisms, and involve the sequential action of a MIP synthase (catalyzing formation of *myo*-inositol- phosphate from glucose 6-phosphate) and a MIP phosphatase. In actinomycetes these are essential activities, required for the biosynthesis of the essential metabolite mycothiol (the major cellular thiol and redox co-catalyst). For this reason, actinobacterial genomes mostly harbor more than one gene, and sometimes have several genes with either L-*myo*-inositol-1-phosphate synthase or inositol monophosphatase signatures (Wehmeier and Piepersberg, 2009). Thus for many aminocyclitol pathways, it appears that genes encoding these two enzymes are not necessarily located within the corresponding biosynthetic gene cluster. In the streptomycin producer *S. griseus*, a MIP synthase has been purified and it has been shown that the corresponding gene is not present in the streptomycin biosynthetic gene cluster (Flatt and Mahmud, 2007; Pittner et al., 1979; Sipos and Szabo, 1989). The MIP synthase is also lacking in the biosynthetic gene clusters of bluensomycin and spectinomycin (Flatt and Mahmud, 2007), although this enzymatic activity is presumably required for formation of these natural products. The partial loss of HA production with deletion of *hyg18* and restoration with *myo*-inositol are consistent with (1) Hyg18 encoding a putative MIP synthase required for efficient production of MIP and (2) the presence of an additional MIP synthase that can catalyze this reaction in *Streptomyces hygroscopicus*. A MIP phosphatase gene is present in the streptomycin (*strO*) and spectinomycin

Please cite this article in press as: Palaniappan et al., Biosynthesis of the Aminocyclitol Subunit of Hygromycin A in *Streptomyces hygroscopicus* NRRL 2388, Chemistry & Biology (2009), doi:10.1016/j.chembiol.2009.10.013

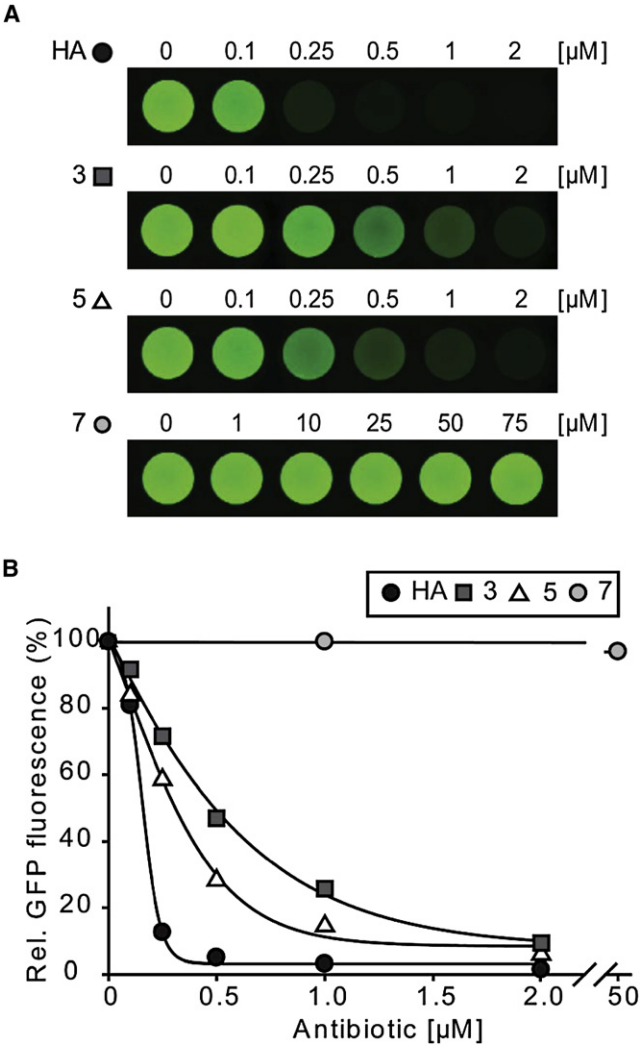

Figure 4. Effect of Hygromycin A and Derivatives on In Vitro Transcription-Translation

(A) Detection of template-dependent synthesis of GFP using fluorescence in the absence or presence of increasing concentrations (μM) of the antibiotic hygromycin A (HA), methoxyhygromycin A (**3**), desmethylenehygromycin A (**5**), or 5″-dihydroAB subunit (**7**) (see Figure 1 for structures).

(B) Quantitation of (A). GFP fluorescence is given as a percentage where 100% is defined as the fluorescence detected in the absence of the antibiotic.

(*speA*) gene clusters. The function of SpeA has also been biochemically confirmed (Ahlert et al., 1997; You-Young et al., 2003), although it has not been determined if these genes are essential for biosynthesis of the antibiotics. The *hyg25* gene product has conserved domains of the haloacid dehalogenase like hydrolase superfamily, which includes phosphatases (although there is no significant sequence similarity between Hyg25, and either known MIP phosphatases, StrO or SpeA). The wild-type production levels of HA by the *hyg25* mutant do not provide evidence that Hyg25 is a MIP phosphatase. However, because this is the only putative phosphatase in the HA biosynthetic gene cluster, the evidence indicates that an enzyme not encoded by the *hyg* gene cluster can catalyze dephosphorylation of MIP.

Steps subsequent to *myo*-inositol intermediate involve introduction of the amine functionality (at the C-5 hydroxyl) and introduction of the methyl group (at the C2 hydroxyl group). Although the exact order of these steps in the normal biosynthetic process is unclear, the production of desmethylenehygromycin A by Δ*hyg6* demonstrates that the amine functionality can be introduced without the methyl group. In such a pathway, the C-5 hydroxyl group would be oxidized to form *neo*-inosose, with a subsequent transamination to form *neo*-inosamine-2 (Figure 1B). The data with Δ*hyg17* strain (an almost a 90% reduction in HA yields relative to wild-type strain, and a 4-fold increase in these yields with supplementation with subunit C, but not *myo*-inositol) support the proposed role of this gene product as an *myo*-inositol dehydrogenase. The continued production of low levels of HA in this strain suggests that another enzyme or enzymes present in *S. hygroscopicus* are able to catalyze C5 oxidation of *myo*-inositol. The data with the Δ*hyg8* mutant (complete loss of HA production and modest HA production on supplementation with the subunit) support the proposed role of the gene product as the pyridoxal-phosphate-dependent aminotransferase that introduces the amine functionality. The poor yields of HA in the chemical complementation experiments with subunit C are puzzling, given how effective this moiety is at restoring HA production in other mutants. The HA shunt product **7,** which would be expected to form in the absence of adequate levels of the aminocyclitol moiety, was not observed in Δ*hyg8.* A polar effect from replacement of *hyg8* with the apramycin resistance marker may account for these observations (the current lack of a genetic complementation system did not permit this possibility to be tested). Another possible explanation is that the intermediate *neo*-inosamine-2 may have a key regulatory role. In principle, only Δ*hyg8* is unable to generate this intermediate.

The production of desmethylene analogs **5** and **6** by the Δ*hyg6* strain provide conclusive evidence that the C4-C5 methylene group in HA (and the methyl group in **3)** is carried out by an *O*-methylation activity of Hyg6 and not by Hyg29, the second methyltransferase homolog in the HA gene cluster (Figure 1). The high titers of **5** and **6** also demonstrate that introduction of the amine functionality in *myo*-inositol is not dependant upon methylation. The MIC analyses showed that the antibacterial activity of **5** against Δ*tolC E. coli* was 15 times less than that of HA. Interestingly, the MIC value of **5** was the same as that of **3**, which has a C5-OCH_3 group instead of the methylenedioxy bridge. The lower antibacterial activity of **3** has been reported previously (Chida et al., 1990; Yoshida et al., 1986). HA analogs in which the aminocyclitol is replaced by aminocyclohexadiols and aminocyclohexatriols have also shown markedly reduced biological activity (Hecker et al., 1992). The MIC data on the new shunt product **5** finalize these analyses, demonstrating that for maximal antibiotic activity subunit C must be an aminocyclitol and that this must be modified through formation of the methylenedioxy bridge. An unexpected observation is that removal of the methylenedioxy ring does not lead to a loss in the in vitro protein synthesis inhibition activity. Compounds **3** and **5**, where the methylenedioxy ring is disrupted, both retained potent protein synthesis inhibitory activity despite showing poor MIC values (Figure 4, Table 2). In contrast compound **7**, which lacks the aminocyclitol ring, is totally inactive. In fact, the IC_{50}

CHBIOL 1595

Please cite this article in press as: Palaniappan et al., Biosynthesis of the Aminocyclitol Subunit of Hygromycin A in *Streptomyces hygroscopicus* NRRL 2388, Chemistry & Biology (2009), doi:10.1016/j.chembiol.2009.10.013

of these compounds (0.3–0.5 μM) is comparable to that of the macrolide antibiotic tylosin (~0.4 μM) in the same in vitro transcription-translation assay (A.L.S. and D.N.W., unpublished data). These data suggest that the aminocyclitol ring is indeed essential for translation inhibition activity, whereas an intact methylenedioxy ring is not. It appears that the loss in biological activity due to methylenedioxy ring disruption stems from another factor, potentially a reduced uptake of the drug into the cell rather than abolishing the ribosome binding ability of the compound.

Inactivation of the second methyltransferase homolog, *hyg29*, resulted in a decrease in the yield of HA, although the antibiotic production profile and self-resistance were not affected. Because HA binds to the ribosomes, rRNA methylation by Hyg29 may provide a self-resistance mechanism in *S. hygroscopicus*. There is as yet no evidence to support such a role for *hyg29* and, moreover, ribosomal self-resistance is not always observed for ribosome-targeting antibiotics (e.g., oleandomycin) (Cundliffe, 1989). If the *hyg29* gene product is indeed an rRNA methylase, the high level of HA resistance of the Δ*hyg29* mutant suggests that in the absence of target-site modification by *hyg29*, self-resistance is possibly being conferred by the other resistance determinants in the HA gene cluster, namely a HA inactivating *O*-phosphotransferase (Dhote et al., 2008), and putative efflux pumps encoded by *hyg19* and *hyg28*.

The final step in the proposed pathway for formation of the C-subunit of HA is a oxidative cyclization to provide the methylenedioxy bridge. No gene product likely responsible for catalyzing this step was identified in the initial analyses of the *hyg* biosynthetic gene cluster (Palaniappan et al., 2006). The role of the *hyg7* gene product was unknown. A more detailed analysis has revealed clear homology of Hyg7 with aminoacylases, which catalyze hydrolytic deacetylation of *N*-acetyl-D-amino acids. Furthermore, Hyg7 is a member of the metallo-dependant hydrolase superfamily. Enzymes in this class have hydrolytic activities and typically have two, or less commonly one, metal ion-binding sites (Lai et al., 2004). Our analysis of Hyg7 revealed the four highly conserved residues (a Cys, Asp, and two His) that comprise a single metal-binding site and suggest a role in a hydrolytic process. Nonetheless, the selective production of methoxyhygromycin A (**3**) by Δ*hyg7* and the restoration of HA upon supplementation with subunit C clearly demonstrate that Hyg7 is required for the oxidative cyclization process which forms the methylenedioxy bridge of HA. Natural products with a methylenedioxy bridge have been identified more commonly in plants, and involve an initial methylation with subsequent action by a cytochrome p450 enzyme complex (Ikezawa et al., 2003). There are a limited number of examples of secondary metabolites from actinomycetes possessing methylenedioxy bridge. A 1,3-dioxine ring is found in dioxapyrrolomycin from *Streptomyces fumanus*, simaomicin from *Actinomadura madurae*, and the streptovaricins from *Streptomyces spectabilis* (Charan et al., 2006; Carter et al., 1989; Staley and Rinehart, 1991). FR-900109 from *S. prunicolor*, the dioxolides from *S. tendae*, and pseudoverticin from *S. pseudoverticillus* possess a 1,3-dioxolane ring similar to that seen in HA (Blum et al., 1996; Cui et al., 2007; Koda et al., 1983). Deuterium labeling studies in dioxapyrrolomycin by Charan et al. indicated an oxidative cyclization mechanism for methylenedioxy bridge formation similar to that reported for the plant metabolite berberine (Bjorklund et al., 1995; Charan et al., 2006). The *pyr20* gene product in the biosynthetic gene cluster of pyrrolomycin has resemblance to cytochrome P450 enzymes (and not to Hyg7) and has been proposed to potentially carry out the above function (Zhang and Parry, 2007). However, to the best of our knowledge there have been no genetic or biochemical characterization of the processes that lead to methylenedioxy bridge formation in bacterial natural product biosynthesis. Our results with *hyg7* represent the first example of in vivo characterization of a functional methylenedioxy bridge-forming gene of bacterial origin. Furthermore, the data indicate that a member of the metallo-dependent hydrolase superfamily, rather than a cytochrome p450 enzyme, is involved. The role of Hyg7 in this process, and the need for other enzymes or cofactors, remains to be biochemically determined.

The ability of subunit C to restore HA biosynthesis in most of the mutants described herein, demonstrates that it is an effective substrate for the enzyme that catalyzes amide bond formation. It is thus possible that the normal HA biosynthetic process involves formation of a complete C subunit prior to formation of the amide bond. Formation of **3** and **5**, and the apparent incorporation of valienamine, suggest relaxed substrate specificity of the corresponding coupling enzyme (Figure 1B). However, the data do not preclude the possibility that the final steps of C-subunit biosynthesis (methylation and formation of the methylenedioxy bridge) occur after amide bond formation.

SIGNIFICANCE

The roles of key *hyg* gene products in formation of the structurally unusual, methylene-bridged aminocyclitol of HA have been elucidated. Deletion of key genes in the pathway leads in some cases to accumulation of intermediates in the aminocyclitol biosynthetic process. As such the genetic tools to access novel HAs in *Streptomyces hygroscopicus* and to generate various aminocyclitols for combinatorial biosynthetic processes (generating new structurally diverse compounds) have been identified. The methylenedioxy bridge in HA has been shown not to be required for in vivo versus translation inhibition activity, but is required for biological uptake. These discoveries may help in the continued evaluation of HA-based structures for development of novel antibacterials. The discovery of the need for Hyg7 in the oxidative cyclization that yields the methylene-bridged aminocyclitol suggests a new enzymatic paradigm for formation of these unusual structural moieties.

EXPERIMENTAL PROCEDURES

Chemicals, Bacterial Strains, Growth Conditions, and General Procedures

Hygromycin A and 2L-2-amino-2-deoxy-4,5-*O*-methylene-*neo*-inositol (subunit C) were kindly supplied by Pfizer Inc. [2-^{3}H] *myo*-inositol (20.0 Ci/mmol) was purchased from Moravek Biochemicals. [carboxyl-^{14}C]-4-hydroxybenzoic acid was obtained from American Radiolabeled Chemicals Inc. All other antibiotics and chemicals were purchased from Sigma Aldrich. The *E. coli* Δ*tolC* strain, deficient in the outer membrane protein TolC, was procured from the *E. coli* Genetic Stock Center at Yale University. All *E. coli* strains were grown following standard protocols (Sambrook and Russell, 2001). *S. hygroscopicus* wild-type and mutant strains were maintained using media

Please cite this article in press as: Palaniappan et al., Biosynthesis of the Aminocyclitol Subunit of Hygromycin A in *Streptomyces hygroscopicus* NRRL 2388, Chemistry & Biology (2009), doi:10.1016/j.chembiol.2009.10.013

Table 3. PCR Primers Used for Gene Disruptions

Gene	Putative Function	Primer Name	Primer Sequence (5′-3′)
hyg6	Methyltransferase	*hyg6*_Forw	CGCCCCTCGACCGCGAAGACCTTCTGGGGGCAGCGGATG*ATTCCGGGGATCCGTCGACC*
		*hyg6*_Rev	ATGGTGGTCCGGCCTCCTCGTGTCGTCTGCGTGCCACTG*TGTAGGCTGGAGCTGCTTC*
hyg7	D-aminoacylase	*hyg7*_Forw	GACGACACGAGGAGGCCGGACCACCATGCATGACCTGAT*ATTCCGGGGATCCGTCGACC*
		*hyg7*_Rev	TCGCGCGCCCCGCCGGTGCGGCGGGCCGCCTCGCGGTC*ATGTAGGCTGGAGCTGCTTC*
hyg8	Aminotransferase	*hyg8*_Forw	CTGTCCGAGAAGGACTACGTCATCGAGCGGGACCGGCTG*ATTCCGGGGATCCGTCGACC*
		*hyg8*_Rev	GGTTTCCGCGAAGAACGCGTCCTGCATCGCCCGTGACCG*TGTAGGCTGGAGCTGCTTC*
hyg17	*myo*-inositol dehydrogenase	*hyg17*_Forw	TTCCGCCGTCGTGCGGGCCGCGGGGGTGAGCCGGTGAGC*ATTCCGGGGATCCGTCGACC*
		*hyg17*_Rev	GTCATCCCCTCGCGCCGCCGGCCAGGACGCCACCGGTC*ATGTAGGCTGGAGCTGCTTC*
hyg18	*myo*-inositol-1-phosphate synthase	*hyg18*_Forw	GGCCTGCGGCCCGGAGATTTCGCGAAGGGAAGAACCATG*ATTCCGGGGATCCGTCGACC*
		*hyg18*_Rev	CACGGGTCGGATCTCGGTTCGGAAACGCCCGGCGGCTCA*TGTAGGCTGGAGCTGCTTC*
hyg25	*myo*-inositol-1-phosphatase	*hyg25*_Forw	CACGCATGTCCGATACGACCGAATCGGGGTTGAGTGATG*ATTCCGGGGATCCGTCGACC*
		*hyg25*_Rev	GCGTCAGCGAATTCTGAGCCGCGCAACCGTCCGCGGTCA*TGTAGGCTGGAGCTGCTTC*
hyg29	Methyltransferase	*hyg29*_Forw	GCCGCCCGACCCGAGGCGCCCGGAGACGCCGCCGCGATG*ATTCCGGGGATCCGTCGACC*
		*hyg29*_Rev	GCCGTCCGGCCTCTGTCCACCAGCTGTGCGCCGCCTCCA*TGTAGGCTGGAGCTGCTTC*

The 39-nucleotide homologous region flanking the targeted gene is indicated in normal font. The italicized primer region is homologous to pIJ773.

and culture conditions as described earlier (Habib et al., 2003; Palaniappan et al., 2006). For qualitative analysis of the fermentation broths, the mycelium was removed by centrifugation and the supernatant was examined by HPLC and LC-MS as described previously (Palaniappan et al., 2006).

Targeted Disruption of the Aminocyclitol Biosynthetic Genes

The individual *hyg* genes were individually replaced with apramycin resistance cassette using the PCR-targeted *Streptomyces* gene replacement method (Gust et al., 2003; Palaniappan et al., 2006). The primer sequences used to amplify the resistance cassette from pIJ773 plasmid are listed in Table 3. All of the genes, except *hyg29*, were first disrupted in cosmid 17E3. For *hyg29* disruption, cosmid 15A10 was used. The recombinant cosmids were subsequently transferred to *S. hygroscopicus* wild-type by conjugation and the exoconjugants resulting from homologous recombination were selected based on resistance to apramycin. The genotype of the mutant strains was confirmed by PCR amplification using an appropriate set of outer primers (Table 3), and by sequencing the PCR product.

In the studies on *hyg8*, the apramycin resistance gene was removed from the *hyg8* mutant cosmid 17E3 using FLP recombinase. This cosmid with the 81 bp scar in place of *hyg8* sequence was then used to for replacement of *hyg7* with the apramycin resistance gene. The resulting 17E3 cosmid derivative was introduced into the wild-type *S. hygroscopicus* to provide the desired *hyg7+hyg8* deletion mutant.

Chemical Complementation Studies

The wild-type and appropriate mutant strains were grown in 5 ml production medium and treated with an amino sugar (the HA C subunit, glucosamine, galactosamine, or valienamine,) after 24 hr of fermentation to a final concentration of 5 mM. [2-^{3}H] *myo*-inositol and [carboxyl-^{14}C] 4-hydroxybenzoic acid were added to a final concentration of 0.4 μCi/ml. The supernatant was analyzed by HPLC and LC-MS after 6 days of fermentation (Palaniappan et al., 2006). Fermentation broths from the radiolabeled precursor feeding studies were analyzed by Beckman HPLC system linked to Beta-Ram (R) radioactivity quantization system (IN/US Systems, Inc.).

Quantitative Analysis of Antibiotic Production

Quantitative analyses of production of HA and its analogs were determined from triplicate cultures of the wild-type and mutant strains. Pure HA was used to generate a standard curve of peak area versus amount in μg within a 5 to 50 μg range. Then 50 μl filtered fermentation broth from each culture was used for HPLC analyses. The amounts of HA and related products in each injection sample were determined from their individual peak areas using the standard curve as reference and used to determine total production in the fermentations.

Purification and Characterization of Desmethylenehygromycin A (5) and 5″-Dihydrodesmethylenehygromycin A (6)

The desmethylene HA analogs (**5**, **6**) (Figure 1) produced by the Δ*hyg6* strain were extracted from culture filtrate and purified as described earlier (Palaniappan et al., 2006; Habib et al., 2003). The two products were characterized by MS and NMR techniques. ^{1}H-NMR spectra were recorded on a Bruker AMX-400 NMR. Two-dimensional correlated spectography correlation spectra were recorded on a Bruker AMX-600 NMR spectrometer. Coupling constants (*J*) were expressed in Hertz. Abbreviations for multiplicities are: s = singlet, d = doublet, t = triplet, q = quartet, m = multiplet.

Hygromycin A (1)

^{1}H-NMR (400 MHz, D_2O) δ 7.10 (1H, d, *J* = 8.0, H-9′), 7.01 (1H, s, H-3′), 6.88 – 6.91 (2H, m, H-5′, H-8′), 5.69 (1H, d, *J* = 4.4, H-1″), 5.18, 4.83 (2H, -OCH_2O-), 4.50 – 4.48 (1H, m, H-2), 4.40 – 4.18 (5H, m, H-2″, H-4″, H-4, H-5, H-6), 4.08 (1H, t, *J* = 2.8, H-3″), 3.95 (1H, dd, *J* = 5.2, H-1), 3.82 (1H, dd, *J* = 3.6, H-3), 2.16 (3H, s, H-6″), 2.02 (3H, s, α-CH_3).

Desmethylenehygromycin A (5)

^{1}H-NMR (400 MHz, D_2O) δ 7.14 (1H, d, *J* = 8.4, H-9′), 6.99 (1H, s, H-3′), 6.94 (1H, s, H-5′), 6.93 (1H, d, *J* = 8.4, H-8′), 5.72 (1H, d, *J* = 4.4, H-1″), 4.74 – 4.62 (1H, m, H-2), 4.41 – 4.40 (2H, m, H-3″, H-4″), 4.30 – 4.22 (1H, m, H-2″), 4.02 (1H, t, *J* = 2.8, H-5), 3.95 – 3.92 (2H, m, H-1, H-3), 3.72 (2H, dd, *J* = 10.0, 2.8, H-4, H-6), 1.99 (6H, s, α-CH_3, H-6″).

5″-Dihydrodesmethylenehygromycin A (6)

^{1}H-NMR (D_2O, 400 MHz) δ 7.17 (1H,d, *J* = 8.2, H-9′), 7.08 (1H, s, H-3′), 7.01 (1H, s, H-5′), 6.99 (1H, d, *J* = 8.2, H-8′), 5.69 (1H, d, *J* = 4.4, H-1″), ~4.7 (1H, partially obscured by solvent peak, H-2), 4.33-4.29 (2H, m, H-2″, H-3″), 4.11 (1H, t, *J* = 2.8, H-5), 4.03 (2H, dd, *J* = 10.0, 4.2, H-1, H-3), 3.87-3.80 (3H, m, H-4, H-6, H-5″), 3.74 (1H, t, *J* = 6.0, H-4″) 2.08 (3H, s, α-CH_3), 1.13 (3H, d, *J* = 6.8, H-6″).

MIC_{90} of HA and Analogs for Δ*tolC E. coli*

Five microliters of an overnight culture of Δ*tolC E. coli* were added to 195 μl final volume of fresh LB supplemented with HA or its analogs (Figure 1). The tubes were grown with shaking for 2 hr at 37°C and the absorbance at 600 nm was measured. The MIC_{90} was defined as the lowest concentration of the antibiotic at which 90% of growth was inhibited compared to a control *E. coli* culture grown in the absence of any antibiotic.

Coupled Transcription-Translation Assay

All coupled transcription-translation experiments were performed using an *E. coli* lysate-based system in the presence and absence of antibiotics as described previously (Dinos et al., 2004; Szaflarski et al., 2008). Reactions were transferred into 96-well microtiter plates and the GFP fluorescence was measured with a Typhoon Scanner 9400 (Amersham Bioscience) using

a Typhoon blue laser module (Amersham Bioscience). Images were then quantified using ImageQuantTL (GE Healthcare) and represented graphically using SigmaPlot (Systat Software, Inc.).

Hygromycin Sensitivity of Δ*hyg29* strain

The MIC_{95} of HA for the Δ*hyg29* mutant and the wild-type strain were determined by the agar plate dilution method (Dhote et al., 2008). Briefly, spores were plated on ISP2 agar plates containing varying amounts of HA, incubated at 30°C for 48 hr, and scored for growth. The MIC_{95} was defined as the lowest concentration of HA that prevented visible growth of 95% or more of the colony forming units on the agar plate.

ACKNOWLEDGMENTS

A part of this work was supported by the Deutsche Forschungsgemeinschaft (WI3285/1-1 to D.N.W.). We are grateful to Taifo Mahmud for providing valienamine.

Received: June 13, 2009
Revised: September 25, 2009
Accepted: October 16, 2009
Published: November 24, 2009

REFERENCES

Ahlert, J., Distler, J., Mansouri, K., and Piepersberg, W. (1997). Identification of stsC, the gene encoding the L-glutamine:scyllo-inosose aminotransferase from streptomycin-producing Streptomycetes. Arch. Microbiol. *168*, 102–113.

Bjorklund, J.A., Frenzel, T., Rueffer, M., Kobayashi, M., Mocek, U., Fox, C., Beale, J.M., Grtiger, S., Zenk, M.H., and Floss, H.G. (1995). Cryptic stereochemistry of berberine alkaloid biosynthesis. J. Am. Chem. Soc. *117*, 1533–1545.

Blum, S., Groth, I., Rohr, J., and Fielder, H.P. (1996). Biosynthetic capacities of actinomycetes. 5. Dioxolides, novel secondary metabolites from *Streptomyces tendae*. J. Basic Microbiol. *36*, 19–25.

Carter, G.T., Goodman, J.J., Torrey, M.J., Borders, D.B., and Gould, S.J. (1989). Biosynthetic origin of the carbon skeleton of simaomicin alpha., a hexacyclic xanthone antibiotic. J. Org. Chem. *54*, 4321–4323.

Charan, R.D., Schlingmann, G., Bernan, V.S., Feng, X., and Carter, G.T. (2006). Dioxapyrrolomycin biosynthesis in *Streptomyces fumanus*. J. Nat. Prod. *69*, 29–33.

Chida, N., Nakazawa, K., Ohtsuka, M., Suzuki, M., and Ogawa, S. (1990). Total synthesis of methoxyhygromycin and its 5-epimer. Chem. Lett. *19*, 423–426.

Cui, C.B., Han, B., Caib, B., and Wanga, H. (2007). Pseudoverticin, a novel benzoquinone-derived ansamycin antibiotic obtained as new cell cycle inhibitor from Streptomyces pseudoverticillus YN17707. Tetrahedron Lett. *48*, 4839–4843.

Cundliffe, E. (1989). How antibiotic-producing organisms avoid suicide. Annu. Rev. Microbiol. *43*, 207–233.

Dhote, V., Gupta, S., and Reynolds, K.A. (2008). An O-phosphotransferase catalyzes phosphorylation of hygromycin A in the antibiotic-producing organism Streptomyces hygroscopicus. Antimicrob. Agents Chemother. *52*, 3580–3588.

Dinos, G., Wilson, D.N., Teraoka, Y., Szaflarski, W., Fucini, P., Kalpaxis, D., and Nierhaus, K.H. (2004). Dissecting the ribosomal inhibition mechanisms of edeine and pactamycin: the universally conserved residues G693 and C795 regulate P-site RNA binding. Mol. Cell *13*, 113–124.

Flatt, P.M., and Mahmud, T. (2007). Biosynthesis of aminocyclitol-aminoglycoside antibiotics and related compounds. Nat. Prod. Rep. *24*, 358–392.

Guerrero, M.D., and Modolell, J. (1980). Hygromycin A, a novel inhibitor of ribosomal peptidyltransferase. Eur. J. Biochem. *107*, 409–414.

Gust, B., Challis, G.L., Fowler, K., Kieser, T., and Chater, K.F. (2003). PCR-targeted Streptomyces gene replacement identifies a protein domain needed for biosynthesis of the sesquiterpene soil odor geosmin. Proc. Natl. Acad. Sci. USA *100*, 1541–1546.

Habib, el-S.E., Scarsdale, J.N., and Reynolds, K.A. (2003). Biosynthetic origin of hygromycin A. Antimicrob. Agents Chemother. *47*, 2065–2071.

Hayashi, S.F., Norcia, L.J., Seibel, S.B., and Silvia, A.M. (1997). Structure-activity relationships of hygromycin A and its analogs: protein synthesis inhibition activity in a cell free system. J. Antibiot. (Tokyo) *50*, 514–521.

Hecker, S.J., Lilley, S.C., and Werner, K.M. (1992). Hygromycin A: preparation of aminocyclitol analogs defining the minimum functionality required for biological activity. Bioorg. Med. Chem. Lett. *2*, 1043–1046.

Ikezawa, N., Tanaka, M., Nagayoshi, M., Shinkyo, R., Sakaki, T., Inouye, K., and Sato, F. (2003). Molecular cloning and characterization of CYP719, a methylenedioxy bridge-forming enzyme that belongs to a novel P450 family, from cultured Coptis japonica cells. J. Biol. Chem. *278*, 38557–38565.

Kim, S.D., Kweon, M.H., Kim, C.J., and Yoo, I.D. (1990). Hygromycin, a plant growth inhibitor. Korean J. Biochem. *23*, 23–25.

Koda, S., Morimoto, Y., Yamashita, M., Komori, T., and Imanaka, H. (1983). Studies on a new antibiotic FR-900109. 2. X-ray structure determination of FR-900109 p-bromophenyl ester. J. Antibiot. (Tokyo) *36*, 1237–1238.

Lai, W.L., Chou, L.Y., Ting, C.Y., Kirby, R., Tsai, Y.C., Wang, A.H., and Liaw, S.H. (2004). The functional role of the binuclear metal center in D-aminoacylase: one-metal activation and second-metal attenuation. J. Biol. Chem. *279*, 13962–13967.

Lee, H.B., Kim, C.J., Kim, J.S., Hong, K.S., and Cho, K.Y. (2003). A bleaching herbicidal activity of methoxyhygromycin (MHM) produced by an actinomycete strain Streptomyces sp. 8E-12. Lett. Appl. Microbiol. *36*, 387–391.

Mahmud, T. (2003). The C7N aminocyclitol family of natural products. Nat. Prod. Rep. *20*, 137–166.

Mahmud, T. (2009). Progress in aminocyclitol biosynthesis. Curr. Opin. Chem. Biol. *13*, 161–170.

Mahmud, T., Flatt, P.M., and Wu, X. (2007). Biosynthesis of unusual aminocyclitol-containing natural products. J. Nat. Prod. *70*, 1384–1391.

Majumder, A.L., Chatterjee, A., Ghosh Dastidar, K., and Majee, M. (2003). Diversification and evolution of L-myo-inositol 1-phosphate synthase. FEBS Lett. *553*, 3–10.

Mann, R.L., Gale, R.M., and Van Abeele, R.F. (1953). Hygromycin. II. Isolation and properties. Antibiot. Chemother. *3*, 1279–1282.

Nakagawa, A., Fujimoto, T., Omura, S., Walsh, J.C., Stotish, R.L., and George, B. (1987). Hygromycin A, an antitreponemal substance. II. Therapeutic effect for swine dysentery. J. Antibiot. (Tokyo) *40*, 1627–1635.

Omura, S., Nakagawa, A., Fujimoto, T., Saito, K., Otoguro, K., and Walsh, J.C. (1987). Hygromycin A, an antitreponemal substance. I. Screening method and therapeutic effect for Treponema hyodysenteriae-caused infection in CF-1 mice. J. Antibiot. (Tokyo) *40*, 1619–1626.

Palaniappan, N., Ayers, S., Gupta, S., Habib, el-S., and Reynolds, K.A. (2006). Production of hygromycin A analogs in *Streptomyces hygroscopicus* NRRL 2388 through identification and manipulation of the biosynthetic gene cluster. Chem. Biol. *13*, 753–764.

Pittenger, R.C., Wolfe, R.N., Hoehn, P.N., Daily, W.A., and McGuire, J.M. (1953). Hygromycin. I. Preliminary studies in the production and biologic activity on a new antibiotic. Antibiot. Chemother. *3*, 1268–1278.

Pittner, F., Tovarova, I.I., Kornitskaya, E.Y., Khokhlov, A.S., and Hoffmann-Ostenhof, O. (1979). Myo-inositol-1-phosphate synthase from *Streptomyces griseus* (studies on the biosynthesis of cyclitols, XXXVIII). Mol. Cell. Biochem. *25*, 43–46.

Sambrook, J., and Russell, D.W. (2001). Molecular Cloning: A Laboratory Manual, Third Edition (Cold Spring Harbor, NY: Cold Spring Harbor Laboratory Press).

Sipos, L., and Szabo, G. (1989). Myo-inositol-1-phosphate synthase in different *Streptomyces griseus* variants. FEMS Microbiol. Lett. *53*, 339–343.

Staley, A.L., and Rinehart, K.L. (1991). Biosynthesis of the streptovaricins: 3-amino-5-hydroxybenzoic acid as a precursor to the meta-C7N unit. J. Antibiot. (Tokyo) *44*, 218–224.

Please cite this article in press as: Palaniappan et al., Biosynthesis of the Aminocyclitol Subunit of Hygromycin A in *Streptomyces hygroscopicus* NRRL 2388, Chemistry & Biology (2009), doi:10.1016/j.chembiol.2009.10.013

Szaflarski, W., Vesper, O., Teraoka, Y., Plitta, B., Wilson, D.N., and Nierhaus, K.H. (2008). New features of the ribosome and ribosomal inhibitors: non-enzymatic recycling, misreading and back-translocation. J. Mol. Biol. *380*, 193–205.

Uyeda, M., Mizukami, M., Yokomizo, K., and Suzuki, K. (2001). Pentalenolactone I and hygromycin A, immunosuppressants produced by *Streptomyces filipinensis* and *Streptomyces hygroscopicus*. Biosci. Biotechnol. Biochem. *65*, 1252–1254.

Wehmeier, U.F., and Piepersberg, W. (2009). Enzymology of aminoglycoside biosynthesis-deduction from gene clusters. Methods Enzymol. *459*, 459–491.

Yoshida, M., Takahashi, E., Uozumi, T., and Beppu, T. (1986). Hygromycin A and methoxyhygromycin A, novel inhibitors of K88 antigen synthesis of enterotoxic *Escherichia coli* strain. Agric. Biol. Chem. *50*, 143–149.

You-Young, J., Kim, S., Yang, Y.Y., Kang, C., Sohng, J., and Suh, J. (2003). Functional analysis of spectinomycin biosynthetic genes from *Streptomyces spectabilis* ATCC 27741. J. Microbiol. Biotechnol. *13*, 906–911.

Zhang, X., and Parry, R.J. (2007). Cloning and characterization of the pyrrolomycin biosynthetic gene clusters from Actinosporangium vitaminophilum ATCC 31673 and Streptomyces sp. strain UC 11065. Antimicrob. Agents Chemother. *51*, 946–957.

 ©2009 Elsevier Ltd All rights reserved

Paper 2

ANTIMICROBIAL AGENTS AND CHEMOTHERAPY, Dec. 2009, p. 5163–5172 Vol. 53, No. 12
0066-4804/09/$12.00 doi:10.1128/AAC.01069-09
Copyright © 2009, American Society for Microbiology. All Rights Reserved.

The Final Step of Hygromycin A Biosynthesis, Oxidation of C-5″-Dihydrohygromycin A, Is Linked to a Putative Proton Gradient-Dependent Efflux▽

Vidya Dhote,[1] Agata L. Starosta,[2,3] Daniel N. Wilson,[2,3] and Kevin A. Reynolds[1]*

Department of Chemistry, Portland State University, P.O. Box 751, Portland, Oregon 97207-0751,[1] and Center for Integrated Protein Science Munich (CiPS-M)[2] and Gene Center and Department of Chemistry and Biochemistry,[3] Ludwig-Maximilians-Universität München, Feodor-Lynen-Strasse 25, Munich D-81377, Germany

Received 30 July 2009/Returned for modification 28 August 2009/Accepted 9 September 2009

Hygromycin A (HA) is an aminocyclitol antibiotic produced and excreted by *Streptomyces hygroscopicus*. Deletion of *hyg26* from the hygromycin A biosynthetic gene cluster has previously been shown to result in a mutant that produces 5″-dihydrohygromycin A (DHHA). We report herein on the purification and characterization of Hyg26 expressed in *Escherichia coli*. The enzyme catalyzes an NAD(H)-dependent reversible interconversion of HA and DHHA, supporting the role of the reduced HA as the penultimate biosynthetic pathway intermediate and not a shunt product. The equilibrium for the Hyg26-catalyzed reaction heavily favors the DHHA intermediate. The high-titer production of the HA product by *S. hygroscopicus* must be dependent upon a subsequent energetically favorable enzyme-catalyzed process, such as the selective and efficient export of HA. *hyg19* encodes a putative proton gradient-dependent transporter, and a mutant lacking this gene was observed to produce less HA and to produce the DHHA intermediate. The DHHA produced by either the Δ*hyg19* or the Δ*hyg26* mutant had slightly reduced activity against *E. coli* and reduced protein synthesis-inhibitory activity in vitro. The data indicate that Hyg26 and Hyg19 have evolved to produce and export the final potent HA product in a coordinated fashion.

Antibiotic biosynthetic gene clusters contain genes required for the process of assembling the natural product and for the generation of specific biosynthetic precursors that are not readily available from primary metabolism (16). In addition, they often contain genes that are responsible for self-resistance, thereby protecting the organism from its own natural product, and regulatory genes that control the expression of biosynthetic genes. Although these gene classifications are useful, they are often incomplete in their descriptions. In fact, a complex interplay between biosynthesis, resistance, and regulation has been observed for many natural product biosynthetic processes, and it is becoming increasingly evident that some of these gene products perform multiple functions.

Hygromycin A (HA; compound 1) (Fig. 1) is an aminocyclitol antibiotic that acts by inhibiting the peptidyltransferase reaction of protein synthesis in gram-positive and gram-negative bacteria (7, 15, 25). Biosynthetic studies have shown that HA is assembled from three independently synthesized subunits, 5-dehydro-α-L-fucofuranose (subunit A), (*E*)-3-(3,4-dihydroxyphenyl)-2-methylacrylic acid (subunit B), and the aminocyclitol, 2L-2-amino-2-deoxy-4,5-*O*-methylene-*neo*-inositol (subunit C) (6). The corresponding biosynthetic gene cluster has been cloned and sequenced from *Streptomyces hygroscopicus* NRRL 2388, and putative functions have been assigned to the 29 open reading frames (22). The proposed role of *hyg26* as a short-chain dehydrogenase gene has also been verified at the genetic level (22).

Disruption of *hyg26* in *S. hygroscopicus* abolished the production of HA and methoxyhygromycin A (compound 3) and, instead, yielded their reduced analogs, 5″-dihydrohygromycin A (DHHA; compound 2) and 5″-dihydromethoxyhygromycin A (compound 4), respectively, and small amounts of (*E*)-3-(3-hydroxy-4-*O*-α-fucofuranosylphenyl)-2-methylacrylic acid (compound 7). Compound 7 is DHHA without the C subunit (see Fig. 1 for the structures). While these results showed that Hyg26 is required for the dehydrogenation of the C-5″ OH on the fucofuranose moiety, the timing of this reaction in the biosynthetic sequence and, subsequently, the question as to whether DHHA is a shunt metabolite or a precursor of the final product (HA) remain unresolved.

Analysis of the HA biosynthetic gene cluster has also revealed multiple genes likely to be involved in antibiotic resistance. Of these, the function of *hyg21* has been biochemically determined (4). *hyg21* encodes a phosphotransferase that inactivates HA by phosphorylating the C-2″ OH on the fucofuranose. A Δ*hyg21* strain has been shown to retain resistance to HA, indicating the presence of other mechanisms of self-resistance. Antibiotic transporters/efflux pumps are additional mechanisms of self-resistance in antibiotic producers and likely operate in *S. hygroscopicus* also, as all of the HA produced is found outside the cell. The HA biosynthetic gene cluster contains two putative HA transporter genes, *hyg19* and *hyg28*. The *hyg19* gene shows similarity to proton gradient-dependent transporter genes. The *hyg28* gene encodes a putative type II ATP-binding cassette transporter. The role of these gene prod-

* Corresponding author. Mailing address: Department of Chemistry, Portland State University, P.O. Box 751, Portland, OR 97207. Phone: (503) 725-3886. Fax: (503) 725-9525. E-mail: reynoldsk@pdx.edu.

▽ Published ahead of print on 21 September 2009.

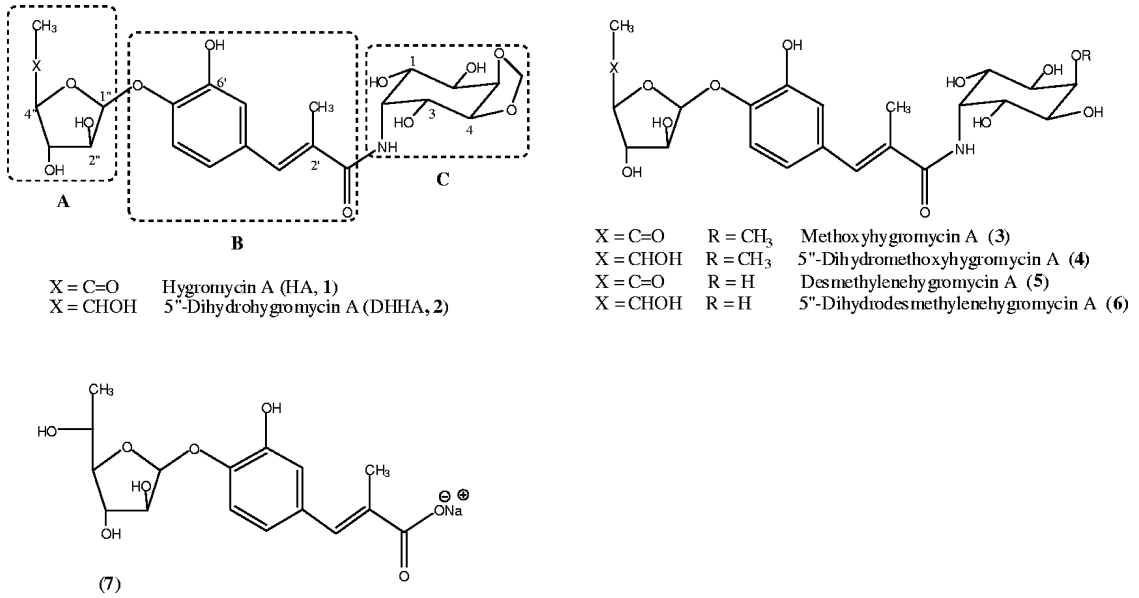

FIG. 1. Structures of HA and related compounds.

ucts in exporting HA or pathway intermediates and in contributing to self-resistance has not been determined.

In the work described here, we show that a recombinant Hyg26 catalyzes the reversible interconversion of DHHA and HA and that the equilibrium for this reaction lies heavily toward the biologically less active, reduced HA product. The putative proton gradient-dependent transporter encoded by *hyg19* is observed to be required for the high-level production of HA and is hypothesized to operate by the selective and efficient exportation of HA. A *hyg19* deletion mutant did not show increased sensitivity to HA, but a mutant in which both *hyg19* and *hyg21* were deleted had markedly increased HA sensitivity. This work has demonstrated that DHHA is likely the final biosynthetic pathway intermediate and that Hyg19 has a role in both self-resistance and biosynthesis, ensuring that the final and most biologically active HA product is generated.

MATERIALS AND METHODS

Chemicals, bacterial strains, and growth conditions. All antibiotics and chemicals were purchased from Sigma Aldrich unless otherwise stated. PCR primers were obtained from Integrated DNA Technologies. The enzymes used for DNA manipulations were obtained from New England Biolabs. HA was kindly provided by Pfizer Inc. DHHA, 5″-dihydromethoxyhygromycin A (compound 4), and (*E*)-3-(3-hydroxy-4-*O*-α-fucofuranosylphenyl)-2-methylacrylic acid (compound 7) were purified from the fermentation broth of mutant strain *S. hygroscopicus* SCH30 by a semipreparative high-performance liquid chromatography (HPLC) method, as described earlier (22). A Δ*hyg7* strain of *S. hygroscopicus* was used as the source for methoxyhygromycin A (compound 3). A Δ*hyg6* disruption strain was used as the source for desmethylenehygromycin A (compound 5) and 5″-dihydrodesmethylenehygromycin A (compound 6) (submitted for publication). The *S. hygroscopicus* strains were propagated by using the media and culture conditions described earlier (6, 22). The *Escherichia coli* strains were cultured by standard protocols (28). *E. coli* Δ*tolC* was procured from the *E. coli* Genetic Stock Center at Yale University.

Nucleotide and protein sequence analysis. Searches for sequences with homology to the sequences of the *hyg19*, *hyg26*, and *hyg28* genes were carried out with the BLAST suite of programs at the National Center for Biotechnology Information website (1). Protein sequence alignments were obtained by using the CLUSTALX program at the European Bioinformatics Institute website (14). Protein motif searches were carried out by using the PROSITE database at the Expasy proteomics server (9). Hydropathy analysis for Hyg19 was based on the amino acid hydropathy values of Kyte and Doolittle (13) and carried out at the Transporter Classification Database server (26, 27). The MEMSAT3 program was also used for prediction of the secondary structure and topology of Hyg19 (10).

Cloning, overexpression, and purification of recombinant Hyg26. The 816-bp *hyg26* gene was amplified from cosmid 17E3 (22). Primers were designed to introduce an NdeI restriction site at the initiation codon and a BamHI restriction site 3′ to the termination codon (Table 1). Amplification was performed by using the following temperature program: initial denaturation at 95°C for 5 min, 25 cycles of amplification (45 s of denaturation at 95°C, 45 s of primer annealing at 56°C, 1 min of extension at 72°C), and a final 7-min extension at 72°C. The gene was subsequently cloned into the NdeI and BamHI restriction sites of the pET15b vector (Novagen). The resulting pET15b-*hyg26* construct was introduced into the *E. coli* BL21-CodonPlus (DE3) expression host (Stratagene) by transformation. For protein expression, cells were grown at 37°C in LB medium containing 100 μg/ml ampicillin and 50 μg/ml chloramphenicol. When an A_{600} of 0.6 was reached, the culture flask was brought to room temperature (~23°C) and expression was induced by adding 0.5 mM isopropyl thio-β-D-galactoside. After a further 6 h of incubation, cells were harvested by centrifugation and stored at −80°C.

The N-terminal His-tagged Hyg26 was purified under native conditions according to Qiagen's Ni-nitrilotriacetic acid protocol. The cells were resuspended in BugBuster master mixture protein extraction reagent (Novagen) and lysed by incubation at room temperature for 30 min. The lysate was cleared by centrifugation; and the supernatant was loaded onto Ni-nitrilotriacetic acid agarose preequilibrated with buffer containing 50 mM NaH_2PO_4, 300 mM NaCl, and 10 mM imidazole (pH 8.0). The column was washed with buffer containing 50 mM NaH_2PO_4, 300 mM NaCl, and 20 mM imidazole (pH 8.0). The protein was eluted with the same buffer containing a higher concentration of imidazole (250 mM). Fractions containing Hyg26 were pooled, dialyzed overnight against a buffer (50 mM Tris-HCl, 20% glycerol, 5 mM 2-mercaptoethanol at pH 7.5), and stored at −80°C until further use.

Determination of molecular mass of Hyg26. The molecular mass of purified His-tagged Hyg26 was determined by size-exclusion chromatography with a Phenomenex BioSep-SEC-S4000 size-exclusion column fitted to an Agilent 1100 series HPLC system. The column was equilibrated and eluted with 20 mM sodium phosphate (pH 7.2) at a flow rate of 0.5 ml/min. Carbonic anhydrase (25 kDa), bovine serum albumin (66 kDa), β-amylase (200 kDa), apoferritin (443 kDa), and thyroglobulin (669 kDa) were used as standards.

Hyg26 enzyme assays and kinetic analyses. Initial enzyme assays were performed at 30°C with 4 μg of purified enzyme in a 100-μl reaction mixture of 50 mM Tris-HCl (pH 7.5) and 2 mM Tris(2-carboxyethyl) phosphine (TCEP). The dehydrogenase activity was studied by incubating Hyg26 with 100 μM DHHA,

TABLE 1. Primers used in this study

Primer purpose and primer	Sequence[a]
Disruption primers for *hyg19* gene	
Forward	**GATCCGACCCGTGCCGGGCGGAAGGGAGCACCAGTGATG***ATTCCGGGGATCCGTCGACC*
Reverse	**GGTGATGAGCGGGGCGCTGAGCCAGAGGAACATCACGAC***TGTAGGCTGGAGCTGCTTC*
Disruption primers for *hyg28* gene	
Forward	**CTGATGACTGCCACTCTCGTCGCCAAGGATCTGGCCGCC***ATTCCGGGGATCCGTCGACC*
Reverse	**CTCGGTGACCCGGCCGTCCGCCACCTCCAGGCGGCGGGT***TGTAGGCTGGAGCTGCTTC*
Disruption primers for *hyg19*, *hyg20*, and *hyg21* genes	
Forward	**GATCCGACCCGTGCCGGGCGGAAGGGAGCACCAGTGATG***ATTCCGGGGATCCGTCGACC*
Reverse	**ACCGTTGACCGAGAATGGGTAAAGGAGCAGAAAACAATG***TGTAGGCTGGAGCTGCTTC*
Expression primers for *hyg26* gene	
Forward	**CATATG**AGTGGACTGATGCGGGAC
Reverse	**GGATCC**TCAGAATTCGCTGACGC

[a] The 39-nucleotide homologous region flanking the targeted gene is indicated in boldface. The italicized primer region is homologous to pIJ773. The NdeI and BamHI sites in *hyg26* expression primers are also indicated in boldface.

compound 4, compound 6, or compound 7 and 1,000 μM NAD or NADP. For lactate dehydrogenase-coupled assays, 1,000 μM sodium pyruvate and 5 U of lactate dehydrogenase were added. The reductase activity was detected using 100 μM HA, compound 3, or compound 5 and 1,000 μM NADH or NADPH. After incubation for 2 h at 30°C, the sample was loaded onto a reverse-phase HPLC column (Agilent Eclipse XDB-C18) to detect the oxidized products (with longer retention times) in the dehydrogenase assay or the reduced products (with shorter retention times) in the reductase assay. Samples were separated at a flow rate of 1 ml/min with a methanol-water gradient, as described earlier (4). The optimal temperature and pH for Hyg26 reductase activity were determined with 100 μM HA and 1,000 μM NADH in a 15-min assay by the use of HPLC analysis and the peak area to quantitate the production of DHHA. The temperatures studied were 23°C (room temperature), 30°C, 37°C, and 42°C. For the pH studies, the following buffers were used: 50 mM potassium acetate, pH 4.0 and 5.0; 50 mM potassium phosphate, pH 6.0 and 7.0; and 50 mM Tris-HCl, pH 7.5, 8.0, and 9.0. The metal requirement was probed by conducting the assay in the presence of 5 mM and 10 mM EDTA. Kinetic analyses of reductase activity were carried out at 37°C for 15 min with 800 ng Hyg26 in 100 μl assay buffer comprised of 50 mM phosphate (pH 6) and 2 mM TCEP. The NADH concentration was fixed at 60 mM, while the antibiotic concentration was varied from 2 mM to 60 mM. For kinetic analyses of NADH, the HA concentration was fixed at 20 mM, while the NADH concentration was varied from 0.25 mM to 10 mM. Each assay was performed in duplicate, and the average values of the two measurements were plotted in the GraFit 4 program to determine the kinetic parameters.

Gene disruption experiments. The *hyg19* and *hyg28* genes and a segment of the HA biosynthetic gene cluster comprised of the *hyg19*, *hyg20*, and *hyg21* genes were individually replaced by the apramycin resistance cassette by the PCR targeted *Streptomyces* gene replacement method (8). The primers used to amplify the disruption cassette from plasmid pIJ773 are listed in Table 1. The primers used for *hyg28* disruption were designed such that the 68-nucleotide overlap between the 3′ end of *hyg28* and the 5′ end of the downstream *hyg29* gene was unaffected. The *hyg19* and the *hyg19*, *hyg20*, and *hyg21* disruptions were carried out in cosmid 17E3, while the *hyg28* gene disruption was done in cosmid 15A10 (22). The recombinant cosmids were introduced into a wild-type *S. hygroscopicus* strain by conjugation and selected for apramycin resistance. The genotype of the mutant strains was confirmed by PCR amplification of the apramycin cassette from chromosomal DNA and by verifying the sequence of the PCR product. Automated DNA sequencing was done at the Molecular Microbiology and Immunology Research Core Facility at Oregon Health and Science University. The DNA sequence data were analyzed by using Accelrys DS Gene software.

Analysis of antibiotic production in *S. hygroscopicus* strains. Fermentation broths of *S. hygroscopicus* disruption strains were analyzed for antibiotic production by HPLC and liquid chromatography-mass spectrometry methods on a Bruker Daltonics MicroTOF-Q instrument fitted with an Agilent 1100 series HPLC system. Cell extracts were generated by methanol lysis of the mycelia and were examined by HPLC (4). The production yields of HA and related metabolites were estimated from their corresponding peak areas in the chromatograms by using a standard curve of HA as a reference.

Susceptibilities of *S. hygroscopicus* strains to HA. The HA susceptibilities of *S. hygroscopicus* wild-type and mutant strains were determined by the agar plate dilution method, as described previously (4). Briefly, spores were plated on yeast extract malt extract agar plates containing various amounts of HA, incubated at 30°C for 48 h, and scored for growth. The MIC was defined as the lowest concentration of HA that prevented the visible growth of 95% or more of the CFU on the agar plate.

Bioactivity of DHHA and other dihydro analogs. The Δ*tolC E. coli* strain was used as the test organism to determine the antibiotic activities of DHHA and compounds 4, 6, and 7. The strain was grown in 200 μl LB medium at 37°C for 2 h in the presence of different concentrations of antibiotic, and the A_{600} was measured. The MIC was defined as the lowest concentration of the antibiotic at which 95% of bacterial growth was inhibited compared to the amount of growth of a control *E. coli* culture grown in the absence of any antibiotic.

Coupled transcription-translation assay. All coupled transcription-translation experiments were performed with an *E. coli* lysate-based system in the presence and absence of antibiotics, as described previously (5, 30). The reaction mixtures were transferred into 96-well microtiter plates, and the fluorescence of the green fluorescent protein (GFP) was measured with a Typhoon 9400 scanner (Amersham Bioscience) and a Typhoon blue laser module (Amersham Bioscience). The images were then quantified with the ImageQuantTL program (GE Healthcare) and are represented graphically by using the SigmaPlot program (Systat Software, Inc.).

RESULTS

Enzymatic characterization of a short-chain dehydrogenase encoded by *hyg26*. The *hyg26* gene from the HA biosynthetic gene cluster shows homology to short-chain dehydrogenase/reductase genes. A previous gene disruption study demonstrated that a Δ*hyg26* mutant accumulates DHHA and that Hyg26 is likely responsible for dehydrogenation of the C-5 OH on the L-fucofuranose moiety (22). It was suggested that this reaction may precede the glycosyltransferase reaction that connects the A subunit of HA to its B subunit. Alternatively, Hyg26 may act at a much later step in the biosynthetic pathway and may be responsible for converting DHHA to HA (Fig. 1). In such a case, DHHA could represent the penultimate pathway intermediate and not a shunt metabolite, and Hyg26 would be responsible for catalyzing the last step of HA biosynthesis. To probe this possibility, we generated and purified recombinant Hyg26 and determined its ability to interconvert HA and DHHA. A pET15b-*hyg26* expression vector was constructed

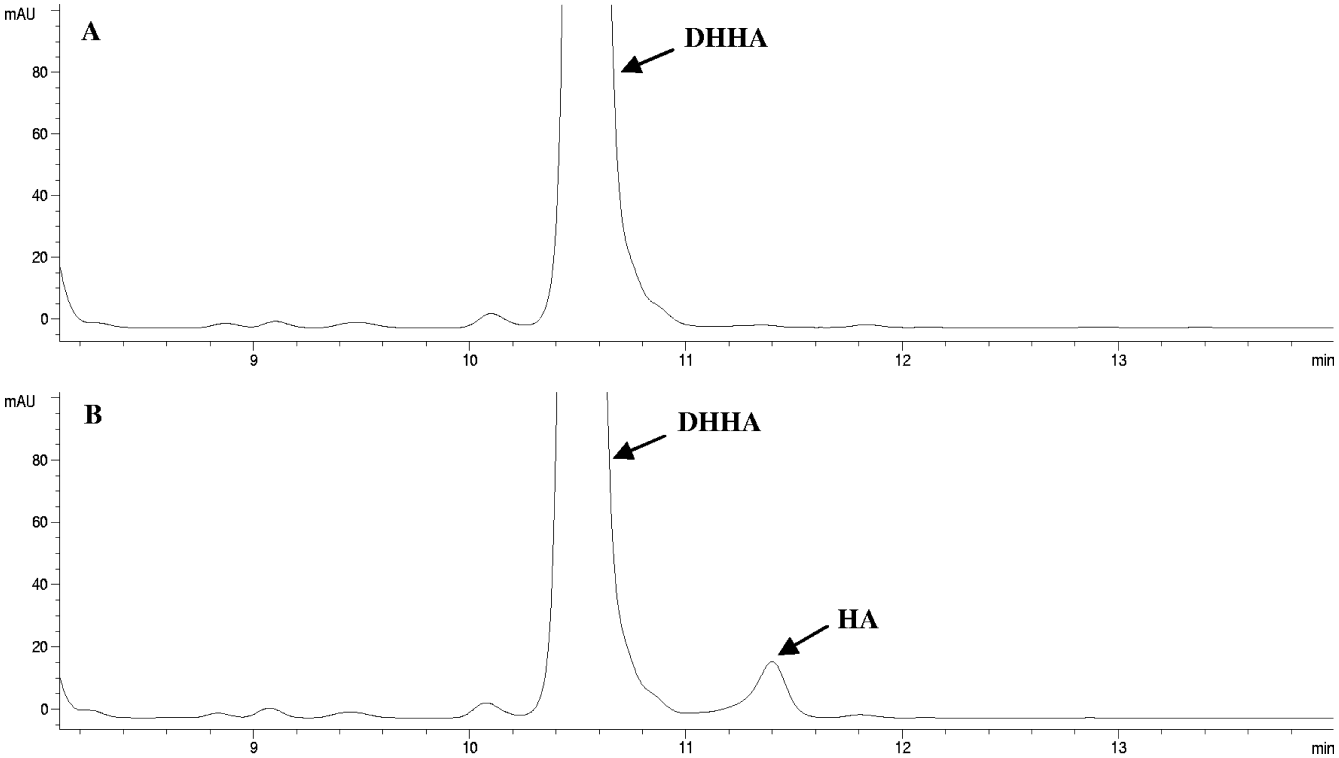

FIG. 2. Reverse-phase HPLC analysis of DHHA (compound 2) dehydrogenation by Hyg26. (A) Control reaction of DHHA and NAD^+ without Hyg26; (B) reaction of DHHA and NAD^+ after incubation with Hyg26 showing the formation of HA. mAU, milli-absorbance units.

and the N-terminal hexahistidine-tagged Hyg26 was purified by Ni^{2+} affinity chromatography. The purified protein showed the expected size of ~30 kDa on sodium dodecyl sulfate-polyacrylamide gel electrophoresis and an apparent molecular mass of 64,000 Da by size-exclusion chromatography, suggesting that recombinant Hyg26 is a dimeric protein.

The dehydrogenase activity was assayed by incubation of DHHA, compound 4, or compound 6 in the presence of NAD^+ or $NADP^+$ as a cofactor. In assays with NAD^+, reverse-phase HPLC analysis of each reaction mixture showed the appearance of a new peak with a retention time longer than that of the substrate (see Fig. 2 for the results of the assay with DHHA). This peak was not observed in a control assay without Hyg26 or in the assay with $NADP^+$. The retention time of the new peak, the results of coinjection experiments with the appropriate standards, and the results of mass spectrometric analyses were all consistent with the formation in the assays of the corresponding C-5″-oxidized analog (HA, compound 3, and compound 5), products of an Hyg26-dependent dehydrogenation. In each case, there was only a low level of product formation (1.2 to 1.5 μM from 100 μM of substrate after 2 h at 30°C). Attempts to increase the conversion level by the use of increased incubation times or by the performance of coupled enzymatic assays that would regenerate NAD^+ (by using pyruvate and lactate dehydrogenase) were unsuccessful.

The ability of Hyg26 to catalyze the reverse reaction (reductase activity) was also investigated. Assays were carried out with HA, compound 3, or compound 5 in the presence of NADH or NADPH, followed by HPLC analyses. Compared to the results for a control without Hyg26, each of the NADH assays showed a significant decrease in the amount of substrate and the appearance of a new peak with a retention time shorter than that of the substrate (see Fig. 3 for the results of the assay with HA). This peak was not observed in the reaction with NADPH. Mass spectrometric analyses of the NADH reaction mixtures showed that the compounds under the new peaks had an increase in mass by 2 atomic mass units with respect to the masses of the substrates, consistent with that expected for the C-5″-reduced analogs. Coinjections of the reaction mixtures with authentic materials provided additional support for the characterization of the reaction products. These observations confirm that Hyg26 is an NAD^+/NADH-dependent oxidoreductase with broad substrate specificity. These data also demonstrated that under the given assay conditions, the enzyme catalyzed the reverse reaction more efficiently than the forward biosynthetic reaction, suggesting that the equilibrium position favors the DHHA product.

The optimal pH for catalysis of the reduction reaction was determined over a pH range of 4.0 to 9.0 and was found to be 6.0. Among the temperatures from 23°C to 42°C that were tested, the optimal temperature was 37°C, although no significant difference was observed between the amounts of product formed at 30°C and 37°C. The metal-chelating reagent EDTA did not reduce the enzyme activity, suggesting that, like other short-chain dehydrogenases, Hyg26 is metal ion independent (24). Analysis of the steady-state kinetic parameters for the reduction of HA, compound 3, and compound 5 showed that Hyg26 has a very low affinity for them, as indicated by the high K_m values (in the millimolar range; Table 2). The catalytic efficiency, as indicated by k_{cat}/K_m, was found to be comparable

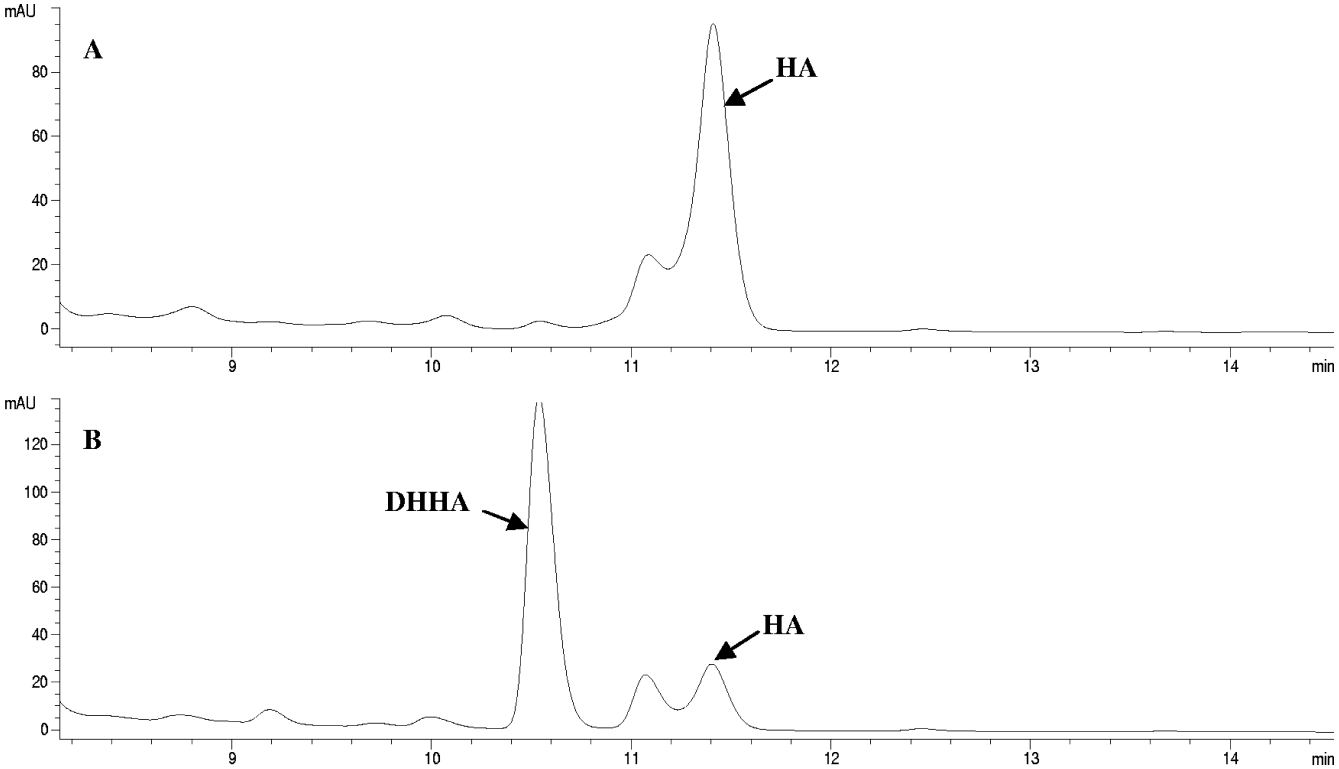

FIG. 3. Reverse-phase HPLC analysis of hygromycin A (HA) reduction by Hyg26. (A) Control reaction of HA and NADH without Hyg26; (B) reaction of HA and NADH after incubation with Hyg26, showing the formation of DHHA. An additional peak (11.1 min) eluting earlier than HA is the C-4″ epimer of HA and not a substrate for Hyg26. mAU, milli-absorbance units.

for all three substrates. The K_m for NADH was determined to be 400 ± 34 μM.

Predicted roles of *hyg19* and *hyg28* genes in the HA biosynthetic gene cluster. The biosynthetic gene cluster of hygromycin A has two genes, *hyg19* and *hyg28*, that encode putative transporter proteins. The predicted translation product of *hyg19* has 416 amino acids with a theoretical molecular mass of 43.8 kDa. A search of the National Center for Biotechnology Information protein sequence database by use of the deduced Hyg19 sequence returned several transmembrane proteins belonging to the major facilitator superfamily (MFS). The highest level of sequence similarity (66%) was observed with a presumptive transmembrane protein, Ata9, from the biosynthetic gene cluster of antibiotic A201A from *Saccharothrix mutabilis* subsp. *capreolus*. The structure of HA resembles that of A201A, particularly in the A and B subunits, and many genes with similar sequences and possibly similar functions have been identified in the biosynthetic gene clusters of these two antibiotics (22). The N-terminal region of Hyg19 specifically shows a high degree of similarity to the MFS proteins involved in drug efflux, such as the TetV tetracycline resistance determinant from *Mycobacterium smegmatis*, the MefA macrolide efflux protein from *Streptococcus pneumoniae*, and the chloramphenicol resistance protein from *Streptomyces lividans*. Hydropathy analysis and transmembrane topology prediction suggest that Hyg19 has 12 transmembrane helices with cytoplasmic N and C termini and, therefore, is likely a member of the proton gradient-dependent DHA12 family of MFS transporters. Five sequence motifs have been identified in the DHA12 efflux proteins (23). Hyg19 does not show full conservation of all the motifs but shows a partially conserved motif C (gxxxGPxxGGrl) in transmembrane 5 (positions 163 to 181), and a partially conserved motif G (GxxxGPL) in transmembrane 11 (positions 373 to 392) can clearly be distinguished. On the basis of these observations, Hyg19 is hypothesized to be a proton gradient-dependent efflux protein that confers resistance to *S. hygroscopicus* by exporting HA out of the cell.

TABLE 2. Kinetic parameters for Hyg26 reductase activity

Substrate	k_{cat} (s^{-1})	K_m (mM)	k_{cat}/K_m (M^{-1} s^{-1})
HA	5.1	5.8 ± 0.8	1.0×10^3
Methoxyhygromycin A (compound 3)	15.5	19.8 ± 1.9	0.9×10^3
Desmethylenehygromycin A (compound 5)	31.7	63.6 ± 24.4	0.9×10^3

The deduced translation product of *hyg28*, with 570 residues and a theoretical molecular mass of 61.5 kDa, shows homology to several ATP-binding cassette (ABC)-type transporter proteins, including Ard1 from the A201A gene cluster that is known to confer resistance to A201A in *S. lividans* (2). Two ABC domains containing the Walker A and Walker B motifs characteristic of ATPases are present in Hyg28. The Walker A motif ([AG]-x_4-G-K-[ST]) is a glycine-rich loop that binds to the phosphates of ATP or GTP (32). The Walker B motif

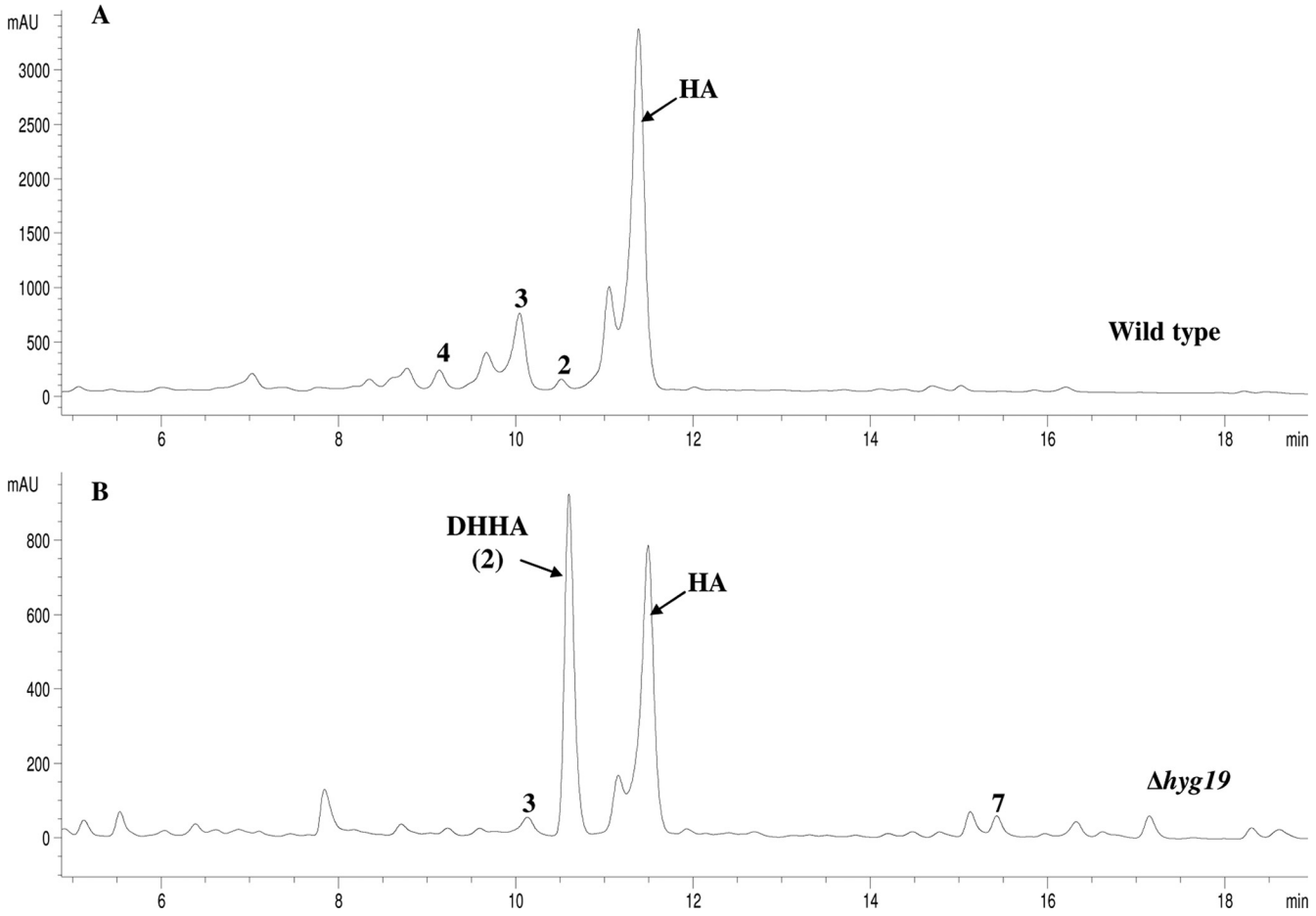

FIG. 4. Reverse-phase HPLC analysis of fermentation broth of the wild-type (A) and Δ*hyg19* (B) strains. Reduced HA production and accumulation of DHHA were observed in the Δ*hyg19* strain. mAU, milli-absorbance units.

(hhhhDEPT, where h indicates a hydrophobic residue) coordinates a magnesium ion (32). Therefore, the *hyg28* gene is predicted to encode a type II ABC transporter protein, which, in association with an unidentified membrane component, constitutes the second transporter system for HA efflux and subsequent self-resistance.

Effect of *hyg19* and *hyg28* gene disruptions on HA biosynthesis and efflux. In order to determine whether Hyg19 and Hyg28 are involved in antibiotic biosynthesis and efflux, the corresponding genes were individually replaced with the apramycin resistance cassette in the *S. hygroscopicus* wild type. The resulting mutant strains, Δ*hyg19* and Δ*hyg28*, were cultured; the mycelia were removed by centrifugation; and the filtered supernatants were analyzed by HPLC and liquid chromatography-mass spectrometry for antibiotic production. Analysis of the fermentation broth of the Δ*hyg28* mutant revealed that the antibiotic production profile was unaffected by the disruption of *hyg28*. The strain produced and excreted nearly the same amount (~1.5 g/liter) of HA as the wild type (data not shown). This clearly indicates that Hyg28 is not essential for antibiotic biosynthesis and efflux. On the other hand, the disruption of *hyg19* caused the level of HA production to drop to ~509 mg/liter, a threefold decrease compared to the HA yield from the wild type (Fig. 4). The levels of methoxyhygromycin A (compound 3) and 5″-dihydromethoxyhygromycin A (compound 4) (Fig. 1) also appeared to be similarly reduced. Interestingly, the yield of DHHA in Δ*hyg19* increased 10-fold to ~380 mg/liter from the ~37 mg/liter seen for the wild type. A slight increase in the amount of compound 7, detected only at trace levels in the wild type, was also observed in Δ*hyg19*. It was speculated that the reduced amount of HA in the fermentation broth of Δ*hyg19* could be a consequence of intracellular HA accumulation due to impaired transmembrane transport. To test this possibility, the mycelium of Δ*hyg19* was lysed by methanol treatment and the lyaste was analyzed by HPLC. The cell lysates of the wild type and Δ*hyg28* were also examined alongside in the same way. However, neither HA nor any known related compounds, including any phosphorylated forms, were detected in the cell lysates of either the Δ*hyg19* or the Δ*hyg28* strain. The data demonstrate that all detectable HA and related products are located outside the cell even in the absence of Hyg19. Nonetheless, the efficient and selective biosynthesis of HA is dependent upon the *hyg19* gene product.

Contribution of *hyg19* and *hyg28* gene products to self-resistance of *S. hygroscopicus*. The wild-type and mutant strains were assessed for their susceptibilities to HA by growing their spores on agar plates with antibiotics at different concentrations. The MIC of HA for the wild type was found to be 400

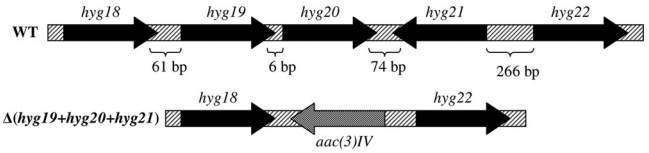

FIG. 5. Schematic representation of replacement of the *hyg19*, *hyg20*, and *hyg21* genes with the apramycin resistance cassette. WT, wild type.

μg/ml. The mutants also showed high levels of resistance, with MICs of 400 μg/ml and 300 μg/ml for Δ*hyg19* and Δ*hyg28*, respectively. These data indicate that the self-resistance of *S. hygroscopicus* is not entirely conferred by *hyg19* or *hyg28*. Another mutant strain was generated by disrupting *hyg19* together with the *hyg20* and *hyg21* genes present immediately downstream of it (Fig. 5). The *hyg20* gene encodes a putative transglucosylase/mutase for the generation of the A subunit, and its disruption has been observed to abolish antibiotic production completely (unpublished data). *hyg21* encodes an antibiotic-modifying *O*-phosphotransferase with a role in self-resistance, and loss of this gene results in reduced HA production (4). The Δ(*hyg19-hyg20-hyg21*) strain did not produce HA and showed significantly increased susceptibility (MIC, 75 μg/ml). A Δ*hyg20* strain had a MIC of 300 μg/ml, which was not significantly lower than that of the wild type. The MIC of *S. lividans* for HA was determined to be 20 μg/ml. These data suggest that the increased susceptibility of Δ(*hyg19-hyg20-hyg21*) is due to the loss of *hyg19* and *hyg21*, implying a synergistic role of these two genes in self-resistance.

Biological activity of C-5″-dihydro analogs. DHHA and compounds 4 and 6 are the C-5″-dihydro analogs of HA, methoxyhygromycin A (compound 3), and desmethylenehygromycin A (compound 5), respectively (Fig. 1). These three C-5″-dihydro compounds and compound 7 were studied for their ability both to inhibit the growth of Δ*tolC E. coli* and to inhibit protein synthesis in an *E. coli* in vitro-coupled transcription-translation system (5, 30). The MICs of DHHA, compound 2, and compound 4 were determined to be 20 μg/ml, 150 μg/ml, and 150 μg/ml, respectively (Table 3). These values are similar to the MICs for the corresponding 5″-oxidized analogs, albeit for the most active pair, HA appeared to be slightly more active (10 μg/ml) than DHHA. The DHHA analog lacking the C subunit (compound 7) was inactive against *E. coli* Δ*tolC* even at 250 μg/ml. The data demonstrate that for in vivo activity, the presence of the methylene bridge on the C subunit is of greater importance than the C-5″ oxidation state of the A subunit. HA

TABLE 3. Comparison of MIC and IC_{50}/IC_{90} data for HA and DHHA analogs

Compound	MIC (μg/ml)	IC_{50} (μM)	IC_{90} (μM)
HA	10	0.18	0.25
DHHA	20	0.3	1.5
3	150	0.5	2
4	150	7.4	50
5	150	0.32	1
6	150	2.7	14.1

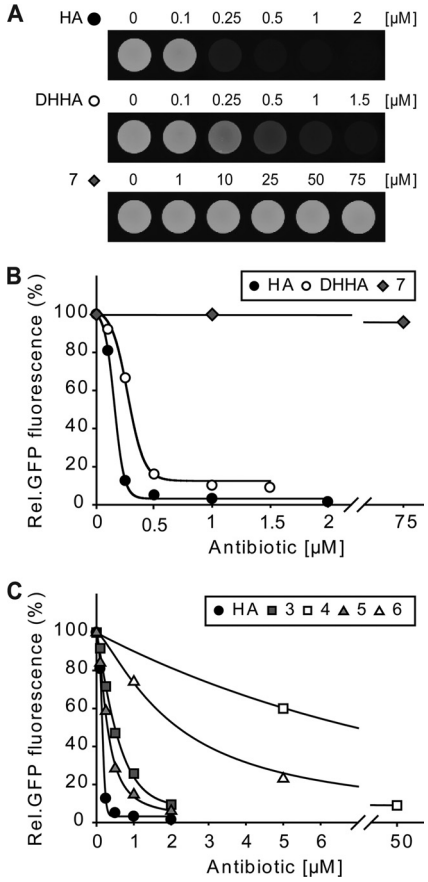

FIG. 6. Effects of HA and derivatives on in vitro transcription-translation. (A) Detection of template-dependent synthesis of GFP by using fluorescence and native polyacrylamide gel electrophoresis in the presence of template with increasing concentrations (μM) of the antibiotic HA, DHHA, and compound 7 on GFP synthesis; (B) quantitation of effects of HA, DHHA, and compound 7 on GFP synthesis; (C) quantitation of effects of HA and compounds 3, 4, 5, and 6 on GFP synthesis. The experiments whose results are shown in panels B and C were performed in triplicate. GFP fluorescence is given as a percentage, where 100% is defined as the fluorescence detected in the absence of the antibiotic. Rel., relative.

was also the most active compound in vitro, having a 50% inhibitory concentration (IC_{50}) and an IC_{90} of 0.18 μM and 0.25 μM, respectively, whereas compound 7 was inactive (consistent with the MICs), exhibiting no effect on translation at 75 μM (Fig. 6A and B and Table 3). On the basis of the IC_{50}s, compounds 3 and 5 were as effective as DHHA and their activities were similar to the activity of HA. In contrast, the reduced forms of these compounds, compounds 4 and 6, had significantly lower (8 to 15 times) potency (Fig. 6C and Table 3). The data demonstrate that for in vitro activity, the presence of the methylene bridge on the C subunit is of lesser importance than the C-5″ oxidation state of the A subunit.

DISCUSSION

hyg26 in the HA biosynthetic gene cluster encodes a protein that is a member of the short-chain dehydrogenase family. The requirement for this gene to obtain HA and not DHHA has

previously been demonstrated by a gene disruption study (22). Most short-chain dehydrogenase enzymes are dimers or tetramers and typically do not need a divalent metal ion for activity, unlike the classical metal-dependent medium-chain alcohol dehydrogenases (11, 18). The results of analyses of recombinant Hyg26 in the present study are consistent with it being a dimeric, metal ion-independent protein. The enzyme showed an absolute preference for NAD(H) and did not utilize NADP(H). The coenzyme-binding site of short-chain dehydrogenases preferring NAD(H) has an acidic residue (Asp or Glu) that forms hydrogen bonds with the hydroxyl groups of the adenine ribose, whereas the binding site for NADP(H) has two basic residues (Arg or Lys) that bind to the phosphate (12, 31). The specificity of Hyg26 for NAD(H) is consistent with the presence of an Asp residue at position 38 in the putative coenzyme-binding region within residues 12 to 38 (V**TG**AAR **GQG**REHAVRMAGE**G**ADVIAI**D**; conserved residues are indicated in boldface). Both the ability of Hyg26 to catalyze the interconversion of DHHA and HA and the production of DHHA by a Δ*hyg26* mutant are consistent with this being the last step of HA biosynthesis. A previous proposal that Hyg26 may catalyze the conversion of L-fucofuranose to 5-dehydro-α-L-fucofuranose during the formation of just the A subunit appears to be less likely.

Additional support for the hypothesis that DHHA is the penultimate intermediate in the HA pathway comes from the analyses of the Δ*hyg19* mutant. The equilibrium for the Hyg26-catalyzed process was observed to heavily favor DHHA, even though HA is the primary fermentation product. Loss of the subsequent energetically favorable step, which would shift the equilibrium toward HA, would be predicted to result in the formation of decreased of levels of HA and the formation of increased levels of DHHA, as seen for the Δ*hyg19* mutant. The possibility that this accumulation of DHHA arises from a polar effect on the adjacent *hyg20* is unlikely, as a *hyg20* deletion mutant does not produce any detectable levels of HA. There are several examples of this, in which the final steps of antibiotic biosynthesis are linked with efflux. In the case of nystatin biosynthesis by *S. noursei*, disruption of the *nysH* and *nysG* genes for a putative type III ABC transporter resulted in the accumulation of 10-deoxynystatin, a precursor of nystatin lacking the hydroxyl at C-10 (29). Furthermore, expression in the mutant strains of an additional copy of *nysL*, which presumably encodes a monooxygenase for C-10 hydroxylation, partially restored nystatin production with a concomitant decrease in 10-deoxynystatin. NysL has been expressed and has been shown to catalyze the hydroxylation of 10-deoxynystatin (29). The reaction has not been shown to be reversible (in contrast to the reaction observed for Hyg26), and there does not appear to be detectable inhibition of NysL by the product nystatin. Thus, while the observations indicate that the final biosynthetic step is balanced with efficient efflux, the biochemical basis seems to be less clear than that proposed herein for HA. A linkage between the final proposed step in chromomycin A3 biosynthesis, the conversion of dideacetylated precursor by a membrane-bound acetyltransferase, and exportation by a type I ABC transporter in *S. griseus* subsp. *griseus* have also been reported (17).

The increased level of production of DHHA by the Δ*hyg19* mutant is consistent with Hyg19 being the primary efflux pump responsible for the selective and efficient transport of HA. In our working hypothesis, Hyg19 is able to preferentially bind to and export HA over the intermediate DHHA (Fig. 7). These properties would contrast with those observed for Hyg26, which, in the reduction reaction, exhibited poor binding for HA (approximately 6 mM) and showed limited evidence of binding specificity (compounds 3 and 5 were also substrates). The poor HA binding by Hyg26 would permit facile transfer to Hyg19 for export. Hyg19 must also export HA sufficiently fast such that it is not phosphorylated by the resistance element, Hyg21 (this enzyme has an observed k_{cat} of 2.2 min^{-1} and a K_m for HA of 30 μM), and gets trapped inside the cell (4).

The presence of HA and DHHA in the fermentation broth of Δ*hyg19* implies the existence of an alternative system for antibiotic efflux (Fig. 7). This system would have reduced selectivity (exporting both HA and DHHA) relative to that for the process mediated by Hyg19. The most obvious candidate within the *hyg* biosynthetic gene cluster is the *hyg28*-encoded ABC transporter. Hyg28 does not appear to have a significant role in efflux in the wild type, as the Δ*hyg28* strain continues to produce wild-type levels of HA in the fermentation broth. The Hyg19 process may be significantly faster that that proposed to be catalyzed by Hyg28, or *hyg28* expression may increase in the Δ*hyg19* strain. Attempts to probe these possibilities by the generation of a mutant in which both genes have been deleted have thus far been unsuccessful. There are numerous precedents for the association of multiple efflux systems with antibiotic biosynthetic processes and, in particular, transporters that can excrete pathway intermediates. The 10-deoxynystatin intermediate, produced by deletion of the putative type III ABC transporter in *S. noursei*, is found in the fermentation broth, suggesting an additional efflux process (29). The premature efflux of landomycin D, an intermediate in landomycin A biosynthesis in *S. cyanogenus*, has been reported with either the overexpression of the proton gradient-dependent transporter gene *lanJ* or the disruption of the regulatory gene, *lanK*, that represses *lanJ* (19).

In addition to ensuring the production of the final HA product, Hyg19 also contributes to HA resistance in the producing organism. The loss of *hyg19* alone did not lead to decreased HA resistance. Similar observations with regard to resistance have been made for the landomycin E producer *S. globisporus* 1912. Self-resistance was not affected when the proton gradient-dependent transporter gene *lndJ* and the ABC transporter gene *lndW*, both of which occur in the landomycin E biosynthetic gene cluster, were independently disrupted. Heterologous expression of these genes, however, conferred resistance to landomycin E, proving their function as resistance genes (20, 21). The intrinsic resistance of an antibiotic producer is often due to the synergistic action of multiple gene products (3). This appears to be the case for HA self-resistance, as the simultaneous deletion of two putative HA resistance determinants, *hyg19* and *hyg21* (in addition to the *hyg20* biosynthetic gene), resulted in an increase in susceptibility greater than that achieved when either of them was individually disrupted (the HA susceptibility of the Δ*hyg21* mutant has been described separately [4]). In this mutant with triple mutations, both the proposed efficient HA efflux system and an enzyme that can modify and inactivate HA inside the cell are absent. The high

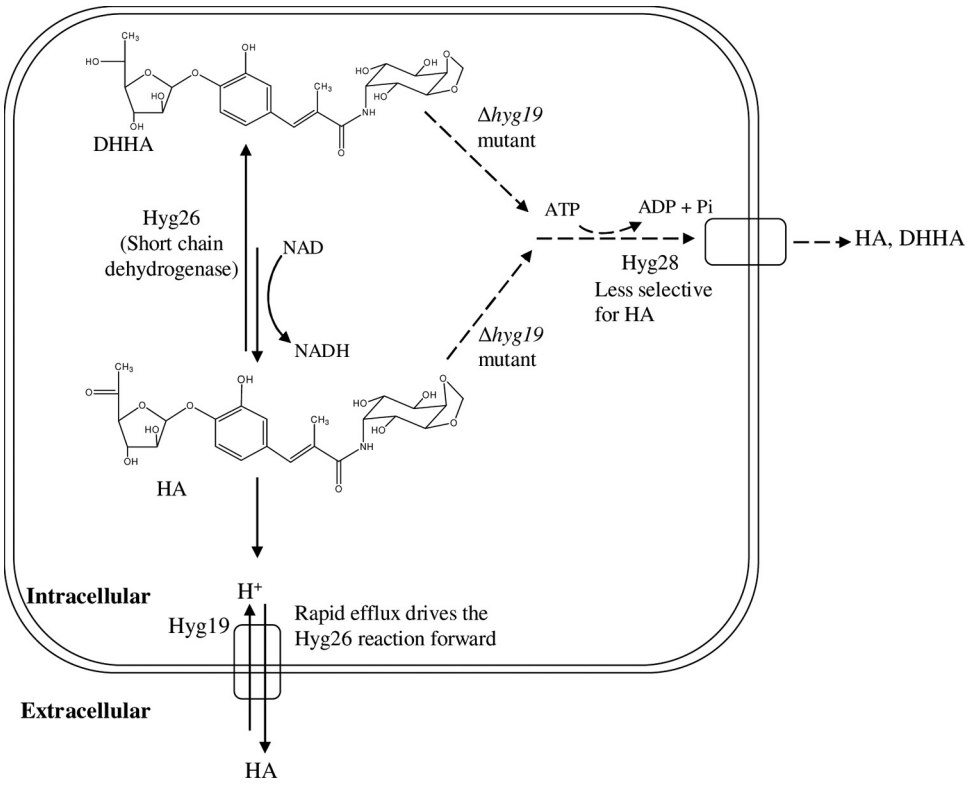

FIG. 7. Working hypothesis for the roles of Hyg19 and Hyg28 in antibiotic efflux. The proton gradient-dependent transporter, Hyg19, is the primary HA transporter in the wild type. Efflux in the Δ*hyg19* strain is hypothesized to be mediated by the ABC transporter, Hyg28, which is less selective for HA.

wild-type level resistance of the Δ*hyg20* HA-nonproducing strain [versus the reduced resistance seen for the mutant with triple mutations, Δ(*hyg19-hyg20-hyg21*)] suggests that HA is not essential for the induction of expression of the resistance genes. It is possible that the *hyg28* gene product and a putative methyltransferase encoded by *hyg29* may also contribute to resistance in the wild-type strain and to residual self-resistance in the Δ(*hyg19-hyg20-hyg21*) mutant with triple mutations. A gene inactivation experiment targeting all four putative resistance determinants has been pursued but has been unsuccessful to date.

These analyses provide compelling evidence that Hyg26 catalyzes the final step in HA biosynthesis and that Hyg19 plays a role in ensuring the efficient production of HA (and not the DHHA intermediate) as well as resistance to HA. The MIC and in vitro translation data indicate that HA is the most potent inhibitor (albeit only in tests against *E. coli*). The presence of the methylene bridge does not significantly affect translation inhibition in vitro but does lead to lower MICs, suggesting the importance of this group for some other aspect of the activity such as cellular uptake. In contrast, changes in the C5″ oxidation state clearly affect the in vitro activity of HA and its analogs, indicating a previously unknown role of this group in interacting with the ribosome target. Thus, the final steps of the HA biosynthetic process lead to a progressively more active compound, culminating in the most active and major product, HA, and have presumably evolved as a result of an ecological advantage to *S. hygroscopicus* in its natural environment.

ACKNOWLEDGMENT

A part of this work was supported by the Deutsche Forschungsgemeinschaft (grant WI3285/1-1 to D.N.W.).

REFERENCES

1. **Altschul, S. F., W. Gish, W. Miller, E. W. Myers, and D. J. Lipman.** 1990. Basic local alignment search tool. J. Mol. Biol. **215:**403–410.
2. **Barrasa, M. I., J. A. Tercero, R. A. Lacalle, and A. Jimenez.** 1995. The *ard1* gene from *Streptomyces capreolus* encodes a polypeptide of the ABC-transporters superfamily which confers resistance to the aminonucleoside antibiotic A201A. Eur. J. Biochem. **228:**562–569.
3. **Cundliffe, E.** 1989. How antibiotic-producing organisms avoid suicide. Annu. Rev. Microbiol. **43:**207–233.
4. **Dhote, V., S. Gupta, and K. A. Reynolds.** 2008. An *O*-phosphotransferase catalyzes phosphorylation of hygromycin A in the antibiotic-producing organism *Streptomyces hygroscopicus*. Antimicrob. Agents Chemother. **52:** 3580–3588.
5. **Dinos, G., D. N. Wilson, Y. Teraoka, W. Szaflarski, P. Fucini, D. Kalpaxis, and K. H. Nierhaus.** 2004. Dissecting the ribosomal inhibition mechanisms of edeine and pactamycin: the universally conserved residues G693 and C795 regulate P-site RNA binding. Mol. Cell **13:**113–124.
6. **el Habib, S. E., J. N. Scarsdale, and K. A. Reynolds.** 2003. Biosynthetic origin of hygromycin A. Antimicrob. Agents Chemother. **47:**2065–2071.
7. **Guerrero, M. D., and J. Modolell.** 1980. Hygromycin A, a novel inhibitor of ribosomal peptidyltransferase. Eur. J. Biochem. **107:**409–414.
8. **Gust, B., G. L. Challis, K. Fowler, T. Kieser, and K. F. Chater.** 2003. PCR-targeted *Streptomyces* gene replacement identifies a protein domain needed for biosynthesis of the sesquiterpene soil odor geosmin. Proc. Natl. Acad. Sci. USA **100:**1541–1546.
9. **Hulo, N., A. Bairoch, V. Bulliard, L. Cerutti, E. De Castro, P. S. Langendijk-Genevaux, M. Pagni, and C. J. Sigrist.** 2006. The PROSITE database. Nucleic Acids Res. **34:**D227–D230.
10. **Jones, D. T.** 2007. Improving the accuracy of transmembrane protein topology prediction using evolutionary information. Bioinformatics **23:**538–544.
11. **Jornvall, H., B. Persson, M. Krook, S. Atrian, R. Gonzalez-Duarte, J. Jeffery, and D. Ghosh.** 1995. Short-chain dehydrogenases/reductases (SDR). Biochemistry **34:**6003–6013.

12. **Kallberg, Y., U. Oppermann, H. Jornvall, and B. Persson.** 2002. Short-chain dehydrogenases/reductases (SDRs). Coenzyme-based functional assignments in completed genomes. Eur. J. Biochem. **269:**4409–4417.
13. **Kyte, J., and R. F. Doolittle.** 1982. A simple method for displaying the hydropathic character of a protein. J. Mol. Biol. **157:**105–132.
14. **Larkin, M. A., G. Blackshields, N. P. Brown, R. Chenna, P. A. McGettigan, H. McWilliam, F. Valentin, I. M. Wallace, A. Wilm, R. Lopez, J. D. Thompson, T. J. Gibson, and D. G. Higgins.** 2007. Clustal W and Clustal X version 2.0. Bioinformatics **23:**2947–2948.
15. **Mann, R. L., R. M. Gale, and R. F. Van Abeele.** 1953. Hygromycin. II. Isolation and properties. Antibiot. Chemother. **3:**1279–1282.
16. **Martin, M. F., and P. Liras.** 1989. Organization and expression of genes involved in the biosynthesis of antibiotics and other secondary metabolites. Annu. Rev. Microbiol. **43:**173–206.
17. **Menendez, N., A. F. Brana, J. A. Salas, and C. Mendez.** 2007. Involvement of a chromomycin ABC transporter system in secretion of a deacetylated precursor during chromomycin biosynthesis. Microbiology **153:**3061–3070.
18. **Oppermann, U., C. Filling, M. Hult, N. Shafqat, X. Wu, M. Lindh, J. Shafqat, E. Nordling, Y. Kallberg, B. Persson, and H. Jornvall.** 2003. Short-chain dehydrogenases/reductases (SDR): the 2002 update. Chem. Biol. Interact. **143–144:**247–253.
19. **Ostash, I., B. Ostash, A. Luzhetskyy, A. Bechthold, S. Walker, and V. Fedorenko.** 2008. Coordination of export and glycosylation of landomycins in *Streptomyces cyanogenus* S136. FEMS Microbiol. Lett. **285:**195–202.
20. **Ostash, I., B. Ostash, S. Walker, and V. Fedorenko.** 2007. Proton-dependent transporter gene *lndJ* confers resistance to landomycin E in *Streptomyces globisporus*. Genetika **43:**1032–1037.
21. **Ostash, I., Y. Rebets, B. Ostash, A. Kobylyanskyy, M. Myronovskyy, T. Nakamura, S. Walker, and V. Fedorenko.** 2008. An ABC transporter encoding gene *lndW* confers resistance to landomycin E. Arch. Microbiol. **190:** 105–109.
22. **Palaniappan, N., S. Ayers, S. Gupta, S. el Habib, and K. A. Reynolds.** 2006. Production of hygromycin A analogs in *Streptomyces hygroscopicus* NRRL 2388 through identification and manipulation of the biosynthetic gene cluster. Chem. Biol. **13:**753–764.
23. **Paulsen, I. T., M. H. Brown, and R. A. Skurray.** 1996. Proton-dependent multidrug efflux systems. Microbiol. Rev. **60:**575–608.
24. **Persson, B., M. Krook, and H. Jornvall.** 1991. Characteristics of short-chain alcohol dehydrogenases and related enzymes. Eur. J. Biochem. **200:**537–543.
25. **Pittenger, R. C., R. N. Wolfe, P. N. Hoehn, W. A. Daily, and J. M. McGuire.** 1953. Hygromycin. I. Preliminary studies in the production and biologic activity on a new antibiotic. Antibiot. Chemother. **3:**1268–1278.
26. **Saier, M. H., Jr., C. V. Tran, and R. D. Barabote.** 2006. TCDB: the Transporter Classification Database for membrane transport protein analyses and information. Nucleic Acids Res. **34:**D181–D186.
27. **Saier, M. H., Jr., M. R. Yen, K. Noto, D. G. Tamang, and C. Elkan.** 2009. The Transporter Classification Database: recent advances. Nucleic Acids Res. **37:**D274–D278.
28. **Sambrook, J., and D. W. Russell.** 2001. Molecular cloning: a laboratory manual, 3rd ed. Cold Spring Harbor Laboratory Press, Cold Spring Harbor, NY.
29. **Sletta, H., S. E. Borgos, P. Bruheim, O. N. Sekurova, H. Grasdalen, R. Aune, T. E. Ellingsen, and S. B. Zotchev.** 2005. Nystatin biosynthesis and transport: *nysH* and *nysG* genes encoding a putative ABC transporter system in *Streptomyces noursei* ATCC 11455 are required for efficient conversion of 10-deoxynystatin to nystatin. Antimicrob. Agents Chemother. **49:**4576–4583.
30. **Szaflarski, W., O. Vesper, Y. Teraoka, B. Plitta, D. N. Wilson, and K. H. Nierhaus.** 2008. New features of the ribosome and ribosomal inhibitors: non-enzymatic recycling, misreading and back-translocation. J. Mol. Biol. **380:**193–205.
31. **Tanaka, N., T. Nonaka, M. Nakanishi, Y. Deyashiki, A. Hara, and Y. Mitsui.** 1996. Crystal structure of the ternary complex of mouse lung carbonyl reductase at 1.8 Å resolution: the structural origin of coenzyme specificity in the short-chain dehydrogenase/reductase family. Structure **4:**33–45.
32. **Walker, J. E., M. Saraste, M. J. Runswick, and N. J. Gay.** 1982. Distantly related sequences in the alpha- and beta-subunits of ATP synthase, myosin, kinases and other ATP-requiring enzymes and a common nucleotide binding fold. EMBO J. **1:**945–951.

Paper 3

doi:10.1016/j.jmb.2008.11.042 J. Mol. Biol. (2009) 385, 1179–1192

JMB

Available online at www.sciencedirect.com

ScienceDirect

ELSEVIER

Time-Resolved Binding of Azithromycin to *Escherichia coli* Ribosomes

Alexandros D. Petropoulos[1]†, Ekaterini C. Kouvela[1]†, Agata L. Starosta[2,3], Daniel N. Wilson[2,3], George P. Dinos[1] and Dimitrios L. Kalpaxis[1]*

[1]*Laboratory of Biochemistry, School of Medicine, University of Patras, 26504 Patras, Greece*

[2]*Gene Center and Department of Chemistry and Biochemistry, Ludwig-Maximilians-Universitat Munchen, Feodor-Lynen-Strasse 25, D-81377 Munich, Germany*

[3]*Munich Center for Integrated Protein Science CiPS, University of Munich, Germany*

Received 8 October 2008; received in revised form 13 November 2008; accepted 18 November 2008
Available online 27 November 2008

Azithromycin is a semisynthetic derivative of erythromycin that inhibits bacterial protein synthesis by binding within the peptide exit tunnel of the 50S ribosomal subunit. Nevertheless, there is still debate over what localization is primarily responsible for azithromycin binding and as to how many molecules of the drug actually bind per ribosome. In the present study, kinetic methods and footprinting analysis are coupled together to provide time-resolved details of the azithromycin binding process. It is shown that azithromycin binds to *Escherichia coli* ribosomes in a two-step process: The first-step involves recognition of azithromycin by the ribosomal machinery and places the drug in a low-affinity site located in the upper part of the exit tunnel. The second step corresponds to the slow formation of a final complex that is both much tighter and more potent in hindering the progression of the nascent peptide through the exit tunnel. Substitution of uracil by cytosine at nucleoside 2609 of 23S rRNA, a base implicated in the high-affinity site, facilitates the shift of azithromycin to this site. In contrast, mutation U754A hardly affects the binding process. Binding of azithromycin to both sites is hindered by high concentrations of Mg^{2+} ions. Unlike Mg^{2+} ions, polyamines do not significantly affect drug binding to the low-affinity site but attenuate the formation of the final complex. The low- and high-affinity sites of azithromycin binding are mutually exclusive, which means that one molecule of the drug binds per *E. coli* ribosome at a time. In contrast, kinetic and binding data indicate that in *Deinococcus radiodurans*, two molecules of azithromycin bind cooperatively to the ribosome. This finding confirms previous crystallographic results and supports the notion that species-specific structural differences may primarily account for the apparent discrepancies between the antibiotic binding modes obtained for different organisms.

© 2008 Elsevier Ltd. All rights reserved.

Keywords: azithromycin; ribosome; peptide exit tunnel; peptidyl transferase; slow binding inhibitors

Edited by D. E. Draper

Introduction

Azithromycin is a semisynthetic derivative of erythromycin, possessing a 15-membered lactone ring that is structurally distinguished by the absence of a keto oxygen at position C9 and the insertion of a methyl-substituted nitrogen at position C10 (Fig. 1). These structural features allow for high stability of azithromycin in acidic aqueous media,[1] better pharmacokinetic characteristics,[2] and improved potency against Gram-negative microorganisms, while retaining the efficacy of erythromycin against Gram-positive microbes.[3] For susceptible *Escherichia coli*

*Corresponding author. E-mail address: dimkal@med.upatras.gr.

† A.D.P. and E.C.K. contributed equally to this work.

Abbreviations used: PTase, peptidyl transferase; DMS, dimethyl sulfate; CMCT, 1-cyclohexyl-3-(2-morpholinoethyl) carbodiimide metho-*p*-toluene; PAE, post antibiotic effect; TRNOE, transferred nuclear Over Hauser effect.

0022-2836/$ - see front matter © 2008 Elsevier Ltd. All rights reserved.

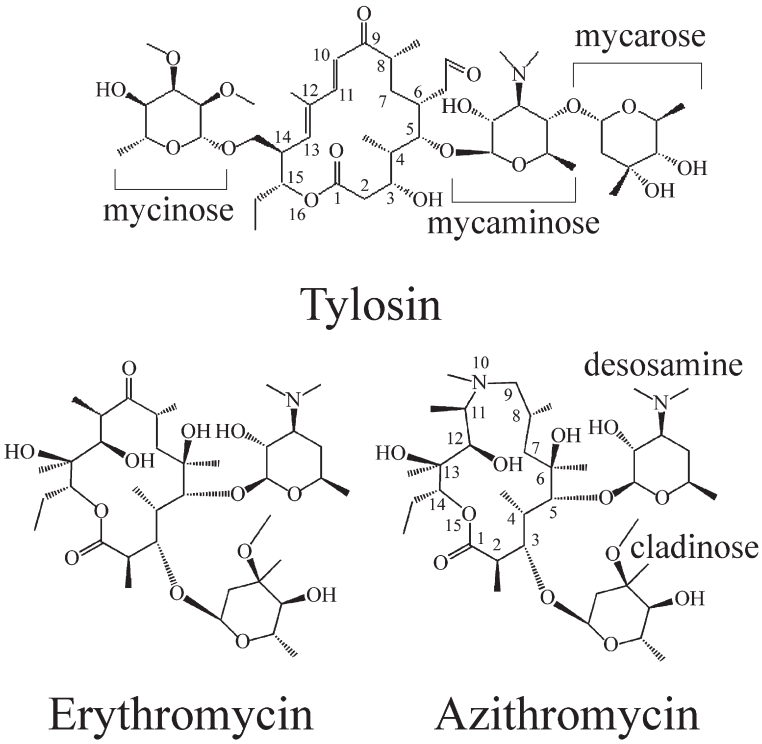

Fig. 1. Chemical structures of tylosin, erythromycin, and azithromycin.

strains, azithromycin is 8 to 15 times more active than erythromycin.[4,5] Although the superior potency of azithromycin has been attributed to its faster penetration of the outer membranes of Gram-negative bacteria,[6,7] this drug also exhibits better ability than erythromycin to compete for [^{14}C]erythromycin-binding sites in *Staphylococcus aureus* ribosomes and higher affinity for *E. coli* ribosomes.[8–11]

Accumulated biochemical and genetic evidence suggests that azithromycin exerts its inhibitory effect on microbial growth by binding in a narrow part of the peptide exit tunnel, at a position that is situated between the peptidyl transferase (PTase) center and a constriction in the tunnel formed by proteins L4 and L22.[5,8,12–17] Binding of the drug at this region occludes the lumen of the tunnel, thus aborting the growth of the nascent peptide chain during the early rounds of translation, eventually leading to peptidyl–tRNA "drop-off".[18] An additional inhibitory target of azithromycin in susceptible bacterial cells is the assembly of the 50S subunit; azithromycin, like erythromycin, stalls the normal assembly sequence, leading to the accumulation of an incomplete ribosomal particle that is subsequently degraded.[19] Moreover, a recent microarray analysis indicated that azithromycin at subinhibitory concentrations can activate as well as repress different subsets of genes in *Pseudomonas aeruginosa*.[20]

In the past few years, the structures of the archaeal and bacterial large ribosomal subunits and their complexes with azithromycin have been solved by X-ray crystallography.[21,22] Not only did this structural information improve our understanding of how azithromycin binds to the ribosome, but it could also provide tools to assess previous findings regarding macrolide resistance conferred by base substitutions or modifications in 23S rRNA and mutations of ribosomal proteins. Although there is an underlying similarity between the archaeal and bacterial crystallographic models in the localization of azithromycin-binding site, the precise position and conformation of the lactone ring of azithromycin seen in these structures differ significantly (Fig. 2). An additional notable difference relates to the number of azithromycin molecules bound per ribosome. In contrast to the one molecule found in the archaeal structure, two molecules of the drug were observed in the structure of *Deinococcus radiodurans* 50S subunit complexed with azithromycin. One of the azithromycin molecules (AZI-1) is found in the conventional macrolide-binding site, while the other (AZI-2) is located directly adjacent to it, but deeper in the tunnel, making direct contacts with proteins L4 and L22 as well as with domain II of 23S rRNA (Fig. 2a). It has been suggested that the mode of dual binding is species specific.[23] Consistent with this suggestion is the finding that, although the general ribosomal architecture between archaea and bacteria is the same, the nature and precise orientation of the rRNA and ribosomal protein residues in their ribosomes differ in details. For instance, wild-type archaeal ribosomes contain a guanosine at position 2058 (*E. coli* numbering is used throughout the text) of 23S rRNA, whereas *D. radiodurans*, like most eubacteria, contains an adenosine at the equivalent position. It is known that mutation A2058G in eubacteria confers resistance against macrolides.[12] Consequently, A/G difference at position 2058 may account for the structural discrepancies obtained. This possibility was investigated by Tu *et al.*, using a *Haloarcula marismortui* strain containing mutation

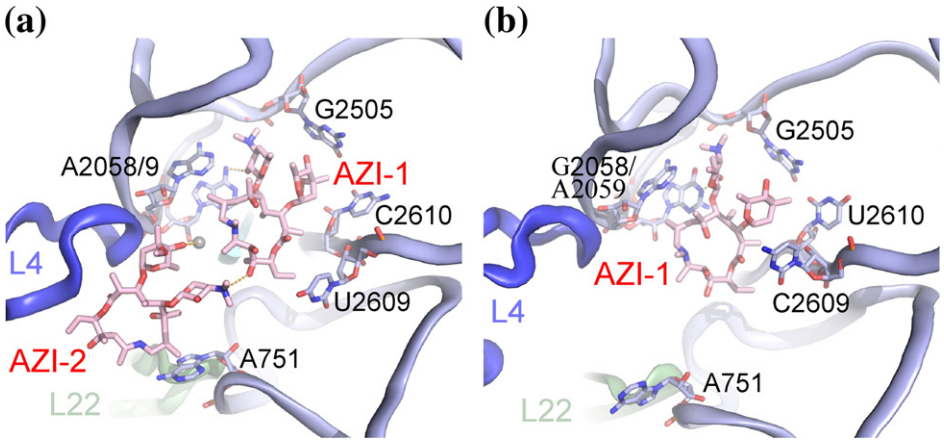

Fig. 2. The binding site(s) of azithromycin on the 50S ribosomal subunit. (a) Binding of two molecules of azithromycin (pink) to the *D. radiodurans* 50S ribosomal subunit (Protein Data Bank accession no. 1NWY). Parts of domain V and helix H35 of 23S rRNA (light blue) as well as parts of ribosomal proteins L4 (dark blue) and L22 (light green) are shown by ribbon representation. Important nucleoside residues for macrolide binding are presented by their structures (*E. coli* numbering); those contributing to hydrogen bonds are connected with the drug by dotted lines. (b) Binding position of azithromycin on the *H. marismortui* 50S ribosomal subunit (Protein Data Bank accession no. 1M1K). Labeling is the same as in (a).

G2058A.[24] It was found that azithromycin binds to wild-type and mutant 50S subunits of *H. marismortui* in a virtually identical way, making impossible the hypothesis that the variability of azithromycin binding to bacterial and archaeal 50S subunits may be attributed to sequence differences at position 2058. However, it is worth considering the possibility that the two azithromycin-bound molecules in the 50S ribosomal subunit from *D. radiodurans* may result from other idiosyncratic structural characteristics of this bacterium[23] and/or the near *in vivo* ionic conditions followed during the crystal preparation[25] or reflect snapshots of azithromycin binding at different steps of the drug binding process. With respect to the latter postulation, it should be mentioned that kinetic and NMR studies have provided evidence that binding of azithromycin to *E. coli* ribosomes occurs in a two-step process, the first one involving the recognition and selection of the drug by the ribosomal machinery and the second one being the strong interaction responsible for the protein synthesis inhibition.[10,26,27]

In the present study, chemical footprinting and kinetic analysis are applied together in a dual strategy to investigate the entire course of azithromycin binding to *E. coli* functional ribosomes and to monitor the effects of ionic environment on the binding process. In the context of this work, we also seize the chance to construct a mechanistic model that explains our results as well as crystallographic and other data collected so far.

Results

Azithromycin is a slow binding ligand of *E. coli* ribosomes

Sixteen-membered macrolides, such as tylosin, possess a disaccharide branch at position C5 of the lactone ring (Fig. 1), from which extending towards the PTase center perturbs the relative positioning of the bound tRNA substrates. Consequently, macrolides of this type inhibit the PTase activity in most reference cell-free systems.[28–30] In contrast, azithromycin has a single desosamine moiety at the C5 position, which is too short to reach the PTase center. Consistently, azithromycin fails to inhibit AcPhe–puromycin formation (Fig. 3). Nevertheless, previous studies have demonstrated that azithromycin

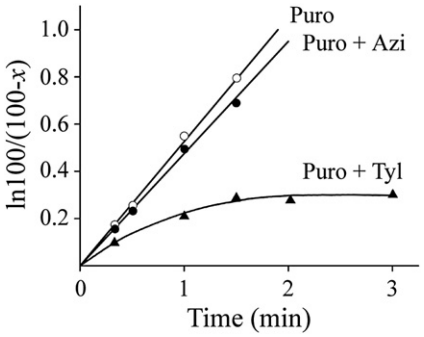

Fig. 3. AcPhe–puromycin synthesis in the absence or presence of antibiotics. Complex C prepared from *E. coli* ribosomes reacted in buffer A for specified time intervals at 25 °C with (○) 200 μM puromycin alone or with a mixture containing both (●) 200 μM puromycin and 0.5 μM azithromycin or (▲) 200 μM puromycin and 2 μM tylosin. The values of the percentage of the initially added complex C, which is converted to product, x, have been corrected by the extent of AcPhe–puromycin synthesis achieved in the absence of azithromycin and tylosin. The two upper lines were drawn by linear fitting of the x and t values to the equation $\ln[100/(100-x)]=k_{obs}\cdot t$, where k_{obs} represents the observed first-order rate constant of the puromycin reaction. The lower line was drawn from the calculated $\ln[100/(100-x)]$ values at each time point, using the B-Spline function of the Microcal Origin 6.1 program (Microcal Software, Inc). Puro, puromycin; Azi, azithromycin; Tyl, tylosin.

competes with tylosin for binding to complex C [post state ribosomes programmed with poly(U) and bearing AcPhe–tRNA and deacylated tRNA at the P- and E-site, respectively].[8,10] This is also shown in Fig. 4; when complex C is added in a solution containing 4 μM tylosin and azithromycin, a progressive decrease in the inactivation of complex C by tylosin occurs as the concentration of azithromycin increases. At high concentrations of azithromycin (>2 μM), the inactivation of complex C is completely reversed. Another feature of the competition mechanism is that the initial slopes of the inactivation plots vary as a function of azithromycin concentration. The overall kinetic pattern is reminiscent of that observed in a recent study of erythromycin binding performed under the same ionic conditions (4.5 mM Mg^{2+}, 150 mM NH_4^+)[30] and is in agreement with previous kinetic studies of azithromycin carried out under conventional ionic conditions (10 mM Mg^{2+}, 100 mM NH_4^+).[10] Thus, it is reasonable to employ a similar kinetic model for the competition of tylosin (T) binding by azithromycin (A), as represented by Scheme 1. The values of $k_{on,A}$, $k_{off,A}$, K_A, and the overall dissociation constant K_A^*, estimated by nonlinear regression fitting of the obtained data to Eq. (7) (see Materials and Methods), are shown in Table 1.

Previous genetic studies have indicated that mutations in hairpin 35 of domain II and in the central loop of domain V of the *E. coli* 23S rRNA confer resistance to low concentrations of erythromycin.[5,31] To check if two of these mutations, U754A and U2609C, also influence the kinetics of azithromycin binding, the affinity of mutant ribosomes for azithromycin was estimated in parallel experiments. As shown in Table 1, mutation U754A

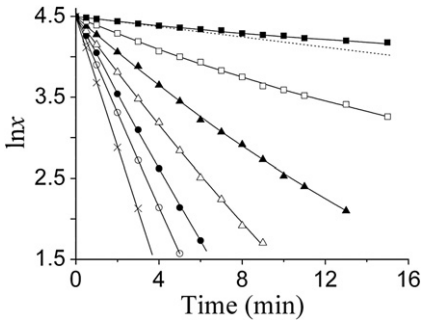

Fig. 4. Inactivation of complex C by tylosin in the absence or presence of azithromycin. Complex C prepared from *E. coli* ribosomes reacted in buffer A with (×) 4 μM tylosin alone or with a mixture containing both 4 μM tylosin and azithromycin at (○) 25 nM, (●) 50 nM, (△) 100 nM, (▲) 200 nM, (□) 500 nM, and (■) 2000 nM. After removing the excess of each antibiotic, the percentage of complex C input remaining active, x, was titrated with 2 mM puromycin. The curves were drawn by nonlinear fitting of the x and t values to Eq. (7). The $k_{on,T}$ and K_T values were measured via experiments performed in the presence of tylosin alone and set in the above computer simulation as constant factors. The tangent at zero time of the nonlinear plot obtained at 4 μM tylosin and 2 μM azithromycin is indicated by a broken line.

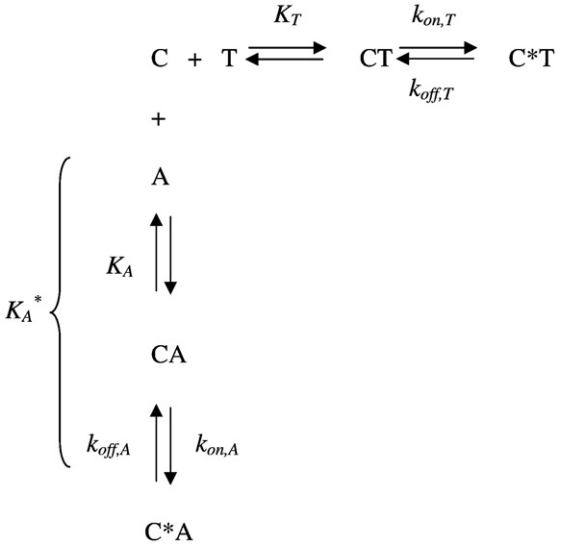

Scheme 1. Competition between tylosin (T) and azithromycin (A) for common binding sites in ribosomal complex C.

hardly affects the affinity of azithromycin, at both the initial and final positions of its accommodation within complex C. The small alterations in the K_A^* and $k_{on,A}/k_{off,A}$ values are not statistically significant ($P<0.05$). In contrast, U2609C mutation increases the isomerization constant $k_{on,A}/k_{off,A}$ by 55%. As a result, the value of the overall dissociation constant for azithromycin, K_A^*, undergoes a 40% reduction, reflecting an increase in affinity of the drug for the mutant ribosome. By repeating the kinetic analysis of azithromycin binding to wild-type ribosomes in the presence of 100 μM spermine, we observed that the $k_{on,A}$ value is decreased by 63%, resulting in a parallel reduction of the isomerization constant. Consistently, the K_A^* value undergoes a twofold enhancement. Similar alterations were recorded by using 50 μM spermine and 2 mM spermidine (optimized Mg^{2+}/NH_4^+/polyamine system[32]), instead of spermine alone (Table 1). Thus, the presence of polyamines leads to an overall decrease in azithromycin binding.

One molecule of azithromycin binds per *E. coli* ribosome

Scheme 1 assumes that only one molecule of azithromycin binds per *E. coli* ribosome at the same time. To verify this assumption, we performed two series of experiments. In the first, C*A complex was exposed to 4 μM tylosin for various time intervals, and its activity, after removing the excess tylosin, was titrated with puromycin. As shown in Fig. 5a, the data of complex C regeneration from complex C*A give a simple first-order time plot, which is consistent with one molecule of azithromycin bound per *E. coli* ribosome. An alternative explanation could be that only one molecule of azithromycin competes with tylosin for a common binding in the ribosome. In any case, $k_{off,A}$ is more than two orders

Table 1. Kinetic parameters derived from analysis of azithromycin interaction with complex C

	Ionic conditions					
		4.5 mM Mg^{2+}, 150 mM NH_4^+		4.5 mM Mg^{2+}, 150 mM NH_4^+, 100 μM spermine	4.5 mM Mg^{2+}, 150 mM NH_4^+, 50 μM spermine, 2 mM spermidine	10 mM Mg^{2+}, 100 mM NH_4^+
Constant (unit)	Wild type	U2609C	U754A	Wild type	Wild type	Wild type[a]
K_A (nM)	29.6±2.6	26.6±1.5	30.5±2.3	25.0±1.8	23.4±1.9	48.0±5.0
$k_{on,A}$ (min^{-1})	0.049±0.004	0.055±0.003	0.045±0.004	0.018±0.001	0.022±0.001	0.0086±0.011
$k_{off,A}$ (min^{-1})	0.0051±0.0004	0.0037±0.0002	0.005±0.0004	0.0053±0.0003	0.0066±0.0005	0.015±0.001
$k_{on,A}/k_{off,A}$	9.66±1.08	15.03±1.00	9.00±0.96	3.40±0.27	3.33±0.29	5.73±0.82
K_A^* (nM)	2.77±0.38	1.66±0.17	3.05±0.43	5.68±0.57	5.32±0.62	7.12±1.17

Data are expressed as means±standard error (duplicate analysis in three ribosomal preparations).
[a] Data taken from Ref. 10.

smaller than $k_{on,T}$. Therefore, the net flux from C*A to C*T depends on this rate-limiting step. From the slope of the plot shown in Fig. 5a, a value of 0.005 min^{-1} is determined, which is quite similar to the $k_{off,A}$ value estimated by nonlinear regression fitting of kinetic data to Eq. (7) (see Table 1).

In the second series of experiments, complex C or 70S ribosomes from *E. coli* were incubated for 2 h in buffer A containing radiolabeled azithromycin at increasing concentrations (equilibrium binding). Azithromycin was present in a molar excess relative to complex C or 70S ribosomes for all of the drug binding assays. The value of bound [^{3}H]azithromycin was measured by nitrocellulose filtration. As shown in Fig. 5b, the binding of azithromycin to complex C follows a rectangular hyperbolic curve. Therefore, the relationship between the amount of bound ligand (B) and the concentration of free ligand (A) can be expressed by the equation:

$$B = \frac{B_{max}[A]}{K_d + [A]} \quad (1)$$

where B_{max} is the maximum level of bound azithromycin and K_d is the dissociation constant of the azithromycin–ribosome complex. The number of drug-binding sites in complex C, estimated after dividing B_{max} by the amount of complex C, is equal to 0.75. Similar results were obtained when 70S ribosomes from *E. coli* were used, instead of complex C (data not shown). In contrast, dissociation of the [^{3}H]azithromycin–ribosome complex prepared from *D. radiodurans* 70S ribosomes follows a clear biphasic curve, suggesting two molecules of azithromycin bound per ribosome, dissociating with rate constants 0.020 min^{-1} and 0.004 min^{-1}, respectively (Fig. 6a). Moreover, binding of radiolabeled azithromycin to *D. radiodurans* ribosomes follows a sigmoid hyperbola (Fig. 6b). Therefore, the data were fitted to the equation

$$B = \frac{B_{max} \cdot [A]^n}{K_d + [A]^n} \quad (2)$$

where n represents the Hill coefficient. The value obtained after dividing B_{max} by the amount of ribosomes (=1.61) and the value of n (=2.31) suggest that two cooperatively interacting sites for azithromycin exist in ribosomes from *D. radiodurans*. It should be mentioned that the ribosomal populations

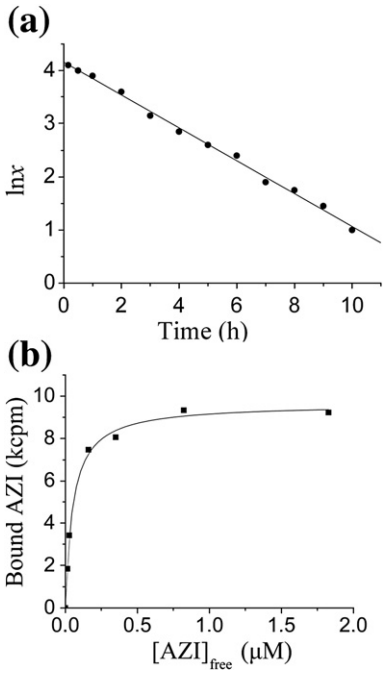

Fig. 5. Analysis of azithromycin dissociation from or binding to complex C prepared from *E. coli*. (a) Dissociation of azithromycin from complex C*A; complex C*A formed by incubating complex C with 1 μM azithromycin for 80 min in buffer A was collected by filtration on a cellulose nitrate filter, exposed to 5 ml of 4 μM tylosin in buffer A for the time intervals indicated, and its percentage remaining active, x, was titrated with 2 mM puromycin. The line was drawn from the calculated ln$x$ values at each time point, using the linear fitting function of the Microcal Origin 6.1 program. (b) Binding of [^{3}H]azithromycin to complex C; each 400-μl reaction mixture containing 6.5 pmol complex C and [^{3}H]azithromycin (1786 dpm/pmol) at various concentrations in buffer A was incubated for 2 h at 25 °C, and the complex formed in each case was isolated by filtration through a nitrocellulose filter. The concentration of free [^{3}H]azithromycin in the reaction mixture is given on the abscissa. The curve was drawn by nonlinear fitting of the bound [^{3}H]azithromycin (B) at each concentration of the free ligand (A) to Eq. (1), using the Hyberbola function of the Microcal Origin 6.1 program.

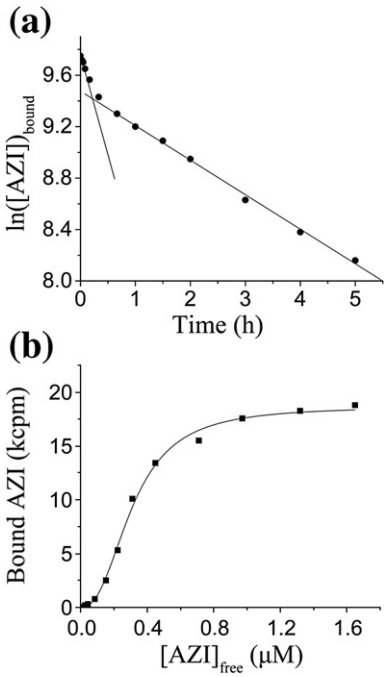

Fig. 6. Analysis of [^{3}H]azithromycin dissociation from or binding to 70S ribosomes from *D. radiodurans*. (a) Dissociation of the azithromycin–ribosome complex; 70S ribosomes (6.5 pmol) were incubated with 30 μl of buffer B containing 1 μM [^{3}H]azithromycin for 80 min at 25 °C, filtered through a nitrocellulose filter, and then exposed to 5 ml of buffer B at 25 °C for the indicated time intervals. After washing with buffer B, the trapped radioactivity on the filters was determined by scintillation counting. The two linear portions of the biphasic curve were drawn from the calculated values of $\ln[AZI]_{bound}$ at each time, using the linear fitting function of the Microcal Origin 6.1 program. (b) Binding of [^{3}H]azithromycin to 70S ribosomes; binding was carried out in buffer B (400 μl) containing 6.5 pmol 70S ribosomes and [^{3}H]azithromycin (1786 dpm/pmol) at various concentrations. The mixture was incubated at 25 °C for 2 h (equilibrium binding) and the amount of bound azithromycin was measured by nitrocellulose filtration and radioactivity counting. The concentration of free [^{3}H]azithromycin in the reaction mixture is given on the abscissa. The curve was drawn by nonlinear fitting of the bound [^{3}H]azithromycin (*B*) at each concentration of the free ligand (*A*) to Eq. (2), using the Hill hyperbola function of the Microcal Origin 6.1 program.

isolated from *E. coli* and *D. radiodurans* were 75% and 84.3% capable of binding, respectively, as found by titration with [^{14}C]erythromycin. Thus, correcting for the binding efficiency, the number of drug molecules bound per *E. coli* and *D. radiodurans* ribosomes becomes 1 and 1.9, respectively.

Footprinting of azithromycin–ribosome complexes

To identify the individual drug–ribosome interactions occurring in the encounter complex CA and the final complex C*A, we followed a kinetic-footprinting approach, recently applied in studying the interactions of erythromycin and tylosin with *E. coli* ribosomes.[30] Footprinting of the CA complex was achieved by incubating complex C prepared from *E. coli* ribosomes with azithromycin in buffer A for 10 s, the latter at concentration $50\times K_A$, thus ensuring that most of the binding sites are occupied. Because the equilibrium C+A⇄CA is established rapidly, while the isomerization reaction proceeds slowly ($t_{1/2}$=13 min), the product during this time interval mainly consists of complex CA (>95%). The formed CA complex was then probed with chemical reagents that attack nucleosides of 23S rRNA that are neither occupied by the drug nor participating in secondary or tertiary interactions. The incubation time of complex C with azithromycin was extended to 100 min to footprint the C*A complex. Because the isomerization constant is higher than 3 (Table 1), it is reasonable to presume that at the end of this time interval ($\approx 8\times t_{1/2}$), most of the added complex C should be in the form of complex C*A.

Representative autoradiograms obtained by primer extension analysis are shown in Figs. 7 and 8. The final modification results are summarized in Table 2. Azithromycin at the CA binding state and in the absence of polyamines strongly protects A2058 and A2059 from dimethyl sulfate (DMS) and G2505 from kethoxal modification, while moderately reducing the accessibility of U2609 to 1-cyclohexyl-3-(2-morpholinoethyl) carbodiimide metho-*p*-toluene (CMCT). A weak protection effect is also observed on C2611, although this residue is not normally accessible to DMS, due to its base pairing with G2057.[33] Interestingly, in the presence of polyamines, the reactivity of C2611 against DMS is lost, both in ribosome–azithromycin complexes and in complex C alone. Consequently, it is reasonable to suppose that at low Mg^{2+} concentrations, polyamines reestablish the C2611/G2057 base pair. In the C*A binding state, new protection effects appear on A788, U790, and U2586. Also, protection of U2609 becomes stronger, whereas protections at A2058 and G2505 soften and the accessibility of A752 is slightly enhanced. The presence of spermine hardly affects the protection pattern of complex CA. However, in complex C*A, it stimulates the accessibility of all nucleotides implicated in the binding of azithromycin, in particular of U2609 and those situated in helix 35 of 23S rRNA. The increased accessibility indicates reduced binding of the drug, in agreement with the increased dissociation constant K_A^* when polyamines are present.

Discussion

High-resolution crystallographic structures of ribosomal particles and their complexes with azithromycin have elucidated basic concepts in azithromycin binding mode at the molecular level.[21,22,24] However, a disadvantage of crystallography is that the structures offer only a snapshot of stably bound azithromycin position on the ribosome, whereas the complete picture of the drug binding process may be significantly more complex. Kinetic

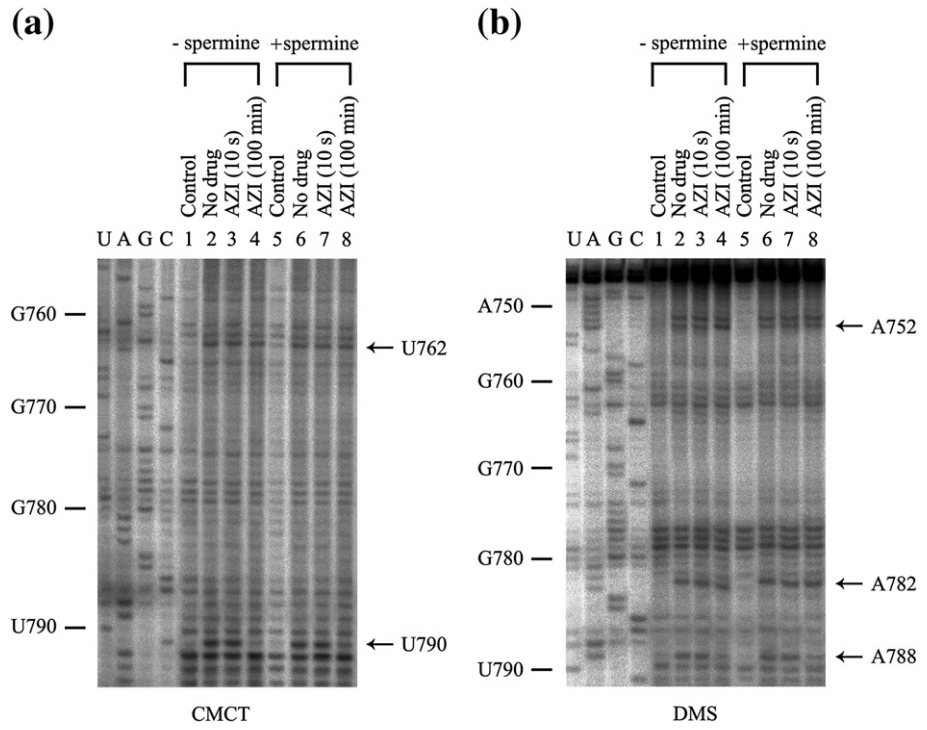

Fig. 7. Alterations in the chemical reactivity of nucleosides in domain II of 23S rRNA, caused by azithromycin binding to complex C prepared from *E. coli* ribosomes. Complex C was incubated in the absence or presence of azithromycin in buffer A (lanes 1 to 4) or in the same buffer also containing 100 μM spermine (lanes 5 to 8). The resulting complexes were then probed with DMS or CMCT. Modification sites were detected by primer extension analysis. U, A, G, and C denote dideoxy sequencing lanes. Lanes 1 and 5, unmodified complex C with no drug present; lanes 2 and 6, complex C probed in the absence of azithromycin; lanes 3 and 7, complex C incubated with azithromycin for 10 s and then probed; lanes 4 and 8, complex C incubated with azithromycin for 100 min and then probed. Numbering of nucleotides for the sequencing lanes is indicated at the left, while nucleotides with altered reactivity against chemical probes as well as reference bands are indicated by arrows. AZI, azithromycin.

analysis and chemical footprinting used in the present work provide additional tools to (i) investigate the entire course of azithromycin binding to *E. coli* ribosomes and (ii) rationalize the available crystallographic, genetic, and other data collected so far.

According to our kinetic results, the overall association rate constant of azithromycin binding to complex C, $(k_{on,A}+k_{off,A})/K_A$, equals 3×10^4 M^{-1} s^{-1}, a value that is two orders below the upper limit set for the characterization of a drug as a slow binding ligand.[34] Corroborative evidence that azithromycin is a slow binder is also derived from the preincubation effect, namely, the strengthening of the azithromycin competition potency against tylosin when complex C is preincubated with azithromycin before the addition of tylosin (data not shown). Moreover, the ratio $k_{on,A}/k_{off,A}$ is much higher than 1, regardless of ionic conditions used, a fact implying that azithromycin is a slowly reversible ligand as well. Another important characteristic of the azithromycin kinetic behavior is that the initial slope of each inactivation plot in Fig. 4 decreases as the concentration of azithromycin increases. This is consistent with a two-step mechanism of binding, since otherwise, the initial slope should be independent of azithromycin concentration. According to this mode, the first step equilibrates rapidly, while the second one representing the accommodation of azithromycin at its final position is established slowly, within the minute timescale ($t_{1/2}=13$ min). A two-step mechanism has also been suggested by transferred nuclear Overhauser effect studies,[26] as well as by previous kinetic studies.[10] Comparing the results presented here with previous studies performed at 10 mM Mg^{2+}, we conclude that a decrease of Mg^{2+} concentration from 10 to 4.5 mM enhances azithromycin affinity at both steps of binding. Noteworthy is the threefold reduction in the $k_{off,A}$ value, suggesting that relatively low Mg^{2+} concentrations preserve complex C*A from disassembly. Although polyamines do not affect the initial step of binding, they obstruct the accommodation of azithromycin at its final position, primarily by lowering the $k_{on,A}$ value. Our results emphasize the role that ionic conditions may have in the ligand/ribosome binding free energy. Comparing azithromycin with erythromycin binding to ribosomes at optimal ionic conditions for efficient and accurate protein synthesis (4.5 mM Mg^{2+}, 150 mM NH_4^+, 50 μM spermine, and 2 mM spermidine),[32] we realize that azithromycin exhibits a higher affinity for complex C ($K_E^*/K_A^*=19.9$) and forms a more stable final complex with ribosomes ($k_{off,E}/k_{off,A}=14.8$). Although the efficacy of a drug depends on many factors, our data at least partially

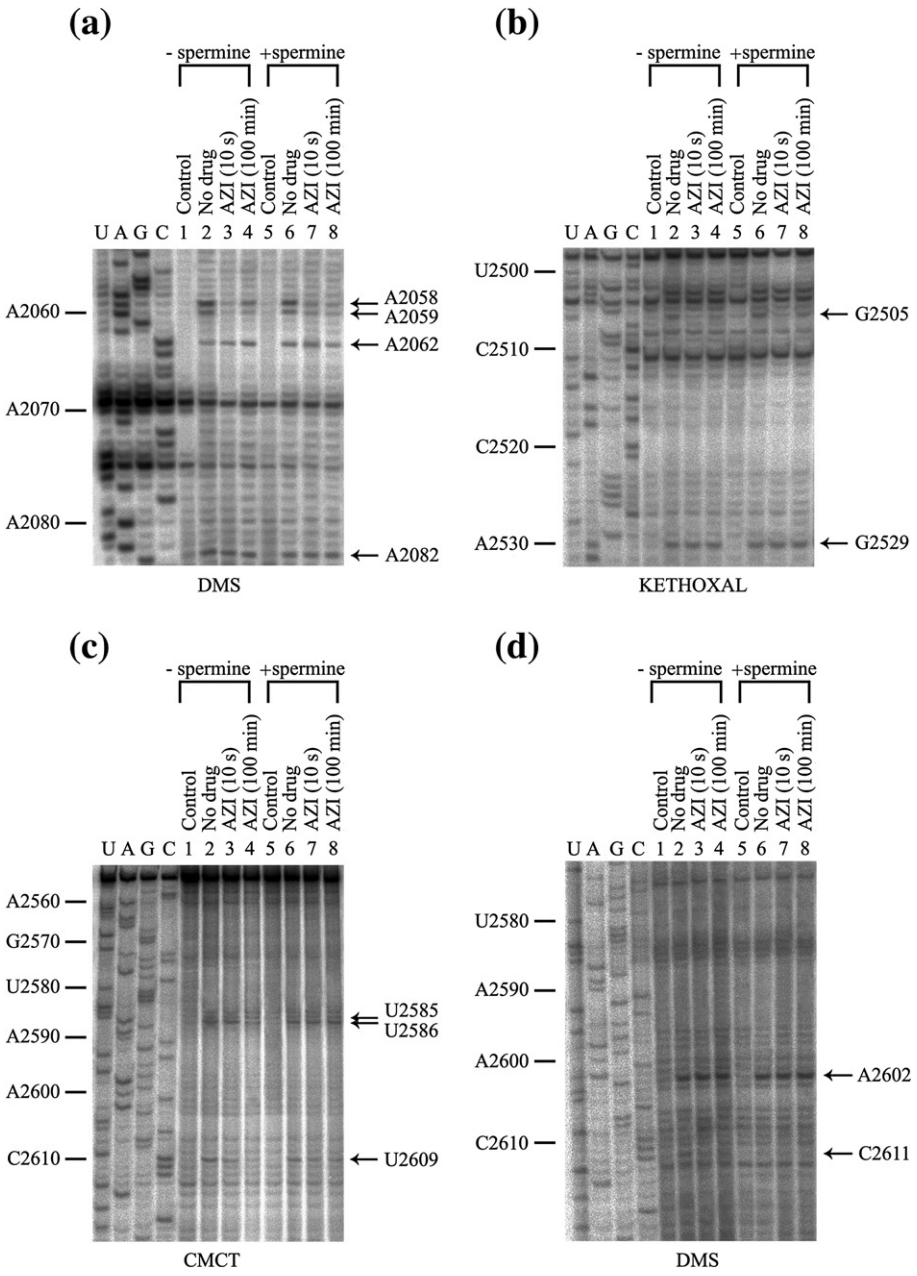

Fig. 8. Alterations in the chemical reactivity of nucleosides in domain V of 23S rRNA, caused by azithromycin binding to complex C prepared from *E. coli* ribosomes. Incubation of complex C with azithromycin was made as in Fig. 7. Samples were modified with DMS, CMCT, or kethoxal and analyzed as in Fig. 7.

explain the superiority of azithromycin as an antimicrobial agent against *E. coli* and are also consistent with its prolonged inhibitory activity on growth following antibiotic removal from the medium (Post Antibiotic Effect)[35] and with its relatively lower efficiency in inducing A2058 dimethylation in cells carrying inducible *erm*(C).[36]

The kinetic model shown in Scheme 1 is based on the assumption that one molecule of azithromycin transiently binds to an initial site in the ribosome and, subsequently, converts to a final position exhibiting high affinity for azithromycin. Consequently, the two binding sites are regarded as mutually exclusive. As can be seen from its outcome, this assumption seems to be right; first, our data fit Eq. (7) well, and second, if two molecules of azithromycin could bind simultaneously per ribosome, then K_A^* representing the overall dissociation constant should depend on drug concentration. As found by calculating the K_A^* value at different azithromycin concentrations, K_A^* value exhibits very little variation (<15%). Dissociation and binding of azithromycin to complex C were analyzed in detail to better address this issue. As shown in Fig. 5a, dissociation of azithromycin from the C*A complex follows a linear first-order plot, suggesting that one molecule of the drug binds per *E. coli* ribosome. However, if a second molecule of azithromycin is actually involved but does not compete with tylosin, then it would not be discriminated by

Table 2. Footprinting of azithromycin bound at the initial and final positions in the large subunit of the *E. coli* ribosomes

23S rRNA residue	Ionic conditions					
	4.5 mM Mg^{2+}, 150 mM NH_4^+			4.5 mM Mg^{2+}, 150 mM NH_4^+, 100 μM spermine		
	C	CA	C*A	C	CA	C*A
A752	++	++	+++	++	++	++
A788	++	++	(+)	++	++	+
U790	++	++	(+)	++	++	+
A2058	++++	+	++	++++	++	++
A2059	+++	+	+	+++	++	++
A2062	+++	+++	+++	+++	++++	+++
G2505	+	0	(+)	+	0	(+)
U2586	+	+	(+)	+	+	+
U2609	+++	++	(+)	+++	++	++
C2611	+	(+)	(+)	0	0	0

Intensities of the modified residues are assigned as follows: ++++, very strong; +++, strong; ++, moderate; +, weak; (+), very weak; 0, no modification. Quantification of the band intensities was made by phosphorimaging of the gels. The accessibility of U762 to CMCT in Fig. 7a was not affected by azithromycin binding, and therefore, this band was used as a reference one to normalize the intensity of U790. Quantification of the band intensities at A752 and A788 in Fig. 7b was made as for Fig. 7a, normalizing against the A782 band. Similarly, quantifications of the band intensities at A2058, A2059, and A2062 in Fig. 8a; G2505 in Fig. 8b; U2586 and U2609 in Fig. 8c; and C2611 in Fig. 8d were made, normalizing against bands A2082, G2529, U2585, and A2602, respectively. The normalized intensity of A2058 was the highest one and assigned as ++++.

C, poly(U)-programmed 70S ribosomes bearing $tRNA^{Phe}$ at the E-site and AcPhe–tRNA at the P-site; CA, encounter complex between C and azithromycin; C*A, final complex resulting from CA by isomerization.

the applied experimental method. Therefore, binding of radioactive azithromycin to complex C was employed to overcome the above limitations: Data collected by binding of [^{3}H]azithromycin to *E. coli* ribosomes yield a rectangular hyperbolic curve (Fig. 5b), from which it is calculated that one molecule of azithromycin binds per ribosome. In contrast, those obtained with *D. radiodurans* ribosomes display a clear sigmoidal hyperbolic curve (Fig. 6b), with a B_{max} corresponding to 1.9 molecules of azithromycin bound per ribosome. The calculated value of the Hill coefficient equals 2.3, a fact suggesting that the binding sites of azithromycin in *D. radiodurans* ribosomes are cooperative. This is consistent with crystallographic data indicating that AZI-1 and AZI-2 bound to the 50S ribosomal subunit of *D. radiodurans* are directly connected by a hydrogen bond and indirectly through a Mg^{+2} ion (Fig. 2).[22] Also, consistent with a 2:1 stoichiometry is the finding that the dissociation of [^{3}H]azithromycin–*D. radiodurans* ribosome complex follows a biphasic curve (Fig. 6a). In summary, our results verify the number of azithromycin molecules observed by crystallography to be bound per *D. radiodurans* ribosome but suggest that for *E. coli* ribosomes, only one binding site is susceptible at any given time.

Structural characterization of CA and C*A complexes was gained by footprinting analysis. As shown in Table 2, the footprinting pattern of complex CA resembles that previously reported for erythromycin.[30] A shift of azithromycin to the high-affinity site (complex C*A) is accompanied by drug interactions with nucleosides A752, A788, and U790 in domain II of 23S rRNA, as well as with U2586 and U2609 in domain V. Meanwhile, the interactions with A2058 and G2505 become weaker. The footprinting pattern of complex C*A correlates better than the CA pattern with crystallographic data regarding the binding of AZI-1 to *D. radiodurans* 50S ribosomal subunits.[22] This may be due to the fact that co-crystallization has been carried out in the presence of sevenfold excess of azithromycin for prolonged time, conditions that favor the C*A formation. Nevertheless, the C*A footprinting pattern does not correlate with the binding of the second molecule of azithromycin, AZI-2, detected by crystallography in *D. radiodurans*.[22]

Drawing clues from the protection experiments, one can envisage that azithromycin binds initially to a hydrophobic crevice of *E. coli* ribosomes, formed by nucleosides G2057–A2059 at the upper part of the exit tunnel (Fig. 9b). The pivotal role of A2058 and A2059 in the contact of azithromycin with the hydrophobic crevice has been well documented by studies testing the resistance against this drug of laboratory strains or clinical isolates of bacteria carrying mutations or methylated bases at these positions.[12,15] Consistently, A2058 has been found to form a hydrogen bond with the 02′ of the desosamine sugar in both archaeal and bacterial crystal structures of 50S ribosomal subunits complexed with azithromycin.[22–24] The accommodation of azithromycin at the CA binding state is also facilitated by drug interaction with the adjacently placed G2505. For thermodynamic reasons ($\Delta\Delta G^o = -1.4$ kcal·mol^{-1}), azithromycin partially loses its interaction with the hydrophobic crevice, a fact resulting in a shift of the drug towards the other side of the tunnel where U2609 and residues of domain II are situated (Fig. 9c). Enhancement of DMS reactivity at A752 upon drug binding to the final position suggests changes in the local conformation of 23S rRNA rather than direct interaction with azithromycin. It is possible that these conformational changes are mediated through U2609, which has been shown in *D. radiodurans* to interact with both A752 and azithromycin.[22,38] It should be mentioned

that upon binding of AZI-2 to the 50S ribosomal subunit of *D. radiodurans*, the loop connecting helices 73 and 93 of 23S rRNA is significantly shifted.[22] In turn, this causes the base of U2609 to adopt a distinctly different orientation that allows hydrophobic interactions with AZI-1.[22] Because azithromycin does not bind to *E. coli* ribosomes in a manner analogous to that of AZI-2, a similar alteration in the orientation of base U2609 in *E. coli* cannot be easily speculated. Therefore, a direct contact of U2609 in *E. coli* with azithromycin, like that observed with erythromycin,[39] seems more probable. Even so, a mutation of U2609 to C is predicted to favor rather than interrupt this contact.[5] Consistently, we found that mutation U2609C increases the formation and stability of complex C*A. In contrast, mutation U754A barely affects the azithromycin–ribosome interaction. Our results obtained with mutant *E. coli* ribosomes are in remarkable agreement with resistance studies performed in *E. coli* by Garza-Ramos *et al.*,[5] but in apparent variance with earlier results published by the same research group.[31] It is possible that the use of a heterogeneous ribosomal population (wild-type plus mutant ribosomes) in this earlier study is the cause of this discrepancy. Another finding of the present work is that interaction of azithromycin with A788 and U790 favors the formation of complex C*A. Both nucleosides are placed on the same side of the exit tunnel, opposite to that forming the G2057–A2059 hydrophobic crevice. Nevertheless, the loop in which A788 and U790 are situated is poorly conserved and relative flexible.[23] Therefore, it is not surprising that interactions of this loop with azithromycin, not detected in crystals of *D. radiodurans* or *H. marismortui* 50S ribosomal subunits, are adopted in *E. coli* ribosomes, probably via a swinging of A788 and U790 towards the drug (shown in Fig. 9c by a double arrow). Polyamines bound to this region may establish a conformational state that disfavors interactions of A752, A788, and U790 with azithromycin, a postulation that could explain their negative effect on C*A formation. Spermine cross-linking to helices 73, 35, and 35a has already been detected.[40]

In conclusion, our results demonstrate that one molecule of azithromycin binds per *E. coli* ribosome. The binding process is characterized by an initial step that rapidly equilibrates, followed by a slower step when the drug accommodates into its final position. Both interactions between azithromycin and the ribosome are Mg^{2+} dependent. Polyamines do not affect the initial binding step but instead hinder the shift of azithromycin to the high-affinity

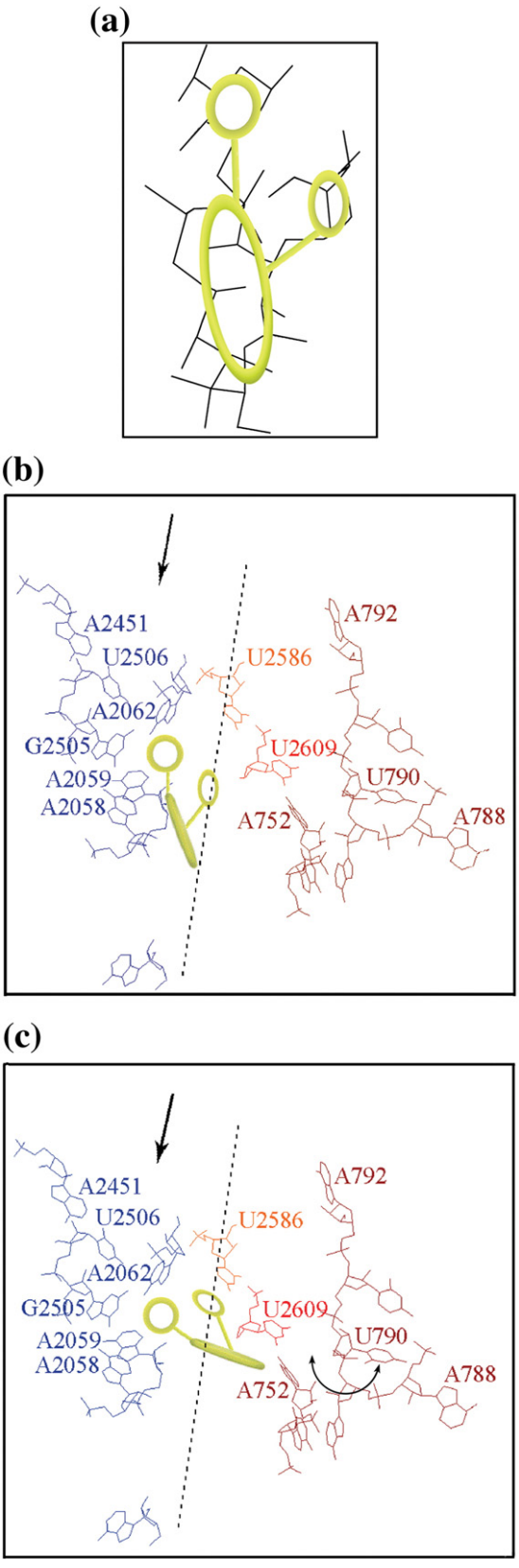

Fig. 9. Schematic representation of azithromycin binding at the low- and high-affinity sites within the ribosomal exit tunnel. (a) Azithromycin crystal structure; the orientation of the molecule is represented by three connected circles reflecting the planes of the lactone ring and the two sugar substituents. (b and c) Positional and orientation clustering of azithromycin within the exit tunnel, at the low- and high-affinity sites, respectively. The broken line represents the tunnel axis, while the position of PTase center is shown by an arrow. A putative rotation of U790 upon binding of azithromycin to the high-affinity site is indicated in (c) by a double arrow. Representations are based on the results of the present study and crystallographic data taken from Refs. 22,37.

site. Nevertheless, the general characteristics of the binding model are conserved, regardless of the ionic conditions used. Therefore, the apparent discrepancies between the antibiotic binding modes obtained for *E. coli* and *D. radiodurans* cannot be attributed to differences in the ionic conditions used. As proposed by Schlünzen *et al.*,[22] it seems more probable that these discrepancies predominantly result from species-specific differences in the ribosomal proteins and rRNA constituting the drug-binding sites. The present work shows that the simultaneous binding of two azithromycin molecules to *D. radiodurans* ribosomes is cooperative. This observation may be important for the future rational design of macrolides that work in a synergistical fashion.

Materials and Methods

Reagents and materials

Puromycin dihydrochloride, tylosin tartrate, spermine tetrahydrochloride, spermidine trihydrochloride, $tRNA^{Phe}$ from *E. coli*, DMS, and DMS stop solution were from Sigma-Aldrich. Kethoxal and CMCT were purchased from MP Biomedicals and Fluka Biochemicals, respectively. Radioactive materials L-[2,3,4,5,6-^{3}H]phenylalanine and [α-^{32}p]ATP were from Amersham Biosciences. AMV reverse transcriptase, dNTPs and ddNTPs were obtained from Roche Diagnostics. Cold and radioactive azithromycin (9.9 Ci/mmol) was kindly provided by Pfizer (Groton/New London Laboratories). Cellulose nitrate filters (type HA; 0.45 μm pore size) were from Millipore Corp.

Bacterial strains and biochemical preparations

70S ribosomes were prepared from *E. coli* K12 and *D. radiodurans* cells as described elsewhere.[41] *E. coli* TA531 cells lacking chromosomal *rrn* alleles but containing pKK3535 plasmids expressing wild-type or mutated 23S rRNA (U2609C or U754A) were kindly provided by Prof. A. S. Mankin, University of Illinois. These strains were used to prepare ribosomes in studying the effect of 23S rRNA mutations on the mechanism of azithromycin binding. Ac[^{3}H]Phe–tRNA charged to 80% and posttranslocation complex of poly(U)-programmed ribosomes, complex C, bearing $tRNA^{Phe}$ at the E-site and Ac[^{3}H]Phe–tRNA at the P-site were prepared and purified according to Dinos *et al.*[41] The percentage of ribosomes, active in AcPhe–tRNA binding, was more than 65%. This fraction was 90–95% reactive towards puromycin.

Inactivation of complex C by tylosin in the absence or presence of azithromycin

Complex C in buffer A [100 mM Tris/HCl, pH7.2, 4.5 mM Mg $(CH_3COO)_2$, 150 mM NH_4Cl, and 6 mM 2-mercaptoethanol] containing 4 μM tylosin and azithromycin at specified concentrations was incubated at 25 °C for the desired time intervals. As previously proved,[30] the apparent rate constant of complex C inactivation, F, is given by the equation

$$F = F_s + (F_o - F_s) \cdot e^{-k' \cdot t} \tag{3}$$

where F_s and F_o are the inactivation constants at the steady state and zero time, respectively, while k' is the apparent equilibration rate constant for the attainment of equilibrium between complex C and the drugs. For the derivation of Eq. (3), we assumed that the equilibria C+T⇄CT and C+A⇄CA in Scheme 1 are established rapidly, while the isomerization reactions CT⇄C*T and CA⇄C*A are established slowly. Additionally, we assumed that the values of $k_{off,T}$ and $k_{off,A}$ might be less than those of $k_{on,T}$ and $k_{on,A}$, respectively, for appreciable formation of C*T and C*A. Each of the kinetic parameters F_s, F_o, and k' in Eq. (3) is related to the concentrations of azithromycin (A) and tylosin (T), through the following equations:

$$F_o = \frac{k_{on,T}[T]}{K_T\left(1 + \frac{[A]}{K_A}\right) + [T]} \tag{4}$$

$$F_s = \frac{k_{on,T}k_{off,A}[T]}{k'K_T\left(1 + \frac{[T]}{K_T} + \frac{[A]}{K_A}\right)} \tag{5}$$

$$k' = k_{off,A} + k_{on,A}\frac{\frac{[A]}{K_A}}{1 + \frac{[T]}{K_T} + \frac{[A]}{K_A}} \tag{6}$$

The values of $k_{on,A}$, $k_{off,}$A, and K_A were calculated by nonlinear regression fitting of kinetic data obtained from three independently performed experiments to the equation

$$\ln x = 4.6 - F_s \cdot t - \frac{(F_o - F_s)}{k'}\left(1 - e^{-k't}\right) \tag{7}$$

that is derived from Eq. (3) by integration. The variable x in Eq. (7) is the percentage of the initially added complex C, which remains active (reactive towards puromycin) with time. The constant factor in Eq. (7) is valid by assuming that the extent of puromycin reaction used for titration of complex C is 100%; otherwise, it is corrected. The $k_{on,T}$ and K_T constants for tylosin, measured via experiments performed in the presence of tylosin alone, were in good agreement with those obtained previously[30] and set in the above computer simulation as constant factors. Once $k_{on,A}$, $k_{off,}$A, and K_A were calculated, the overall dissociation constant K_A^*, concerning both steps of azithromycin binding to complex C, was estimated through the equation

$$K_A^* = K_A\left(\frac{k_{off,A}}{k_{off,A} + k_{on,A}}\right) \tag{8}$$

Details on the derivation of the above equations are available in the Supplementary Data of Ref. 30.

Regeneration of complex C from complex C*A

To determine the $k_{off,A}$ value by an alternative way and to check whether one or more molecules of azithromycin bind per *E. coli* ribosome, complex C*A formed by incubating complex C (6.5 pmol) with 1 μM azithromycin in buffer A (total volume: 30 μl) for 80 min was adsorbed on a cellulose nitrate filter, washed with buffer A, and then immersed in 5 ml of buffer A containing 4 μM tylosin for specified time intervals. After removing the excess of tylosin, the percentage (x) of the complex C remaining active was determined by titration with 2 mM puromycin.

The $k_{off,A}$ value was estimated from the slope of the obtained ln*x versus* time plot and compared with those calculated through Eq. (7).

Kinetic analysis of the dissociation of the azithromycin–ribosome complex was also performed by incubating *E. coli* 70S ribosomes (6.5 pmol) with 1 μM [^{3}H]azithromycin (1786 dpm/pmol) in 30 μl of buffer A for 80 min at 25 °C. The [^{3}H]azithromycin–ribosome complex formed was then collected by filtration through a cellulose nitrate filter, washed with buffer A, and immersed in 5 ml of buffer A at 25 °C. The amount of azithromycin remaining bound to ribosomes with time was monitored by washing the filter rapidly with cold buffer A and measuring the trapped radioactivity on the filter in a scintillation spectrometer. Controls without ribosomes were included in each experiment and the values obtained were subtracted. The same procedure was followed when *D. radiodurans* 70S ribosomes were used. In the later case, however, buffer B [100 mM Tris/HCl, pH7.2, 10 mM Mg $(CH_3COO)_2$, 100 mM NH_4Cl, and 6 mM 2-mercaptoethanol] was used, since 70S ribosomes from *D. radiodurans* were unstable in buffer A.

Binding of azithromycin to complex C or 70S ribosomes

Complex C or 70S ribosomes (6.5 pmol) from *E. coli* or *D. radiodurans* were incubated with varying concentrations of [^{3}H]azithromycin (1786 dpm/pmol) in 400 μl of buffer A or B, respectively, at 25 °C for 2 h (equilibrium binding). The bound drug to complex C or 70S ribosomes was then collected on a nitrocellulose filter, washed three times (3 ml each) with cold buffer, and dissolved in 10 ml of Bray's solution, and its radioactivity was measured in a liquid scintillation spectrometer. Nonspecific binding was determined by assessing the displacement of [^{3}H]azithromycin with a 100-fold excess of unlabeled azalide.

Probing of CA and C*A complexes

Complex C at 100 nM was incubated alone or with 1.4 μM azithromycin ($50 \times K_A$) in 100 μl of buffer C[Hepes/KOH, pH7.2, 4.5 mM $Mg(CH_3COO)_2$, 150 mM NH_4Cl, and 5 mM dithiothreitol] in the absence or presence of 100 μM spermine at 25 °C, either for 10 s (CA probing) or for $8 \times t_{1/2}$ min (C*A probing). The term $t_{1/2}$ represents the half-life for the attainment of equilibrium between complex C and the drug and was calculated through the equation,

$$t_{1/2} = \frac{0.693}{k''} \tag{9}$$

where k'' is given by the equation

$$k'' = k_{off,A} + k_{on,A} \cdot \frac{[A]}{K_A + [A]} \tag{10}$$

Complexes CA and C*A were then probed with DMS, kethoxal, or CMCT, as described previously.[30] Reactions were stopped, and the rRNA was recovered from CA or C*A complexes by extraction with phenol, phenol–chloroform, and chloroform. Finally, rRNA was precipitated by ethanol and resuspended in Milli-Q water.

Primer extension

The modifications in 23S rRNA were monitored by primer extension analysis using reverse transcriptase, according to Stern *et al.*[42] The used primers were complementary to the sequences 888–906, 2099–2116, 2561–2578, and 2677–2694. The cDNA products were separated by electrophoresis on 6% polyacrylamide/7 M urea gels. The positions of stops in cDNA synthesis were identified by reference to dideoxy sequencing reactions, run in parallel on unmodified rRNA template. Three replications were carried out for each experiment. Quantification of the band intensities was made by phosphorimaging of the gels (Fujifilm, FLA-3000, Berthold; Image Quant Software AIDA, Raytest). Background values in each "control" lane were subtracted from the corresponding bands of interest. Each lane was searched for a reference nucleotide whose accessibility to the chemical probe is not affected by azithromycin binding. The intensity of this reference band was then used to normalize the intensities of the bands of interest in this lane (vertical comparison). The relative intensity of the reference band between lanes was finally used to correct for variability between lanes (horizontal comparison).

Statistics

All data indicated in Table 2 and in the figures denote mean values obtained from three independently performed experiments. Data variability was determined by ANOVA. Significant differences between mean values were measured by the *F* Scheffé test.

Acknowledgements

This work was supported by a grant (B115) from the Research Committee of the University of Patras (Programme K. Karatheodori) and the Deutsche Forschungsgemeinschaft (WI3285/1-1 to D.N.W.). We wish to thank Dr. Dennis Synetos and Dr. Dennis Drainas for many fruitful discussions, Spyridoula Angelakopoulou for technical assistance, Elisavet Kalpaxis for generating Fig. 9, and Dr. Alexander S. Mankin (University of Illinois) for providing us with mutated strains of *E. coli*. Also, we wish to thank Dr. Nikos Baibas of Pfizer Hellas A.E. and Dr. Donnie W. Owens, Compound Transfer Manager of Pfizer Inc., for [^{3}H]azithromycin supply.

References

1. Fiese, E. F. & Steffen, S. H. (1990). Comparison of the acid stability of azithromycin and erythromycin A. *J. Antimicrob. Chemother.* **25**, 39–47.
2. Lalak, N. J. & Morris, D. L. (1993). Azithromycin clinical pharmacokinetics. *Clin. Pharmacokinet.* **25**, 370–374.
3. Zuckerman, M. D. (2000). The newer macrolides: azithromycin and clarithromycin. *Infect. Dis. Clin. North Am.* **14**, 449–462.
4. Gordillo, M. E., Singh, K. V. & Murray, B. E. (1993). In vitro activity of azithromycin against bacterial enteric pathogens. *Antimicrob. Agents Chemother.* **37**, 1203–1205.
5. Garza-Ramos, G., Xiong, L., Zhong, P. & Mankin, A. S. (2001). Binding site of macrolide antibiotics on the ribosome: new resistance mutation identifies a specific

interaction of ketolides with rRNA. *J. Bacteriol.* **183**, 6898–6907.
6. Vaara, M. (1993). Outer membrane permeability barrier to azithromycin, clarithromycin, and roxithromycin in gram-negative enteric bacteria. *Antimicrob. Agents Chemother.* **37**, 354–356.
7. Imamura, Y., Higashiyama, Y., Tomono, K., Izumikawa, K., Yanagihara, K., Ohno, H. *et al.* (2005). Azithromycin exhibits bactericide effects on *Pseudomonas aeruginosa* through interaction with the outer membrane. *Antimicrob. Agents Chemother.* **49**, 1377–1380.
8. Retsema, J., Girard, A., Schelkly, W., Manousos, M., Anderson, M., Bright, G. *et al.* (1987). Spectrum and mode of action of azithromycin (CP-62, 993), a new 15-membered-ring macrolide with improved potency against gram-negative organisms. *Antimicrob. Agents Chemother.* **31**, 1939–1947.
9. Goldman, R. C., Fesik, S. W. & Doran, C. C. (1990). Role of protonated and neutral forms of macrolides in binding to ribosomes from Gram-positive and Gram-negative bacteria. *Antimicrob. Agents Chemother.* **34**, 426–431.
10. Dinos, G. P., Michelinaki, M. & Kalpaxis, D. L. (2001). Insights into the mechanism of azithromycin interaction with an *Escherichia coli* functional ribosomal complex. *Mol. Pharmacol.* **59**, 1441–1445.
11. Yan, K., Hunt, E., Berge, J., May, E., Copeland, R. A. & Gontarek, R. R. (2005). Fluorescence polarization method to characterize macrolide–ribosome interactions. *Antimicrob. Agents Chemother.* **49**, 3367–3372.
12. Vester, B. & Douthwaite, S. (2001). Macrolide resistance conferred by base substitutions in 23S rRNA. *Antimicrob. Agents Chemother.* **45**, 1–12.
13. Leclercq, R. & Courvalin, P. (2002). Resistance to macrolides and related antibiotics in *Streptococcus pneumoniae*. *Antimicrob. Agents Chemother.* **46**, 2727–2734.
14. Farrell, D. J., Douthwaite, S., Morrissey, I., Bakker, S., Poehlsgaard, J., Jakobsen, L. & Felmingham, D. (2003). Macrolide resistance by ribosomal mutation in clinical isolates of *Streptococcus pneumoniae* from the PROTECT 1999–2000 study. *Antimicrob. Agents Chemother.* **47**, 1777–1783.
15. Katz, L. & Ashley, G. W. (2005). Translation and protein synthesis: macrolides. *Chem. Rev.* **105**, 499–527.
16. Pfister, P., Corti, N., Hobbie, S., Bruell, C., Zarivach, R., Yonath, A. & Böttger, E. C. (2005). 23S rRNA base pair 2057–2611 determines ketolide susceptibility and fitness cost of the macrolide resistance mutation 2058A→G. *Proc. Natl Acad. Sci. USA*, **102**, 5180–5185.
17. Pereyre, S., Renaudin, H., Charron, A., Bébéar, C. & Bébéar, C. M. (2006). Emergence of a 23S rRNA mutation in *Mycoplasma hominis* associated with a loss of the intrinsic resistance to erythromycin and azithromycin. *J. Antimicrob. Chemother.* **57**, 753–756.
18. Lovmar, M., Tenson, T. & Ehrenberg, M. (2004). Kinetics of macrolide action: the josamycin and erythromycin cases. *J. Biol. Chem.* **279**, 53506–53515.
19. Chittum, H. S. & Champney, W. S. (1995). Erythromycin inhibits the assembly of the large ribosomal subunit in growing *Escherichia coli* cells. *Curr. Microbiol.* **30**, 273–279.
20. Nalca, Y., Jänsch, L., Bredenbruch, F., Geffers, R., Buer, J. & Häussler, S. (2006). Quorum-sensing antagonistic activities of azithromycin in *Pseudomonas aeruginosa* PAO1: a global approach. *Antimicrob. Agents Chemother.* **50**, 1680–1688.
21. Hansen, J. L., Ippolito, J. A., Ban, N., Nissen, P., Moore, P. B. & Steitz, T. A. (2002). The structures of four macrolide antibiotics bound to the large ribosomal subunit. *Mol. Cell*, **10**, 117–128.
22. Schlünzen, F., Harms, J. M., Franceschi, F., Hansen, H.A. S., Bartels, H., Zarivach, R. & Yonath, A. (2003). Structural basis for the antibiotic activity of ketolides and azalides. *Structure*, **11**, 329–338.
23. Wilson, D. N., Harms, J. M., Nierhaus, K. H., Schlünzen, F. & Fucini, P. (2005). Species-specific antibiotic–ribosome interactions: implications for drug development. *Biol. Chem.* **386**, 1239–1252.
24. Tu, D., Blaha, G., Moore, P. B. & Steitz, J. A. (2005). Structures of MLS_BK antibiotics bound to mutated large ribosomal subunits provide a structural explanation for resistance. *Cell*, **121**, 257–270.
25. Berisio, R., Corti, N., Pfister, P., Yonath, A. & Böttger, E. C. (2006). 23S rRNA 2058A→G alteration mediates ketolide resistance in combination with deletion in L22. *Antimicrob. Agents Chemother.* **50**, 3816–3823.
26. Bertho, G., Gharbi-Benarous, J., Delaforge, M. & Girault, J. P. (1998). Transferred nuclear Overhauser effect study of macrolide–ribosome interactions: correlation between antibiotic activities and bound conformations. *Bioorg. Med. Chem.* **6**, 209–221.
27. Novak, P., Tatić, I., Tepeš, P., Koštrum, S. & Barber, J. (2006). Systematic approach to understanding macrolide–ribosome interactions: NMR and modeling studies of oleandomycin and its derivatives. *J. Phys. Chem. A*, **110**, 572–579.
28. Dinos, G., Synetos, D. & Coutsogeorgopoulos, C. (1993). Interaction between the antibiotic spiramycin and a ribosomal complex active in peptide bond formation. *Biochemistry*, **32**, 10638–10647.
29. Poulsen, S. M., Kofoed, C. & Vester, B. (2000). Inhibition of the ribosomal peptidyl transferase reaction by the mycarose moiety of the antibiotics carbomycin, spiramycin and tylosin. *J. Mol. Biol.* **304**, 471–481.
30. Petropoulos, A. D., Kouvela, E. C., Dinos, G. P. & Kalpaxis, D. L. (2008). Step-wise binding of tylosin and erythromycin to *Escherichia coli* ribosomes, characterized by kinetic and footprinting analysis. *J. Biol. Chem.* **283**, 4756–4765.
31. Xiong, L., Shah, S., Mauvais, P. & Mankin, A. S. (1999). A ketolide resistant mutation in domain II of 23S rRNA reveals the proximity of hairpin 35 to the peptidyl transferase centre. *Mol. Microbiol.* **31**, 633–639.
32. Szaflarski, W., Vesper, O., Teraoka, Y., Phitta, B., Wilson, D. N. & Nierhaus, K. H. (2008). New features of the ribosome and ribosomal inhibitors: non enzymatic recycling, misreading and back-translocation. *J. Mol. Biol.* **380**, 193–205.
33. Egebjerg, J., Larsen, N. & Garrett, R. A. (1990). Structural map of 23S rRNA. In *The Ribosome: Structure, Function and Evolution* (Dahlberg, A., Hill, W. E., Garrett, R. A., Moore, P. B., Schlessinger, D. & Warner, J. R., eds), pp. 168–179, American Society for Microbiology, Washington, DC.
34. Morrison, J. F. & Walsh, C. T. (1988). The behavior and significance of slow-binding enzyme inhibitors. *Adv. Enzymol. Relat. Areas Mol. Biol.* **61**, 201–301.
35. Fuentes, F., Izquierdo, J., Martin, M. M., Gomez-Lus, M. L. & Prieto, J. (1998). Postantibiotic and sub-MIC effects of azithromycin and isepamicin against *Staphylococcus aureus* and *Escherichia coli*. *Antimicrob. Agents Chemother.* **42**, 414–418.
36. Bailey, M., Chettiath, T. & Mankin, A. S. (2008). Induction of *erm*(C) expression by noninducing antibiotics. *Antimicrob. Agents Chemother.* **52**, 866–874.
37. Schuwirth, B. S., Borovinskaya, M. A., Hau, C. W.,

Zhang, W., Vila-Sanjurjo, A., Holton, J. M. & Cate, J. H. (2005). Structures of the bacterial ribosome at 3.5 Å resolution. *Science*, **310**, 827–834.
38. Davydova, N., Streltsov, V., Wilce, M., Liljas, A. & Garber, M. (2002). L22 ribosomal protein and effect of its mutation on ribosome resistance to erythromycin. *J. Mol. Biol.* **322**, 635–644.
39. Schlünzen, F., Zarivach, R., Harms, J., Bashan, A., Tocilj, A., Albrecht, R. *et al.* (2001). Structural basis for the interaction of antibiotics with the peptidyl transferase centre in eubacteria. *Nature*, **413**, 814–821.
40. Xaplanteri, M. A., Petropoulos, A. D., Dinos, G. P. & Kalpaxis, D. L. (2005). Localization of spermine binding sites in 23S rRNA by photoaffinity labeling: parsing the spermine contribution to ribosomal 50S subunit functions. *Nucleic Acids Res.* **33**, 2792–2805.
41. Dinos, G., Wilson, D. N., Teraoka, Y., Szaflarski, W., Fucini, P., Kalpaxis, D. L. & Nierhaus, K. H. (2004). Dissecting the ribosomal inhibition mechanisms of edeine and pactamycin: the universally conserved residues G693 and C795 regulate P-site RNA binding. *Mol. Cell*, **13**, 113–124.
42. Stern, S., Moazed, D. & Noller, H. F. (1988). Structural analysis of RNA using chemical and enzymatic probing monitored by primer extension. *Methods Enzymol.* **164**, 481–489.

Paper 4

Chemistry & Biology
Article

Interplay between the Ribosomal Tunnel, Nascent Chain, and Macrolides Influences Drug Inhibition

Agata L. Starosta,[1,2] Viktoriya V. Karpenko,[3] Anna V. Shishkina,[4] Aleksandra Mikolajka,[1,2] Natalia V. Sumbatyan,[3] Frank Schluenzen,[5] Galina A. Korshunova,[4] Alexey A. Bogdanov,[3,4,*] and Daniel N. Wilson[1,2,*]
[1]Gene Center and Department of Biochemistry
[2]Center for Integrated Protein Science Munich
University of Munich, LMU, Munich D-81377, Germany
[3]Department of Chemistry
[4]A.N. Belozersky Institute of Physico-Chemical Biology,
M.V. Lomonosov Moscow State University, Moscow 119992, Russia
[5]Deutsches Elektronen-Synchrotron, Hamburg D-22603, Germany
*Correspondence: bogdanov@genebee.msu.su (A.A.B.), wilson@lmb.uni-muenchen.de (D.N.W.)
DOI 10.1016/j.chembiol.2010.04.008

SUMMARY

Accumulating evidence suggests that, during translation, nascent chains can form specific interactions with ribosomal exit tunnel to regulate translation and promote initial folding events. The clinically important macrolide antibiotics bind within the exit tunnel and inhibit translation by preventing progression of the nascent chain and inducing peptidyl-tRNA drop-off. Here, we have synthesized amino acid– and peptide-containing macrolides, which are used to demonstrate that distinct amino acids and peptides can establish interaction with components of the ribosomal tunnel and enhance the ribosome-binding and inhibitory properties of the macrolide drugs, consistent with the concept that the exit tunnel is not simply a Teflon-like channel. Surprisingly, we find that macrolide antibiotics do not inhibit translation of all nascent chains similarly, but rather exhibit polypeptide-specific inhibitory effects, providing a change to our general mechanistic understanding of macrolide inhibition.

INTRODUCTION

The translational machinery represents one of the major targets within the cell for antibiotics (reviewed by Spahn and Prescott, 1996; Wilson, 2009). The majority of antibiotics inhibit protein synthesis by binding at the active centers on the ribosome; for example, the tetracyclines and aminoglycosides (gentamicin) bind within the decoding site on the small subunit, whereas the phenylpropanoids (chloramphenicol) and oxazolidinones (linezolid) bind within the A-site of peptidyltransferase center (PTC) to block peptide-bond formation. In contrast, the clinically important class of macrolide antibiotics bind within the ribosomal exit tunnel, where they are thought to inhibit translation by blocking elongation of the nascent polypeptide chain, which, in turn, induces peptidyl-tRNA drop-off (Mankin, 2008; Poehlsgaard and Douthwaite, 2003).

Macrolides are a diverse family of antibiotics that contain a central 12–16-membered lactone ring to which various sugar substituent's are attached; for example, erythromycin has a 14-membered ring with C3 cladinose and C5 desosamine sugars (Figure 1), whereas tylosin has a 16-membered ring with a C5 mycaminose-mycarose disaccharide as well as a C23 mycinose (Figures 1 and 2). Crystal structures of macrolides bound to the large ribosomal subunit reveal that the drugs bind within the ribosomal exit tunnel adjacent to the peptidyltransferase center (Figures 2A and 2B) (Hansen et al., 2002; Schlünzen et al., 2001). Surprisingly, 16-membered macrolides that have a C6 ethyl aldehyde (with the aldehyde functional group at C20), such as tylosin (Figure 1), form a reversible covalent bond with the N6 of adenine 2062 (A2062; *Escherichia coli* numbering used throughout) of the 23S ribosomal RNA (Figure 2B) (Hansen et al., 2002). The lactone rings of different macrolides are generally positioned in the tunnel with very similar orientations, such that the C5 sugars extend up the tunnel toward the PTC (Hansen et al., 2002; Poulsen et al., 2000; Schlünzen et al., 2001; Wilson et al., 2005) (Figure 2B). Consistently, macrolides such as erythromycin with only a single C5 sugar allow synthesis of short oligopeptides of six to eight amino acids before peptidyl-tRNA drop-off occurs, whereas macrolides with C5 disaccharides, such as tylosin, allow only two to four amino acids to be synthesized (Tenson et al., 2003), and can even directly inhibit the peptidyltransferase reaction (Karahalios et al., 2006).

It should be noted, however, that the length of the peptide synthesized before peptidyl-tRNA drop-off appears to be dependent on the sequence being translated (Tenson et al., 2003). Translation of short nascent pentapeptides of defined sequence can lead to dissociation of macrolide antibiotics from the ribosome and thus confer macrolide resistance (Lovmar et al., 2006; Tenson et al., 1996; Tenson and Mankin, 2001). Moreover, different pentapeptide sequences can confer resistance to distinct macrolide members, suggesting a direct and discriminating interaction between the nascent chain and the

 ©2010 Elsevier Ltd All rights reserved

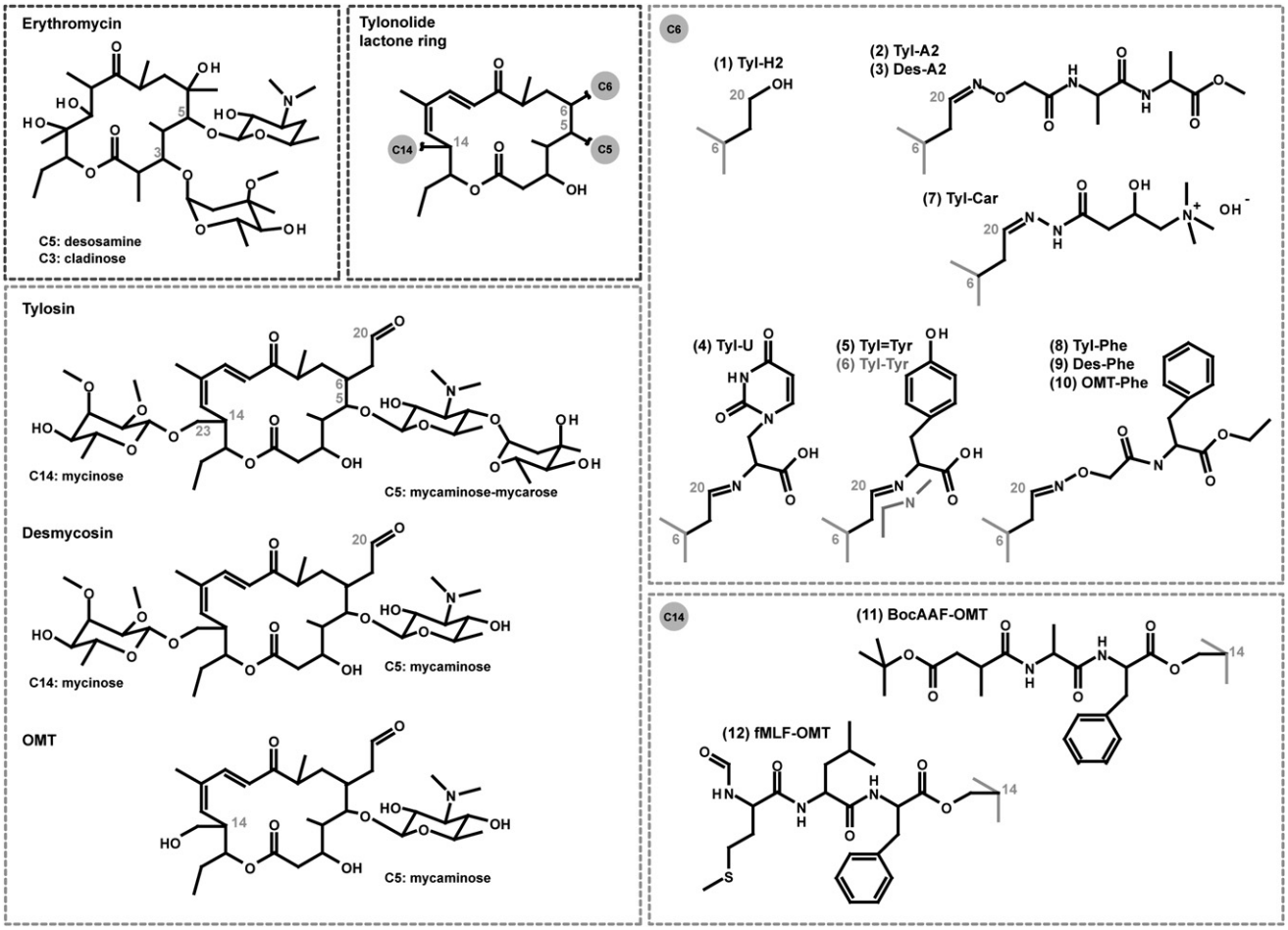

Figure 1. Chemical Structures of Macrolide Antibiotics

Chemical structures of tylosin (Tyl), desmycosin (Des), OMT, erythromycin, and derivatives used in this study (**1**)–(**12**) are depicted.

macrolide (Tenson et al., 1997; Tripathi et al., 1998; Vimberg et al., 2004). Inducible expression of some macrolide resistance genes, such as the methyltransferase encoded by the *ermC* gene, requires macrolide-dependent translational stalling during the synthesis of an upstream leader peptide (Mayford and Weisblum, 1989; Ramu et al., 2009; Vazquez-Laslop et al., 2008). Mutations in the ErmC leader peptide as well as within components of the ribosomal exit tunnel, namely A2062 of the 23S rRNA, have been identified that relieve the translational stalling (Ramu et al., 2009; Vazquez-Laslop et al., 2008), suggesting

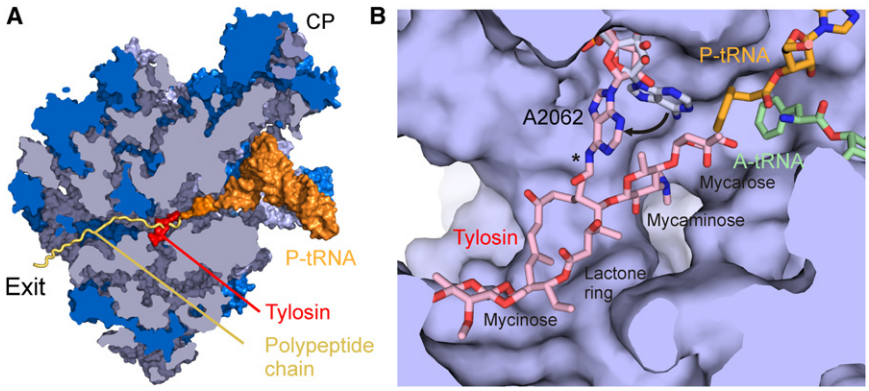

Figure 2. Binding of Macrolide Antibiotics Within the Ribosomal Tunnel

(A) Transverse section through the large subunit of the ribosome to visualize the ribosomal exit tunnel. The position of tylosin (red), P-site tRNA (orange), and a mock polypeptide chain (yellow) are indicated. CP, central protuberance; rRNA, gray and ribosomal proteins (dark blue).

(B) Zoom in on the macrolide-binding site within the ribosomal tunnel. Tylosin (pink) shown with lactone ring, C23-mycinose, and C5-mycaminose-mycarose are labeled. The asterisk indicates the carbinolamine bond that forms between tylosin and the N6 of 23S rRNA nucleotide A2062, whereas the arrow indicates the shift in A2062 seen upon ligand binding. The positions of A- and P-site aminoacyl-tRNAs are shown in green and orange, respectively.

a complex interplay between the antibiotic, the tunnel, and the nascent polypeptide chain.

Although the ribosomal tunnel has for many years been thought of as a passive conduit for the nascent chain, accumulating evidence indicates the existence of many specific leader peptides that induce translational stalling by directly interacting with the ribosomal tunnel, and in doing so regulate translation of a downstream gene (Tenson and Ehrenberg, 2002). Indeed, recent cryo-EM reconstructions directly visualize interaction between the nascent polypeptide chain and components of the ribosomal tunnel (Becker et al., 2009; Bhushan et al., 2010; Seidelt et al., 2009). Moreover, interaction between the nascent chain and tunnel has been proposed to play a more general role in modulating translation rate (Lu and Deutsch, 2008; Seidelt et al., 2009) as well as influencing initial protein folding events (Bhushan et al., 2010; Kosolapov and Deutsch, 2009; Lu and Deutsch, 2005a, 2005b; Woolhead et al., 2004).

Here, we demonstrate that abolishing the potential of tylosin to form a covalent bond with A2062 of the ribosome dramatically reduces the binding and inhibitory properties of the drug, but that this can be reversed by the addition of amino acid and peptide side chains that enable interaction to be reestablished with the ribosomal exit tunnel. A number of the macrolide-peptide compounds are even more potent inhibitors of translation than their parent compounds. Surprisingly, we find that macrolides exhibit nascent chain-specific effects: 5-O-mycaminosyl-tylonolid (OMT), a precursor of tylosin, has excellent antimicrobial activity and is a potent inhibitor of firefly luciferase synthesis. In contrast, OMT is a very poor inhibitor of green fluorescent protein synthesis and can even protect the translational apparatus from the inhibitory effects of other macrolides, such as erythromycin and tylosin. Differential effects are also observed for other macrolide antibiotics but are not seen for non-macrolide antibiotics, such as tetracyclines and chloramphenicols. Collectively, our results demonstrate the direct and specific interaction between peptides and the ribosomal tunnel and suggest that the inhibitory effect of macrolides is dependent on the sequence of the nascent polypeptide chain being translated.

RESULTS

Peptide Interaction with the Tunnel Compensates for Loss of the Covalent Bond

To investigate the effect of the covalent linkage between the C6 ethyl aldehyde of tylosin and the N6 of A2062 of the 23S rRNA (Figure 2B), we synthesized a reduced form of tylosin, (**1**) Tyl-H2, where the C6 ethyl aldehyde is replaced by hydroxyethyl group (Figure 1A). Binding of (**1**) Tyl-H2 to the ribosome was monitored by competition with radiolabeled [^{14}C]-erythromycin (apparent K_d calculations in Table S1, available online, are based on a 2 hr incubation; see Experimental Procedures). In the control experiment, we demonstrate that tylosin is an excellent competitor, completely abolishing the binding of erythromycin at ~0.1 μM (Figure 3A). In contrast, (**1**) Tyl-H2 was totally inactive, and no significant loss in erythromycin binding was observed with 100× higher concentrations (10 μM) of the compound (Figure 3A). These results support the importance of the carbinolamine covalent linkage for efficient ribosome binding, in agreement with previous findings that modification of the C20 aldehyde group leads to a ~100-fold increase in the MIC value for a variety of gram-positive bacteria (Kirst et al., 1988; Narandja et al., 1994; Omura et al., 1982; Omura and Tishler, 1972).

Next, we synthesized a series of macrolide derivatives where amino acids and peptides were attached to the C20 aldehyde position to investigate whether amino acids can establish defined interactions with the ribosomal exit tunnel. We reasoned that if this is indeed the case, then the peptide-tunnel interactions should improve the binding affinity of the compounds. As can be seen in Figure 3A, the presence of Ala-Ala at the C20 position to generate (**2**) Tyl-A2 dramatically improves the ability of the compound to compete with erythromycin for ribosome binding. Similar results were also obtained when Ala-Ala was attached to the C20 position of desmycosin, a degradation product of tylosin differing by the absence of a C5 mycarose, to generate (**3**) Des-A2 (Figure 3A). This finding suggests that, indeed, the Ala-Ala peptides establish interaction with the tunnel to improve the binding of the compounds compared with the Tyl-H2; however, it should be noted that the K_d of (**2**) Tyl-A2 and (**3**) Des-A2 (~18 nM for both compounds) are still significantly worse than their C6 ethyl aldehyde–containing parent compounds tylosin (0.65 nM) and desmycosin (0.3 nM) (Table S1; Figure 3A).

To test the inhibitory activity of the compounds, we utilized an *E. coli* lysate–based, in vitro, coupled transcription-translation system (Dinos et al., 2004; Starosta et al., 2009), where the synthesis of green fluorescent protein (GFP) was monitored by directly measuring fluorescence (Figure 3B). Consistent with the ribosome binding results, tylosin was found to be an excellent inhibitor, with an IC_{50} of 0.25 μM and abolishing translation at ~1 μM (Figures 3B and 3C), whereas (**1**) Tyl-H2 had an IC_{50} > 10× higher (4 μM) (Table S1) and did not even completely abolish translation at 25 μM (data not shown). (**2**) Tyl-A2 exhibited improved inhibitory characteristics, with an IC_{50} of 0.5 μM—only slightly worse than that of tylosin (Figure 3C; Table S1). This contrasts with the binding assay results where (**2**) Tyl-A2 was a significantly worse competitor of erythromycin than tylosin for ribosome binding (Figure 3A). A similar trend was observed when comparing desmycosin with (**3**) Des-A2, in that (**3**) Des-A2 was a slightly more effective inhibitor than desmycosin. However, unlike (**2**) Tyl-A2, both desmycosin and (**3**) Des-A2 could not fully abolish translation even at high concentrations (Figure 3C; Table S1).

We have previously determined a crystal structure of (**2**) Tyl-A2 bound to the *Deinococcus radiodurans* large ribosomal subunit (Wilson et al., 2005), which shows that the lactone ring binds in a similar position to that seen for tylosin (Hansen et al., 2002). The C20 Ala-Ala peptide protrudes into a small alcove or pocket within the tunnel wall, where it stacks against the base of A2062 (Figure 3E). The presence of the C20 Ala-Ala peptide on (**2**) Tyl-A2 precludes formation of the carbinolamine bond with the N6 of A2062, and as a result A2062 is in a shifted position compared to the tylosin-50S structure (Hansen et al., 2002) (Figure 3D).

Optimized Stacking Interactions with A2062 Improves Inhibition

On the basis of the structure of the (**2**) Tyl-A2 bound to the large subunit, a series of novel C6 tylosin derivatives were synthesized that can potentially form better stacking interactions with the

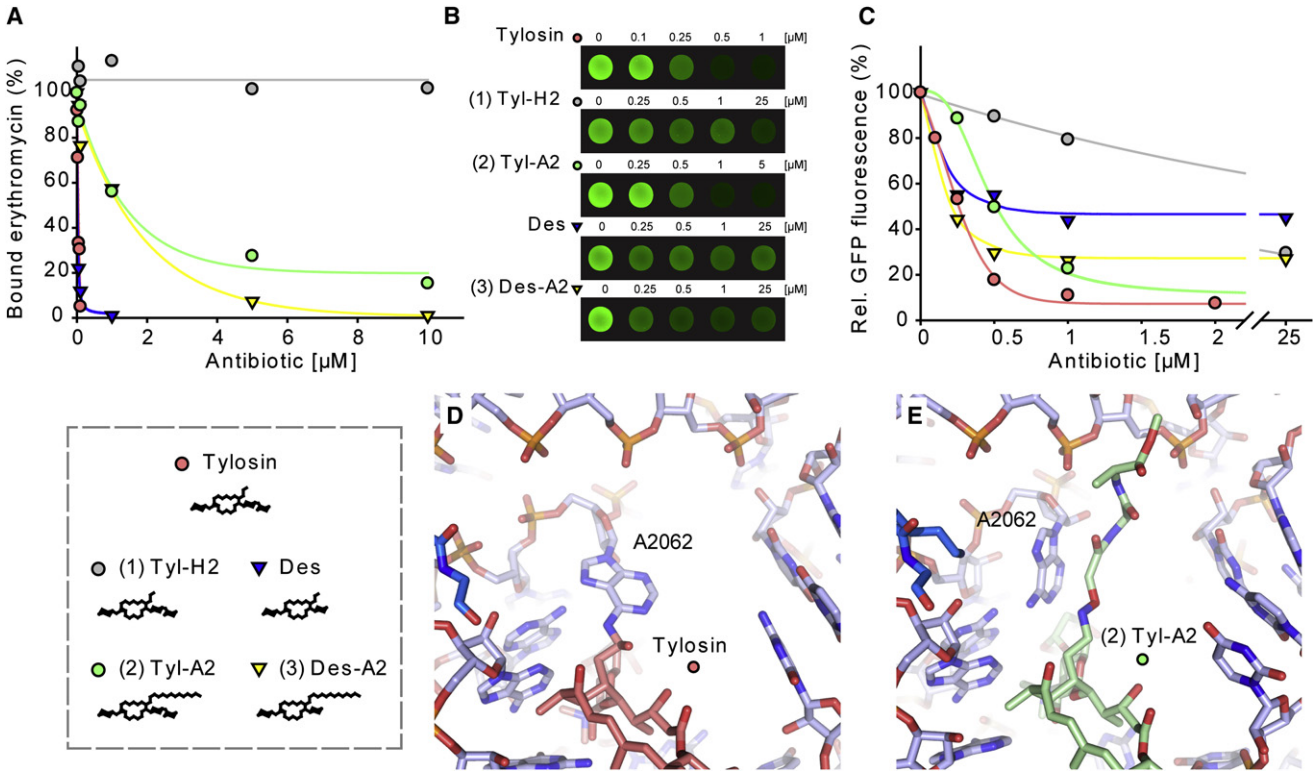

Figure 3. Inhibitory Effect of Tylosin and Desmycosin Ala2 Derivatives

(A) The ability of tylosin (pink), Tyl-H2 (gray), desmycosin (Des, blue), (**2**) Tyl-A2, and (**3**) Des-A2 to compete with radiolabeled erythromycin for binding to *E. coli* 70S ribosomes was determined. The binding of erythromycin in the absence of competing ligand was assigned as 100%.

(B) The amount of GFP produced in an *E. coli* in vitro transcription-translation assay in the presence or absence of tylosin, (**1**) Tyl-H2 and (**2**) Tyl-A2, Des, and (**3**) Des-A2 was determined by monitoring fluorescence of GFP. The fluorescence of GFP in the absence of antibiotic was assigned as 100%.

(C) Quantification of (B) with symbols and colors for each compound as in (A).

(D) The binding site of tylosin on the *H. marismortui* 50S subunit showing the formation of a covalent carbinolamine bond between the C6 ethyl-aldehyde of tylosin (red) and the N6 of the base of A2062 of the 23S rRNA (Hansen et al., 2002).

(E) The binding site of (**2**) Tyl-A2 (green) on the *D. radiodurans* 50S subunit showing the stacking interaction between the Ala-Ala side chain of (**2**) Tyl-A2 and the base of A2062 of the 23S rRNA (Wilson et al., 2005).

base of A2062, namely by introducing aromatic or heterocyclic groups that replace the Ala amino acids. Because base-stacking between RNA nucleotides is an efficient and highly ubiquitous interaction mode within RNA particles, the first compound, (**4**) Tyl-U, was designed with an uridine (U) RNA nucleobase linked to the lactone C6 carbon by a four-atom linker (Figure 1). In the translation assay, (**4**) Tyl-U was still a worse inhibitor than (**2**) Tyl-A2, but was superior to (**1**) Tyl-H2 (Figure 4A; Table S1).

In parallel, we investigated the effect of replacing the Ala-Ala peptide with the amino acid tyrosine (Tyr) to generate the (**5**) Tyl=Tyr derivative, which also utilizes a five-atom linker. Although this compound had improved binding and inhibitory activity with respect to (**1**) Tyl-H2, it was still significantly worse than (**2**) Tyl-A2 (Figures 4A and 4B; Table S1). We rationalized that the double bond in the linker may restrict the conformational freedom of the side chain and therefore synthesized a second compound (**6**) Tyl-Tyr with a fully saturated linker. In the translation assays, (**6**) Tyl-Tyr was a significantly better inhibitor than (**5**) Tyl=Tyr and (**2**) Tyl-A2 (Figure 4B; Table S1), which was consistent with the improved binding properties of (**6**) Tyl-Tyr (Figure 4A). What was curious was (**6**) Tyl-Tyr had an IC_{50} comparable to that of tylosin (Figure 4B; Table S1), despite being less effective than tylosin at competing for ribosome binding with erythromycin (Figure 3A).

In a separate approach, we also attached carnitine to the C20 position to generate (**7**) Tyl-Car (Figure 1). The positively charged side chain improves the aqueous solubility, compared with tylosin, but was also intended to improve interactions with the highly electronegative cleft in the ribosomal tunnel. Indeed, (**7**) Tyl-Car displayed binding (K_d, 0.6 nM) and inhibition (IC_{50}, 0.3) properties very similar to those of tylosin (Figures 4A and 4B; Table S1), suggesting that, like (**2**) Tyl-A2, the side chain of (**7**) Tyl-Car establishes interaction with the ribosomal tunnel that compensate for the loss of the carbinolamine bond. (**7**) Tyl-Car was modeled in the tunnel with the constraint that the lactone ring and A2062 were positioned as in (**2**) Tyl-A2 structure (Wilson et al., 2005). The most energetically favorable solution indicated that the carnitine side chain adopted a conformation that establishes stacking interactions with A2062 (Figure 4C).

Enhanced Tylosin Antibiotics That Utilize Peptide-Tunnel Interaction

To further explore the stacking potential of the C20 side chains with the nucleobase of A2062, we decided to introduce

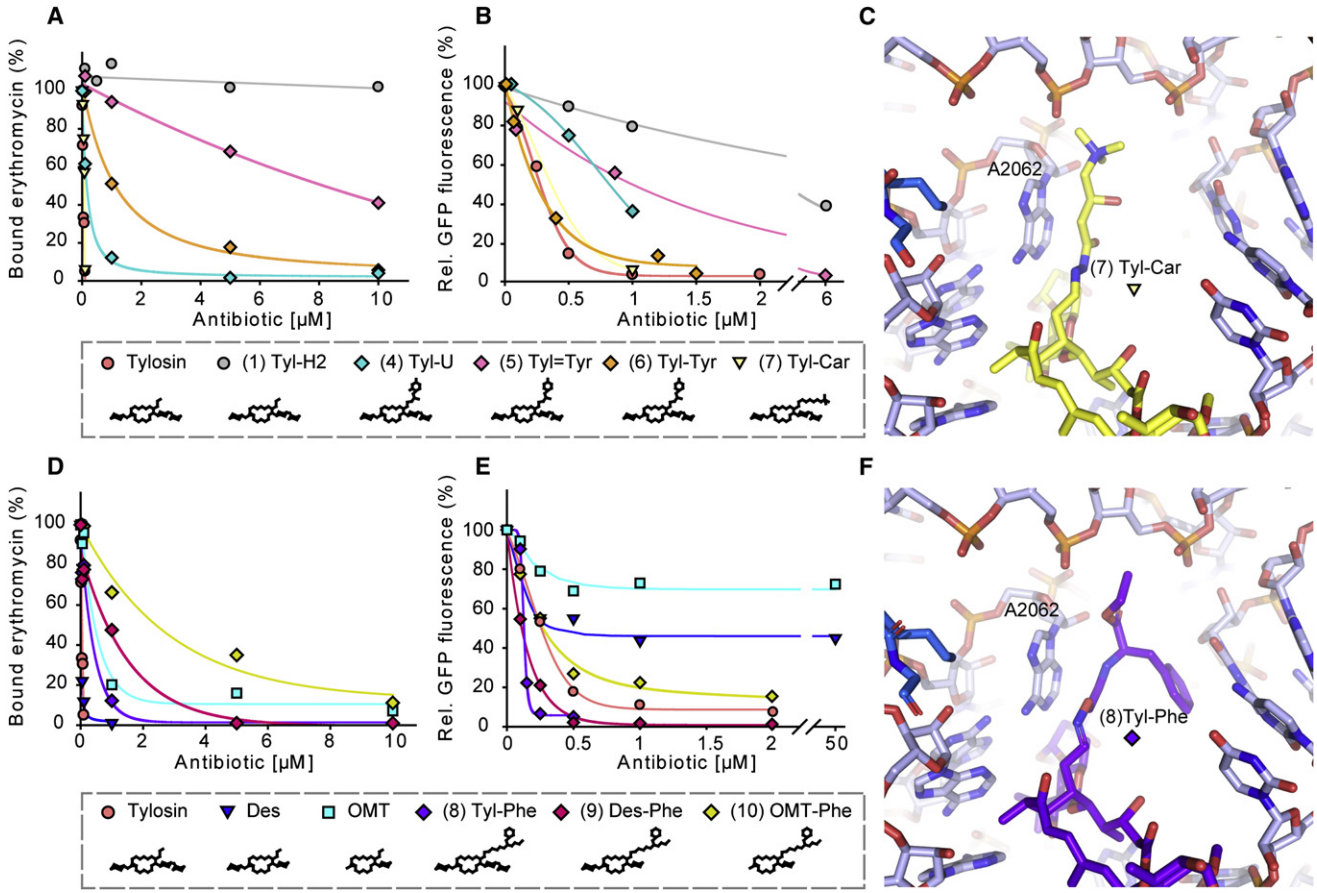

Figure 4. Stacking Interaction with A2062

(A) The ability of tylosin, (**1**) Tyl-H2, (**4**) Tyl-U, (**5**) Tyl=Tyr, (**6**) Tyl-Tyr, and (**7**) Tyl-Car to compete with radiolabeled erythromycin for binding to *D. radiodurans* 70S ribosomes was determined. The binding of erythromycin in the absence of competing ligand was assigned as 100%.

(B) Quantification of the fluorescence of GFP produced in an *E. coli* in vitro transcription-translation assay in the presence or absence of tylosin, (**1**) Tyl-H2, (**4**) Tyl-U, (**5**) Tyl=Tyr, (**6**) Tyl-Tyr, and (**7**) Tyl-Car. The fluorescence of GFP in the absence of antibiotic was assigned as 100%.

(C) Model based on Tyl-A2 for the binding site of (**7**) Tyl-Car (yellow) on the *D. radiodurans* 50S subunit showing the stacking interaction between the carinitine sidechain of (**7**) Tyl-Car and the base of A2062 of the 23S rRNA.

(D) The ability of tylosin, desmycosin (Des), OMT, (**8**) Tyl-Phe, (**9**) Des-Phe, and (**10**) OMT-Phe to compete with radiolabeled erythromycin for binding to *D. radiodurans* 70S ribosomes was determined. The binding of erythromycin in the absence of competing ligand was assigned as 100%.

(E) Quantification of the fluorescence of GFP produced in an *E. coli* in vitro transcription-translation assay in the presence or absence of tylosin, desmycosin (Des), OMT, (**8**) Tyl-Phe, (**9**) Des-Phe, and (**10**) OMT-Phe. The fluorescence of GFP in the absence of antibiotic was assigned as 100%.

(F) Model based on (**2**) Tyl-A2 for the binding site of (**8**) Tyl-Phe (purple) on the *D. radiodurans* 50S subunit showing the stacking interaction between the linker of (**8**) Tyl-Phe and the base of A2062, as well as a between the phenylalanine aromatic residue and the base of C2586 of the 23S rRNA.

a nonpolar phenylalanine (Phe), while extending the linker, but maintaining its overall flexibility. Binding studies indicate that this compound, (**8**) Tyl-Phe, improved the ribosome binding affinity (K_d, 3.6 nM) compared to (**1**) Tyl-H2 (Figure 4D; Table S1). Consistently, (**8**) Tyl-Phe was found to be a very potent inhibitor of translation (Figure 4E), performing slightly better than tylosin but significantly better than (**2**) Tyl-A2 and (**1**) Tyl-H2 (Table S1). The Phe side chain may stabilize the binding of (**8**) Tyl-Phe by establishing additional stacking interactions with 23S rRNA nucleotides (Figure 4F). However, the improved ribosome binding affinity cannot be the sole explanation for the increased translational inhibitory activity relative to tylosin, because (**8**) Tyl-Phe was significantly less effective compared to tylosin at competing erythromycin from the ribosome (Figure 4D).

We also synthesized (**9**) Des-Phe and (**10**) OMT-Phe, where the Phe-containing linker side chain was attached to the C20 position of desmycosin and OMT, respectively (Figure 1). OMT is a precursor of tylosin, which lacks both the C5 mycarose and the C23 mycinose (Figure 1). Our erythromycin competition studies indicate that both (**9**) Des-Phe and (**10**) OMT-Phe were worse competitors than their respective parent compounds (Figure 4D). The order of affinities of (**8**) Tyl-Phe > (**9**) Des-Phe > (**10**) OMT-Phe is the same as for tylosin > desmycosin > OMT, and correlates with the predicted surface areas that these compounds bury on the ribosome; that is, more surface area buried equals higher binding affinity (Hansen et al., 2002). However, that each derivative had a lower binding affinity than the parent compound emphasizes again the important influence that the C6-ethyl aldehyde and presumably the carbinolamine

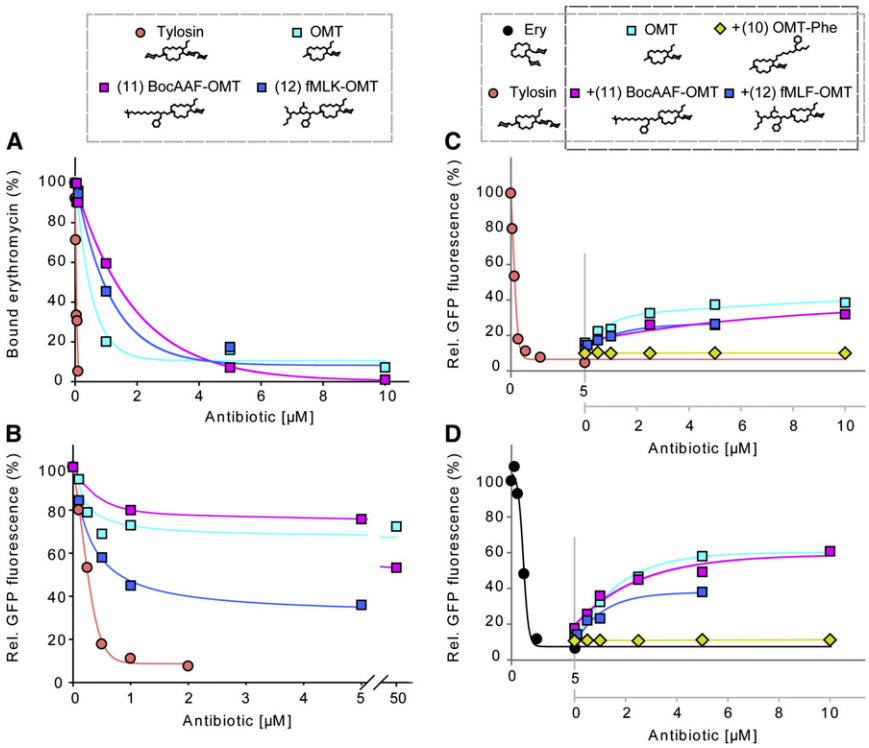

Figure 5. Protective Effects of OMT Compounds

(A) The ability of tylosin, OMT, (**11**) BocAAF-OMT, and (**12**) fMLF-OMT to compete with radiolabeled erythromycin for binding to *D. radiodurans* 70S ribosomes was determined. The binding of erythromycin in the absence of competing ligand was assigned as 100%.

(B) Quantification of the fluorescence of GFP produced in an *E. coli* in vitro transcription-translation assay in the presence or absence of tylosin, OMT, (**11**) BocAAF-OMT, and (**12**) fMLF-OMT. The fluorescence of GFP in the absence of antibiotic was assigned as 100%.

(C) Quantification of the fluorescence of GFP produced in an *E. coli* in vitro transcription-translation assay in the presence of increasing concentrations (upper *x*-axis) of erythromycin (Ery) to 5 μM, then with additional presence of increasing concentrations (lower *x*-axis) of OMT (cyan), (**11**) BocAAF-OMT (magenta), (**12**) fMLF-OMT (blue), or (**10**) OMT-Phe (yellow).

(D) Quantification of the fluorescence of GFP produced in an *E. coli* in vitro transcription-translation assay in the presence of increasing concentrations (upper *x*-axis) of tylosin (Ery) to 5 μM, then with additional presence of increasing concentrations (lower *x*-axis) of OMT (cyan), (**11**) BocAAF-OMT (magenta), (**12**) fMLF-OMT (blue), or (**10**) OMT-Phe (yellow).

bond has on stabilizing the C6-ethyl aldehyde–containing macrolides on the ribosome.

In the translation system, (**9**) Des-Phe and (**10**) OMT-Phe, like (**8**) Tyl-Phe, were more potent inhibitors than would have been expected on the basis of their K_d values. (**9**) Des-Phe and (**10**) OMT-Phe had IC_{50} values (0.1 μM and 0.3 μM, respectively) similar to that of tylosin (0.25 μM) (Figure 4E; Table S1), thus indicating that the presence of the peptide and its interaction with the tunnel can compensate for loss in binding affinity resulting from disruption of the covalent linkage with the ribosome. In contrast, we found unexpectedly that desmycosin and OMT were very poor inhibitors of translation. Even with high concentrations of antibiotic (50–100 μM), desmycosin never inhibited translation by more than 50% (Figure 3B), and OMT had little or no significant inhibitory effect (Figure 4E). This finding was surprising because (1) both OMT and desmycosin bound efficiently to an empty ribosome (Figure 4D), with K_d values of 3 nM and 0.3 nM, respectively (Table S1), similar to that previously reported (Karahalios et al., 2006) and that is 5- and 50-fold better than that of erythromycin (K_d, 15 nM) (Karahalios et al., 2006); and (2) both OMT and desmycosin have potent antimicrobial activity (data not shown). Indeed, OMT and desmycosin are known to have MIC values similar to tylosin for a number of gram-positive bacterial strains (e.g., *Streptococcus pyogenes*, *Staphlococcus aureus*, and *Enterococcus faecalis*) (Fu et al., 2006; Kirst et al., 1988; Mutak et al., 2004).

Protective Effects of Peptide-OMT Precursor Compounds Against Translation Inhibition

To investigate the differential effects of OMT in more detail, we synthesized a series of peptide-OMT compounds, where BocAlaAlaPhe and fMetLeuPhe peptides were attached to C14(C23) of OMT to generate (**11**) BocAAF-OMT and (**12**) fMLF-OMT derivatives, respectively. These compounds still retain a C5 sugar and the C6 ethyl aldehyde, and the placement of the peptide side chain on the C14(C23) position of the lactone ring orients it such that it would penetrate deeper into the ribosomal tunnel. Like OMT, both (**11**) BocAAF-OMT and (**12**) fMLF-OMT were excellent competitors of erythromycin, although the presence of the peptide did not enhance the affinity of the derivative for the ribosome (Figure 5A). In contrast, the presence of the peptide improved the inhibitory effect of the OMT derivatives, particularly, (**12**) fMLF-OMT, which inhibited the in vitro translation reaction by 50% at ~1 μM (Figure 5B).

Because OMT and some of the derivatives were shown to bind efficiently to an empty ribosome, but were poor inhibitors in the translation assay, we decided to test whether the compounds could relieve the translation inhibition effect that results from other more effective macrolide antibiotics, such as tylosin and erythromycin. Figure 5C shows that, at 5 μM erythromycin, the translation of GFP is totally abolished, whereas when OMT, (**11**) BocAAF-OMT, or (**12**) fMLF-OMT are additionally titrated into the reaction, the inhibition of translation was gradually alleviated. As a control, (**10**) OMT-Phe, which was shown itself to be a potent inhibitor (Figure 4E), could not relieve the inhibitory effect due to erythromycin (Figure 5C). Indeed, the extent of relief appeared to correlate inversely with the innate inhibitory activity of the compound; for example, OMT and (**11**) BocAAF-OMT, which were the poorest inhibitors, yielded the strongest relief (up to 40% with 5 μM—that is, equimolar concentration to erythromycin), whereas (**12**) fMLF-OMT, which was a slightly better inhibitor, only restored translation by up to 20% at 5 μM final

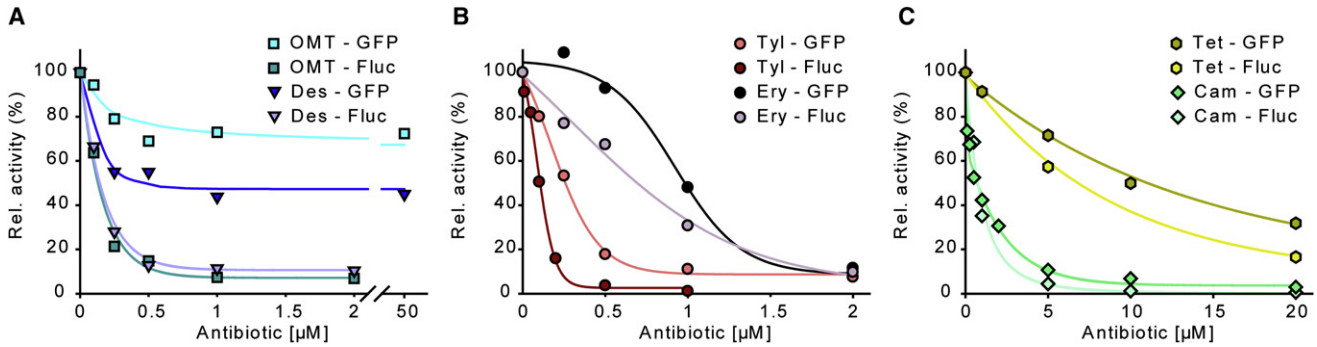

Figure 6. Polypeptide Chain-Dependency of Macrolide Antibiotics

(A) Comparison of the effect of desmycosin (Des) and OMT on the in vitro transcription-translation of green fluorescent protein (GFP) and firefly luciferase (Fluc).

(B) Comparison of the effect of tylosin (Tyl) and erythromycin (Ery) on the in vitro transcription-translation of GFP and Fluc.

(C) Comparison of the effect of chloramphenicol (Cam) and tetracycline (Tet) on the in vitro transcription-translation of GFP and Fluc. In (A)–(C), the fluorescence of GFP or luminescence of Fluc in the absence of antibiotic was assigned as 100%.

concentration (Figure 5C). This latter result was slightly surprising, since at 5 μM of (**12**) fMLF-OMT, the drug itself reduces translation by 60% (to 40%). Similar results were observed when 5 μM tylosin was used instead of erythromycin; however, higher excesses of OMT and the derivatives were required to obtain the equivalent inhibitory relief that was observed with erythromycin (Figure 5D). For example, 10 μM (2× tylosin concentration) of OMT produced only ~30% relief (Figure 5D). This trend is consistent with the higher affinity and IC_{50} of tylosin over erythromycin (Table S1) and thus supports the idea that the relief is due to direct competition between the OMT/OMT-derivative and the inhibitory compound (tylosin or erythromycin). Additional evidence includes the observations that (1) OMT/OMT-derivatives could not relieve the translation inhibition resulting from nonmacrolide antibiotics, such as tetracycline or thiostrepton (data not shown), and (2) compounds that were very poor competitors with erythromycin, such as (**1**) Tyl-H2 (Figure 3A), produced very low inhibition relief with extremely high excesses of compound—for example, 25 μM (5× excess) (**1**) Tyl-H2 produced 4% relief for 5 μM tylosin (data not shown).

Macrolide Antibiotics Exhibit Polypeptide-Specific Inhibitory Effects

Because of the inconsistency between the potent antimicrobial activity of OMT and the poor inhibitory activity in the in vitro translation assay, we decided to test whether OMT displayed some template-specific effects. To do this, we substituted the GFP template with firefly luciferase (Fluc) and monitored translation of Fluc using luminescence. Figure 6A shows that OMT is an excellent inhibitor of translation of Fluc, with an IC_{50} of 0.15 μM, similar to that observed for the inhibition of GFP synthesis by tylosin (0.25 μM). Similarly, we found that Des, which we had shown to be a poor inhibitor of GFP (Figure 3C), was a potent inhibitor of Fluc synthesis (Figure 6A). Less dramatic differences were observed when comparing the effect of tylosin and erythromycin on GFP and Fluc synthesis (Figure 6B). The effect of tylosin on GFP and Fluc synthesis was similar, whereas the corresponding values for erythromycin were 1 μM (GFP) and 0.75 μM (Fluc) (Table S1). We believe that this template dependency in inhibition is specific for the macrolide class of antibiotics, because we do not find such distinct inhibitory effects when examining the inhibition of other antibiotic classes, such as the tetracyclines or phenylpropanoids (i.e., chloramphenicol) (Figure 6C). Tetracycline inhibits GFP synthesis with an IC_{50} of 11 μM and Fluc with an IC_{50} of 7 μM, and chloramphenicol inhibits GFP and Fluc with the same IC_{50} of ~1 μM (Figure 6C).

DISCUSSION

The surface of the exit tunnel is largely hydrophilic and has no patches of hydrophobic surface large enough to form a significant binding site for hydrophobic sequences in nascent polypeptide chains (Nissen et al., 2000). Although this general "nonstick" characteristic of the exit tunnel may hold for the majority of polypeptides being synthesized by the ribosome, growing evidence indicates that particular nascent chain sequences interact with the ribosomal tunnel during their egression (Becker et al., 2009; Bhushan et al., 2010; Cruz-Vera et al., 2005; Cruz-Vera and Yanofsky, 2008; Gong and Yanofsky, 2002; Kosolapov and Deutsch, 2009; Lawrence et al., 2008; Lu and Deutsch, 2005a, 2005b, 2008; Nakatogawa and Ito, 2002; Seidelt et al., 2009; Tenson and Ehrenberg, 2002; Vazquez-Laslop et al., 2008; Woolhead et al., 2004). Here, we have utilized macrolide antibiotics to direct amino acid and peptide sequences to bind and interact with the ribosomal tunnel. Our results indicate that specific amino acid and peptide sequences can indeed establish distinct interactions with components of the ribosomal tunnel, such as stacking interactions between the backbone and aromatic moieties with nucleotide A2062 of the 23S rRNA. A2062 is a universally conserved nucleotide that appears to adopt different conformations within the ribosomal tunnel dependent upon the functional state of the ribosome. In the crystal structure of the apo *Haloarcula marismortui* 50S subunit, A2062 lies flat against the tunnel wall, whereas when P-site ligands are bound A2062 shifts position to extend into the lumen of the ribosomal tunnel (Figure 2B). It appears that A2062 also establishes interaction with the nascent polypeptide chains, as observed by cryo-EM of stalled translating ribosomes (Bhushan et al., 2010; Seidelt et al., 2009). Mutations of A2062 relieve the translational arrest resulting during synthesis of the ErmC leader peptide,

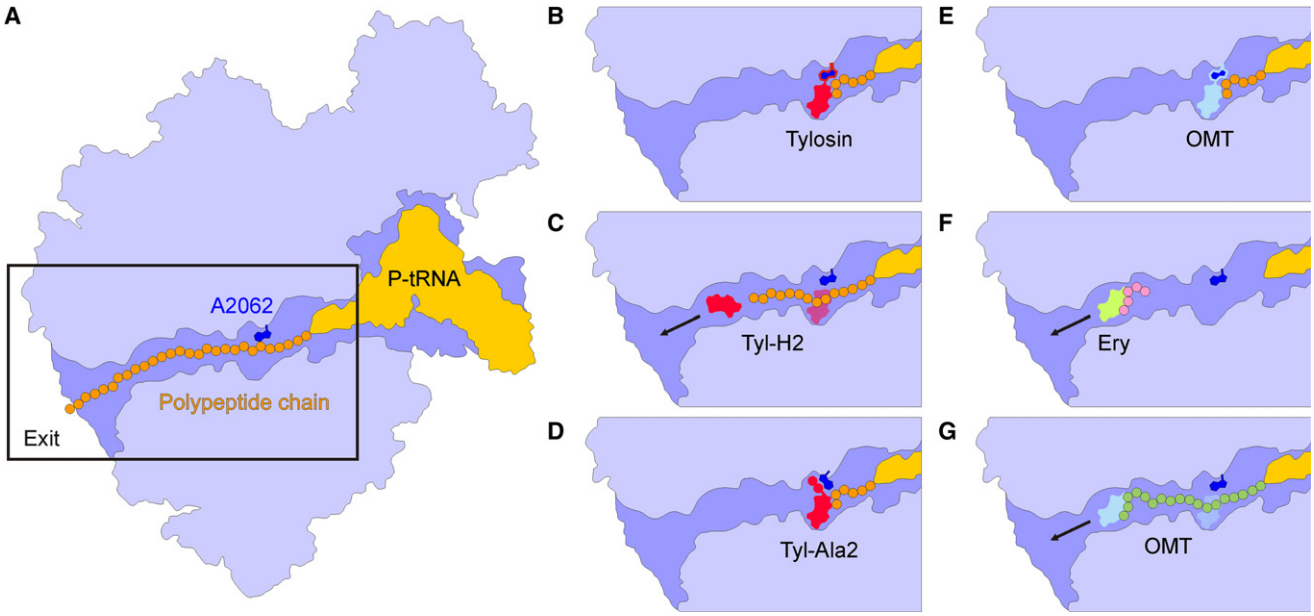

Figure 7. Factors Influencing Macrolide Inhibition

(A) Schematic view of a transverse section through the large ribosomal subunit revealing a P-site tRNA (yellow) attached to a polypeptide chain (orange) in the tunnel exit. The nucleotide A2062 (blue) has been proposed to interact with some polypeptide chains (Ramu et al., 2009; Vazquez-Laslop et al., 2008).

(B) Tylosin (red) binds within the tunnel where it forms a covalent bond with A2062 of the 23S rRNA and allows only translation of short peptides.

(C) Reducing the C6 ethylaldehyde of tylosin to produce (**1**) Tyl-H2 prevents the covalent interaction with A2062, reducing the binding affinity and allowing translation in the presence of the drug.

(D) Addition of amino acids or peptides to the C20 position prevents the covalent interaction with A2062, but establishes new compensatory interaction with the tunnel that increases the binding affinity and thus allows only translation of short peptides.

(E) OMT (cyan) binds within the tunnel where it forms a covalent bond with A2062 of the 23S rRNA and allows only translation of short peptides of the Fluc protein.

(F) Translation of short pentapeptide sequences confers resistance to macrolide antibiotics, such as erythromycin (Tenson et al., 1996). The peptide is thought to interact with the drug and remove it from the binding site when the peptide is released from the tRNA (Tenson and Mankin, 2001).

(G) Translation of GFP is not inhibited by OMT (cyan) either because the polypeptide chain removes the drug from its binding site or can pass the drug undisturbed.

suggesting that this nucleotide might be involved in monitoring the nascent chain as it passes through the tunnel (Figure 7A) (Vazquez-Laslop et al., 2008).

A2062 is also involved in the interaction of 16-membered macrolides, such as tylosin, with the ribosome because it forms a covalent bond with the drug. Here we show that reducing the C6-ethyl aldehyde of tylosin (Tyl-H2), which abolishes the potential to form a covalent linkage with the N6 of A2062, dramatically reduces the K_d value by >100-fold (Table S1). The corresponding loss in effectiveness of this antibiotic in translation inhibition is seen by a reduction in IC_{50} by >10-fold (Table S1), suggesting that the nascent polypeptide chain can now expel the drug from the ribosome (Figure 7C). It should be noted, however, that the presence of a C6-ethyl aldehyde is not strictly necessary for efficient binding and potent inhibitory activity because erythromycin has a C6-hydroxyl and thus cannot and does not form the carbinolamine bond (Tu et al., 2005). The differences in orientation (Hansen et al., 2002; Tu et al., 2005; Wilson et al., 2005) and kinetics (Petropoulos et al., 2009) of binding between 14-membered macrolides, such as erythromycin, and 16-membered macrolides, such as tylosin, seems to obviate the C6-ethyl aldehyde in the former case. It would be interesting in the future to analyze the characteristics of C6-ethyl aldehyde containing 14-membered macrolides, with respect to binding modes, kinetics, and formation of the carbinolamine interaction with A2062. Nevertheless, we could show that the loss of the covalent bond can be compensated for by addition of amino acid or peptide side chains to the C6(C23) position of the drug (Figure 7D). On the basis of the observation that (**2**) Tyl-A2 stacks upon the nucleobase of A2062 (Figures 3E and 7D), a series of compounds was designed to explore different modes of interactions with this region of the ribosome, culminating in a series of compounds—(**6**) Tyl-Tyr, (**7**) Tyl-Car, (**8**) Tyl-Phe, (**9**) Des-Phe, and (**10**) OMT-Phe—that were similar or better inhibitors of translation compared to tylosin (Figure 4; Table S1). These results also demonstrate the potential to use the ribosome antibiotic structures as a basis for rational design of novel derivatives of antimicrobial agents.

One observation with respect to many of the macrolide-peptide derivatives is the lack of correlation between the K_d and IC_{50} values, namely that all of the macrolide-peptide derivatives are less effective at competing erythromycin from the ribosome than are tylosin, but are relatively better inhibitors of translation. This suggests that the binding affinity per se does not solely determine the effectiveness of the compound and that the C20-side chains contribute an additional factor, perhaps by sterically blocking the path of the nascent polypeptide chain (Figure 7D). The most dramatic example of this is seen for

OMT and (**10**) OMT-Phe, because OMT has a K_d value ~9× lower than that of (**10**) OMT-Phe (Table S1), yet (**10**) OMT-Phe is a vastly superior inhibitor of GFP synthesis (Figure 4E). The ability of OMT and the peptide-OMT derivatives, (**11**) BocAAF-OMT and (**12**) fMLF-OMT to restore translation in the presence of inhibitory concentrations of erythromycin or tylosin (Figures 5C and 5D) is consistent with the binding data (Figures 4D and 5A), supporting the conclusion that these compounds do bind to the ribosome, and thus are likely to reverse the effect of erythromycin and tylosin by competing the drugs from their binding site in tunnel.

The lack of effect of OMT on GFP synthesis (Figures 5E and 6A) was surprising because OMT is known to be a potent antimicrobial agent that targets the translation machinery (Fu et al., 2006; Kirst et al., 1988; Mutak et al., 2004). This finding prompted us to test the effect of macrolides on translation of Fluc, which we could monitor using luminescence. OMT was found to be a potent inhibitor of Fluc synthesis (Figure 7E), as was tylosin (Figure 6A). Similarly, we found differential effects for desmycosin, which was a poor inhibitor of GFP but an excellent inhibitor of Fluc synthesis (Figure 6A). In contrast, few significant differences were observed between the inhibition of GFP and Fluc synthesis by other macrolides, such as tylosin (Figure 6B), erythromycin, (Figure 6C), nor for other classes of antibiotics, such as chloramphenicols and tetracyclines (Figure 6C). We also generated chimeric Fluc-GFP templates where the first 5–15 amino acids of Fluc were placed at the N terminus of GFP and vice versa. Unfortunately, the efficiency of translation of these proteins appeared to be dramatically affected, such that the interpretation of the results was inconclusive (data not shown).

Collectively, the data suggest that the sequence of the nascent chain may influence the inhibitory ability of particular macrolide antibiotics. Precedents for this include the observation that translation of specific pentapeptides can confer resistance to macrolide antibiotics by chasing the drug from the ribosome (Figure 7F). Distinct pentapeptides sequences are specific for particular macrolide or ketolide members, leading to the proposal of a direct interaction between the nascent chain and the drug in the ribosomal tunnel (Lovmar et al., 2006; Tenson et al., 1996; Tenson and Mankin, 2001; Tenson et al., 1997; Tripathi et al., 1998; Vimberg et al., 2004). By analogy, we propose that the GFP nascent polypeptide chain establishes specific interactions with OMT, leading to its removal from the ribosome (Figure 7G).

Because macrolide antibiotics cannot bind to and inhibit translating ribosomes (Contreras and Vazquez, 1977; Tai et al., 1974), we do not believe that the differential inhibitory effects of OMT on GFP and Fluc synthesis result from the ability of the GFP, but not Fluc, nascent polypeptide chain to pass the drug in the exit tunnel, but we cannot totally exclude this possibility. Macrolide antibiotics have been shown to allow synthesis of up to six to eight amino acids before peptidyl-tRNA drop-off occurs (Tenson et al., 2003). This may hint that the N-terminal six to eight residues of translating nascent chains, in this case GFP, interacts with drug (OMT) and removes it from the tunnel by continued translation of the nascent chain (Figure 7G) as suggested previously (Mankin, 2008), in contrast to drug removal via peptidyl-tRNA hydrolysis, as occurs in the case of the macrolide-resistance peptides (Figure 7F) (Tenson and Ehrenberg, 2002).

The proposed model suggests that the translation of a particular subset of proteins in vivo may not be inhibited by macrolide antibiotics, which could potentially provide the cell an additional regulatory mechanism, for example, to up-regulate relevant resistance genes. Future works needs to address the ubiquity of this "translating nascent chain-mediated macrolide resistance" and to determine whether specific consensus sequences exist for distinct macrolides.

EXPERIMENTAL PROCEDURES

Synthesis of Peptide Derivatives of Macrolides

(**1**) Tyl-H2 was prepared by reduction of Tyl with sodium borohydride (Kirst et al., 1988). (**2**) Tyl-A2 and (**3**) Des-A2 were synthesized as described elsewhere (Sumbatyan et al., 2003). (**8**) Tyl-Phe, (**9**) Des-Phe, and (**10**) OMT-Phe were prepared by analogy with (**2**) Tyl-A2 and (**3**) Des-A2 (Sumbatyan et al., 2003) by the condensation of 2-aminooxyacetylphenylalanyl ethyl ester with Tyl (Des or OMT) in 0.4 M Na-acetate buffer (pH 4.7) at 50°C (Sumbatyan et al., 2010). (**4**) Tyl-U and (**5**) Tyl = Tyr were prepared by coupling of Tyl with 3-(uracyl-1-yl)alanine (or tyrosine) in methanol in the presence of sodium methylate at room temperature. (**5**) Tyl = Tyr was reduced with sodium borohydride to give (**6**) Tyl-Tyr (Sumbatyan et al., 2010). The compounds were purified by the column chromatography on silica gel, and their homogeneity and structure were confirmed by TLC, HPLC, NMR, and mass spectra. BocAAF-OMT and fMLF-OMT were synthesized as described elsewhere (Korshunova et al., 2007). (**7**) Tyl-Car was synthesized starting from tylosin (24 mg, 0.026 mmol, 1 eq.) and carnitine hydrazide (Oka et al., 1963) (8 mg, 0.045 mmol, 1.7 eq.), which were dissolved in Na-acetate buffer (pH 4.7) (1.5 ml), and the mixture was stirred for 12 hr at 50°C. The crude product was extracted with chloroform and purified by silica gel column chromatography in chloroform-methanol (3:1, v/v) system to give (**7**) Tyl-Car as white crystals: the yield, 42% (11.1 mg, 0.011 mmol); TLC: R_f ($CHCl_3$ - CH_3OH, 3:1) 0;7, R_f ($CHCl_3$ - CH_3OH – CH_3COOH, 6:1:0.1) 0;25, R_f ($CHCl_3$ - CH_3OH, 6:1) 0;28, HPLC: t_R = 19.7 min (gradient of CH_3CN in 0,1% CF_3COOH 0%–60%); MALDI MS: m/z calculated. for $C_{53}H_{93}N_4O_{18}$ 1073.7; found 1070.6; NMR ^1H (600 MHz, 303K, DMSO): 0.86 (3H, t, H17), 0.94 (3H, d, H18), 1.08 (3H, d, H5"CH_3), 1.15 (3H, s, H3"CH_3), 1.23 (3H, d, H21), 1.25 (3H, d, H5′CH_3), 1.28 (3H, d, H5′"CH_3), 1.58 (1H, m, H16), 1.65 (2H, m, H4, H2"), 1.80 (3H, s, H22), 1.82 (4H, m, H7, H16, H2," $H^{\alpha\ Car}$), 1.90 (3H, m, H2, H7, H16), 1.95 (1H, m, H2), 2.48 (6H, 1H, s, m, $N(CH_3)_3$, H3′), 2.77 (2H, m, H6, H19), 2.88 (1H, m, H14), 2.98 (1H, dd, H2′"), 3.13 (m, 4H, H8, H4′, H5′), 3.38 (1H, m, H2′), 3.39 (9H, s, $N^+(CH_3)_3^{Car}$), 3.41 (2H, m, H5," H3), 3.44 (3H, s, H2′"OCH_3), 3.50 (3H, s, H3′"OCH_3), 3.52 (3H, m, $H^{\gamma\ Car}$, H23), 3.61 (3H, m, H3′", H5, H5′"), 3.80 (1H, m, H23), 4.12 (3H, m, H1′, H4," $H^{\beta\ Car}$), 4.38 (1H, m, H4′"), 4.47 (1H, d, H1′"), 4.95 (3H, m, H15, H1," NH^{Car}), 5.82 (1H, d, H13), 6.49 (1H, d, H10), 7.10 (1H, d, H11), 8.16 (1H, s, H20).

In Vitro Transcription-Translation Assay

All coupled transcription-translation experiments were performed using an *E. coli* lysate–based system in the presence and absence of antibiotics, as described elsewhere (Dinos et al., 2004; Starosta et al., 2009; Szaflarski et al., 2008). Two microliters of each reaction was diluted with 50 μL of buffer A (10 mM HEPES/KOH [pH 7.8], 10 mM $MgCl_2$, 60 mM NH_4Cl, and 4 mM β-mercaptoethanol), mixed, and then transferred into black 96-well chimney flat bottom microtiter plates. The GFP fluorescence was either on a Tecan Infinite® M1000 with an excitation wavelength of 395 nm and emission 509 nm, or measured at 520 nm (filter cutoff) with a Typhoon Scanner 9400 (Amersham Bioscience) using a Typhoon blue laser module (excited at 488 nm). Images were then quantified using ImageQuantTL (GE Healthcare) and were represented graphical using SigmaPlot (Systat Software, Inc.). Synthesis of firefly luciferase (Fluc) was performed as described above for GFP, but using pIVEX-2.3MCS with Fluc cloned into the NdeI and SacI restriction sites as a template. After incubation at 30°C with shaking for 4–5 hr, 2 μL of each reaction was added directly to white 96-well chimney flat bottom microtiter plates, after which 50 μL of luminol substrate (Promega) was quickly added, shaken for 3 s, and the luminescence was immediately detected using

a Tecan Infinite® M1000. All measurements were repeated in triplicate and had a standard deviation of less than 10%.

Binding Assay

Binding of all compounds to empty ribosomes was examined using a competition assay with radiolabeled [^{14}C]Erythromycin (Perkin Elmer), as described elsewhere (Karahalios et al., 2006; Petropoulos et al., 2009). Briefly, all reactions contained 0.25 μM *D. radiodurans* 70S ribosomes and 1.25 μM [^{14}C]erythromycin in binding buffer (10 mM HEPES/KOH [pH 7.8], 30 mM $MgCl_2$, 150 mM NH_4Cl, and 6 mM β-mercaptoethanol), which equated with 60% binding from the saturation curve (data not shown). The saturation curve indicated that 80% of ribosomes were active (data not shown). To measure the apparent K_d value for each of the compound, reactions were performed in the absence or presence of increasing concentrations of the competing compounds. After incubation at room temperature for 2 hr, reactions were passed through nitrocellulose filters, type HA, 0.45 μm pore size (Millipore). Filters were washed three times with binding buffer and then scintillation counted in the presence of Filtersafe (Zinsser Analytic) scintillant. All measurements were repeated in duplicate and had a standard deviation of 5%–10%.

Modeling and Figure Preparation

All chemical structures were drawn with ChemSketch and then were modified with Adobe Illustrator. Small molecule structures for macrolide-peptide derivatives were generated using ChemSketch. The lactone rings were then replaced with the lactone ring from *D. radiodurans* 50S subunit in complex with (**2**) Tyl-A2 (Wilson et al., 2005), and the derivative sidechains were modeled on the basis of the position of the Ala-Ala sidechain of (**2**) Tyl-A2. The models of the macrolide-peptide compounds in complex with the large subunit were then minimized using CNS (Brünger et al., 1998). All 3D structural figures were produced using PyMol (http://www.pymol.org).

SUPPLEMENTAL INFORMATION

Supplemental information includes one table and can be found with this article online at doi:10.1016/j.chembiol.2010.04.008.

ACKNOWLEDGMENTS

We thank Shura Mankin and Roland Beckmann for helpful discussions, and the Beckmann laboratory for generous support and creating a stimulating work environment. This study was financed by the Deutsche Forschungsgemeinschaft (grant WI3285/1-1 to D.N.W.) and the Russian Foundation for Basic Research (grant 07-04-00902a to G.A.K.). V.K. would like to acknowledge the FEBS Fellowship Committee for granting her a Collaborative Experimental Scholarship for Central and Eastern Europe. A.A.B. would like to thank the Alexander von Humboldt Foundation for a very generous support.

Received: February 23, 2010
Revised: March 22, 2010
Accepted: April 2, 2010
Published: May 27, 2010

REFERENCES

Becker, T., Bhushan, S., Jarasch, A., Armache, J.P., Funes, S., Jossinet, F., Gumbart, J., Mielke, T., Berninghausen, O., Schulten, K., et al. (2009). Structure of monomeric yeast and mammalian Sec61 complexes interacting with the translating ribosome. Science *326*, 1369–1373.

Bhushan, S., Gartmann, M., Halic, M., Armache, J.P., Jarasch, A., Mielke, T., Berninghausen, O., Wilson, D.N., and Beckmann, R. (2010). α-helical nascent polypeptide chains visualized within distinct regions of the ribosomal exit tunnel. Nat. Struct. Mol. Biol. *17*, 313–317.

Brünger, A.T., Adams, P.D., Clore, G.M., DeLano, W.L., Gros, P., Grosse-Kunstleve, R.W., Jiang, J.S., Kuszewski, J., Nilges, M., Pannu, N.S., et al. (1998). Crystallography & NMR system: a new software suite for macromolecular structure determination. Acta Crystallogr. D Biol. Crystallogr. *54*, 905–921.

Contreras, A., and Vazquez, D. (1977). Cooperative and antagonistic interactions of peptidyl-tRNA and antibiotics with bacterial ribosomes. Eur. J. Biochem. *74*, 539–547.

Cruz-Vera, L.R., and Yanofsky, C. (2008). Conserved residues Asp16 and Pro24 of TnaC-tRNAPro participate in tryptophan induction of Tna operon expression. J. Bacteriol. *190*, 4791–4797.

Cruz-Vera, L.R., Rajagopal, S., Squires, C., and Yanofsky, C. (2005). Features of ribosome-peptidyl-tRNA interactions essential for tryptophan induction of tna operon expression. Mol. Cell *19*, 333–343.

Dinos, G., Wilson, D.N., Teraoka, Y., Szaflarski, W., Fucini, P., Kalpaxis, D., and Nierhaus, K.H. (2004). Dissecting the ribosomal inhibition mechanisms of edeine and pactamycin: the universally conserved residues G693 and C795 regulate P-site tRNA binding. Mol. Cell *13*, 113–124.

Fu, H., Marquez, S., Gu, X., Katz, L., and Myles, D.C. (2006). Synthesis and in vitro antibiotic activity of 16-membered 9-O-arylalkyloxime macrolides. Bioorg. Med. Chem. Lett. *16*, 1259–1266.

Gong, F., and Yanofsky, C. (2002). Instruction of translating ribosome by nascent peptide. Science *297*, 1864–1867.

Hansen, J.L., Ippolito, J.A., Ban, N., Nissen, P., Moore, P.B., and Steitz, T.A. (2002). The structures of four macrolide antibiotics bound to the large ribosomal subunit. Mol. Cell *10*, 117–128.

Karahalios, P., Kalpaxis, D.L., Fu, H., Katz, L., Wilson, D.N., and Dinos, G.P. (2006). On the mechanism of action of 9-O-arylalkyloxime derivatives of 6-O-mycaminosyltylonolide, a new class of 16-membered macrolide antibiotics. Mol. Pharmacol. *70*, 1271–1280.

Kirst, H.A., Toth, J.E., Debono, M., Willard, K.E., Truedell, B.A., Ott, J.L., Counter, F.T., Felty-Duckworth, A.M., and Pekarek, R.S. (1988). Synthesis and evaluation of tylosin-related macrolides modified at the aldehyde function: a new series of orally effective antibiotics. J. Med. Chem. *31*, 1631–1641.

Korshunova, G.A., Sumbatyan, N.V., Fedorova, N.V., Kuznetsova, I.V., Shishkina, A.V., and Bogdanov, A.A. (2007). Peptide derivatives of tylosin-related macrolides [in Russian]. Bioorg. Khim. *33*, 235–244.

Kosolapov, A., and Deutsch, C. (2009). Tertiary interactions within the ribosomal exit tunnel. Nat. Struct. Mol. Biol. *16*, 405–411.

Lawrence, M.G., Lindahl, L., and Zengel, J.M. (2008). Effects on translation pausing of alterations in protein and RNA components of the ribosome exit tunnel. J. Bacteriol. *190*, 5862–5869.

Lovmar, M., Nilsson, K., Vimberg, V., Tenson, T., Nervall, M., and Ehrenberg, M. (2006). The molecular mechanism of peptide-mediated erythromycin resistance. J. Biol. Chem. *281*, 6742–6750.

Lu, J., and Deutsch, C. (2005a). Folding zones inside the ribosomal exit tunnel. Nat. Struct. Mol. Biol. *12*, 1123–1129.

Lu, J., and Deutsch, C. (2005b). Secondary structure formation of a transmembrane segment in Kv channels. Biochemistry *44*, 8230–8243.

Lu, J., and Deutsch, C. (2008). Electrostatics in the ribosomal tunnel modulate chain elongation rates. J. Mol. Biol. *384*, 73–86.

Mankin, A.S. (2008). Macrolide myths. Curr. Opin. Microbiol. *11*, 414–421.

Mayford, M., and Weisblum, B. (1989). ermC leader peptide: amino acid sequence critical for induction by translational attenuation. J. Mol. Biol. *206*, 69–79.

Mutak, S., Marsic, N., Kramaric, M.D., and Pavlovic, D. (2004). Semisynthetic macrolide antibacterials derived from tylosin: synthesis and structure-activity relationships of novel desmycosin analogues. J. Med. Chem. *47*, 411–431.

Nakatogawa, H., and Ito, K. (2002). The ribosomal exit tunnel functions as a discriminating gate. Cell *108*, 629–636.

Narandja, A., Suskovic, B., Kelneric, Z., and Djokic, S. (1994). Structure-activity relationship among polyhydro derivatives of tylosin. J. Antibiot. (Tokyo) *47*, 581–587.

Nissen, P., Hansen, J., Ban, N., Moore, P.B., and Steitz, T.A. (2000). The structural basis of ribosome activity in peptide bond synthesis. Science *289*, 920–930.

Oka, Y., Yonemoto, H., and Yurugi, S. (1963). Carnitine derivatives. Takeda Kenkyusho Nenpo *22*, 13–18.

Omura, S., and Tishler, M. (1972). Relationship of structures and microbiological activities of the 16-membered macrolides. J. Med. Chem. *15*, 1011–1015.

Omura, S., Miyano, K., Matsubara, H., and Nakagawa, A. (1982). Novel dimeric derivatives of leucomycins and tylosin, sixteen-membered macrolides. J. Med. Chem. *25*, 271–275.

Petropoulos, A.D., Kouvela, E.C., Starosta, A.L., Wilson, D.N., Dinos, G.P., and Kalpaxis, D.L. (2009). Time-resolved binding of azithromycin to *Escherichia coli* ribosomes. J. Mol. Biol. *385*, 1179–1192.

Poehlsgaard, J., and Douthwaite, S. (2003). Macrolide antibiotic interaction and resistance on the bacterial ribosome. Curr. Opin. Investig. Drugs *4*, 140–148.

Poulsen, S.M., Kofoed, C., and Vester, B. (2000). Inhibition of the ribosomal peptidyl transferase reaction by the mycarose moiety of the antibiotics carbomycin, spiramycin and tylosin. J. Mol. Biol. *304*, 471–481.

Ramu, H., Mankin, A., and Vazquez-Laslop, N. (2009). Programmed drug-dependent ribosome stalling. Mol. Microbiol. *71*, 811–824.

Schlünzen, F., Zarivach, R., Harms, J., Bashan, A., Tocilj, A., Albrecht, R., Yonath, A., and Franceschi, F. (2001). Structural basis for the interaction of antibiotics with the peptidyl transferase centre in eubacteria. Nature *413*, 814–821.

Seidelt, B., Innis, C.A., Wilson, D.N., Gartmann, M., Armache, J.P., Villa, E., Trabuco, L.G., Becker, T., Mielke, T., Schulten, K., et al. (2009). Structural insight into nascent polypeptide chain-mediated translational stalling. Science *326*, 1412–1415.

Spahn, C.M.T., and Prescott, C.D. (1996). Throwing a spanner in the works: antibiotics and the translational apparatus. J. Mol. Med. *74*, 423–439.

Starosta, A.L., Qin, H., Mikolajka, A., Leung, G.Y., Schwinghammer, K., Nicolaou, K.C., Chen, D.Y., Cooperman, B.S., and Wilson, D.N. (2009). Identification of distinct thiopeptide-antibiotic precursor lead compounds using translation machinery assays. Chem. Biol. *16*, 1087–1096.

Sumbatyan, N.V., Korshunova, G.A., and Bogdanov, A.A. (2003). Peptide derivatives of antibiotics tylosin and desmycosin, protein synthesis inhibitors. Biochemistry (Mosc.) *68*, 1156–1158.

Sumbatyan, N.V., Kuznetsova, I.V., Karpenko, V.V., Federova, N.V., Chertkov, V.A., Korshunova, G.V., and Bogdanov, A.A. (2010). Amino acid and peptide derivatives of the tylosin family of antibiotics modified by aldehyde function. Russ. J. Bioorganic Chem. *36*, 245–256.

Szaflarski, W., Vesper, O., Teraoka, Y., Plitta, B., Wilson, D.N., and Nierhaus, K.H. (2008). New features of the ribosome and ribosomal inhibitors: non-enzymatic recycling, misreading and back-translocation. J. Mol. Biol. *380*, 193–205.

Tai, P.-C., Wallace, B.J., and Davis, B.D. (1974). Selective action of erythromycin on initiating ribosomes. Biochemistry *13*, 4653–4659.

Tenson, T., and Ehrenberg, M. (2002). Regulatory nascent peptides in the ribosomal tunnel. Cell *108*, 591–594.

Tenson, T., and Mankin, A. (2001). Short peptides conferring resistance to macrolide antibiotics. Peptides *22*, 1661–1668.

Tenson, T., Deblasio, A., and Mankin, A. (1996). A functional peptide encoded in the *Escherichia coli* 23S rRNA. Proc. Natl. Acad. Sci. USA *93*, 5641–5646.

Tenson, T., Xiong, L.Q., Kloss, P., and Mankin, A.S. (1997). Erythromycin resistance peptides selected from random peptide libraries. J. Biol. Chem. *272*, 17425–17430.

Tenson, T., Lovmar, M., and Ehrenberg, M. (2003). The mechanism of action of macrolides, lincosamides and streptogramin B reveals the nascent peptide exit path in the ribosome. J. Mol. Biol. *330*, 1005–1014.

Tripathi, S., Kloss, P.S., and Mankin, A.S. (1998). Ketolide resistance conferred by short peptides. J. Biol. Chem. *273*, 20073–20077.

Tu, D., Blaha, G., Moore, P., and Steitz, T. (2005). Structures of MLSBK antibiotics bound to mutated large ribosomal subunits provide a structural explanation for resistance. Cell *121*, 257–270.

Vazquez-Laslop, N., Thum, C., and Mankin, A.S. (2008). Molecular mechanism of drug-dependent ribosome stalling. Mol. Cell *30*, 190–202.

Vimberg, V., Xiong, L., Bailey, M., Tenson, T., and Mankin, A. (2004). Peptide-mediated macrolide resistance reveals possible specific interactions in the nascent peptide exit tunnel. Mol. Microbiol. *54*, 376–385.

Wilson, D.N. (2009). The A-Z of bacterial translation inhibitors. Crit. Rev. Biochem. Mol. Biol. *44*, 393–433.

Wilson, D.N., Harms, J.M., Nierhaus, K.H., Schlünzen, F., and Fucini, P. (2005). Species-specific antibiotic-ribosome interactions: Implications for drug development. Biol. Chem. *386*, 1239–1252.

Woolhead, C.A., McCormick, P.J., and Johnson, A.E. (2004). Nascent membrane and secretory proteins differ in FRET-detected folding far inside the ribosome and in their exposure to ribosomal proteins. Cell *116*, 725–736.

 ©2010 Elsevier Ltd All rights reserved

Paper 5

Chemistry & Biology
Article

Identification of Distinct Thiopeptide-Antibiotic Precursor Lead Compounds Using Translation Machinery Assays

Agata L. Starosta,[1,2,5] Haiou Qin,[3,5] Aleksandra Mikolajka,[1,2,5] Gulice Y.C. Leung,[4] Kathrin Schwinghammer,[1,2] Kyriacos C. Nicolaou,[4] David Y.-K. Chen,[4] Barry S. Cooperman,[3,*] and Daniel N. Wilson[1,2,*]
[1]Gene Center and Department of Chemistry and Biochemistry
[2]Center for Integrated Protein Science Munich
Ludwig-Maximilians University of Munich, Feodor Lynen Strasse 25, 81377, Munich, Germany
[3]Department of Chemistry, University of Pennsylvania, Philadelphia, PA 19104-6323, USA
[4]Chemical Synthesis Laboratory @ Biopolis, Institute of Chemical and Engineering Sciences, Agency for Science, Technology and Research, 11 Biopolis Way, The Helios Block, #03-08, Singapore 138667, Singapore
[5]These authors contributed equally to this work
*Correspondence: wilson@lmb.uni-muenchen.de (D.N.W.), cooprman@pobox.upenn.edu (B.S.C.)
DOI 10.1016/j.chembiol.2009.09.016

SUMMARY

Most thiopeptide antibiotics target the translational machinery: thiostrepton (ThS) and nosiheptide (NoS) target the ribosome and inhibit translation factor function, whereas GE2270A/T binds to the elongation factor EF-Tu and prevents ternary complex formation. We have used several in vitro translational machinery assays to screen a library of thiopeptide antibiotic precursor compounds and identified four families of precursor compounds that are either themselves inhibitory or are able to relieve the inhibitory effects of ThS, NoS, or GE2270T. Some of these precursors represent distinct compounds with respect to their ability to bind to ribosomes. The results not only provide insight into the mechanism of action of thiopeptide compounds but also demonstrate the potential of such assays for identifying lead compounds that might be missed using conventional inhibitory screening protocols.

INTRODUCTION

The translational machinery represents one of the major targets within the cell for antibiotics (reviewed by Spahn and Prescott, 1996; Wilson, 2004). Many clinical important classes of antibiotics, such as the tetracyclines, phenylpropanoids (chloramphenicol), macrolides (erythromycin), and aminoglycosides (gentamicin), inhibit translation by binding to the ribosome. Despite the potency of many of these drug classes, antibiotic resistance among clinically relevant pathogens is an increasing problem and thus the need for new antibiotics is more urgent than ever before. One class of antibiotics that has received renewed interest in recent years is the thiopeptide family (reviewed by Bagley et al., 2005; Nicolaou et al., 2009) because of their effectiveness against Gram-positive bacteria, in particular, methicillin-resistant *Staphlococcus aureus*, as well as against the malarial parasite *Plasmodium falciparum* (McConkey et al., 1997). Thiopeptide antibiotics are composed of oxazoles and thiazoles, as well as non-natural amino acids that are linked together to form complex macrocyclic frameworks (Figures 1A–1D).

Two distinct families of thiopeptide compounds target the translational apparatus, one that targets the ribosome, referred to here as Class I thiopeptides, and the other, referred to as Class II thiopeptides, which targets the elongation factor EF-Tu. The best characterized of the Class I compounds include thiostrepton (ThS) and nosiheptide (NoS) (Figures 1A and 1B), both of which have been crystallized bound to the large ribosomal subunit (Harms et al., 2008) (see later Figures 6A, 6B, and 6G). These structures reveal that the Class I thiopeptides bind within a region of the ribosome that is part of the GTPase-associated center, so-named because it is involved in translation G protein factor binding and stimulation of GTPase activity (Wilson and Nierhaus, 2005). Biochemically, Class I thiopeptides have been shown to inhibit 70S initiation complex (70SIC) formation by interfering with the initiation G protein IF2 (Brandi et al., 2004, and references therein; Grigoriadou et al., 2007) as well as elongation by interfering with both the G proteins EF-Tu (Gale et al., 1981; Gonzalez et al., 2007; Modolell et al., 1971), which is necessary for rapid cognate aminoacyl-tRNA binding to the ribosome, and EF-G, which catalyzes translocation of the $tRNA_2$-mRNA complex from the A and P sites to the P and E sites (Pan et al., 2007; Pestka, 1970; Rodnina et al., 1999; Seo et al., 2006; Weisblum and Demohn, 1970). In contrast, the structurally similar Class II thiopeptides (Figure 1D) do not bind to the ribosome, but instead interact directly with EF-Tu (reviewed by Parmeggiani and Nissen, 2006). The crystal structure of the Class II thiopeptide GE2270A bound to EF-Tu reveals that the drug binds within a cleft between domains I and II of EF-Tu and directly overlaps with the binding site of the terminal end of the aminoacyl-tRNA (Parmeggiani et al., 2006; Parmeggiani and Nissen, 2006) (see later Figures 7A–7C). GE2270A is thought to prevent the closing of domain I and II, which is necessary for the induced-fit binding of EF-Tu to the tRNA, thereby preventing ternary complex formation (Parmeggiani and Nissen, 2006).

Although ThS is already in veterinary usage, its low water solubility and poor bioavailability has so far precluded its use in

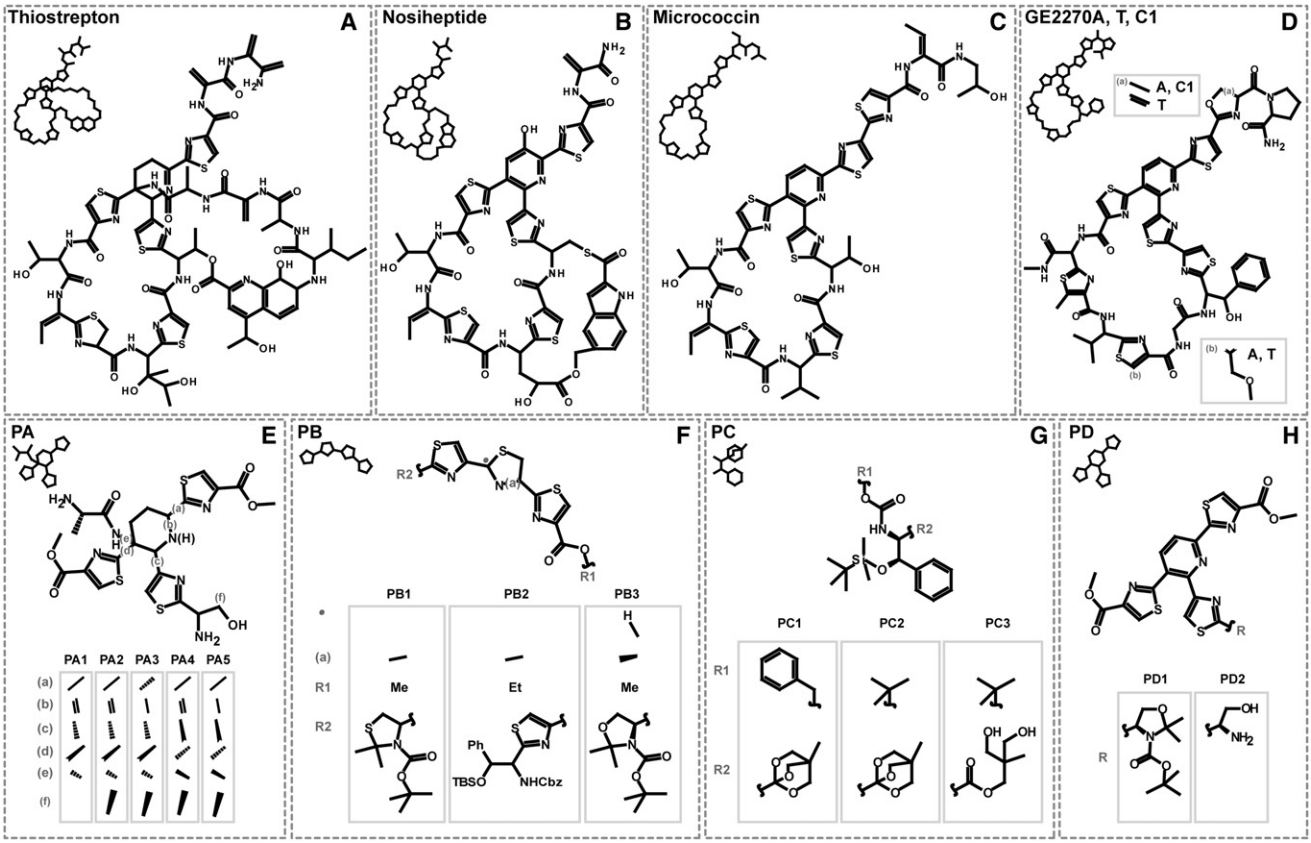

Figure 1. Chemical Structures of Thiopeptide Antibiotics and Precursor Families PA–PD

Chemical structures of the thiopeptide antibiotics ThS (A), NoS (B), micrococcin (MiC) (C), and GE2270A/T/C1 (D) and precursor families PA1-5 (E), PB1-3 (F), PC1-3 (G), and PD1-2 (H).

human medicine. Recent success has been reported in the total synthesis of a number of Class I and II thiopeptides (reviewed by Hughes and Moody, 2007; Nicolaou et al., 2009), including among others ThS (Nicolaou et al., 2005a, 2005c) and GE2270A (Nicolaou et al., 2006, 2008b). Such synthetic studies pave the way to generating improved thiopeptide derivatives by identifying synthetic fragments (or derivatives thereof) that display biological activity or can act as new lead compounds.

We have used a series of translation machinery assays to screen a library of thiopeptide antibiotic precursor compounds. Unlike the parent antibiotics ThS, NoS, and GE2270T, only a few of the precursor compounds display any significant inhibitory properties, even at high concentrations. Instead, however, four structurally distinct families of precursor compounds (Figures 1E–1H) were discovered that relieve the inhibitory effect imparted by the parent compounds. The different precursor families exhibit differential effects with respect to the inhibitory antibiotic that is counteracted as well as to the target, whether it is the ribosome or EF-Tu. Two of the families represent completely new compounds with respect to their ability to bind to ribosomes and thus open the path to the development of novel antimicrobials. The application of such screening strategies will enable the identification of new lead compounds that are not detected using conventional inhibitory screening protocols.

RESULTS

Several assays were used to examine thiopeptide precursor compounds for their abilities to bind to the ThS binding site, either by mimicking ThS inhibition of specific ribosomal functions or by protecting the ribosome against the inhibitory effects of ThS via a competition effect. These assays, which are discussed in turn below, measure (1) IF2 conformational change during the conversion of 30S initiation complex (30SIC) to 70SIC, (2) ribosome-dependent stimulation of the GTPase activity of EF-G, and (3) the cell-free synthesis of green fluorescent protein (GFP) using an *Escherichia coli* in vitro-coupled transcription-translation (TT) assay.

The Thiopeptide Precursor PA1 Inhibits 70SIC Formation

The initiation factor IF2 is essential for 70SIC formation from 30SIC and 50S subunits (Antoun et al., 2003; Grigoriadou et al., 2007). Elsewhere we have shown that the fluorescence of a Cy3 derivative of IF2 ($IF2^{Cy3}$) increases on 70SIC formation resulting from the binding of a 50S subunit to a 30SIC-containing $IF2^{Cy3}$ (Qin et al., 2009). This increase is inhibited by both ThS and NoS (Figure 2A), largely as a result of the effect of these antibiotics in inhibiting both the rate and extent of 70SIC formation (Grigoriadou et al., 2007; data not shown). Measuring the extent

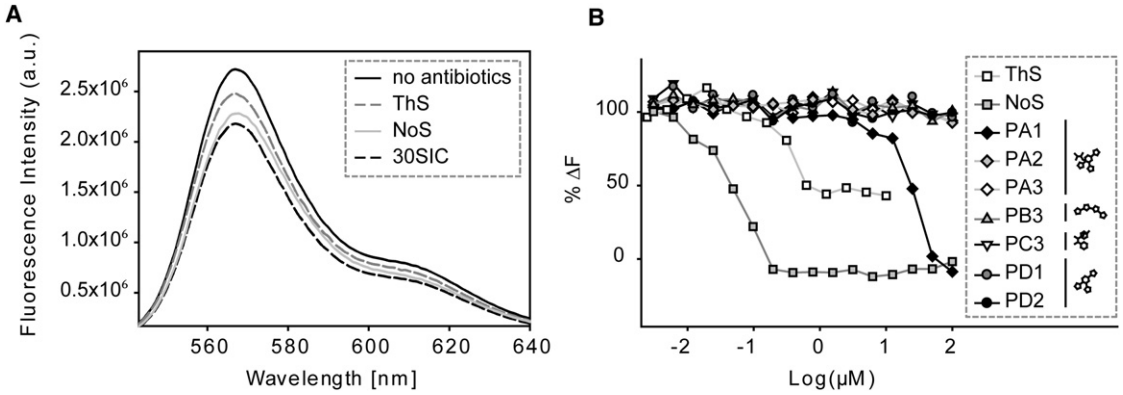

Figure 2. The IF2 Fluorescence Change Assay

(A) Emission spectra of $IF2^{Cy3}$-containing 30SIC mixed with 50S subunits in the presence of ThS or NoS. 50S was preincubated with antibiotics for 5 min at 37°C and then rapidly mixed with 30SIC at 20°C, followed by 5 min incubation before measurements. Black solid trace, no antibiotics; gray dashed trace, ThS; gray solid trace, NoS; black dashed trace, 30SIC alone. The final concentrations are IF1, IF3, and $fMet\text{-}tRNA^{fMet}$, 0.45 μM; $IF2^{Cy3}$, 0.15 μM; mRNA, 0.90 μM; 30S, 0.30 μM; 50S, 0.30 μM; GTP, 100 μM; ThS or NoS, 1.5 μM.

(B) Dose-response curves for the inhibition of fluorescence change on mixing $IF2^{Cy3}$-containing 30SIC with 50S subunits in the presence of thiopeptide compounds. The y axis indicates the percent ΔF in the presence of added compound relative to the ΔF in the absence of added compound relative to the fluorescence of 70SIC by itself. Final concentrations are $IF2^{Cy3}$, 0.15 μM; IF1, IF3, and $fMet\text{-}tRNA^{fMet}$, 0.45 μM; 022AUGmRNA, 0.9 μM; 30S, 0.30 μM; 50S, 0.30 μM; GTP, 100 μM.

of fluorescence change is thus a convenient way of monitoring thiopeptide precursor effects on 70SIC formation. A library of thiopeptide precursor compounds, as well three forms of the EF-Tu inhibitor GE2270 (A, T, and C1), were screened for this activity, along with ThS and NoS as positive controls. Only one precursor, denoted PA1 (Figure 2B), showed any measurable activity in inhibiting the fluorescence change, with an apparent K_i of 25 μM, some 60- to 400-fold higher than for ThS or NoS, respectively. Although PA1 does not bind with very high affinity, it apparently does so with considerable structural specificity, since the inhibitory effect was not seen for compounds PA2 and PA3, which have either stereochemical or minor constitutional differences from PA1 (Figure 1E). The thiopeptide precursors were also screened for their abilities to reverse ThS inhibition of the $IF2^{Cy3}$ fluorescence increase on 70SIC formation. In no case was such reversal observed.

Differential Effects of Precursor Compounds on Factor-Dependent GTPase Assays

Vacant 70S ribosomes are known to stimulate the GTPase activity of EF-G via formation of a 70S•EF-G•GTP complex. Such stimulation is strongly inhibited by ThS (Pestka, 1970; Weisblum and Demohn, 1970). We used two multiple turnover GTPase assays to screen thiopeptide precursors for inhibitory activity.

The first assay measured EF-G GTPase activity via formation of a Malachite Green complex (see Experimental Procedures) for hundreds of turnovers. Under conditions for which ThS (1 μM) almost completely abolished such activity, we identified three distinct classes of precursor compounds (PA–PC; Figures 1E–1G) that exhibited modest inhibitory effects when added at 50 μM (Figure 3A). However, we note that none of these compounds added at 10 μM showed appreciable inhibition (data not shown). As expected, the negative control, GE2270T, had no effect at a concentration of 50 μM (Figure 3A). In order to determine whether the modest inhibitory effects seen in Figure 3A were specific for EF-G, we next checked whether these compounds could also inhibit the ribosome-dependent stimulation of the Tet(M) GTPase. Tet(M) is a GTPase that binds to the ribosome analogously to EF-G and confers resistance to the antibiotic tetracycline by weakening its binding to the ribosome (reviewed by Connell et al., 2003). Similar to the results for EF-G, representatives of the PA and PC families exhibited modest inhibitory effects on Tet(M) GTPase at high concentration (100 μM) (Figure 3B). However, in contrast to EF-G, little or no inhibition was observed for the PB family, suggesting that it is specific for EF-G.

The second assay measured EF-G GTPase activity from the fluorescence increase of released Pi binding to the fluorescent phosphate binding protein MDCC-PBP (Brune et al., 1994; Seo et al., 2006). This assay, which can in principle be used for single turnover measurement, was here used to measure several turnovers, as determined by the stoichiometric ratio (5:1) of MDCC-PBP to ribosome. As performed, this assay could only detect very potent inhibitors of EF-G GTPase, since fluorescence was not measured until 1 min after initiation of reaction, whereas in the absence of inhibition the full fluorescence change is complete within 5–10 s (data not shown). It is thus no surprise, given the results presented in Figure 3A, that although ThS inhibited this assay with an apparent K_i of 1.1 μM none of the precursors tested, nor even NoS or MiC, showed measurable inhibition up to a concentration of 100 μM (Figure 3C). In contrast, both NoS and MiC added at very low concentration protected against inhibition by 1.2 μM ThS, with half-maximal effects seen at 0.04 μM and 0.11 μM, respectively (Figure 3D). However, none of the precursor compounds afforded similar protective effects up to 50–100 μM of added precursor.

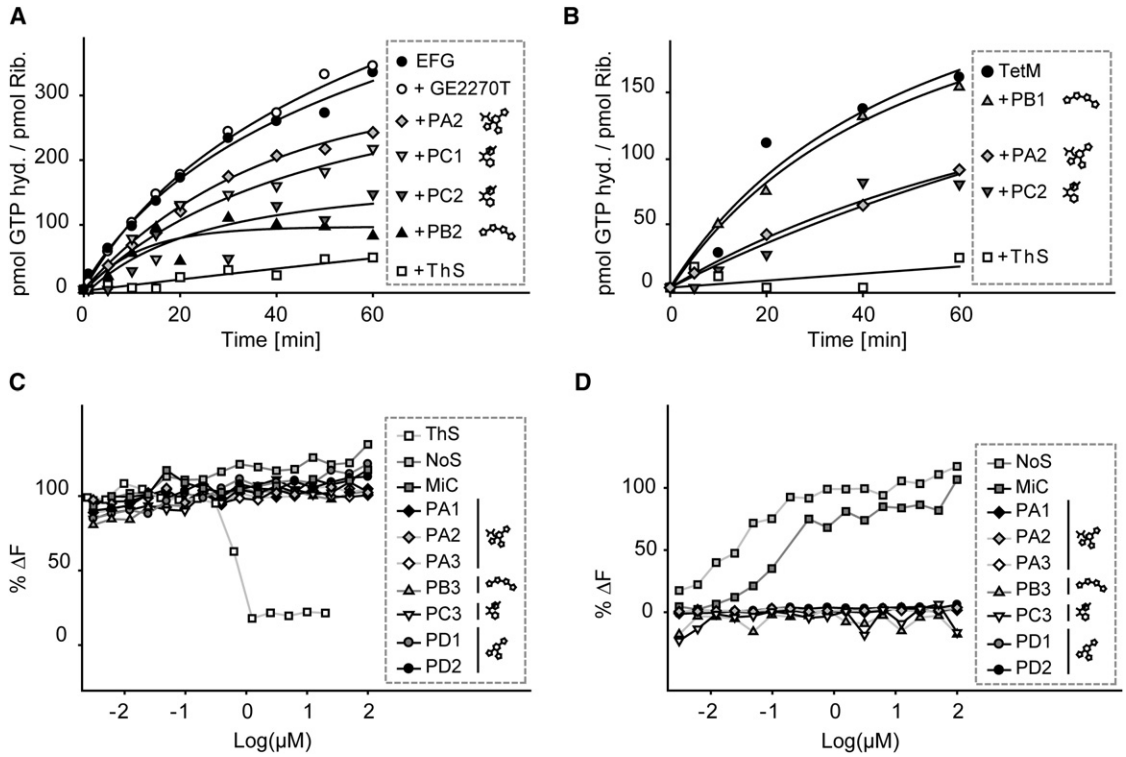

Figure 3. Effect of Thiopeptides and Precursor Compounds on GTPase Activity of EF-G and Tet(M)

(A) Inhibition of uncoupled ribosome-dependent Tet(M) GTPase by ThS (1 μM) and precursors PA2, PB2, and PC2 (50 μM). Closed circles indicate GTPase activity of Tet(M) in the absence of antibiotic.

(B) Inhibition of uncoupled ribosome-dependent TetM GTPase by ThS (1 μM) and precursors PA2, PB1, and PC2 (100 μM). Closed circles indicate GTPase activity of TetM in the absence of antibiotic.

(C) The dose-response curves of Pi release in the presence of ThS, NoS, MiC, or precursor compounds. The y axis indicates the percent ΔF due to Pi release in the presence of added compound relative to the ΔF in the absence of added compound relative to the fluorescence from EF-G interaction with the ribosome in the absence of any compound. The final concentrations are 70S, 0.3 μM; EF-G, 0.75 μM; MDCC-PBP, 1.5 μM; GTP, 100 μM;7-methylguanine, 200 μM; nucleotide phosphorylase, 0.3 U/ml.

(D) Dose-response curves for reversal of ThS inhibition of Pi release by NoS, MiC, or precursor compounds. The final concentrations for each component are 70S, 0.3 μM; EF-G, 0.75 μM; ThS, 1.2 μM; MDCC-PBP, 1.5 μM; GTP, 100 μM; 7-methylguanine, 200 μM; nucleotide phosphorylase, 0.3 U/ml.

Protective Effects of Precursor Compounds on Thiopeptide-Mediated Translation Inhibition

Although, as expected, ThS, NoS, and GE2270T were potent inhibitors of GFP synthesis using an in vitro TT assay (Figure 4, lanes 2–4), none of the precursor compounds tested displayed any significant inhibitory activity in this assay (Figure 4, white bars), even at high concentrations (50–100 μM). In contrast, addition of 50 μM of representative precursor compounds from four structural distinct classes PA–PD (Figures 1E–1G) could reverse the inhibitory effect of 5 μM ThS (Figure 4, gray bars). The most effective protection was seen with PA2, which restored translation back to levels observed in the absence of antibiotic (Figure 4, lane 6). In comparison, PB1, PC1, and PD1 restored translation to 40%–60% of the original levels (Figure 4, lanes 13–28). Additionally, we find that the 5S, 6R stereoisomer of PA2 (PA4) exhibited some protective properties (~35% compared to 100% for PA2). The structural specificity of these effects is clear from the failure of precursors that are chemically related to PA2 to exhibit similar protective effects against ThS inhibition. These include PA3 (Figure 4, lanes 6 and 8), which differs from PA2 by lacking only a double bond within the central dehydropiperidine ring (Figure 1E), and PD2 (Figure 4, lanes 26 and 28), which, with respect to PD1, has an altered side chain on one of the thiazole rings (Figure 1H).

Interestingly, PA2, PB1, PC1, and PD1 displayed marked differences in their abilities to reverse the inhibitory effects of NoS (5 μM) and GE2270T (25 μM), as compared to the inhibitory effects of ThS. Thus, as shown in Figure 5, PA2 was an omnipotent protector of translation, restoring translation levels in the presence of all three thiopeptide inhibitors, with the following order of efficiency: ThS (100%) > GE2270T (80%) > NoS (60%). PD1 rescued translation in the presence of ThS and GE2270T, but not NoS, and PB1 and PC1 efficiently rescued translation only against ThS. As was true for ThS, neither PA3, PB2, PC2, nor PD2 were able to reverse inhibition by NoS or GE2270T (data not shown).

Interaction of Thiopeptide Precursors with the Ribosome

The specific protective effect of the precursor compounds against ThS suggests that these compounds specifically compete with ThS for binding to the ribosome. Structural (Harms

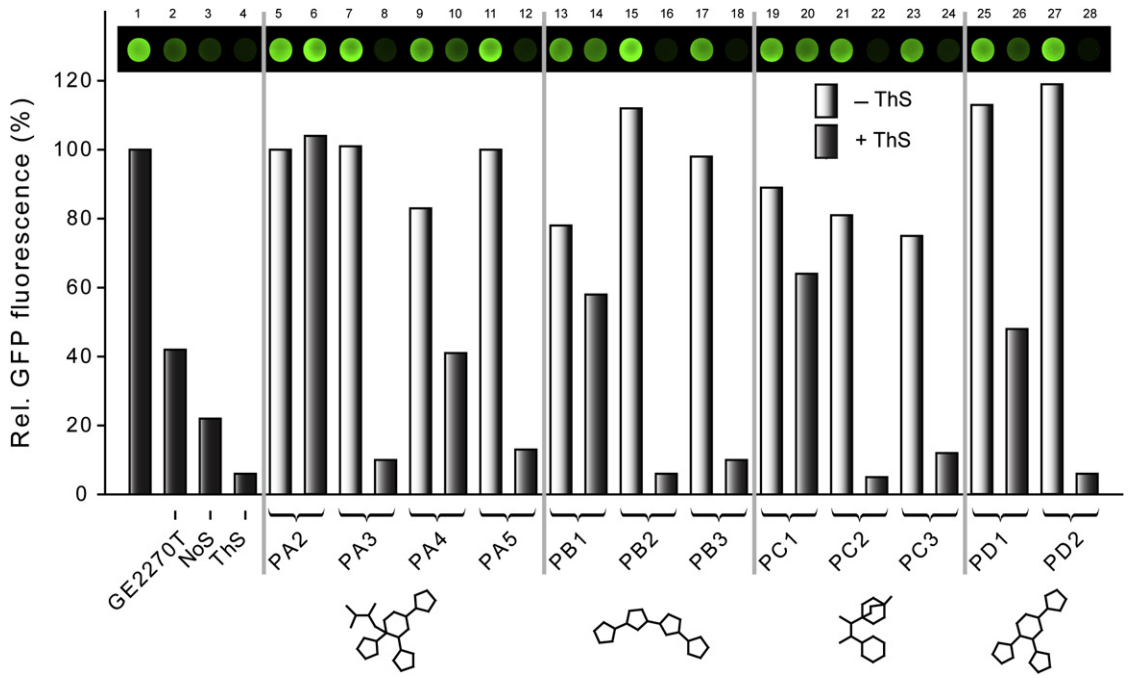

Figure 4. Precursor Compounds Protect Translation from ThS Inhibition

In vitro TT of GFP in the absence or presence of 25 μM GE2270T, 5 μM NoS, and 5 μM ThS (black bars) or in the presence (50 μM) of precursor families PA2-5, PB1-3, PC1-3, and PD1-2 (−ThS; white bars) alone or with additional presence of 5 μM ThS (+ThS; gray bars). GFP fluorescence from microtiter plate wells shown above each lane were quantified and represented as bars, with the fluorescence detected in the absence of antibiotic assigned as 100%.

et al., 2008; Jonker et al., 2007) and biochemical data (Spahn and Prescott, 1996; Xing and Draper, 1996) for ThS suggests that the high affinity of this drug for the ribosome results from cooperative interaction between nucleotides in H43/44 of the 23S rRNA and the L11-NTD (Figures 6A and 6B). Given the structural similarity between PA2 and ThS, it is possible to model the position of this compound bound to the ribosome (Figure 6C; Harms et al., 2008). The substitution of the double bond in the piperidine ring of PA2 to generate PA3 abolishes the protective effect of the compound (Figure 4). This is likely to result from differences in the planarity of the piperidine ring between PA3 and PA2, which in turn leads to differences in the relative position (by 0.5 Å) of the attached thiazole moiety, which, based on the model, would shift it toward Pro27 of L11-NTD and thus encroach on the thiopeptide binding site (data not shown). Such modest displacements within drug binding sites have been shown to have dramatic effects on the affinity of compounds and often lead to antibiotic resistance (Blaha et al., 2008; Tu et al., 2005).

Although it is more difficult to model the PB and PC series of compounds based on the available structures, it is clear that the aromatic rings within these families suggest a potential mode of binding that establishes simultaneous stacking interactions with both H43/44 and L11-NTD (Figures 6D and 6E). Alterations that disrupt these rings, as seen for PC2 (Figure 6F), could explain a reduced binding and corresponding loss in protection (Figure 4). The PD class of precursors is structurally most similar to the pyridine core of NoS (Figure 1). NoS is oriented differently on the ribosome compared to ThS, establishing stacking interactions with Pro22 but not Pro26 (Figure 6G; Harms et al., 2008). Based on our modeling, PD1 can make analogous interactions with Pro22 as NoS (Figure 6H), whereas the inactive PD2 cannot (Figure 6I).

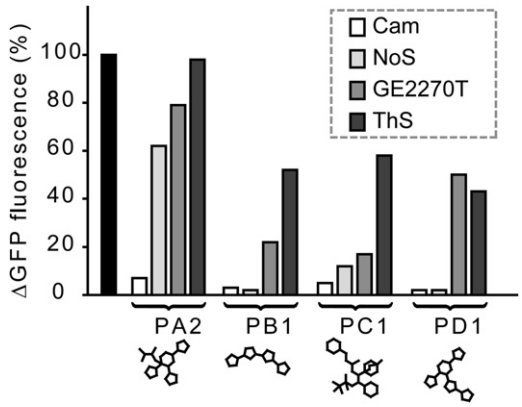

Figure 5. Differential Protective Effects of Precursors Against Thiopeptide Inhibition

Protection profiles of representative precursors from all described groups against chloramphenicol (Cam; 10 μM), NoS (5 μM), GE2270T (25 μM), and ThS (5 μM). GFP fluorescence in the absence of antibiotic is assigned as 100%, whereas the precursor results are presented as the percentage of protection, given as the difference between the inhibition of translation by the active compound (Cam, NoS, GE2270T, or ThS) in the presence and absence of the precursor compound (50 μM).

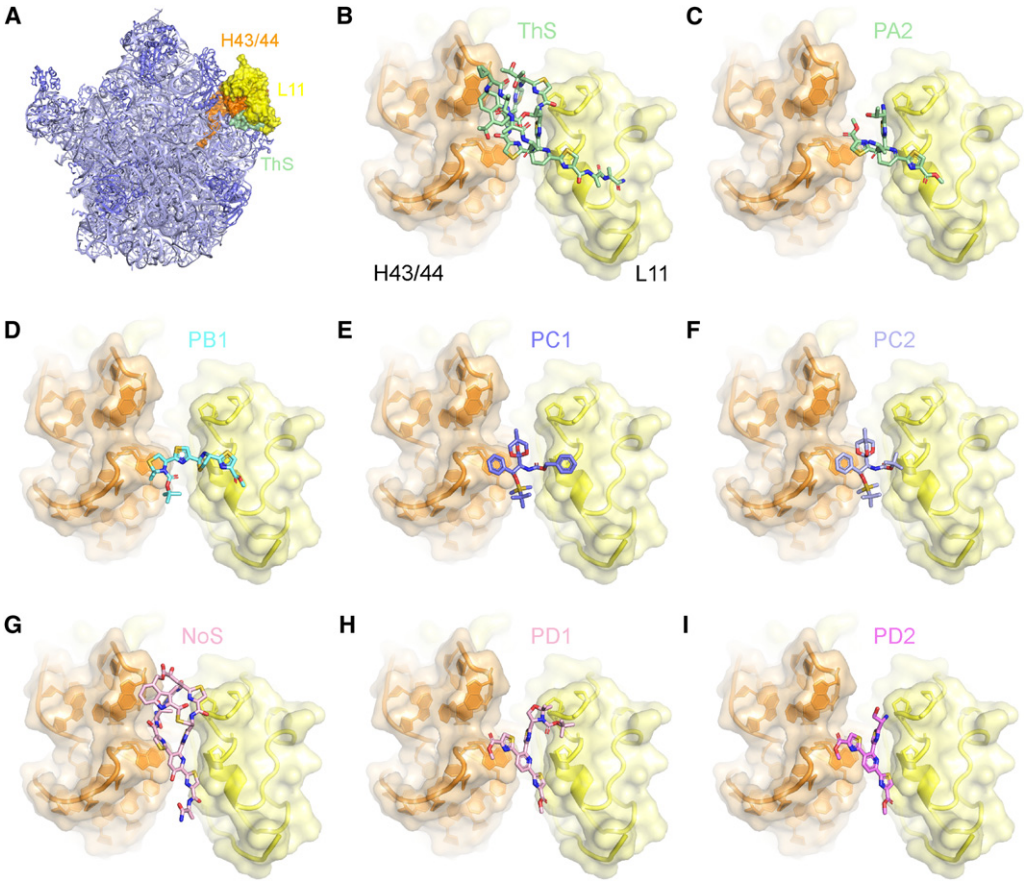

Figure 6. Binding Site of Precursor Compounds on the Ribosome

(A) Overview of thiopeptide binding site on the large ribosomal subunit. Interface view with helix 43 and 44 (H43/44; orange), L11 (yellow), and ThS (green) highlighted with surface representation (from PDB ID 3CF5) (Harms et al., 2008).

(B) The thiazole rings of ThS (green) interact with the RNA bases at the tips of H43/44 as well as the prolines in the N-terminal domain of L11 (yellow).

(C) Model for precursor PA2 bound to the ribosome, based on the position of ThS. PA1, but not PA3 (see text), bind similarly.

(D–F) Possible modes of binding for precursors PB1 and PC1 based on ring stacking interactions with RNA and protein components of the ribosome, whereas PC2 lacks one phenyl ring compared to PC1.

(G) NoS (pink) interacts with the RNA bases at the tips of H43/44 as well as the N-terminal domain of L11 (yellow), but in a distinct manner compared to ThS (using PDB ID 2ZJP) (Harms et al., 2008).

(H and I) Model for precursor PD1 and PD2 bound to the ribosome, based on the position of NoS. PD2 lacks one ring moiety, suggesting binding would be destabilized.

Interaction of Thiopeptide Precursors with EF-Tu

The thiopeptide GE2270A has been crystallized in complex with EF-Tu, revealing that the drug binds within a covered groove in domain II and spans across the active site cleft of EF-Tu, the G domain, to interact with the domain I (Figure 7A; Parmeggiani et al., 2006). GE2270A overlaps the binding site of the terminal A76 and aminoacyl moiety of the tRNA (Figure 7B) and is believed to prevent the closing of domains I and II necessary for the induced fit binding of aa-tRNA (Figure 7C), thereby preventing ternary complex (EF-Tu•GTP•tRNA) formation (reviewed by Parmeggiani and Nissen, 2006). The structural similarities between PA and PD and GE2270A (Figure 1) suggest that these compounds would also bind within the groove of domain II of EF-Tu (Figure 7D) and overlap with the A76 of the tRNA (Figure 7E). However, the truncated nature of these compounds prevents them from establishing additional interactions with domain I, even in the closed tRNA-bound ternary complex state of EF-Tu (Figure 7F).

DISCUSSION

Development of improved antimicrobial agents will be necessary to combat the prevalence of multi-drug-resistant bacteria. A number of biochemical approaches have been taken to identify functionally important hotspots on the ribosome that do not overlap with previously known antibiotic binding sites (Laios et al., 2004; Llano-Sotelo et al., 2009b; Yassin et al., 2005; Yassin and Mankin, 2007). In addition, a recent study has developed an assay using fluorescently labeled ribosomal proteins to monitor binding of small molecules, such as antibiotics, to the ribosome, which is amenable to high-throughput screening (Llano-Sotelo et al., 2009a). Here we present several translation-related assays

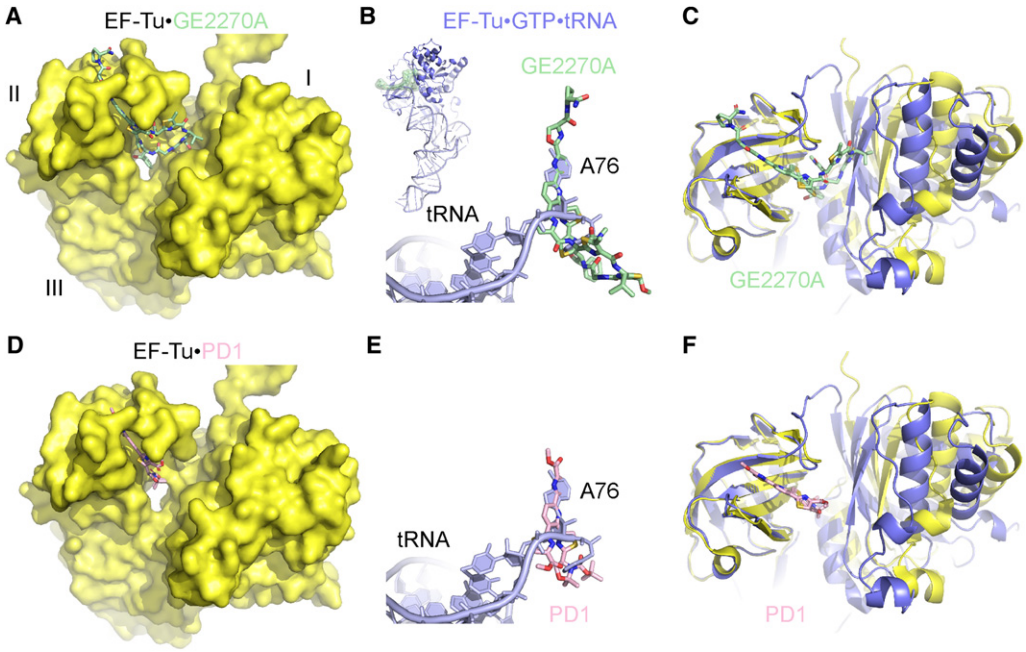

Figure 7. Binding Site of Precursor Compounds on EF-Tu

(A) Structure of the thiopeptide GE2270A (green) bound to EF-Tu (yellow), with domains I, II, and III indicated (PDB ID 2C77) (Parmeggiani et al., 2006).

(B) GE2270A overlaps the binding position on EF-Tu of the terminal A76 and aminoacyl moiety of tRNA. Inset shows overview of EF-Tu•tRNA ternary complex (PDB ID 1TTT) (Nissen et al., 1995) with superimposition of GE2270A.

(C) Superimposition of EF-Tu•GE2270A (yellow) and EF-Tu•tRNA (blue) aligned on basis of domain II. Note that GE2270A (green) clashes with domain I of EF-Tu from the ternary complex (blue).

(D) Model for precursor PD1 bound to EF-Tu based on EF-Tu•GE2270A complex (PDB ID 2C77) (Parmeggiani et al., 2006).

(E) PD1 (pink) overlaps the binding position on EF-Tu of the terminal A76 and aminoacyl moiety of tRNA (blue).

(F) As (C) but with PD1 instead of GE2270A. Note that PD1 does not clash with domain I of EF-Tu from the ternary complex (blue).

using high-throughput 96 or 384 microtiter plate formats that have been used to screen a library of thiopeptide precursor compounds for their abilities to inhibit one or more aspects of translation and/or reverse the inhibition of known thiopeptide antibiotics. These screens identified four distinct families of precursor compounds, termed PA–PD, which could act as potential lead compounds for development of novel antimicrobials.

Two of the families identified, PA and PD, contain a six-membered nitrogen heterocycle core (PA, dehydropiperidine; PD, pyridine) analogous to the thiopeptide antibiotics ThS and GE2270A (Figure 1). The crystal structures of thiopeptides bound to the ribosome (Harms et al., 2008) and of GE2270A bound to EF-Tu (Parmeggiani et al., 2006) reveal the importance of the heterocycle core of these compounds for interaction with their respective targets and allows modeling of how PA and PD members are likely to interact with the ribosome and/or EF-Tu (Figures 5 and 6). The resulting models are consistent with the rescue of translation in the presence of ThS and GE2270T by family members, such as PA2 and PD2, probably by direct competition for binding between the precursor compound and the thiopeptide antibiotic. In addition, PA1 and PA2 displayed inhibitory activity against translational GTPases IF2 (Figure 2B) and EF-G and Tet(M) (Figures 3A and 3B), respectively. However, compared to the parent thiopeptide compounds, much higher concentrations of the precursor compounds were necessary to exhibit similar effects, most likely indicating the much lower binding affinity of the precursors. The ineffectiveness of precursor compound PA2 as a direct inhibitor was surprising, since this compound has been previously reported to exhibit antimicrobial activity against methicillin-resistant *Staphlococcus aureus* and vancomycin-resistant *Enterococcus faecalis* with a minimal inhibitory concentration (MIC) of 5 μM (Nicolaou et al., 2005b). Our results suggest therefore that the inhibitory effect of PA2 in vivo may in fact not be related to translation, but verification of this point will require further investigation.

The other two families identified in our screen, PB and PC, have not, to our knowledge, been previously reported to target the translational machinery. PB1 is chemically similar to the thiazolidine precursor compound used to generate the pyridine core of amythiamicins (Nicolaou et al., 2008a), which target EF-Tu analogously to GE2270A (Parmeggiani et al., 2006; Parmeggiani and Nissen, 2006). The PC series of compounds contain a protected β-hydroxy-α-aminoacid, which is a precursor in the synthesis of GE2270A/T/C1. Curiously, the PB and PC families display much higher specificity for the ribosome than for EF-Tu, as shown by the ability of PB1 and PC1 to restore translation more efficiently in the presence of ThS, as compared with GE2270A (Figure 5). Although PB1 and PC1 are structurally distinct (Figure 1), we believe the common aromatic/cyclic nature of both these compounds is important for ribosome binding. Accommodation of EF-G on the ribosome involves the

insertion of domain V of EF-G into the crevice between H43/44 and L11-NTD. Inhibition by Class I thiopeptides has been proposed to stem in part from their physically linking L11-NTD to H43/44, thereby locking the cleft shut (Harms et al., 2008). We suggest that PB1 and PC1 can also span the L11-rRNA crevice (Figures 6D and 6E) and perform this locking function, analogous to ThS/PA2 (Figures 6B and 6C) and NoS/PD1 (Figures 6G and 6H). Similarly to PA/D, the high concentrations of PB/C required to inhibit the ribosome-dependent GTPase activity of EF-G are indicative of their low binding affinities for the ribosome. Such low affinity may allow facile displacement of precursors from the ribosome, as a result of translation factors (IF2 or EF-G) binding, or from EF-Tu, during ternary complex formation, thus explaining the absence of any direct inhibitory effect of any of the precursors on GFP synthesis. The differential effects of the precursors on the GTPase assays compared to the TT assay is probably related to the ribosome concentrations in the GTPase assays being ~10×–100× less (30–300 nM) compared to the TT assay (~2 μM) and to the putative higher affinity of EF-G for translating rather than empty ribosomes (Sergiev et al., 2005).

The majority of clinically used antibiotics targeting the ribosome bind either to the decoding region on the small subunit or within either the peptidyltransferase center or the adjacent peptide exit tunnel of the large subunit, where they interact almost exclusively with ribosomal RNA (Spahn and Prescott, 1996; Wilson, 2004). The Class I thiopeptide compounds, however, are distinct in that they target a different region of the ribosome, namely the GTPase-associated region or translation factor binding site, where they interact with both rRNA and ribosomal protein L11. As a consequence, no cross-resistance has been found between thiopeptide antibiotics and other clinically important drugs. The compounds such as PA–PD identified in our study provide lead structures for the development of novel antimicrobial agents that target this region of the ribosome. Furthermore, the ability of some precursor compounds, such as PA1 and PD1, to bind both EF-Tu and the ribosome suggests the feasibility of developing antimicrobials that are dual inhibitors of ribosomes and ternary complex formation.

SIGNIFICANCE

The translational machinery represents one of the major targets within the cell for antibiotics, with many clinical important classes of antibiotics inhibiting translation by binding to the ribosome. Despite the potency of many of these drug classes, antibiotic resistance among clinically relevant pathogens is an increasing problem and there is an urgent need for improved antibiotics. We present herein a series of translation machinery assays that can be used to screen for lead compounds that not only inhibit specific steps of translation but also relieve the inhibitory effects of other inhibitory compounds. Using these assays to screen a library of thiopeptide precursor compounds, we have identified four distinct families of compounds that inhibit either IF2, EF-G, and/or Tet(M), as well as confer protective effects against thiopeptide translation inhibitors of both the ribosome and EF-Tu. Our findings not only elucidate the mechanism of action of thiopeptide compounds but also illustrate the potential of such high-throughput assays to identify distinct lead compounds that might be missed using conventional inhibitory screening protocols. Whereas the IF2 and EF-G GTPase assays are specifically useful for screening antibiotics interfering with translation G factor proteins, the TT assay is generally applicable for screening all classes of translation inhibitors, including those targeting the peptidyltransferase, and decoding centers of the ribosome and other ribosomal sites, in addition to those interfering with translation G factor proteins.

EXPERIMENTAL PROCEDURES

Component Preparation

GE2270A, T, and C1 and the library of thiopeptide precursor compounds were synthesized as described previously (Nicolaou et al., 2005b, 2006, 2008a, 2008b). ThS was purchased from Sigma, whereas NoS was a gift from H.G. Floss and micrococcin P1 was supplied by T. Stachlhaus. The *tetM* gene (Tn916) cloned into the pET24b vector was a gift from V. Burdett. Tet(M) protein was expressed in BL21 (DE3) pRIL cells in 20°C with 0.2 mM IPTG. *E. coli* EF-G cloned into pQE70 vector was expressed in XL1 blue cells. Both proteins were purified using Ni-NTA metal affinity chromatography (QIAGEN), followed by gel filtration chromatography on a HiLoad 26/60 Superdex 75 prep grade column (GE Healthcare). For the experiments described in Figures 2 and 3C and 3D, ribosomes, $IF2^{Cy3}$, IF1, IF3, 30S subunits, MDCC-labeled phosphate-binding protein (MDCC-PBP), 022AUG mRNA, and $fMet\text{-}tRNA^{fMet}$ were prepared as described previously (Qin et al., 2009) as was EF-G (Pan et al., 2007).

$IF2^{Cy3}$ Fluorescence Change Assay

Reactions were carried out in a 384 well assay plate. 50S subunits were preincubated (15 min at 37°C) with a series of concentrations of the test compounds in DMSO that are transferred from a premade compound plate to the assay plate by a PerkinElmer Evolution P3 liquid handler. Reaction was initiated by addition of 30SIC to each well of the plate. Fluorescence (579 nm) was read with a 2103 EnVision Multilabel Plate Reader on excitation at 550 nm. For the reversal experiment, 30SIC was preincubated with ThS (10 min at 37°C), followed by a second preincubation with test compounds (10 min at 37°C), and reaction was initiated by 50S addition.

GTPase Activity Assays

For both assays described below, reactions performed in the absence of ribosomes were used as a background signal to account for the intrinsic GTPase activity of EF-G or Tet(M).

By Malachite Green

GTPase activity was measured using the Malachite Green Phosphate Kit (BioAssay) that quantifies the green complex formed between Malachite Green, molybdate, and free orthophosphate. All reactions contained 30 nM *E. coli* 70S ribosomes, 20 μM GTP, and 60 nM protein in the presence or absence of antibiotics as necessary. Reactions were transferred into 96 well microtiter plates and color formation was measured on Tecan Infinite M1000 microplate reader at 650 nm.

By MDCC-Labeled PBP

GTPase activity was measured using the MDCC-labeled PBP complex, which measures free phosphate release as an increase in fluorescence and uses a Pi-MOP system to minimize the background due to phosphate present in the original medium (Brune et al., 1994; Seo et al., 2006). Reactions were carried out in a 384 well assay plate. Ribosomes were preincubated (15 min at 37°C) with a series of concentrations of the test compounds in DMSO that are transferred from a premade compound plate to the assay plate by a PerkinElmer Evolution P3 liquid handler. Reaction was initiated by addition of an ice-cold solution containing EF-G, MDCC-PBP, and GTP to each well of the plate, a process that was completed in under 30 s. Fluorescence (450 nm) was read within 1 min using a 2103 EnVision Multilabel Plate Reader, on excitation at 405 nm. For the reversal experiment, ribosomes were preincubated with ThS (10 min at 37°C), followed by a second preincubation with test

compounds (10 min at 37°C), and reaction was initiated by EF-G, MDCC-PBP, and GTP as above.

In Vitro Transcription-Translation Assay

All coupled TT experiments were performed using an *E. coli* lysate-based system in the presence and absence of antibiotics as described previously (Dinos et al., 2004; Szaflarski et al., 2008). Reactions were transferred into 96 well microtiter plates and the GFP fluorescence was measured with a Typhoon Scanner 9400 (GE Healthcare) using a Typhoon blue laser module (GE Healthcare). Images were then quantified using ImageQuantTL (GE Healthcare) and represented graphically using SigmaPlot (Systat Software, Inc.).

Modeling and Figure Preparation

Chemical structures for the precursor compounds were drawn and converted to 3D coordinates using ChemDraw (Advanced Chemistry Development, Inc.). PA2 models used the ThS binding position on the *Deinococcus radiodurans* 50S (D50S) subunit (PDB ID 3CF5) (Harms et al., 2008), whereas PD1 and PD2 were based on the D50S-NoS complex (PDB ID 2ZJP) (Harms et al., 2008). PyMol (http://www.pymol.org) was used to model the PB1 and PC compounds, align EF-Tu•GE2270A (yellow; PDB ID 2C77) (Parmeggiani et al., 2006) and EF-Tu•tRNA (blue; PDB ID 1TTT) (Nissen et al., 1995) on the basis of domain II, as well as to prepare all X-ray structure figures.

ACKNOWLEDGMENTS

We would like to thank R. Beckmann and his coworkers for generous support and creating a stimulating work environment. This work was financed by the Deutsche Forschungsgemeinschaft (WI3285/1-1 to D.N.W.) and by the National Institutes of Health (GM071014 to B.S.C.).

Received: July 28, 2009
Revised: September 6, 2009
Accepted: September 10, 2009
Published: October 30, 2009

REFERENCES

Antoun, A., Pavlov, M.Y., Andersson, K., Tenson, T., and Ehrenberg, M. (2003). The roles of initiation factor 2 and guanosine triphosphate in initiation of protein synthesis. EMBO J. *22*, 5593–5601.

Bagley, M.C., Dale, J.W., Merritt, E.A., and Xiong, X. (2005). Thiopeptide antibiotics. Chem. Rev. *105*, 685–714.

Blaha, G., Gurel, G., Schroeder, S.J., Moore, P.B., and Steitz, T.A. (2008). Mutations outside the anisomycin-binding site can make ribosomes drug-resistant. J. Mol. Biol. *379*, 505–519.

Brandi, L., Marzi, S., Fabbretti, A., Fleischer, C., Hill, W., Lodmell, J., and Gualerzi, C. (2004). The translation initiation functions of IF2: targets for thiostrepton inhibition. J. Mol. Biol. *335*, 881–894.

Brune, M., Hunter, J.L., Corrie, J.E., and Webb, M.R. (1994). Direct, real-time measurement of rapid inorganic phosphate release using a novel fluorescent probe and its application to actomyosin subfragment 1 ATPase. Biochemistry *33*, 8262–8271.

Connell, S.R., Tracz, D.M., Nierhaus, K.H., and Taylor, D.E. (2003). Ribosomal protection proteins and their mechanism of tetracycline resistance. Antimicrob. Agents Chemother. *47*, 3675–3681.

Dinos, G., Wilson, D.N., Teraoka, Y., Szaflarski, W., Fucini, P., Kalpaxis, D., and Nierhaus, K.H. (2004). Dissecting the ribosomal inhibition mechanisms of edeine and pactamycin: the universally conserved residues G693 and C795 regulate P-site tRNA binding. Mol. Cell *13*, 113–124.

Gale, E.F., Cundliffe, E., Reynolds, P.E., Richmond, M.H., and Waring, M.J. (1981). Antibiotic inhibitors of ribosome function. In The Molecular Basis of Antibiotic Action, E.F. Gale, E. Cundliffe, P.E. Reynolds, M.H. Richmond, and M.J. Waring, eds. (Bristol, UK: John Wiley and sons), pp. 278–379.

Gonzalez, R.L., Jr., Chu, S., and Puglisi, J.D. (2007). Thiostrepton inhibition of tRNA delivery to the ribosome. RNA *13*, 2091–2097.

Grigoriadou, C., Marzi, S., Kirillov, S., Gualerzi, C.O., and Cooperman, B.S. (2007). A quantitative kinetic scheme for 70 S translation initiation complex formation. J. Mol. Biol. *373*, 562–572.

Harms, J.M., Wilson, D.N., Schluenzen, F., Connell, S.R., Stachelhaus, T., Zaborowska, Z., Spahn, C.M., and Fucini, P. (2008). Translational regulation via L11: molecular switches on the ribosome turned on and off by thiostrepton and micrococcin. Mol. Cell *30*, 26–38.

Hughes, R.A., and Moody, C.J. (2007). From amino acids to heteroaromatics—thiopeptide antibiotics, nature's heterocyclic peptides. Angew. Chem. Int. Ed. Engl. *46*, 7930–7954.

Jonker, H.R., Ilin, S., Grimm, S.K., Wohnert, J., and Schwalbe, H. (2007). L11 domain rearrangement upon binding to RNA and thiostrepton studied by NMR spectroscopy. Nucleic Acids Res. *35*, 441–454.

Laios, E., Waddington, M., Saraiya, A.A., Baker, K.A., O'Connor, E., Pamarathy, D., and Cunningham, P.R. (2004). Combinatorial genetic technology for the development of new anti-infectives. Arch. Pathol. Lab. Med. *128*, 1351–1359.

Llano-Sotelo, B., Hickerson, R.P., Lancaster, L., Noller, H.F., and Mankin, A.S. (2009a). Fluorescently labeled ribosomes as a tool for analyzing antibiotic binding. RNA *15*, 1597–1604.

Llano-Sotelo, B., Klepacki, D., and Mankin, A.S. (2009b). Selection of small peptides, inhibitors of translation. J. Mol. Biol. *391*, 813–819.

McConkey, G.A., Rogers, M.J., and McCutchan, T.F. (1997). Inhibition of Plasmodium falciparum protein synthesis. Targeting the plastid-like organelle with thiostrepton. J. Biol. Chem. *272*, 2046–2049.

Modolell, J., Cabrer, B., Parmeggiani, A., and Vazquez, D. (1971). Inhibition by siomycin and thiostrepton of both aminoacyl-tRNA and factor G binding to ribosomes. Proc. Natl. Acad. Sci. USA *68*, 1796–1800.

Nicolaou, K.C., Safina, B.S., Zak, M., Lee, S.H., Nevalainen, M., Bella, M., Estrada, A.A., Funke, C., Zécri, F.J., and Bulat, S. (2005a). Total synthesis of thiostrepton. Retrosynthetic analysis and construction of key building blocks. J. Am. Chem. Soc. *127*, 11159–11175.

Nicolaou, K.C., Zak, M., Rahimipour, S., Estrada, A.A., Lee, S.H., O'Brate, A., Giannakakou, P., and Ghadiri, M.R. (2005b). Discovery of a biologically active thiostrepton fragment. J. Am. Chem. Soc. *127*, 15042–15044.

Nicolaou, K.C., Zak, M., Safina, B.S., Estrada, A.A., Lee, S.H., and Nevalainen, M. (2005c). Total synthesis of thiostrepton. Assembly of key building blocks and completion of the synthesis. J. Am. Chem. Soc. *127*, 11176–11183.

Nicolaou, K.C., Zou, B., Dethe, D.H., Li, D.B., and Chen, D.Y. (2006). Total synthesis of antibiotics GE2270A and GE2270T. Angew. Chem. Int. Ed. Engl. *45*, 7786–7792.

Nicolaou, K.C., Dethe, D.H., and Chen, D.Y. (2008a). Total syntheses of amythiamicins A, B and C. Chem. Commun. (Camb.) 2632–2634.

Nicolaou, K.C., Dethe, D.H., Leung, G.Y., Zou, B., and Chen, D.Y. (2008b). Total synthesis of thiopeptide antibiotics GE2270A, GE2270T, and GE2270C1. Chem. Asian J. *3*, 413–429.

Nicolaou, K.C., Chen, J.S., Edmonds, D.J., and Estrada, A.A. (2009). Recent advances in the chemistry and biology of naturally occurring antibiotics. Angew. Chem. Int. Ed. Engl. *48*, 660–719.

Nissen, P., Kjeldgaard, M., Thirup, S., Polekhina, G., Reshetnikova, L., Clark, B.F., and Nyborg, J. (1995). Crystal structure of the ternary complex of Phe-tRNAPhe, EF-Tu, and a GTP analog. Science *270*, 1464–1472.

Pan, D., Kirillov, S.V., and Cooperman, B.S. (2007). Kinetically competent intermediates in the translocation step of protein synthesis. Mol. Cell *25*, 519–529.

Parmeggiani, A., and Nissen, P. (2006). Elongation factor Tu-targeted antibiotics: four different structures, two mechanisms of action. FEBS Lett. *580*, 4576–4581.

Parmeggiani, A., Krab, I.M., Okamura, S., Nielsen, R.C., Nyborg, J., and Nissen, P. (2006). Structural basis of the action of pulvomycin and GE2270 A on elongation factor Tu. Biochemistry *45*, 6846–6857.

Pestka, S. (1970). Thiostrepton: a ribosomal inhibitor of translocation. Biochem. Biophys. Res. Commun. *40*, 667–674.

 ©2009 Elsevier Ltd All rights reserved

Qin, H., Grigoriadou, C., and Cooperman, B.S. (2009). Interaction of IF2 with the ribosomal GTPase-associated center during 70S initiation complex formation. Biochemistry *48*, 4699–4706.

Rodnina, M.V., Savelsbergh, A., Matassova, N.B., Katunin, V.I., Semenkov, Y.P., and Wintermeyer, W. (1999). Thiostrepton inhibits the turnover but not the GTPase of elongation factor G on the ribosome. Proc. Natl. Acad. Sci. USA *96*, 9586–9590.

Seo, H.S., Abedin, S., Kamp, D., Wilson, D.N., Nierhaus, K.H., and Cooperman, B.S. (2006). EF-G-dependent GTPase on the ribosome. Conformational change and fusidic acid inhibition. Biochemistry *45*, 2504–2514.

Sergiev, P.V., Lesnyak, D.V., Kiparisov, S.V., Burakovsky, D.E., Leonov, A.A., Bogdanov, A.A., Brimacombe, R., and Dontsova, O.A. (2005). Function of the ribosomal E-site: a mutagenesis study. Nucleic Acids Res. *33*, 6048–6056.

Spahn, C.M.T., and Prescott, C.D. (1996). Throwing a spanner in the works: antibiotics and the translational apparatus. J. Mol. Med. *74*, 423–439.

Szaflarski, W., Vesper, O., Teraoka, Y., Plitta, B., Wilson, D.N., and Nierhaus, K.H. (2008). New features of the ribosome and ribosomal inhibitors: non-enzymatic recycling, misreading and back-translocation. J. Mol. Biol. *380*, 193–205.

Tu, D., Blaha, G., Moore, P., and Steitz, T. (2005). Structures of MLSBK antibiotics bound to mutated large ribosomal subunits provide a structural explanation for resistance. Cell *121*, 257–270.

Weisblum, B., and Demohn, V. (1970). Inhibition by thiostrepton of the formation of a ribosome-bound guanine nucleotide complex. FEBS Lett. *11*, 149–152.

Wilson, D.N. (2004). Antibiotics and the inhibition of ribosome function. In Protein Synthesis and Ribosome Structure, K. Nierhaus and D. Wilson, eds. (Weinheim: Wiley-VCH), pp. 449–527.

Wilson, D.N., and Nierhaus, K.H. (2005). Ribosomal proteins in the spotlight. Crit. Rev. Biochem. Mol. Biol. *40*, 243–267.

Xing, Y., and Draper, D.E. (1996). Cooperative interactions of RNA and thiostrepton antibiotic with two domains of ribosomal protein L11. Biochemistry *35*, 1581–1588.

Yassin, A., and Mankin, A.S. (2007). Potential new antibiotic sites in the ribosome revealed by deleterious mutations in RNA of the large ribosomal subunit. J. Biol. Chem. *282*, 24329–24342.

Yassin, A., Fredrick, K., and Mankin, A.S. (2005). Deleterious mutations in small subunit ribosomal RNA identify functional sites and potential targets for antibiotics. Proc. Natl. Acad. Sci. USA *102*, 16620–16625.

 ©2009 Elsevier Ltd All rights reserved

Paper 6

[redacted]

Chemistry & Biology
Article

Differential Effects of Thiopeptide and Orthosomycin Antibiotics on Translational GTPases

Aleksandra Mikolajka,[1,2,4] Hanqing Liu,[3,4] Yuanwei Chen,[3] Agata L. Starosta,[1] Viter Márquez,[1] Marina Ivanova,[1] Barry S. Cooperman,[3,*] and Daniel N. Wilson[1,2,*]
[1]Gene Center and Department of Biochemistry
[2]Center for Integrated Protein Science Munich (CiPSM)
University of Munich, LMU, Feodor Lynen Str. 25, 81377 Munich, Germany
[3]Department of Chemistry, University of Pennsylvania, Philadelphia, PA 19104-6323, USA
[4]These authors contributed equally to this work
*Correspondence: cooprman@pobox.upenn.edu (B.S.C.), wilson@lmb.uni-muenchen.de (D.N.W.)
DOI 10.1016/j.chembiol.2011.03.010

SUMMARY

The ribosome is a major target in the bacterial cell for antibiotics. Here, we dissect the effects that the thiopeptide antibiotics thiostrepton (ThS) and micrococcin (MiC) as well as the orthosomycin antibiotic evernimicin (Evn) have on translational GTPases. We demonstrate that, like ThS, MiC is a translocation inhibitor, and that the activation by MiC of the ribosome-dependent GTPase activity of EF-G is dependent on the presence of the ribosomal proteins L7/L12 as well as the G′ subdomain of EF-G. In contrast, Evn does not inhibit translocation but is a potent inhibitor of back-translocation as well as IF2-dependent 70S-initiation complex formation. Collectively, these results shed insight not only into fundamental aspects of translation but also into the unappreciated specificities of these classes of translational inhibitors.

INTRODUCTION

Protein synthesis occurs on large macromolecular particles called ribosomes, which are composed of RNA and protein. In bacteria the 70S ribosome can be split into a small (30S) and large (50S) subunit. The bacterial translational machinery represents a major target within the cell for antibiotics (reviewed by Blanchard et al., 2010; Wilson, 2009). Many clinically important classes of antibiotics inhibit translation by binding to the active centers of ribosome. For example the tetracyclines and aminoglycosides bind at the decoding site on the small subunit, and the chloramphenicols, macrolides/ketolides, oxazolidinones, and lincosamides bind at the peptidyltransferase center (PTC) on the large subunit (Sohmen et al., 2009a, 2009b). Despite the potency of many of these drug classes, antibiotic resistance among clinically relevant pathogens is an increasing problem, and thus, the need for new antibiotics is more urgent than ever before. Ideally, the new antibiotics should have nonoverlapping sites with the currently used antimicrobial agents, so that the occurrence of cross-resistance is reduced or prevented. Two such classes are the thiopeptides and orthosomycins (Figures 1A–1C), which bind to distinct sites on the large ribosomal subunit that are located far from the PTC (Figures 1D and 1E).

The orthosomycins, such as evernimicin (Evn), are oligosaccharide antibiotics (Figure 1A) that display excellent antimicrobial activity against a broad range of Gram-positive bacteria, both in vivo and in vitro. Although attempts to introduce Evn clinically as Ziracin (Schering-Plough) were unsuccessful, a related compound, avilamycin (Avn), is used as a growth promoter in animal feeding. A multitude of resistance mutation/modification and chemical footprinting studies indicate that the orthosomycin-binding site is located at the base of the L7/L12 stalk (Figures 1D and 1E), ~50 Å from the PTC. Mutations in ribosomal protein L16 (Aarestrup and Jensen, 2000; Adrian et al., 2000b; McNicholas et al., 2001; Zarazaga et al., 2002), and in helix 89 (H89) and H91 of the 23S rRNA, as well as methylation of G2470 (*E. coli* numbering used throughout) in H89 (Mann et al., 2001), confer resistance to Evn and Avn (Adrian et al., 2000a; Belova et al., 2001). In addition, Evn and Avn protect 23S rRNA nucleotides, e.g., A2482 in H89 and A2534 in H91, from chemical modification (Belova et al., 2001; Kofoed and Vester, 2002). It is also noteworthy that mutations in *rplP* (L16 gene) confer relatively low-level resistance (MIC <12 μg ml^{-1}), whereas higher-level resistance (MIC >256 μg ml^{-1}) is obtained by EmtA-mediated methylation or rRNA mutations (Belova et al., 2001; Mann et al., 2001). Taken together, these results suggest that the orthosomycin-binding site spans from the minor groove of H89 to the loop region of H91 (Figure 1E) and that mutations in L16 confer resistance indirectly via perturbation of the 23S rRNA. In agreement with this novel location, Evn does not inhibit peptide-bond formation (Belova et al., 2001) or compete with several other ribosomal antibiotics for ribosome binding (McNicholas et al., 2000). Although some effect of Avn on aa-tRNA binding to ribosomes has been observed (Wolf, 1973), Evn is better known as an initiation inhibitor; Evn inhibits the formation of fMet-puromycin in an IF2-dependent manner (Belova et al., 2001), although the exact step of inhibition remains unclear. Moreover, to our knowledge, the effects of orthosomycins on translation factors other than IF2 and EF-Tu have not yet been addressed.

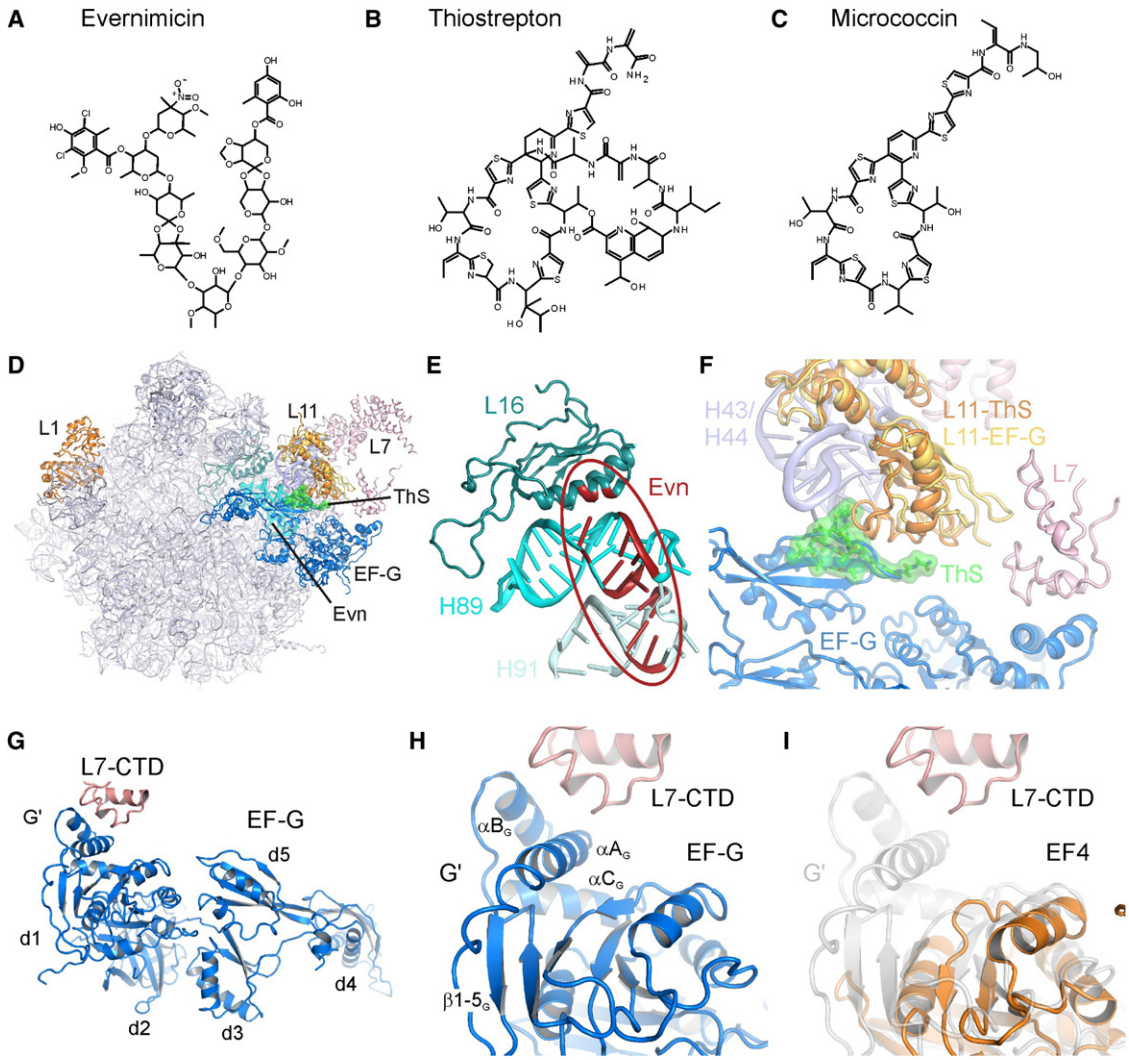

Figure 1. Chemical Structures and Ribosomal-Binding Sites of Thiopeptide and Orthosomycin Antibiotics

(A–C) Chemical structures of the (A) orthosomycin Evn, and the thiopeptide antibiotics (B) ThS and (C) MiC.

(D) Overview of the binding sites of orthosomycins and thiopeptides on the large subunit relative to EF-G. R-proteins L1, L11, and L7 are shown for reference.

(E) Putative binding site of orthosomycins spanning from H89 and H91 of the 23S rRNA. Residues highlighted in red have been associated biochemically with Evn or Avn (reviewed by Wilson, 2009).

(F) Binding site of ThS (green) in the cleft between H43 and H44 of the 23S rRNA and the NTD of L11 (L11-ThS) (Harms et al., 2008). The relative positions of EF-G (blue), C-terminal domain of L7/L12 (L7-CTD), and of a different conformation of L11 (L11-EF-G) are from Gao et al. (2009).

(G) Overview of domain arrangement of EF-G with contact between the L7-CTD and the G′ domain of EF-G as observed in the 70S-EF-G crystal structure (Gao et al., 2009).

(H) Expansion of (G) highlighting the secondary structure elements of the G′ subdomain.

(I) Juxtaposition of the G′ subdomain of EF-G (gray transparency) with the G-domain of EF4 (orange) (Evans et al., 2008) that lacks a G′ subdomain.

See also Figure S1.

In contrast, thiopeptides, such as thiostrepton (ThS), have been extensively studied (reviewed by Bagley et al., 2005; Nicolaou et al., 2009; Wilson, 2009). Although ThS is already in veterinary usage, its low water solubility and poor bioavailability has so far precluded its use in human medicine. Nevertheless, the thiopeptide class of antibiotics has received renewed interest in the recent years because (i) of its effectiveness against Gram-positive bacteria, in particular, methicillin-resistant *Staphylococcus aureus* (MRSA), and against the malarial parasite *Plasmodium falciparum* (McConkey et al., 1997), as well as (ii) recent successes in the total synthesis of a number of thiopeptides (reviewed by Hughes and Moody, 2007; Nicolaou et al., 2009), including among others, ThS (Nicolaou et al., 2005a, 2005b) and micrococcin (MiC) (Lefranc and Ciufolini, 2009). Thiopeptide antibiotics, such as ThS and MiC, are composed of oxazoles and thiazoles, as well as nonnatural amino acids that are linked together to form complex macrocyclic frameworks (Figures 1B and 1C).

Both ThS and MiC have been crystallized in complex with the large ribosomal subunit, revealing their binding site to be located

in a cleft formed by the N-terminal domain (NTD) of ribosomal protein L11 and H43/H44 of the 23S rRNA (Figures 1D and 1F) (Harms et al., 2008), consistent with a vast wealth of prior biochemical studies (reviewed by Wilson, 2009). This region is part of the GTPase-associated center (GAC), so named because it is involved in binding of translation factors and stimulation of their GTPase activities. Consistently, thiopeptide antibiotics have been shown to inhibit IF2-dependent 70S-initiation complex (70SIC) formation (Brandi et al., 2004; Grigoriadou et al., 2007), EF-Tu-dependent delivery of aminoacyl-tRNAs to the ribosome (Brandi et al., 2004; Gonzalez et al., 2007; Modolell et al., 1971; Otaka and Kaji, 1974), translocation of the $tRNA_2$-mRNA complex through the ribosome (Munro et al., 2010; Pan et al., 2007; Pestka, 1970; Pestka and Brot, 1971; Rodnina et al., 1997), and stringent factor RelA-dependent synthesis of ppGpp (Cundliffe and Thompson, 1981; Knutsson Jenvert and Holmberg Schiavone, 2005). Surprisingly, however, ThS and MiC exhibit differential effects on the uncoupled ribosome-dependent EF-G GTPase activities: ThS strongly inhibits multiple-turnover GTP hydrolysis of EF-G (Pestka, 1970; Weisblum and Demohn, 1970) by preventing inorganic phosphate (Pi) release and, thus, trapping EF-G on the ribosome (Rodnina et al., 1999; Seo et al., 2006). The overlap between the ThS and EF-G binding sites on the ribosome (Figures 1D and 1F) (Harms et al., 2008) suggests that ThS stabilizes an initial binding state of EF-G (Rodnina et al., 1999; Seo et al., 2006), which has weaker affinity than a subsequently formed, accommodated state (Cameron et al., 2002; Seo et al., 2006). In contrast, MiC does not prevent Pi release (Starosta et al., 2009) and actually stimulates the multiple-turnover GTP hydrolysis activity of EF-G (Cameron et al., 2002; Cundliffe and Thompson, 1981; Lentzen et al., 2003).

The G domains of translational GTPases have a well-conserved architecture, with the exception of a region located between the G4 and G5 motifs, which, in EF-G, are termed the G′ subdomain (see Figure S1 available online). In EF-G the G′ subdomain consists of ~90 amino acids that form four consecutive β strands (2_G–5_G) followed by three α helices (A_G–C_G) (Figures 1G and 1H; Figure S1). In contrast, translational GTPases, such as elongation factor EF-Tu, initiation factor IF2, the ribosome-associated stress response factor BipA (deLivron et al., 2009; deLivron and Robinson, 2008; Owens et al., 2004), and the back-translocation factor LepA (EF4) (Liu et al., 2010; Qin et al., 2006), are completely lacking the G′ subdomain (Figure 1I), whereas the ribosomal protection protein TetM (Connell et al., 2003a) has a partial G′ subdomain, lacking three β strands (3_G–5_G) (Figure S1). Interaction of the G′ subdomain of EF-G with the C-terminal domain of ribosomal protein L7/L12 (L7-CTD) is observed structurally (Connell et al., 2007; Datta et al., 2005; Gao et al., 2009; Harms et al., 2008; Helgstrand et al., 2007) (Figures 1G and 1H) and is required for efficient GTP hydrolysis (Diaconu et al., 2005; Nechifor et al., 2007; Savelsbergh et al., 2000, 2005) and Pi release (Diaconu et al., 2005; Savelsbergh et al., 2005), leading to the suggestion that enhanced recycling of EF-G by MiC results from stabilization of this interaction (Harms et al., 2008).

Here, we show that although MiC stimulates the multiple-turnover ribosome-dependent EF-G GTPase, it inhibits the GTPase activities of other translational GTPases, such as TetM, EF4, BipA, and IF2, which have reduced, or completely absent, G′ subdomains. Furthermore, deletion of the G′ subdomain from EF-G removes the stimulatory effect of MiC, as does the absence of L7/L12 on the ribosome. Despite the differential effects of MiC and ThS on EF-G GTPase, we show that MiC, like ThS, is a potent inhibitor of the EF-G catalyzed translocation process. In contrast the orthosomycin Evn, although not interfering with EF-G GTPase and translocation activities, is a potent inhibitor of the ribosome-dependent IF2 and EF4 GTPase activities, as well as of EF4-mediated back-translocation and IF2-dependent 70SIC formation. Collectively, our results delineate the specific steps of interference and reveal the differential effects that these inhibitors have on translocation factor function—an important step for the development of new, improved antimicrobial agents.

RESULTS

Differential Effects of Thiopeptide Antibiotics on GTPase Activities of Translational Factors

The suggestion that MiC stimulates the uncoupled ribosome-dependent GTPase (rdGTPase) of EF-G by stabilizing the interaction of L7-CTD with the G′ subdomain of EF-G (Harms et al., 2008) prompted us to investigate the effect of MiC on the uncoupled rdGTPase activities of other translational GTPases that have reduced or completely absent G′ subdomains (such as TetM, EF4, and BipA), as determined using the malachite green assay (Starosta et al., 2009). We found rdGTPase activity of EF-G to be inhibited by ThS (Figure 2A), as expected from previous reports (Pan et al., 2007; Pestka, 1970; Rodnina et al., 1999; Weisblum and Demohn, 1970). The rdGTPase activities of TetM, EF4, and BipA were also inhibited by ThS (1 μM) (Figures 2B–2D), as was the rdGTPase activity of IF2 (Figure 2E), as reported previously (Grunberg-Manago et al., 1972). Similar trends were found for all factors independent of the excess of the factor over the ribosome (Figure S2) or the concentration of antibiotics used (data not shown). Consistent with these results, ThS has been shown previously to inhibit the rdGTPase activity of a related ribosome protection protein, TetO (Connell et al., 2003b), the formation of a stable complex between TetM and the ribosome in the presence of GDPNP and GTP (Dantley et al., 1998), and the IF2-dependent formation of 70SIC (Grigoriadou et al., 2007). However, we could not reproduce the recently reported stimulatory effects of ThS on IF2 GTPase (Brandi et al., 2004; Cameron et al., 2002).

Guided by a comparison of the crystal structures of *T. thermophilus* EF-G (PDB 1FNM; Laurberg et al., 2000) with *E. coli* EF4 (PDB 3CB4; Evans et al., 2008), we also generated an *E. coli* EF-G lacking the G′ subdomain (EF-GΔG′): EF-GΔG′ has a deletion of amino acids 172–265, thus truncating the G′ subdomain before $\beta 3_G$ and after $\beta 6_1$ (Figure S1). In contrast to previous attempts to produce an EF-GΔG′ protein (Nechifor et al., 2007), soluble protein was obtained under native conditions, and therefore, refolding or purification under denaturing conditions was unnecessary (see Experimental Procedures). The purified *E. coli* EF-GΔG′ had an intrinsic GTPase activity comparable with that of wild-type *E. coli* EF-G (data not shown), suggesting that the protein was not misfolded. Moreover, although the rdGTPase was significantly slower (>10×) than wild-type

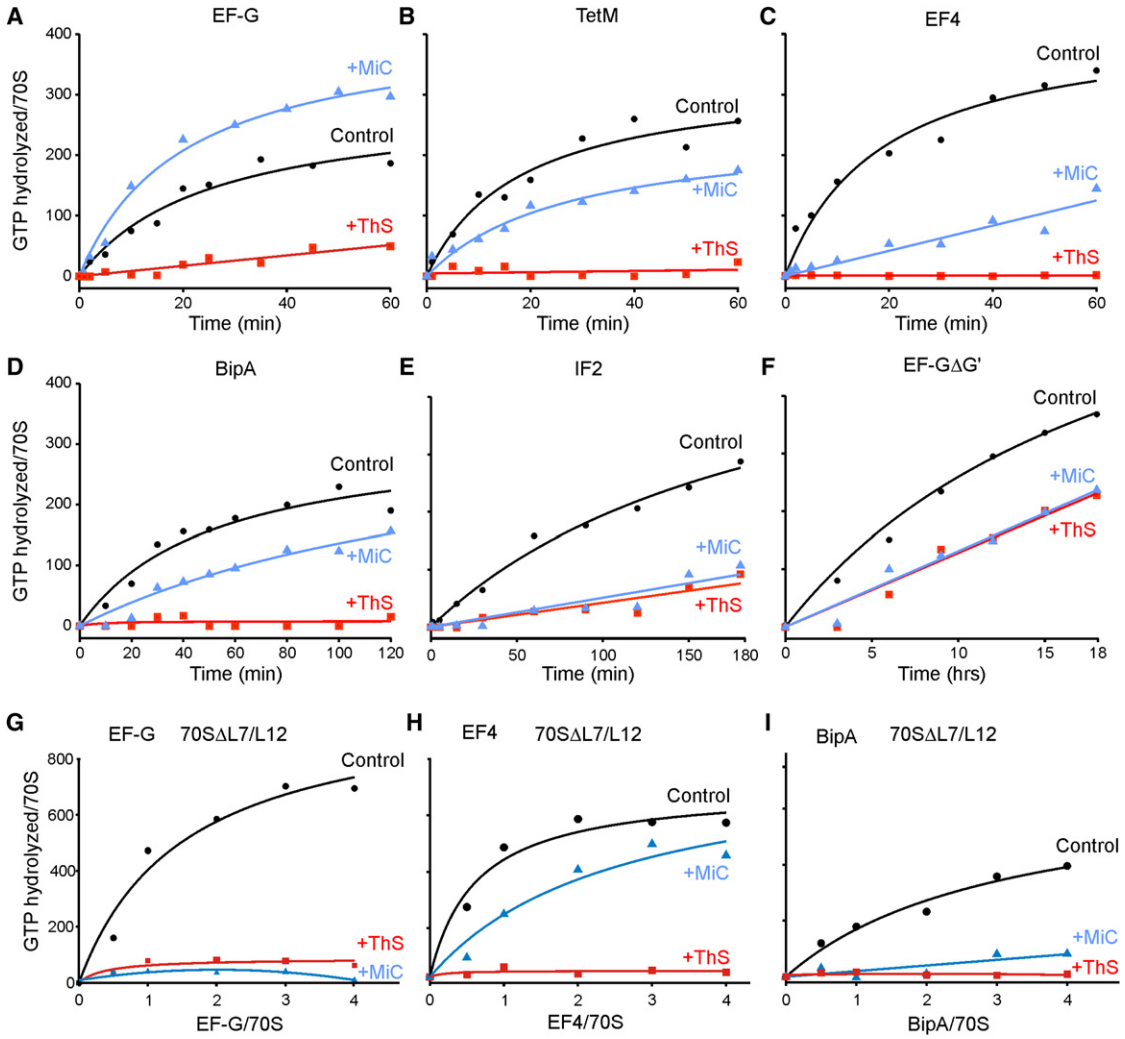

Figure 2. Effect of ThS and MiC on GTPase Activity of Various Translation Factors

(A–F) The rdGTPase activities of translation factors (A) *E. coli* EF-G, (B) TetM, (C) *E. coli* EF4, (D) *E. coli* BipA, (E) *E. coli* IF2, and (F) *E. coli* EF-GΔG′, using *E. coli* 70S ribosomes in the absence (black circles) and presence of 1 μM ThS (red squares) or 5 μM MiC (blue triangles).

(G–I) The rdGTPase activities of *E. coli* translation factors (G) EF-G, (H) EF4, and (I) BipA, using *E. coli* 70S ribosomes lacking L7/L12. Reactions in (G)–(I) were incubated for 12 hr at 20°C.

In all cases, background hydrolysis due to the intrinsic GTPase activity of each factor has been subtracted. See also Figure S2.

E. coli EF-G, it was nevertheless inhibited by ThS (Figure 2F), albeit more weakly than for wild-type EF-G. As expected from previous studies (Cameron et al., 2002; Cundliffe and Thompson, 1981; Lentzen et al., 2003), we also observed that MiC enhanced the rdGTPase activity of EF-G (Figure 2A). Conversely, we could show that MiC inhibited the rdGTPase of all other translational GTPases that were tested, namely TetM, EF4, BipA, and IF2 (Figures 2B–2E). Additionally, deletion of the G′ subdomain of EF-G also produced a change in the activity of MiC because MiC was seen to inhibit, rather than stimulate, the rdGTPase of EF-GΔG′ (Figure 2F). We note that deletion of the G′ subdomain of EF-G greatly reduced (>10-fold) the rdGTPase activity of the factor, similar to the previously reported introduction of mutations within αA_G of the G′ subdomain (Nechifor et al., 2007). Similarly, ThS and MiC also inhibited the rdGTPase activities of EF-G, EF4, and BipA when *E. coli* 70S ribosomes were used that lacked L7/L12 (70SΔL7/L12) (Figures 2G–2I). Defects in rdGTPase of EF-G have also been seen when the ribosomal proteins L7/L12 are selectively removed from the ribosome (Diaconu et al., 2005; Kischa et al., 1971; Nechifor et al., 2007) or mutations are made within the L7-CTD (Diaconu et al., 2005).

Inhibition of Translocation by Thiopeptide Antibiotics, but Not by Evn

The translocation reaction occurs after peptide-bond formation and involves the EF-G catalyzed movement of the peptidyl- and deacylated-tRNAs in the A and P sites into the P and E sites, respectively (Figure 3A) (reviewed by Schmeing and Ramakrishnan, 2009). Conversion of the pretranslocational (PRE) complex into a posttranslocational (POST) complex proceeds through (A/P and P/E) hybrid states, where the CCA 3′ ends of the tRNAs move with respect to the large subunit while remaining

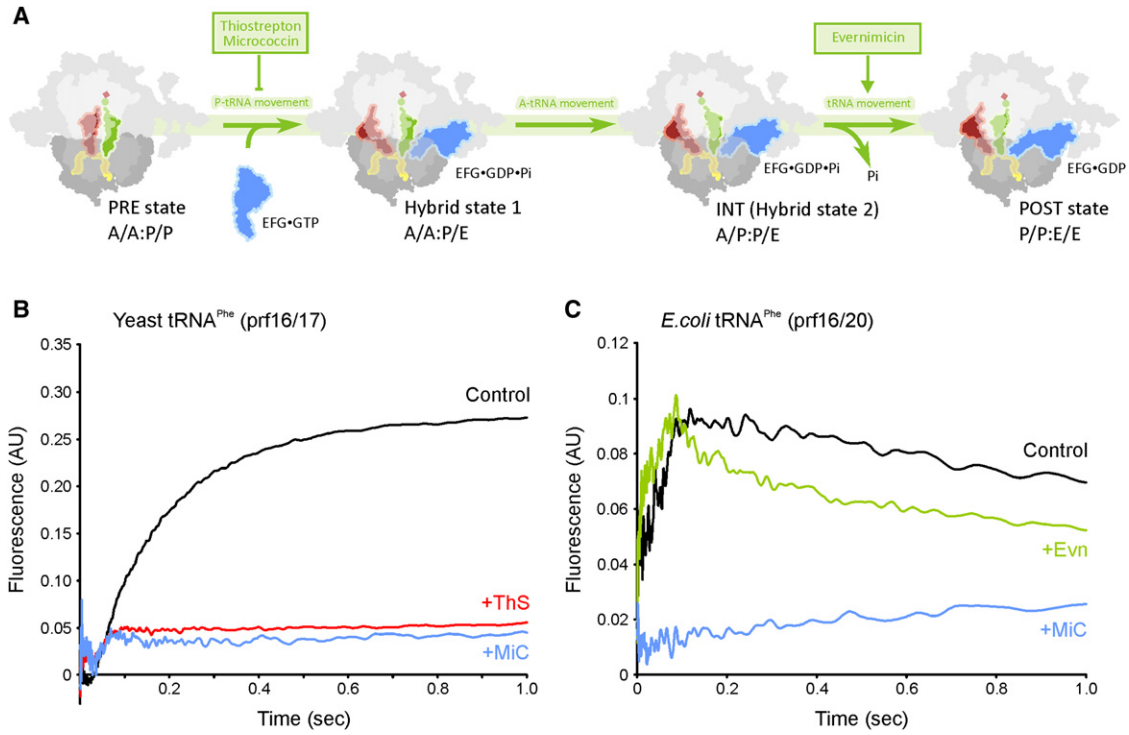

Figure 3. Effect of the MiC and Evn on Translocation

(A) Scheme for EF-G catalyzed translocation with sites of antibiotic inhibition.

(B) Isolated PRE complex (0.1 μM) containing yeast fMetPhe-tRNA^{Phe}(Prf16/17) in the A site and tRNA^{fMet} in the P site, either in the absence of antibiotic (black trace) or in the presence of ThS (10 μM; red trace) or MiC (10 μM; blue trace), was rapidly mixed in a stopped-flow spectrophotometer with 5 μM EF-G and 1 mM GTP.

(C) Isolated PRE complex (0.1 μM) containing *E. coli* fMetPhe-tRNA^{Phe}(Prf16/20) and tRNA^{fMet} in the P site, in the absence of antibiotic (black trace) or in the presence of Evn (10 μM; green trace) or MiC (10 μM; blue trace), was rapidly mixed in a stopped-flow spectrophotometer with 5 μM EF-G and 1 mM GTP. All concentrations are final after mixing. The traces in the control and +Evn traces are each fit to a two-step process (Pan et al., 2007) yielding the following rate constants: Control: 20.7 ± 0.6 s^{-1}, 1.3 ± 0.1 s^{-1}; +Evn: 28.1 ± 0.7 s^{-1}, 3.5 ± 0.2 s^{-1}.

See also Figure S3.

relatively fixed with respect to the small subunit (Blanchard et al., 2004; Moazed and Noller, 1989; Ratje et al., 2010). To monitor translocation rates, PRE complexes were assembled containing proflavin (prf)-labeled tRNAs, thus enabling tRNA movement to be followed by stopped-flow monitoring of the fluorescence change following delivery of EF-G•GTP (Pan et al., 2007; Rodnina et al., 1997; Savelsbergh et al., 2003). In Figure 3B, rapid addition of EF-G•GTP to PRE complexes formed with unlabelled *E. coli* tRNA$_f^{Met}$ in the P site and yeast fMetPhe-tRNA^{Phe} (prf16/17) in the A site leads to an apparent monophasic increase in fluorescence as A-site tRNA is translocated to the P site (Pan et al., 2007; Rodnina et al., 1997; Savelsbergh et al., 2003). Preincubation of the PRE complex with (10 μM) MiC or ThS completely abolished fluorescence, as reported previously for ThS (Pan et al., 2007; Rodnina et al., 1997).

By contrast, translocation clearly proceeds via a two-step reaction for PRE complexes containing *E. coli* tRNA$_f^{Met}$ in the P site and *E. coli* fMetPhe-tRNA^{Phe} (Prf16/20) in the A site (Figure 3C) (Pan et al., 2007). In this case an initial rapid increase in fluorescence intensity is followed by a gradual decrease, with respective apparent rate constants of 20.7 ± 0.6 s^{-1} and 1.3 ± 0.1 s^{-1}. The presence of MiC abolishes almost all fluorescent change (Figure 3C), strongly inhibiting step 1 and, thus, step 2, as reported previously for ThS (Pan et al., 2007). In contrast, Evn does not inhibit the translocation reaction. In fact the apparent rate constants (step 1, 28.1 ± 0.7 s^{-1}; step 2, 3.5 ± 0.2 s^{-1}) suggest that the drug actually accelerates the process, particularly the second step (Figure 3C).

Evn Inhibits IF2-Dependent 70SIC Formation

In bacteria, formation of the 70SIC involves the association of the large 50S subunit with a 30S-initiation complex (30SIC) comprising the 30S subunit, mRNA; initiator fMet-tRNA and three initiation factors IF1, IF2, and IF3 (Figure 4A) (reviewed by Laursen et al., 2005; Simonetti et al., 2009). Binding of the 50S subunit to the 30SIC stimulates the GTPase activity of IF2, leading to release of IF2•GDP and resulting in a puromycin-reactive 70SIC (Figure 4A) (Grigoriadou et al., 2007).

Evn has previously been shown to inhibit IF2-dependent formation of fMet-puromycin (Belova et al., 2001), leading to its classification as a translation initiation inhibitor. However, to our knowledge, the exact step of inhibition has not been determined. To examine this further, 70SIC formation has been monitored kinetically using light scattering as described previously

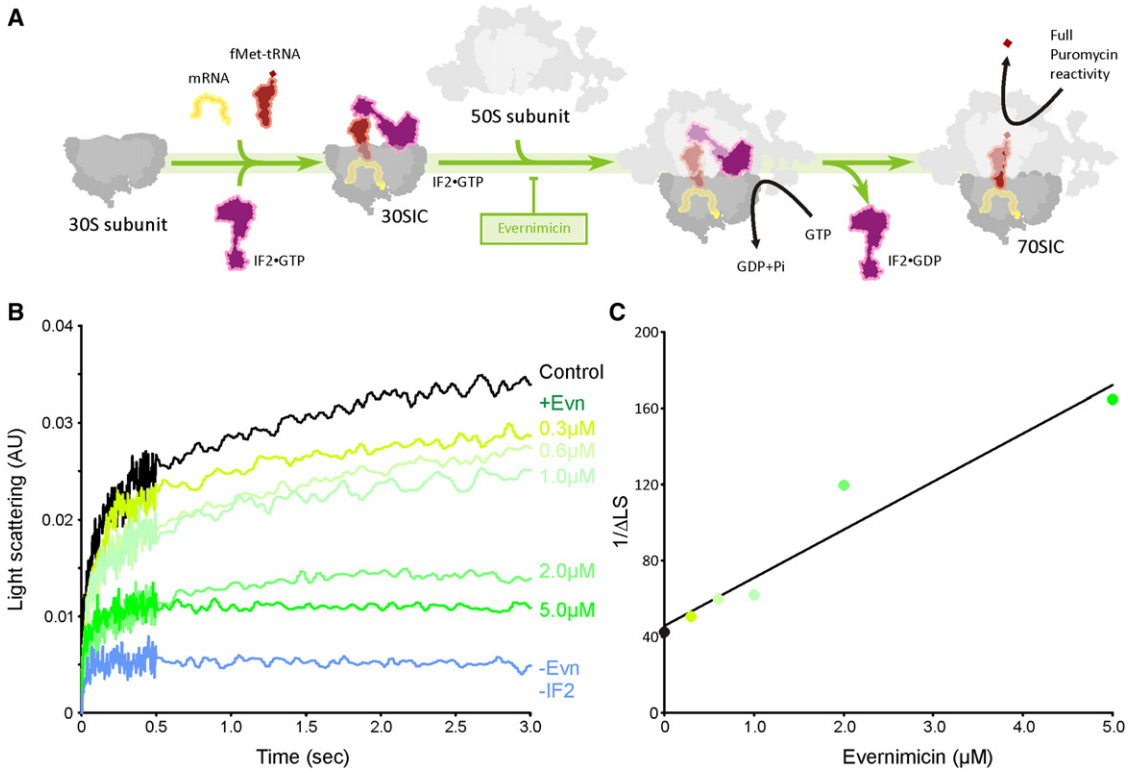

Figure 4. Evn Inhibits IF2-Dependent 70SIC Formation

(A) Scheme for 70SIC formation with site of Evn inhibition.

(B) 30SIC (0.3 μM) was premixed with various concentrations of Evn (0–5 μM) and then rapidly mixed with 50S subunits (0.3 μM) in a KinTek stopped-flow spectrophotometer. The sample from which IF2 was omitted demonstrates the dependence of 70SIC formation on IF2.

(C) A plot of the reciprocal of IF2-dependent light-scattering increase at 1 s versus Evn concentration, allowing calculation of an apparent K_i for Evn of 1.8 ± 0.2 μM.

(Grigoriadou et al., 2007): 30SIC programmed with 022AUG mRNA was rapidly mixed with 50S subunits, and the increase in light scattering due to 70SIC formation (black control trace in Figure 4B) was monitored using stopped-flow spectrophotometry. In the absence of IF2, no increase in light scattering was observed (blue trace in Figure 4B), illustrating the IF2-dependence for 70SIC reported previously (Antoun et al., 2006; Grigoriadou et al., 2007). Pre-incubation of the 30SIC with increasing concentrations of Evn before 50S addition led to a corresponding decrease in IF2-dependent light scattering (green traces in Figure 4B). At 5 μM Evn, almost all IF2-dependent light scattering was abolished, indicating that Evn inhibits the IF2-dependent association of the 30SIC with the 50S subunit. A plot of the reciprocal of the increase of IF2-dependent light scattering at 1 s versus Evn concentration (Figure 4C) yields an apparent K_i for Evn of 1.8 ± 0.2 μM.

Differential Effects of Evn on GTPase Activity of Translational GTPases

Evn strongly inhibits the rdGTPase activity of IF2 (Figure 5A) but has little or no effect on the rdGTPase activities of EF-G (Figure 5B), or EF-GΔG′ (Figure 5C), or of the EF-G paralog Tet(M) (Figure 5D), consistent with the potency of Evn in inhibiting 70SIC formation (Figure 4B) and with the lack of effect of Evn on EF-G-dependent translocation (Figure 3C). Surprisingly, Evn was also found to inhibit the rdGTPase of BipA (Figure 5E) and especially EF4 (Figure 5F). Indeed, the inhibitory activity of Evn toward EF4 (IC_{50} = ~3 μM) was higher than that toward IF2 (IC_{50} = ~7 μM), and much higher than toward BipA (IC_{50} = ~20 μM).

EF4-Dependent Back-Translocation Is Inhibited by Evn

EF4 catalyzes partial back-translocation, i.e., the movements of mRNA and tRNAs from POST toward the PRE state (Figure 6A) (Liu et al., 2010; Qin et al., 2006). As described previously (Liu et al., 2010), EF4-mediated partial back-translocation was monitored using prf-labeled tRNAs: POST state ribosomes containing fMetPhe-$tRNA^{Phe}$(Prf16/20) in the P site and $tRNA^{fMet}$ in the E site were rapidly mixed in a stopped-flow spectrophotometer with EF4 and GDPNP, with fluorescence change being monitored over time (Figure 6B). In the absence of antibiotic, back-translocation proceeds via a three-step process (blue trace in Figure 6B) consistent with movement through a series of three intermediate states as reported (Liu et al., 2010) (INT1–3 in Figure 6A). In the presence of increasing concentrations of Evn, both the fluorescence change and rates of each step in the partial back-translocation were inhibited by Evn, (Figure 6B), leading to an apparent K_i for Evn binding to the POST complex of 0.6 μM (Figure 6C). High concentrations of Evn (5 μM in Figure 6B) completely abolished the EF4-catalyzed component of

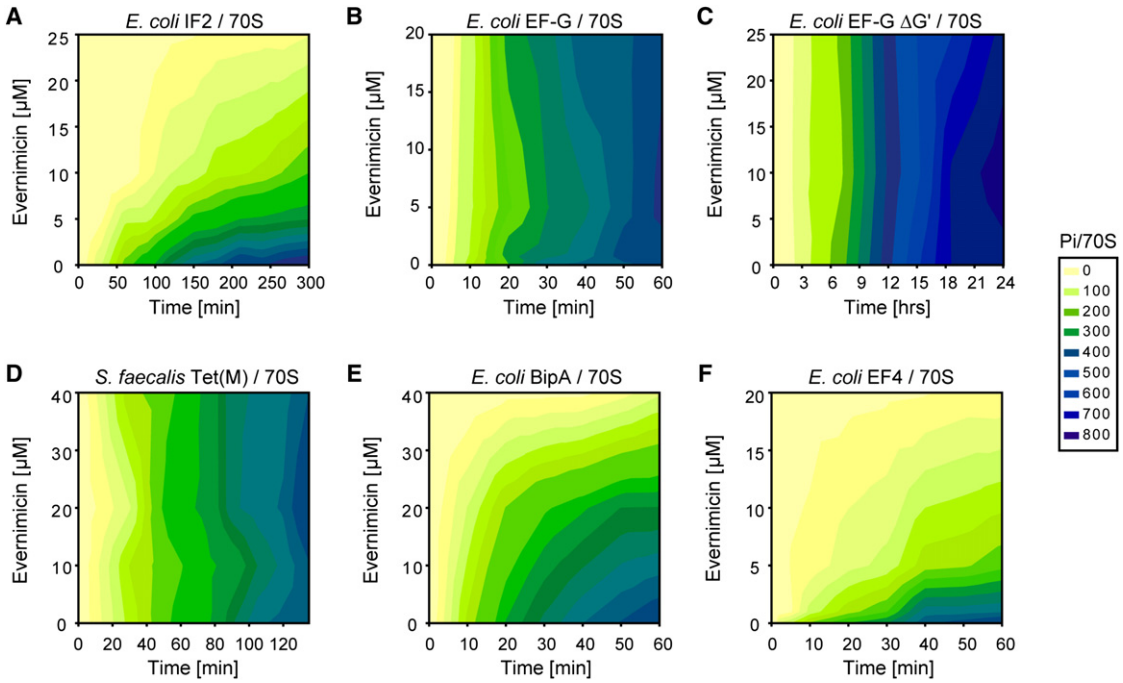

Figure 5. Effect of Evn on the GTPase Activity of Various Translation Factors

(A–F) Activation of uncoupled rdGTPases of translation factors (A) *E. coli* IF2, (B) *E. coli* EF-G, (C) *E. coli* EF-GΔG′, (D) *S. faecalis* TetM, (E) *E. coli* BipA, and (F) *E. coli* EF4, in the presence of increasing concentrations of Evn. The inset shows the color gradient scale from 0 (yellow) to 800 pmol (blue) of Pi produced per pmol of 70S ribosomes, following subtraction of background intrinsic GTPase activities.

the back-translocation, and only the two-step spontaneous reverse-translocation process that occurs in the absence of EF4 was observed (Liu et al., 2010). Evn inhibition of EF4-dependent partial back-translocation is similar to that reported earlier using spectinomycin (Liu et al., 2010), a well-characterized translocation inhibitor (Wilson, 2009), and is consistent with the observation that Evn is a potent inhibitor of the EF4 rdGTPase activity (Figure 5F).

DISCUSSION

Influence of Thiopeptides on Translocation and Translation Factor GTPase Activities

Although both ThS and MiC inhibit the multiple-turnover rdGTPase activities of IF2, TetM, EF4, and BipA (Figures 2B–2E), MiC differs from ThS in stimulating the rdGTPase of EF-G, an activity that is strongly inhibited by ThS (Figure 2A). Our results suggest that ThS inhibition and MiC stimulation of EF-G rdGTPase arise ultimately from differential effects on the interactions between the G′ subdomain of EF-G and L7-CTD.

ThS allows ribosome-binding and single-turnover GTPase activity of EF-G but prevents the stable accommodation of EF-G on the ribosome, which is necessary for tRNA translocation (Rodnina et al., 1999; Seo et al., 2006). Part of the accommodation of EF-G encompasses the movement of EF-G toward L11-NTD, which is inhibited by ThS (Seo et al., 2006), consistent with the structural overlap between the binding site of ThS and domain V of EF-G, both locating to the cleft formed by H43/44 and L11-NTD (Figure 1F) (Harms et al., 2008). Because ThS also prevents multiple-turnover GTPase activity of EF-G by inhibiting Pi release (Savelsbergh et al., 2003; Seo et al., 2006), EF-G remains trapped on the ribosome but in an unaccommodated state. In contrast, MiC allows Pi release from EF-G (Starosta et al., 2009) and, thus, stimulates the multiple-turnover rdGTPase activity of EF-G, as observed here (Figure 2A) and reported previously (Cameron et al., 2002; Cundliffe and Thompson, 1981; Lentzen et al., 2003). In agreement with the idea that MiC stimulates the rdGTPase of EF-G by stabilization of the interaction between the L7-CTD and the G′ subdomain of EF-G (Harms et al., 2008), we could show that the MiC-dependent stimulation of EF-G rdGTPase activity was lost when the G′ subdomain of EF-G was removed (Figure 2F) or the ribosomes lacked L7/L12 (Figures 2G–2I). Moreover, the rdGTPase activities of translation factors that naturally lack or have a reduced G′ subdomain (TetM, EF4, BipA, IF2) were also inhibited by MiC (Figures 2B–2E).

Although many translation factors lack the complete G′ subdomain, NMR studies indicate that IF2, EF-Tu, and RF3 interact with the same conserved region of L7-CTD as EF-G (Helgstrand et al., 2007). L7/L12 has been proposed to interact with helix αD_1 of domain I of EF-Tu. However, this interaction is more important for initial binding of EF-Tu•GTP•aa-tRNA to the ribosome, rather than for subsequent steps, such as A-site binding and GTPase activation (Kothe et al., 2004). Nevertheless, like EF-G, the rdGTPase activity of EF-Tu is dramatically reduced when ribosomes are depleted of L7/L12 (Diaconu et al., 2005; Mohr et al., 2002). In contrast, depletion of L7/L12 reduces the rate of association of IF2 with the ribosome, rather than directly

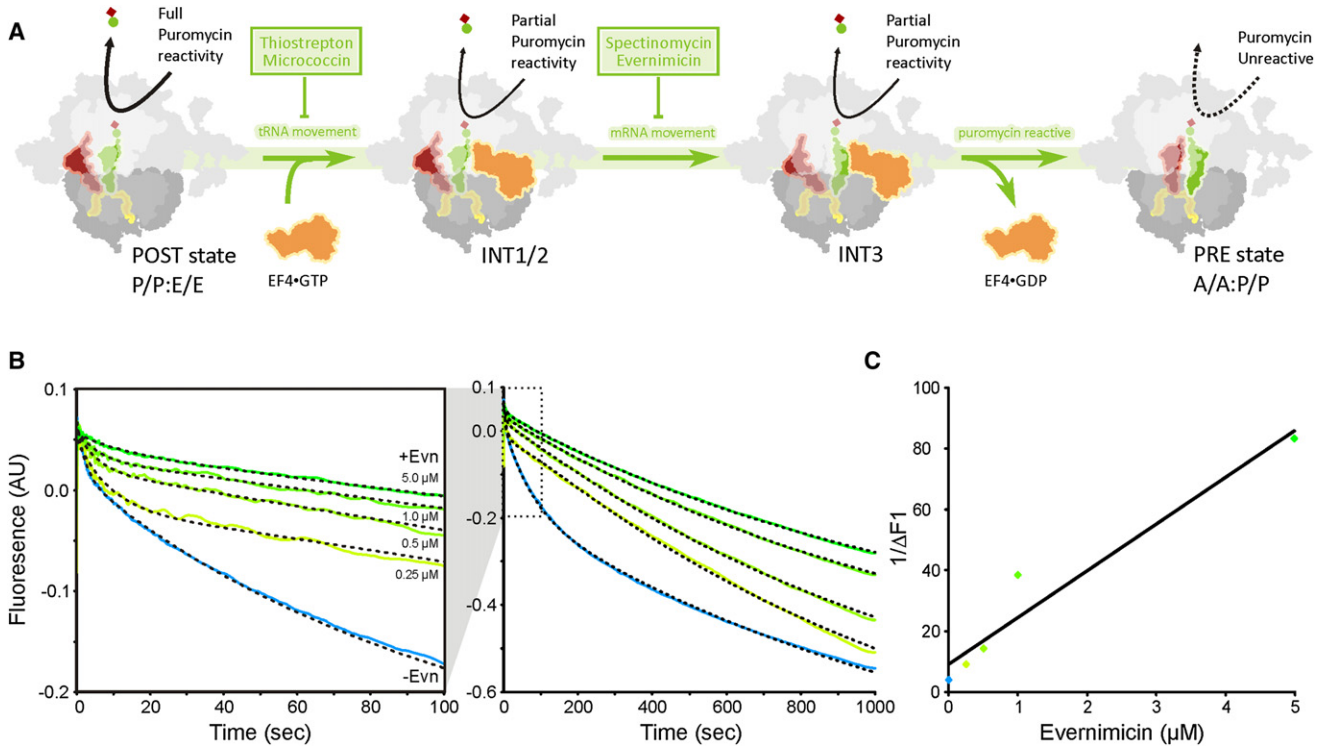

Figure 6. Evn Inhibits EF4-Mediated Back-Translocation

(A) Scheme for EF4-catalyzed back-translocation with sites of antibiotic inhibition.

(B) Fluorescence changes over different time scales. Isolated POST complex (0.1 μM) containing fMetPhe-tRNA^{Phe}(Prf) in the P site and tRNA^{fMet} in the E site, premixed with 0.15 μM tRNA^{fMet}, to increase E-site occupancy, were rapidly mixed in a stopped-flow spectrophotometer with 3 μM EF4, 0.5 mM GDPNP, and different concentrations of Evn as indicated on the figure. All concentrations are final after mixing. Lines through the traces are fit to a kinetic model (Liu et al., 2010) in which back-translocation proceeds via a three-step process in the absence of Evn (the first two of which are catalyzed by EF4) and via a two-step process at saturating Evn.

(C) A plot of the reciprocal of the apparent magnitude of the fluorescence change for the second, EF4-catalyzed step versus Evn concentration, giving an apparent K_i for Evn binding to the POST complex of 0.6 ± 0.1 μM.

affecting GTP hydrolysis and Pi release (Huang et al., 2010). We observed that the rdGTPase of LepA and BipA with 70SΔL7/L12 was significantly reduced but was also inhibited by both MiC and ThS (Figures 2H and 2I). Further work will be needed to distinguish between factor binding versus GTPase activity defects.

Despite the contrasting effects of MiC and ThS on the GTPase activities of EF-G (Figure 2A) (Cameron et al., 2002; Cundliffe and Thompson, 1981; Lentzen et al., 2003), our kinetic analysis demonstrates that MiC, like ThS, is a potent inhibitor of the translocation reaction (Figure 3B). The finding that MiC targets translocation is in agreement with original conclusions of Pestka and Brot (1971), which were based upon its inhibition of poly(U)-dependent poly(Phe) synthesis but its lack of affect on either aa-tRNA binding or peptide-bond formation. Given the similarity in binding site between MiC and ThS, it thus appears likely that both MiC and ThS inhibit translocation analogously—namely, by preventing the transition of EF-G from an initially weaker binding state to a fully accommodated state on the ribosome, which, we would suggest, is necessary for translocation (Seo et al., 2006). We note that despite their diverse effects on the rdGTPase of EF-G, the inhibitory potency of MiC and ThS with respect to in vitro transcription-translation systems is comparable (both have an IC_{50} of ~3 μM) (Figure S3).

Influence of the Orthosomycin Evn on Translation Factor Activities

Unlike thiopeptides, we find that the orthosomycin Evn has no inhibitory effect on rdGTPase activity of EF-G (Figure 5B) or on the EF-G-mediated translocation reaction (Figure 3C). This is consistent with the lack of overlap between the putative Evn-binding site and the binding position of EF-G determined by structural studies (Connell et al., 2007; Gao et al., 2009; Ratje et al., 2010) (Figure 7A). Similarly, Evn does not inhibit the rdGTPase of Tet(M) (Figure 5D) or of Tet(O) (data not shown), which interacts with the ribosome in an analogous manner to EF-G (Spahn et al., 2001). In contrast we find that Evn is a potent inhibitor of the rdGTPase activity of IF2 (Figure 5A), BipA, and EF4 (Figures 5E and 5F). Although little is known about the structure or function of BipA on the ribosome (deLivron et al., 2009), structures of EF4 alone (Evans et al., 2008) and bound to the ribosome (Connell et al., 2008) reveal an overall similarity with EF-G. One exception is the unique CTD of EF4 (Evans et al., 2008), which on the ribosome is oriented back toward the large subunit (Connell et al., 2008) and encroaches upon the Evn-binding site (Figure 7B). Such overlap is consistent with our finding that Evn is a potent inhibitor EF4-mediated back-translocation reaction (Figure 6B). Our results demonstrating potent

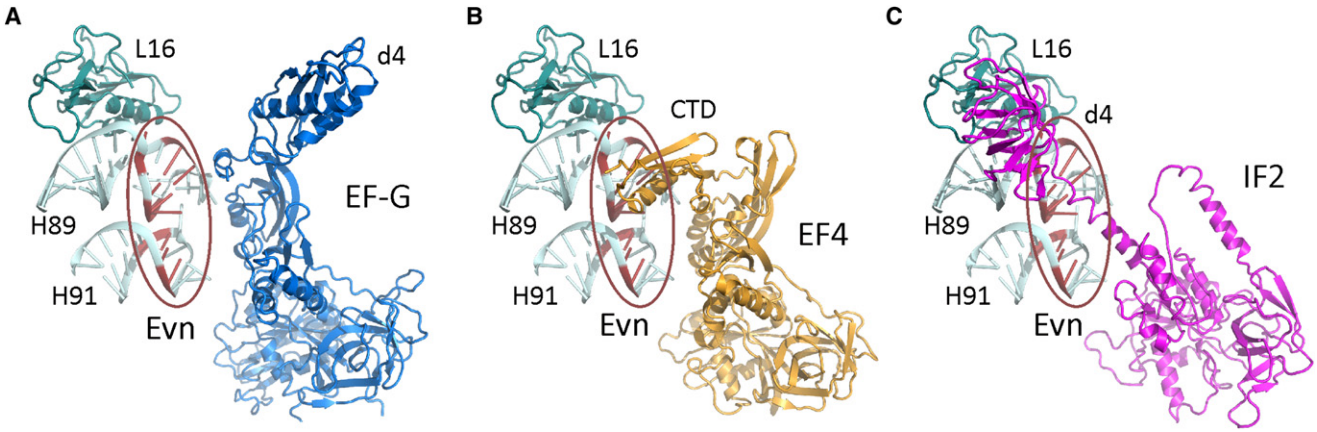

Figure 7. Putative Binding Sites of Orthosomycin Antibiotics Relative to Translation Factors EF-G, EF4, and IF2

(A–C) Relative position of (A) EF-G (blue) (Connell et al., 2007; Gao et al., 2009), (B) EF4 (orange) (Connell et al., 2008), and (C) IF2 (purple) (Allen et al., 2005; Marzi et al., 2003) to the putative Evn-binding site (encircled in red) (Belova et al., 2001; Wilson, 2009). Nucleotides associated with Evn binding in H89 and H91 are colored red, and L16 (teal) is shown for reference. Note the overlap in positions of the CTD of EF4 and domain 4 (d4) of IF2 with the putative Evn-binding site.

Evn inhibitory effects on noninitiation translation factors, such as BipA and EF4, suggest that Evn can no longer be considered exclusively as an initiation inhibitor, as it has been heretofore. Indeed, Evn is a slightly stronger inhibitor of the rdGTPase activity of EF4 compared with IF2, and the K_i (0.6 μM) for Evn binding to the POST complex (Figure 6C) is a little lower than the K_i (1.8 μM) for Evn inhibition of IF2-dependent 70SIC formation.

Nevertheless, because the gene for EF4 is not essential for survival in *E. coli* (Dibb and Wolfe, 1986), the principal antimicrobial target of Evn is most likely IF2. Here, we demonstrate that Evn can inhibit the rdGTPase activity of IF2 (Figure 5A) as well as prevent the IF2-dependent association of the 30SIC with the large ribosomal subunit (Figure 4B). These findings support an earlier suggestion that Evn inhibits 70SIC formation, which was based on the ability of Evn to prevent the formation of fMet-puromycin in an IF2-dependent manner (Belova et al., 2001). Models for IF2 bound to the ribosome derived from biochemical (Marzi et al., 2003) and cryo-EM data (Allen et al., 2005; Myasnikov et al., 2005) suggest that domain 4 of IF2 and the associated linker region encroach on the Evn-binding site (Figure 7C). Thus, we believe that Evn sterically interferes with IF2 binding to the large ribosomal subunit, accounting for the Evn-dependent reduction in rdGTPase activity of IF2 with 70S ribosomes (Figure 5A) as well as the reduction in 70SIC as observed using light scattering (Figure 4B). The similarity between the K_i (1.8 μM) of Evn inhibition for 70SIC formation and the half-inhibitory concentration (IC_{50} = ~2 μM) of Evn for synthesis of GFP as measured in an *E. coli* in vitro-coupled transcription-translation system (Figure S3) also supports the claim that Evn targets predominantly the initiation phase of protein synthesis (Belova et al., 2001).

SIGNIFICANCE

Insight into the mechanism of action of diverse classes of antibiotics, such as the thiopeptides and orthosomycins, to inhibit distinct steps during translation can provide insight into the fundamental process of translation. Here, we demonstrate that although the thiopeptides MiC and ThS have contrasting effects on the rdGTPase activity of EF-G, both antibiotics are potent inhibitors of EF-G-dependent translocation reaction. Our results demonstrate that the MiC-dependent stimulation of the rdGTPase of EF-G requires the presence of the G′ subdomain of EF-G as well as ribosomal proteins L7/L12. This finding supports the idea that recycling of EF-G from the ribosome, which occurs upon release of Pi, is mediated via the interaction of L7-CTD with the G′ subdomain of EF-G. In contrast we can demonstrate that Evn does not influence EF-G rdGTPase, or EF-G dependent translocation, but is a potent inhibitor of EF4-dependent back-translocation reaction as well as IF2-dependent 70S-initiation complex formation. These findings are in agreement with the predicted binding site of the orthosomycins relative to the binding sites of EF-G, EF4, and IF2 on the ribosome. Understanding mechanistically how antibiotics perturb the translational apparatus is an important step for the future development of new improved antimicrobial agents to overcome the emerging resistant bacterial pathogens.

EXPERIMENTAL PROCEDURES

Component Preparation

ThS was purchased from Sigma, MiC P1 was a kind gift of Dr. Torsten Stachelhaus, and gDNA from *S. faecalis* was kindly provided by Dr. Vincent Perreten. *E. coli fusA* and *bipA*, *S. faecalis tetM* as well as *T. thermophilus* (HB8) *fusA* full-length genes were cloned into pET-46 Ek/LIC vector, and *E. coli infB* gene was cloned into pET-14b, in accordance with the manufacturer's instructions (Novagen). EF-GΔG′ mutants were prepared using QuikChange Site-Directed Mutagenesis Kit (Stratagene). *E. coli* EF4 was expressed in pET14b as described previously (Qin et al., 2006). Recombinant proteins were expressed in *BL21* (DE3) cells, at 20°C with 0.2 mM IPTG, then purified with a Ni^{2+}-NTA affinity column (QIAGEN), followed by gel-filtration chromatography on a HiLoad 16/60 Superdex 75 prep grade column (Amersham-Pharmacia) in a buffer containing 10 mM Tris (pH 7.8), 100 mM NaCl, and 10 mM 2-mercaptoethanol. *E. coli* 70S ribosomes lacking L7/L12 were prepared as described by Hamel et al. (1972) and Wystup et al. (1979). Tight-coupled *E. coli*

ribosomes, cloned *E. coli* His-tagged proteins EF-G, EF-Tu, IF1, IF2, and IF3, and *E. coli* [^{35}S]fMet-tRNA^{fMet}; *E. coli* [^{3}H]Phe-tRNA^{Phe} were prepared as described (Liu et al., 2010). MFK-mRNA was purchased from Dharmacon (Lafayette, CO, USA) with sequences 5′-GGG AAG GAG GUA AAA AUG UUU AAA CGU AAA UCU ACU-3′ (initiator codon underlined).

IF2-Dependent 70SIC Formation Light-Scattering Assay

This assay was performed as described (Grigoriadou et al., 2007). 30SIC was formed by mixing 0.3 μM 30S, 0.45 μM IF1, 0.45 μM IF3, 0.45 μM fMet-tRNA$_f^{Met}$, 0.15 μM IF2, 0.9 μM AUG022-mRNA (Grigoriadou et al., 2007), and 100 μM GTP, premixed with various concentrations of Evn (0–5 μM) and then rapidly mixed with 50S subunits (0.3 μM) in a KinTek stopped-flow spectrophotometer. Excitation was at 436 nm, and light scattering was determined using a 455 nm cutoff filter. All concentrations are final after mixing.

Back-Translocation Assay

All of the following complexes were made up in buffer A (20 mM HEPES-KOH [pH 7.5], at 0°C, 150 mM NH_4Ac, 4.5 mM $MgAc_2$, 4 mM β-mercaptoethanol, 0.05 mM spermine, and 2 mM spermidine) at 37°C. Initiation complex was formed by incubating WT ribosomes (2 μM) with mRNA MFK (8 μM), IF1 (3 μM), IF2 (3 μM), IF3 (3 μM), GTP (1 mM), and [^{35}S]fMet-tRNA^{fMet} (3 μM) for 25 min. Ternary complex was formed by incubating EF-Tu (6 μM) with labeled Phe-tRNA^{Phe} (3 μM), GTP (1 mM), phosphoenolpyruvate (Roche Diagnostics) (1.5 mM), and pyruvate kinase (Roche Diagnostics) (0.015 mg/ml) for 15 min. POST complexes were formed by incubating ternary complex and initiation complex at 37°C briefly for 45 s and then in the presence of EF-G (molar ratio of EF-G:ribosome was 0.2:1) and GTP (1 mM) at 37°C for 10 min. Then they were purified by ultracentrifugation through a 1.1 M Sucrose cushion in buffer A (450,000 × g, 40 min, 4°C). POST complex concentration was calculated from the amount of ribosome-bound fMet-[^{3}H]Phe-tRNA^{Phe}. Stopped-flow fluorescence experiments were performed using an SX.18MV Stopped-Flow Spectrofluorometer (Applied Photophysics). POST complex (0.1 μM) containing fMetPhe-tRNA^{Phe}(Prf) in the P site and tRNA^{fMet} in the E site was rapidly mixed with 0.15 μM tRNA^{fMet}, 3 μM EF4•GDPNP, and various concentrations of Evn (0–5 μM). prf was excited at 460 nm, and fluorescence was monitored using a 495 nm long-pass filter. Lines through the data are fit to triple-exponential equations using the program IGOR Pro (WaveMetrics).

Translocation Assay

PRE complexes were formed by incubating initiation complex and ternary complex at 37°C for 45 s. Then they were purified by ultracentrifugation through a 1.1 M Sucrose cushion in buffer A with 20 mM Mg^{2+} (450,000 × g, 40 min, 4°C). PRE complex concentration was calculated from the amount of ribosome-bound fMet-[^{3}H]Phe-tRNA^{Phe}. Stopped-flow fluorescence experiments were performed using an SX.18MV Stopped-Flow spectrofluorometer. prf was excited at 460 nm, and fluorescence was monitored using a 495 nm long-pass filter. Data are fit to double-exponential equations using the program IGOR Pro (WaveMetrics).

Malachite Green GTPase Activity Assays

GTPase activity was measured using the Malachite Green Phosphate Kit (BioAssay) that quantifies the green complex formed between malachite green, molybdate, and free orthophosphate. Unless otherwise mentioned, all reactions contained 30 nM *E. coli* 70S ribosomes, 20 μM GTP, and 60 nM protein in the presence or absence of antibiotics as necessary. Reactions were transferred into 96-well microtiter plates, and color formation was measured on Tecan Infinite M1000 microplate reader at 650 nm. Reactions performed in the absence of ribosomes were used as a background signal to account for the intrinsic GTPase activity of the translation factor.

In Vitro Transcription-Translation Assay

All coupled transcription-translation experiments were performed using an *E. coli* lysate-based system in the presence and absence of antibiotics as described previously (Starosta et al., 2009, 2010). Reactions were transferred into 96-well microtiter plates, and the GFP fluorescence was measured with a Typhoon Scanner 9400 (Amersham Bioscience) using a Typhoon blue laser module (Amersham Bioscience). Images were then quantified using ImageQuant TL (GE Healthcare) and represented graphically using SigmaPlot (Systat Software, Inc.).

Figure Preparation

Chemical structures for the precursor compounds were drawn using ChemDraw (Advanced Chemistry Development, Inc., Toronto, Canada), and all structural figures were prepared with PyMOL (http://www.pymol.org).

SUPPLEMENTAL INFORMATION

Supplemental Information includes three figures and can be found with this article online at doi:10.1016/j.chembiol.2011.03.010.

ACKNOWLEDGMENTS

We would like to thank Torsten Stachelhaus for preparation of the Micrococcin P1 and Dr. Vincent Perreten for providing *S. faecalis* gDNA. This work was financed by the EMBO young investigator program (to D.N.W.), Deutsche Forschungsgemeinschaft (WI3285/1-1 to D.N.W.), and by the National Institutes of Health (GM071014 to B.S.C.).

Received: February 6, 2011
Revised: March 7, 2011
Accepted: March 14, 2011
Published: May 26, 2011

REFERENCES

Aarestrup, F.M., and Jensen, L.B. (2000). Presence of variations in ribosomal protein L16 corresponding to susceptibility of *enterococci* to oligosaccharides (Avilamycin and evernimicin). Antimicrob. Agents Chemother. *44*, 3425–3427.

Adrian, P.V., Mendrick, C., Loebenberg, D., McNicholas, P., Shaw, K.J., Klugman, K.P., Hare, R.S., and Black, T.A. (2000a). Evernimicin (SCH27899) inhibits a novel ribosome target site: analysis of 23S ribosomal DNA mutants. Antimicrob. Agents Chemother. *44*, 3101–3106.

Adrian, P.V., Zhao, W., Black, T.A., Shaw, K.J., Hare, R.S., and Klugman, K.P. (2000b). Mutations in ribosomal protein L16 conferring reduced susceptibility to evernimicin (SCH27899): implications for mechanism of action. Antimicrob. Agents Chemother. *44*, 732–738.

Allen, G.S., Zavialov, A., Gursky, R., Ehrenberg, M., and Frank, J. (2005). The cryo-EM structure of a translation initiation complex from *Escherichia coli*. Cell *121*, 703–712.

Antoun, A., Pavlov, M.Y., Lovmar, M., and Ehrenberg, M. (2006). How initiation factors tune the rate of initiation of protein synthesis in bacteria. EMBO J. *25*, 2539–2550.

Bagley, M.C., Dale, J.W., Merritt, E.A., and Xiong, X. (2005). Thiopeptide antibiotics. Chem. Rev. *105*, 685–714.

Belova, L., Tenson, T., Xiong, L.Q., McNicholas, P.M., and Mankin, A.S. (2001). A novel site of antibiotic action in the ribosome: interaction of evernimicin with the large ribosomal subunit. Proc. Natl. Acad. Sci. USA *98*, 3726–3731.

Blanchard, S.C., Kim, H.D., Gonzalez, R.L., Jr., Puglisi, J.D., and Chu, S. (2004). tRNA dynamics on the ribosome during translation. Proc. Natl. Acad. Sci. USA *101*, 12893–12898.

Blanchard, S.C., Cooperman, B.S., and Wilson, D.N. (2010). Probing translation with small-molecule inhibitors. Chem. Biol. *17*, 633–645.

Brandi, L., Marzi, S., Fabbretti, A., Fleischer, C., Hill, W., Lodmell, J., and Gualerzi, C. (2004). The translation initiation functions of IF2: targets for thiostrepton inhibition. J. Mol. Biol. *335*, 881–894.

Cameron, D.M., Thompson, J., March, P.E., and Dahlberg, A.E. (2002). Initiation factor IF2, thiostrepton and micrococcin prevent the binding of elongation factor G to the *Escherichia coli* ribosome. J. Mol. Biol. *319*, 27–35.

Connell, S.R., Tracz, D.M., Nierhaus, K.H., and Taylor, D.E. (2003a). Ribosomal protection proteins and their mechanism of tetracycline resistance. Antimicrob. Agents Chemother. *47*, 3675–3681.

 ©2011 Elsevier Ltd All rights reserved

Connell, S.R., Trieber, C.A., Dinos, G.P., Einfeldt, E., Taylor, D.E., and Nierhaus, K.H. (2003b). Mechanism of Tet(O)-mediated tetracycline resistance. EMBO J. *22*, 945–953.

Connell, S.R., Takemoto, C., Wilson, D.N., Wang, H., Murayama, K., Terada, T., Shirouzu, M., Rost, M., Schuler, M., Giesebrecht, J., et al. (2007). Structural basis for interaction of the ribosome with the switch regions of GTP-bound elongation factors. Mol. Cell *25*, 751–764.

Connell, S.R., Topf, M., Qin, Y., Wilson, D.N., Mielke, T., Fucini, P., Nierhaus, K.H., and Spahn, C.M. (2008). A new tRNA intermediate revealed on the ribosome during EF4-mediated back-translocation. Nat. Struct. Mol. Biol. *15*, 910–915.

Cundliffe, E., and Thompson, J. (1981). Concerning the mode of action of micrococcin upon bacterial protein synthesis. Eur. J. Biochem. *118*, 47–52.

Dantley, K.A., Dannelly, H.K., and Burdett, V. (1998). Binding interaction between Tet(M) and the ribosome: requirements for binding. J. Bacteriol. *180*, 4089–4092.

Datta, P.P., Sharma, M.R., Qi, L., Frank, J., and Agrawal, R.K. (2005). Interaction of the G′ domain of elongation factor G and the C-terminal domain of ribosomal protein L7/L12 during translocation as revealed by cryo-EM. Mol. Cell *20*, 723–731.

deLivron, M.A., and Robinson, V.L. (2008). Salmonella enterica serovar Typhimurium BipA exhibits two distinct ribosome binding modes. J. Bacteriol. *190*, 5944–5952.

deLivron, M.A., Makanji, H.S., Lane, M.C., and Robinson, V.L. (2009). A novel domain in translational GTPase BipA mediates interaction with the 70S ribosome and influences GTP hydrolysis. Biochemistry *48*, 10533–10541.

Diaconu, M., Kothe, U., Schlunzen, F., Fischer, N., Harms, J.M., Tonevitsky, A.G., Stark, H., Rodnina, M.V., and Wahl, M.C. (2005). Structural basis for the function of the ribosomal L7/12 stalk in factor binding and GTPase activation. Cell *121*, 991–1004.

Dibb, N.J., and Wolfe, P.B. (1986). lep operon proximal gene is not required for growth or secretion by *Escherichia coli*. J. Bacteriol. *166*, 83–87.

Evans, R.N., Blaha, G., Bailey, S., and Steitz, T.A. (2008). The structure of LepA, the ribosomal back translocase. Proc. Natl. Acad. Sci. USA *105*, 4673–4678.

Gao, Y.G., Selmer, M., Dunham, C.M., Weixlbaumer, A., Kelley, A.C., and Ramakrishnan, V. (2009). The structure of the ribosome with elongation factor G trapped in the posttranslocational state. Science *326*, 694–699.

Gonzalez, R.L., Jr., Chu, S., and Puglisi, J.D. (2007). Thiostrepton inhibition of tRNA delivery to the ribosome. RNA *13*, 2091–2097.

Grigoriadou, C., Marzi, S., Kirillov, S., Gualerzi, C.O., and Cooperman, B.S. (2007). A quantitative kinetic scheme for 70 S translation initiation complex formation. J. Mol. Biol. *373*, 562–572.

Grunberg-Manago, M., Dondon, J., and Graffe, M. (1972). Inhibition by thiostrepton of the IF-2-dependent ribosomal GTPase. FEBS Lett. *22*, 217–221.

Hamel, E., Koka, M., and Nakamoto, T. (1972). Requirement of an *E. coli* 50S ribosomal protein component for effective interaction of the ribosome with T and G factors and with guanosine triphosphate. J. Biol. Chem. *247*, 805–814.

Harms, J.M., Wilson, D.N., Schluenzen, F., Connell, S.R., Stachelhaus, T., Zaborowska, Z., Spahn, C.M., and Fucini, P. (2008). Translational regulation via L11: molecular switches on the ribosome turned on and off by thiostrepton and micrococcin. Mol. Cell *30*, 26–38.

Helgstrand, M., Mandava, C.S., Mulder, F.A., Liljas, A., Sanyal, S., and Akke, M. (2007). The ribosomal stalk binds to translation factors IF2, EF-Tu, EF-G and RF3 via a conserved region of the L12 C-terminal domain. J. Mol. Biol. *365*, 468–479.

Huang, C., Mandava, C.S., and Sanyal, S. (2010). The ribosomal stalk plays a key role in IF2-mediated association of the ribosomal subunits. J. Mol. Biol. *399*, 145–153.

Hughes, R.A., and Moody, C.J. (2007). From amino acids to heteroaromatics—thiopeptide antibiotics, nature's heterocyclic peptides. Angew. Chem. Int. Ed. Engl. *46*, 7930–7954.

Kischa, K., Möller, W., and Stöffler, G. (1971). Reconstitution of a GTPase activity by a 50S ribosomal protein from *E. coli*. Nat. New Biol. *233*, 62–63.

Knutsson Jenvert, R.M., and Holmberg Schiavone, L. (2005). Characterization of the tRNA and ribosome-dependent pppGpp-synthesis by recombinant stringent factor from *Escherichia coli*. FEBS J. *272*, 685–695.

Kofoed, C.B., and Vester, B. (2002). Interaction of avilamycin with ribosomes and resistance caused by mutations in 23S rRNA. Antimicrob. Agents Chemother. *46*, 3339–3342.

Kothe, U., Wieden, H.J., Mohr, D., and Rodnina, M.V. (2004). Interaction of helix D of elongation factor Tu with helices 4 and 5 of protein L7/12 on the ribosome. J. Mol. Biol. *336*, 1011–1021.

Laurberg, M., Kristensen, O., Martemyanov, K., Gudkov, A.T., Nagaev, I., Hughes, D., and Liljas, A. (2000). Structure of a mutant EF-G reveals domain III and possibly the fusidic acid binding site. J. Mol. Biol. *303*, 593–603.

Laursen, B.S., Sorensen, H.P., Mortensen, K.K., and Sperling-Petersen, H.U. (2005). Initiation of protein synthesis in bacteria. Microbiol. Mol. Biol. Rev. *69*, 101–123.

Lefranc, D., and Ciufolini, M.A. (2009). Total synthesis and stereochemical assignment of micrococcin P1. Angew. Chem. Int. Ed. Engl. *48*, 4198–4201.

Lentzen, G., Klinck, R., Matassova, N., Aboul-ela, F., and Murchie, A. (2003). Structural basis for contrasting activities of ribosome binding thiazole antibiotics. Chem. Biol. *10*, 769–778.

Liu, H., Pan, D., Pech, M., and Cooperman, B.S. (2010). Interrupted catalysis: the EF4 (LepA) effect on back-translocation. J. Mol. Biol. *396*, 1043–1052.

Mann, P.A., Xiong, L., Mankin, A.S., Chau, A.S., Mendrick, C.A., Najarian, D.J., Cramer, C.A., Loebenberg, D., Coates, E., Murgolo, N.J., et al. (2001). EmtA, a rRNA methyltransferase conferring high-level evernimicin resistance. Mol. Microbiol. *41*, 1349–1356.

Marzi, S., Knight, W., Brandi, L., Caserta, E., Soboleva, N., Hill, W.E., Gualerzi, C.O., and Lodmell, J.S. (2003). Ribosomal localization of translation initiation factor IF2. RNA *9*, 958–969.

McConkey, G.A., Rogers, M.J., and McCutchan, T.F. (1997). Inhibition of Plasmodium falciparum protein synthesis. Targeting the plastid-like organelle with thiostrepton. J. Biol. Chem. *272*, 2046–2049.

McNicholas, P.M., Najarian, D.J., Mann, P.A., Hesk, D., Hare, R.S., Shaw, K.J., and Black, T.A. (2000). Evernimicin binds exclusively to the 50S ribosomal subunit and inhibits translation in cell-free systems derived from both Gram-positive and Gram-negative bacteria. Antimicrob. Agents Chemother. *44*, 1121–1126.

McNicholas, P.M., Mann, P.A., Najarian, D.J., Miesel, L., Hare, R.S., and Black, T.A. (2001). Effects of mutations in ribosomal protein L16 on susceptibility and accumulation of evernimicin. Antimicrob. Agents Chemother. *45*, 79–83.

Moazed, D., and Noller, H.F. (1989). Intermediate states in the movement of transfer RNA in the ribosome. Nature *342*, 142–148.

Modolell, J., Cabrer, B., Parmeggiani, A., and Vazquez, D. (1971). Inhibition by siomycin and thiostrepton of both aminoacyl-tRNA and factor G binding to ribosomes. Proc. Natl. Acad. Sci. USA *68*, 1796–1800.

Mohr, D., Wintermeyer, W., and Rodnina, M.V. (2002). GTPase activation of elongation factors Tu and G on the ribosome. Biochemistry *41*, 12520–12528.

Munro, J.B., Wasserman, M.R., Altman, R.B., Wang, L., and Blanchard, S.C. (2010). Correlated conformational events in EF-G and the ribosome regulate translocation. Nat. Struct. Mol. Biol. *17*, 1470–1477.

Myasnikov, A.G., Marzi, S., Simonetti, A., Giuliodori, A.M., Gualerzi, C.O., Yusupova, G., Yusupov, M., and Klaholz, B.P. (2005). Conformational transition of initiation factor 2 from the GTP- to GDP-bound state visualized on the ribosome. Nat. Struct. Mol. Biol. *12*, 1145–1149.

Nechifor, R., Murataliev, M., and Wilson, K.S. (2007). Functional interactions between the G′ subdomain of bacterial translation factor EF-G and ribosomal protein L7/L12. J. Biol. Chem. *282*, 36998–37005.

Nicolaou, K.C., Safina, B.S., Zak, M., Lee, S.H., Nevalainen, M., Bella, M., Estrada, A.A., Funke, C., Zécri, F.J., and Bulat, S. (2005a). Total synthesis of thiostrepton. Retrosynthetic analysis and construction of key building blocks. J. Am. Chem. Soc. *127*, 1159–1175.

Nicolaou, K.C., Zak, M., Safina, B.S., Estrada, A.A., Lee, S.H., and Nevalainen, M. (2005b). Total synthesis of thiostrepton. Assembly of key building blocks and completion of the synthesis. J. Am. Chem. Soc. *127*, 11176–11183.

Nicolaou, K.C., Chen, J.S., Edmonds, D.J., and Estrada, A.A. (2009). Recent advances in the chemistry and biology of naturally occurring antibiotics. Angew. Chem. Int. Ed. Engl. *48*, 660–719.

Otaka, T., and Kaji, A. (1974). Micrococcin: acceptor-site-specific inhibitor of protein synthesis. Eur. J. Biochem. *50*, 101–106.

Owens, R.M., Pritchard, G., Skipp, P., Hodey, M., Connell, S.R., Nierhaus, K.H., and O'Connor, C.D. (2004). A dedicated translation factor controls the synthesis of the global regulator Fis. EMBO J. *23*, 3375–3385.

Pan, D., Kirillov, S.V., and Cooperman, B.S. (2007). Kinetically competent intermediates in the translocation step of protein synthesis. Mol. Cell *25*, 519–529.

Pestka, S. (1970). Thiostrepton: a ribosomal inhibitor of translocation. Biochem. Biophys. Res. Commun. *40*, 667–674.

Pestka, S., and Brot, N. (1971). Studies on the formation of transfer ribonucleic acid-ribosome complexes. IV. Effect of antibiotics on steps of bacterial protein synthesis: some new ribosomal inhibitors of translocation. J. Biol. Chem. *246*, 7715–7722.

Qin, Y., Polacek, N., Vesper, O., Staub, E., Einfeldt, E., Wilson, D.N., and Nierhaus, K.H. (2006). The highly conserved LepA is a ribosomal elongation factor that back-translocates the ribosome. Cell *127*, 721–733.

Ratje, A., Loerke, J., Mikolajka, A., Brünner, M., Hildebrand, P.W., Starosta, A.L., Dönhöfer, A., Connell, S.R., Fucini, P., Mielke, T., et al. (2010). Head swivel on the ribosome facilitates translocation by means of intra-subunit tRNA hybrid sites. Nature *468*, 713–716.

Rodnina, M.V., Savelsbergh, A., Katunin, V.I., and Wintermeyer, W. (1997). Hydrolysis of GTP by elongation factor G drives tRNA movement on the ribosome. Nature *385*, 37–41.

Rodnina, M.V., Savelsbergh, A., Matassova, N.B., Katunin, V.I., Semenkov, Y.P., and Wintermeyer, W. (1999). Thiostrepton inhibits the turnover but not the GTPase of elongation factor G on the ribosome. Proc. Natl. Acad. Sci. USA *96*, 9586–9590.

Savelsbergh, A., Mohr, D., Wilden, B., Wintermeyer, W., and Rodnina, M.V. (2000). Stimulation of the GTPase activity of translation elongation factor G by ribosomal protein L7/12. J. Biol. Chem. *275*, 890–894.

Savelsbergh, A., Katunin, V.I., Mohr, D., Peske, F., Rodnina, M.V., and Wintermeyer, W. (2003). An elongation factor G-induced ribosome rearrangement precedes tRNA-mRNA translocation. Mol. Cell *11*, 1517–1523.

Savelsbergh, A., Mohr, D., Kothe, U., Wintermeyer, W., and Rodnina, M.V. (2005). Control of phosphate release from elongation factor G by ribosomal protein L7/12. EMBO J. *24*, 4316–4323.

Schmeing, T.M., and Ramakrishnan, V. (2009). What recent ribosome structures have revealed about the mechanism of translation. Nature *461*, 1234–1242.

Seo, H.S., Abedin, S., Kamp, D., Wilson, D.N., Nierhaus, K.H., and Cooperman, B.S. (2006). EF-G-dependent GTPase on the ribosome. Conformational change and fusidic acid inhibition. Biochemistry *45*, 2504–2514.

Simonetti, A., Marzi, S., Jenner, L., Myasnikov, A., Romby, P., Yusupova, G., Klaholz, B.P., and Yusupov, M. (2009). A structural view of translation initiation in bacteria. Cell. Mol. Life Sci. *66*, 423–436.

Sohmen, D., Harms, J.M., Schlünzen, F., and Wilson, D.N. (2009a). Enhanced SnapShot: antibiotic inhibition of protein synthesis II. Cell *139*, 212–212.e1.

Sohmen, D., Harms, J.M., Schlünzen, F., and Wilson, D.N. (2009b). SnapShot: antibiotic inhibition of protein synthesis I. Cell *138*, 1248.e1.

Spahn, C.M., Blaha, G., Agrawal, R.K., Penczek, P., Grassucci, R.A., Trieber, C.A., Connell, S.R., Taylor, D.E., Nierhaus, K.H., and Frank, J. (2001). Localization of the ribosomal protection protein Tet(O) on the ribosome and the mechanism of tetracycline resistance. Mol. Cell *7*, 1037–1045.

Starosta, A.L., Qin, H., Mikolajka, A., Leung, G.Y., Schwinghammer, K., Nicolaou, K.C., Chen, D.Y., Cooperman, B.S., and Wilson, D.N. (2009). Identification of distinct thiopeptide-antibiotic precursor lead compounds using translation machinery assays. Chem. Biol. *16*, 1087–1096.

Starosta, A.L., Karpenko, V.V., Shishkina, A.V., Mikolajka, A., Sumbatyan, N.V., Schluenzen, F., Korshunova, G.A., Bogdanov, A.A., and Wilson, D.N. (2010). Interplay between the ribosomal tunnel, nascent chain, and macrolides influences drug inhibition. Chem. Biol. *17*, 1–10.

Weisblum, B., and Demohn, V. (1970). Inhibition by thiostrepton of the formation of a ribosome-bound guanine nucleotide complex. FEBS Lett. *11*, 149–152.

Wilson, D.N. (2009). The A-Z of bacterial translation inhibitors. Crit. Rev. Biochem. Mol. Biol. *44*, 393–433.

Wolf, H. (1973). Avilamycin, an inhibitor of the 30S ribosomal subunits function. FEBS Lett. *36*, 181–186.

Wystup, G., Teraoka, H., Schulze, H., Hampl, H., and Nierhaus, K.H. (1979). 50S subunit from *Escherichia coli* ribosomes. Isolation of active ribosomal proteins and protein complexes. Eur. J. Biochem. *100*, 101–113.

Zarazaga, M., Tenorio, C., Del Campo, R., Ruiz-Larrea, F., and Torres, C. (2002). Mutations in ribosomal protein L16 and in 23S rRNA in *Enterococcus* strains for which evernimicin MICs differ. Antimicrob. Agents Chemother. *46*, 3657–3659.

 ©2011 Elsevier Ltd All rights reserved

Paper 7

[redacted]

LETTER

doi:10.1038/nature09547

Head swivel on the ribosome facilitates translocation by means of intra-subunit tRNA hybrid sites

Andreas H. Ratje[1,2], Justus Loerke[1], Aleksandra Mikolajka[3,4], Matthias Brünner[1], Peter W. Hildebrand[1], Agata L. Starosta[3], Alexandra Dönhöfer[3], Sean R. Connell[5], Paola Fucini[5], Thorsten Mielke[1,6], Paul C. Whitford[7], José N. Onuchic[8], Yanan Yu[9], Karissa Y. Sanbonmatsu[7], Roland K. Hartmann[2], Pawel A. Penczek[10], Daniel N. Wilson[3,4] & Christian M. T. Spahn[1]

The elongation cycle of protein synthesis involves the delivery of aminoacyl-transfer RNAs to the aminoacyl-tRNA-binding site (A site) of the ribosome, followed by peptide-bond formation and translocation of the tRNAs through the ribosome to reopen the A site[1,2]. The translocation reaction is catalysed by elongation factor G (EF-G) in a GTP-dependent manner[3]. Despite the availability of structures of various EF-G–ribosome complexes, the precise mechanism by which tRNAs move through the ribosome still remains unclear. Here we use multiparticle cryoelectron microscopy analysis to resolve two previously unseen subpopulations within *Thermus thermophilus* EF-G–ribosome complexes at subnanometre resolution, one of them with a partly translocated tRNA. Comparison of these substates reveals that translocation of tRNA on the 30S subunit parallels the swivelling of the 30S head and is coupled to unratcheting of the 30S body. Because the tRNA maintains contact with the peptidyl-tRNA-binding site (P site) on the 30S head and simultaneously establishes interaction with the exit site (E site) on the 30S platform, a novel intra-subunit 'pe/E' hybrid state is formed. This state is stabilized by domain IV of EF-G, which interacts with the swivelled 30S-head conformation. These findings provide direct structural and mechanistic insight into the 'missing link' in terms of tRNA intermediates involved in the universally conserved translocation process.

After peptide-bond formation, pre-translocational (PRE) ribosomes carry a peptidyl-tRNA at the A site and a deacylated tRNA at the P site[1,3,4]. This is a highly dynamic state of the ribosome, which fluctuates between classical states with A tRNA and P tRNA and hybrid states with A/P tRNAs (A/P denotes that the tRNA is in the A site on the 30S subunit and the P site on the 50S subunit) and P/E tRNAs[5–8]. Hybrid state formation is coupled to spontaneous rotation of the 30S subunit relative to the 50S subunit[9–11] and is stabilized by the binding of EF-G[12–14]. The ratchet-like subunit rearrangement induced by EF-G and eukaryotic elongation factor 2 (eEF2) also includes a swivel movement of the head that is roughly orthogonal to the inter-subunit rotation of the ribosomal subunits[14–16]. EF-G catalyses translocation of the hybrid-state tRNAs on the 30S subunit to form a post-translocational (POST) state ribosome with tRNAs located at classical P and E sites. The translocation process is accelerated by the GTPase activity of EF-G stimulated by the ribosome[17,18]. However, it is still not known how tRNAs are translocated with respect to the 30S subunit and how the messenger RNA is advanced by one codon.

Structural snapshots of the translocation process come from cryoelectron microscopy and X-ray analysis of EF-G bound to ribosome complexes[12–14,19]. Despite considerable effort[12,20–22], no direct structural information is available for ribosomal PRE complexes simultaneously containing EF-G and an A tRNA. It seems that this state is too dynamic and transient to be captured, resulting in either a POST state containing EF-G or a PRE state without EF-G bound[20,22]. Indeed, the stable EF-G-bound POST state determined by X-ray crystallography reveals a non-ratcheted ribosome with tRNAs in classical P/P and E/E sites[19]. Therefore, structural insights into intermediate states of translocation—that is, ratcheted ribosomal EF-G complexes—have used complexes without an A-site peptidyl-tRNA[12–14].

In this study we used the antibiotic fusidic acid (FA) to stall EF-G on the 70S ribosome. FA permits the hydrolysis of GTP by EF-G but prevents the associated changes in EF-G that normally accompany hydrolysis[19]. After complex formation and the collection of cryoelectron microscopy data, we employed multiparticle refinement to resolve the heterogeneity of the data (Supplementary Fig. 1). In the first phase of multiparticle refinement a large population of particle images of ribosomes containing EF-G was obtained that yielded a structure in a ratcheted conformation. As refinement progressed to higher resolution, the presence of intrinsic conformational heterogeneity necessitated a second phase of multiparticle refinement, resulting in two final reconstructions of the 70S–EF-G–GDP–FA complex (Fig. 1), at resolutions of 7.6 Å and 7.8 Å (using a 0.5 Fourier shell correlation cut-off criterion), respectively (Supplementary Fig. 2). Both maps have density attributed to EF-G, but they show significant conformational differences (Supplementary Movies 1 and 2): specifically, the substates are distinguished by different degrees of subunit ratcheting and positioning of the L1 protuberance, and also by the swivel movement of the head of the 30S subunit relative to the body/platform (Fig. 1e, f, Supplementary Figs 3 and 4, and Supplementary Table 1). Unlike previous cryoelectron microscopy and X-ray structures of ribosome–EF-G complexes, movement of the head and body/platform of the 30S subunit is uncoupled: in substate I, the 30S subunit is ratcheted by about 7° relative to the 50S subunit, but there is only a modest (roughly 5°) swivelling of the 30S head. In contrast, the 30S in substate II is only ratcheted by about 4°, but there is a very large (roughly 18°) swivel of the head (Supplementary Table 1).

The identification of two different ratcheted substates within the 70S–EF-G–GDP–FA complex prompted us to investigate whether such intrinsic heterogeneity also exists in our previous 70S–EF-G–GMPPNP cryoelectron microscopy data set[14]. Additional multiparticle refinement did indeed reveal that the 70S–EF-G–GMPPNP complex could be subdivided into two substates that seemed to be equivalent to those identified in the 70S–EF-G–GDP–FA complex (Supplementary Fig. 5 and Supplementary Table 1). Our findings here provide evidence supporting the emerging energy-landscape model that allows the sampling of several metastable conformations for a defined ribosomal

[1]Institut für Medizinische Physik und Biophysik, Charite – Universitätsmedizin Berlin, Ziegelstrasse 5–9, 10117-Berlin, Germany. [2]Institut für Pharmazeutische Chemie, Philipps-Universität Marburg, 35037 Marburg, Germany. [3]Gene Center and Department of Biochemistry, Ludwig-Maximilians-Universität, Feodor-Lynenstrasse 25, 81377 München, Germany. [4]Center for Integrated Protein Science, Ludwig-Maximilians-Universität München, 81377 München, Germany. [5]Frankfurt Institute for Molecular Life Sciences, Institute of Organic Chemistry and Chemical Biology, Goethe University Frankfurt, Max-von Laue-Strasse 7, D-60438 Frankfurt am Main, Germany. [6]UltraStrukturNetzwerk, Max Planck Institute for Molecular Genetics, 14195 Berlin, Germany. [7]Theoretical Biology and Biophysics Group, Theoretical Division, Los Alamos National Laboratory, Los Alamos, New Mexico 87545, USA. [8]Center for Theoretical Biological Physics and Department of Physics, University of California, San Diego, La Jolla, California 92093, USA. [9]Florida State University, Department of Computer Science, Tallahassee, Florida 32306, USA. [10]The University of Texas – Houston Medical School, 6431 Fannin, Houston, Texas 77030, USA.

©2010 Macmillan Publishers Limited. All rights reserved

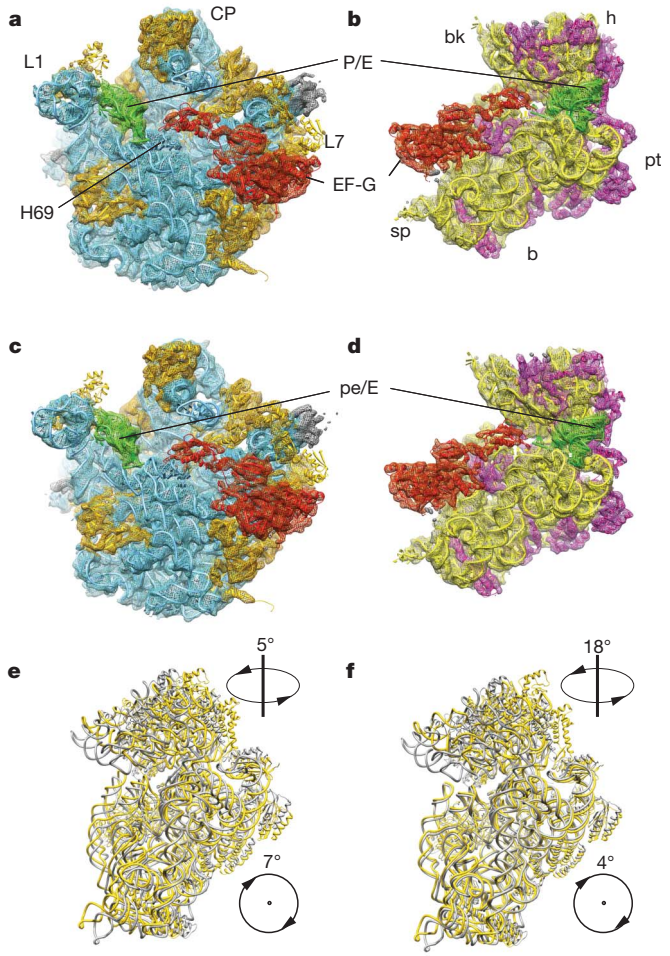

Figure 1 | Substates I (TI^{PRE}) and II (TI^{POST}) of the 70S–EF-G–GDP–FA complex. **a**–**d**, Cryoelectron microscopy maps of TI^{PRE} (**a**, **b**) and TI^{POST} (**c**, **d**) of the 70S–EF-G–GDP–FA complex are shown in mesh form with docked models in ribbon representation: EF-G (red), tRNA (green), 23S/5S rRNA (blue), 50S ribosomal proteins (orange), 16S rRNA (yellow) and the 30S ribosomal proteins (magenta). The maps are shown from the 30S side with the 30S subunit computationally removed (**a**, **c**) and from the 50S side with the 50S subunit computationally removed (**b**, **d**). CP, central protuberance; bk, beak; sp, spur; pt, platform; h, head; b, back; L1 and L7, ribosomal proteins L1 and L7, respectively; H69, helix 69 of 23S rRNA. **e**, **f**, The 30S subunit of TI^{PRE} (**e**) and TI^{POST} (**f**) (yellow) is compared with the 30S subunit of the POST state[19] (grey) by aligning the respective 50S subunits. Arrows with numbers indicate the direction and magnitude (Supplementary Table 1) of the inter-subunit rotation and the head-swivel from the unrotated state to TI^{PRE} or TI^{POST}, respectively.

complex[8]. The subnanometre resolution of the 70S–EF-G–GDP–FA subpopulations enabled the visualization of secondary structure and thus the generation of molecular models (Fig. 1) by applying our newly developed MDFIT algorithm (see Methods). Comparison with available structures reveals that substate I is similar in conformation to the ratcheted substate of the PRE complex[9,10] (Supplementary Table 1) and also that the tRNA is bound in a hybrid P/E site (Fig. 2a). We therefore consider substate I to be related to a pre-translocational intermediate (TI^{PRE}).

In contrast, substate II of the 70S–EF-G–GDP–FA complex represents a novel conformational state of the 70S ribosome. The anticodon stem-loop (ASL) of the tRNA has moved by 8–10 Å compared with the P/E position of TI^{PRE} as it maintains strong association with the P-site components of the head and follows the large 18° swivel movement of the head (Fig. 2b and Supplementary Movie 3). Because the tRNA interacts simultaneously with P-site components of the head as well as E-site components of the platform, it can be thought of as a 30S

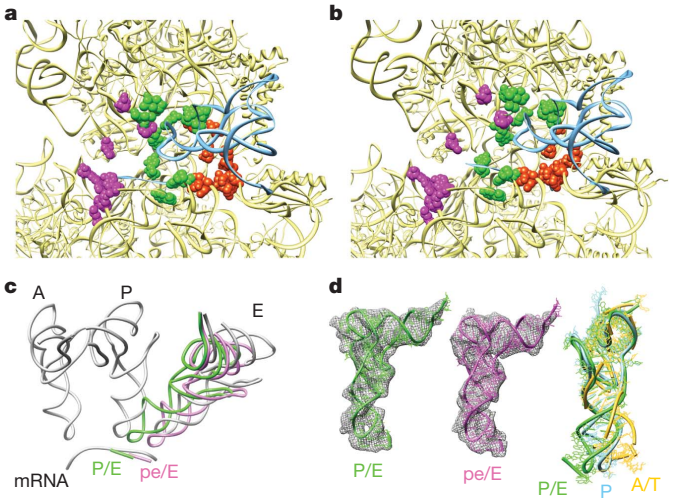

Figure 2 | Localization and conformation of the tRNA of substates I (TI^{PRE}) and II (TI^{POST}). **a**, **b**, Close-up of the tRNA-binding regions of the 30S subunit of TI^{PRE} (**a**) and TI^{POST} (**b**). The 30S subunit and tRNAs are shown as yellow and blue ribbons, respectively; ribosomal residues that contact A, P and E tRNA (magenta, green and orange) are shown as spheres. **c**, In a common 50S alignment, the P/E tRNA (green) of TI^{PRE} and the pe/E tRNA (magenta) of TI^{POST} together with their respective mRNA codons are compared with mRNA and classical A, P and E tRNA positions (grey). **d**, Density for the tRNAs (wire mesh) with molecular models for the P/E tRNA of TI^{PRE} (left, green) and the pe/E tRNA of TI^{POST} (middle, magenta). On the right, the model for P/E tRNA (green), which is essentially the same as that for pe/E-tRNA (root mean squared deviation 1.5 Å), is compared with a classical P tRNA (blue) and an A/T tRNA (yellow) by alignment of the acceptor-stem, D-stem and T-stem loops.

intra-subunit hybrid site (Fig. 2b). Moreover, because the contacts of the CCA end of the tRNA with the E site on the 50S subunit remain unaffected, we extend the previous nomenclature of hybrid sites[5] and refer to this newly identified state as a pe/E hybrid state (P site on head and E site on platform of the 30S subunit, and E site on the 50S subunit).

The ASL of the pe/E tRNA together with the bound mRNA codon is very close to the position of a fully translocated E/E tRNA (Fig. 2c and Supplementary Movie 4). Apparently, head-swivelling coupled with partial unratcheting of the body/platform of the 30S subunit leads to tRNA translocation, suggesting that substate II of the 70S–EF-G–GDP–FA complex is related to a post-translocational intermediate state (TI^{POST}). We note that although the intermediate states visualized here contain only one tRNA, a second tRNA (ap/P) can be superimposed on the TI^{POST} state without steric interference with the binding position of EF-G (Supplementary Fig. 6). Thus, the structures presented here seem to be valid models for translocation intermediates (see also Supplementary Information for further discussion), but structures of translocation intermediates with two tRNAs will be necessary for the validation of these predictions. The presence of the ratchet-like subunit rearrangement in the yeast 80S–eEF2–sordarin complex[15] hints that translocation in prokaryotes and eukaryotes may use related intermediate conformations. This structure showed a strong head swivel comparable to that of bacterial TI^{POST} combined with a strong inter-subunit rotation of bacterial TI^{PRE}. Thus, the conformation of the 80S–eEF2–sordarin complex[15], although obtained by classical single-particle methods, may present a further intermediate between TI^{PRE} and TI^{POST}.

Whereas the P/E and pe/E tRNAs are in a twisted conformation (Fig. 2d), the overall conformations of EF-G in TI^{PRE} and TI^{POST} are remarkably similar to each other (Fig. 1) and to that observed in the cryoelectron microscopy reconstruction of the 70S–EF-G–GMPPNP[14] as well as in the recent X-ray structure of EF-G–GDP–FA bound to a POST-state ribosome[19] (Fig. 3a). However, one difference between the two EF-G–GDP–FA substates relates to the interaction patterns of domain IV of EF-G: in the TI^{PRE} state, domain IV does not seem to

©2010 Macmillan Publishers Limited. All rights reserved

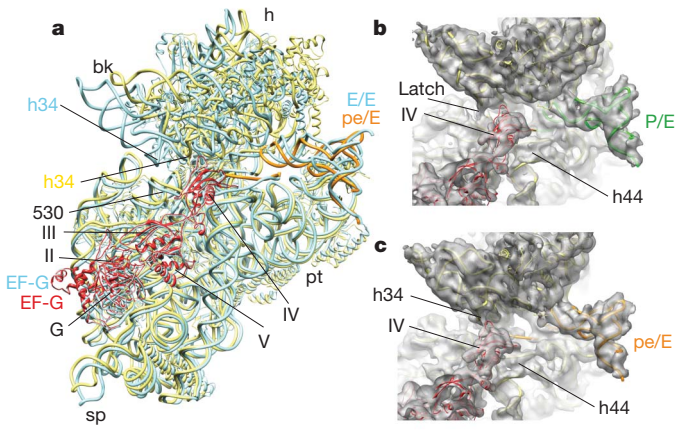

Figure 3 | EF-G stabilizes the swivelled head movement in the TI^{POST} state. **a**, Comparison of the position of FA-stalled EF-G and the 30S subunit between TI^{POST} and the POST-state 70S–EF-G–GDP–FA complex[19]. All shown components of the POST-state 70S–EF-G–GDP–FA complex[19] are depicted as blue ribbons. The 30S, EF-G and pe/E tRNA of TI^{POST} are represented by yellow, red and orange ribbons, respectively. **b**, **c**, Close-up of the decoding region and domain IV of EF-G in the same orientation as in **a**. The surfaces of TI^{PRE} (**b**) and TI^{POST} (**c**) are transparent with molecular models in ribbon representation (30S subunit, yellow; EF-G, red, P/E tRNA, green; pe/E tRNA, orange). The arrows mark the closed latch between helix h34 and the 530 region of TI^{PRE} (**b**) and the interaction between h34 and domain IV of EF-G within TI^{POST}.

interact significantly with the ribosome (Fig. 3b), whereas a small shift in the binding position of EF-G and the large swivel of the head facilitate a more extensive interaction of domain IV of EF-G with helix h34 of the 16S rRNA in the TI^{POST} state (Fig. 3c). Together, h34 and the nucleotide 530 region of 16S rRNA form the so-called latch of the mRNA entry channel. Because of the head-swivel in the TI^{POST} state, h34 has moved about 12 Å away from the 530 region, leading to an opening of the latch (Fig. 3c) similar to that observed previously when eEF2 was trapped on the yeast 80S ribosome with sordarin[15]. This may facilitate the movement of the mRNA–tRNA$_2$ complex. Consistent with this observation, transient protection of h34 by EF-G against chemical modification during the translocation reaction has been reported previously[23]. The direct interaction of domain IV of EF-G with h34 may therefore bias the energy landscape of the ribosome towards TI^{POST}.

Until now, intermediate states of inter-subunit rotation have been considered to be intermediates on the pathway to the fully rotated state[16]. The present findings implicate unratcheting (in combination with the large swivel of the 30S head), rather than ratcheting, as being coupled to the translocation movement of the tRNAs and the mRNA with respect to the 30S subunit. Collectively, the insights gained from the structures of the TI^{PRE} and TI^{POST} states enable us to provide a structural explanation for the process of translocation in a model in which tRNA movements are facilitated by head-swivel, ratcheting and unratcheting motions of the ribosome (Fig. 4). These motions may be influenced by the GTPase reaction on EF-G; a network of interactions involving domain III and the ordered switch I region of EF-G and the γ-phosphate of GTP was proposed to stabilize the rotated state of the 30S subunit[14]. Accordingly, fast GTP hydrolysis by EF-G[17] could destabilize the direct and indirect interactions of switch I of EF-G with the maximally rotated 30S subunit[14,24], therefore increasing the propensity of the 30S subunit to rotate backwards. The unratcheting motion produces a counter-movement of the body/platform with respect to the head, thereby reducing the distance that the tRNAs have to travel during translocation. Intra-subunit hybrid states allow the 30S subunit to maintain partial contacts with the tRNAs at any time of the translocation reaction. In the context of the ribosome's functioning during translocation as a Brownian ratchet machine[25], our model suggests that EF-G acts as a dynamic pawl, decoupling the unratcheting motions of the ribosome from the transition of hybrid-state tRNAs back into classical states. EF-G thereby provides directionality and accelerates translocation of the tRNAs by means of several intermediate inter-subunit and intra-subunit hybrid states into the classical P/P and E/E sites of the POST state.

METHODS SUMMARY

Tight-coupled 70S ribosomes from *Thermus thermophilus* were isolated by sucrose-gradient centrifugation and incubated with EF-G in the presence of GTP and FA. The resulting complexes were flash-frozen and imaged under low-dose conditions

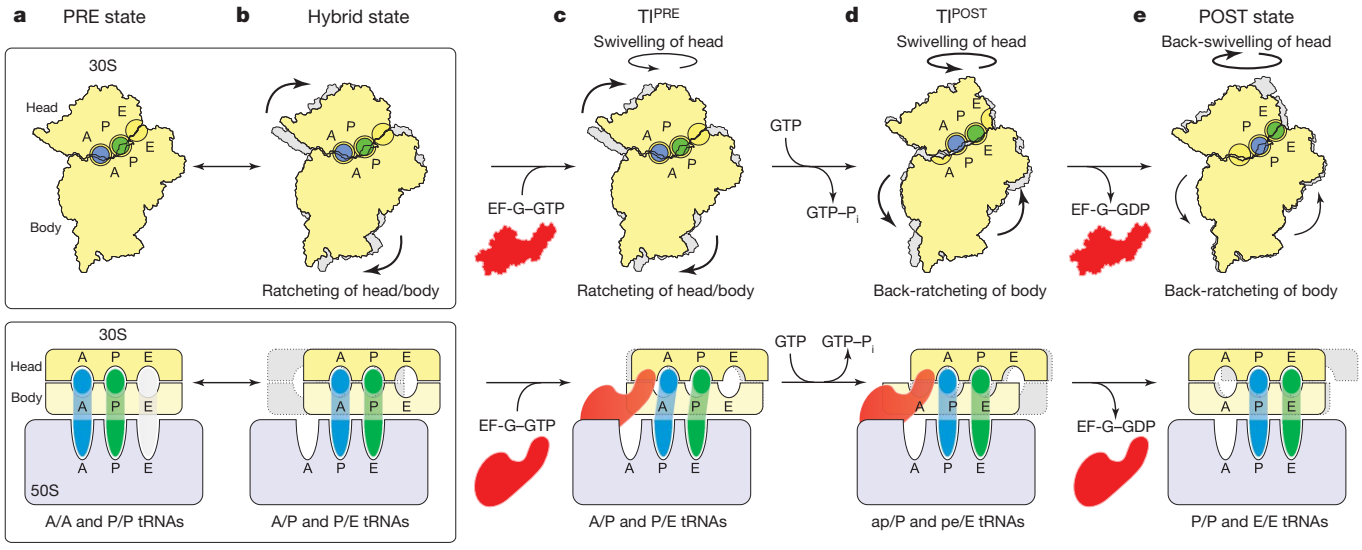

Figure 4 | Model for translocation. **a**, **b**, The PRE ribosome exists in a dynamic equilibrium between base states with classical A/A and P/P tRNAs (**a**) and rotated states with hybrid A/P and P/E tRNAs[6,7,9–11] (**b**). **c**, Binding of EF-G–GTP to PRE state (**a**) or hybrid state (**b**) stabilizes the ratcheted state[12] as observed in TI^{PRE}. **d**, Fast GTP hydrolysis by EF-G[17] accelerates translocation by means of an unlocking step on the 30S subunit[18]. Domain IV of EF-G uncouples unratcheting from the reverse movement of the A/P and P/E tRNAs back into classical states; that is, a doorstop function. Through a head-swivelling and unratcheting motion, the tRNAs move from aa/P and pp/E into the 30S intra-subunit ap/P and pe/E hybrid states. **e**, Complete unratcheting of the 30S subunit leads to the POST-state 70S–EF-G complex[19]. Back-swivelling of the 30S head re-establishes tRNAs in the classical (pp/P) P and E (ee/E) states. Translocation is completed by the dissociation of EF-G–GDP.

©2010 Macmillan Publishers Limited. All rights reserved

with the use of an FEI Polara G2 electron microscope. The collected data were digitized and processed with multiparticle refinement protocols implemented in SPIDER[26]. To interpret the resulting cryoelectron microscopy maps in molecular terms, a newly developed algorithm (MDFIT)[27] that integrates molecular simulation with experimental maps was employed.

Full Methods and any associated references are available in the online version of the paper at www.nature.com/nature.

Received 5 February; accepted 30 September 2010.

1. Frank, J. & Spahn, C. M. The ribosome and the mechanism of protein synthesis. *Rep. Prog. Phys.* **69,** 1383–1417 (2006).
2. Schmeing, T. M. & Ramakrishnan, V. What recent ribosome structures have revealed about the mechanism of translation. *Nature* **461,** 1234–1242 (2009).
3. Shoji, S., Walker, S. E. & Fredrick, K. Ribosomal translocation: one step closer to the molecular mechanism. *ACS Chem. Biol.* **4,** 93–107 (2009).
4. Ramakrishnan, V. Ribosome structure and the mechanism of translation. *Cell* **108,** 557–572 (2002).
5. Moazed, D. & Noller, H. F. Intermediate states in the movement of transfer RNA in the ribosome. *Nature* **342,** 142–148 (1989).
6. Munro, J. B., Altman, R. B., O'Connor, N. & Blanchard, S. C. Identification of two distinct hybrid state intermediates on the ribosome. *Mol. Cell* **25,** 505–517 (2007).
7. Blanchard, S. C. *et al.* tRNA dynamics on the ribosome during translation. *Proc. Natl Acad. Sci. USA* **101,** 12893–12898 (2004).
8. Munro, J. B., Sanbonmatsu, K. Y., Spahn, C. M. & Blanchard, S. C. Navigating the ribosome's metastable energy landscape. *Trends Biochem. Sci.* **34,** 390–400 (2009).
9. Agirrezabala, X. *et al.* Visualization of the hybrid state of tRNA binding promoted by spontaneous ratcheting of the ribosome. *Mol. Cell* **32,** 190–197 (2008).
10. Julian, P. *et al.* Structure of ratcheted ribosomes with tRNAs in hybrid states. *Proc. Natl Acad. Sci. USA* **105,** 16924–16927 (2008).
11. Fischer, N. *et al.* Ribosome dynamics and tRNA movement by time-resolved electron cryomicroscopy. *Nature* **466,** 329–333 (2010).
12. Valle, M. *et al.* Locking and unlocking of ribosomal motions. *Cell* **114,** 123–134 (2003).
13. Frank, J. & Agrawal, R. K. A ratchet-like inter-subunit reorganization of the ribosome during translocation. *Nature* **406,** 318–322 (2000).
14. Connell, S. R. *et al.* Structural basis for interaction of the ribosome with the switch regions of GTP-bound elongation factors. *Mol. Cell* **25,** 751–764 (2007).
15. Spahn, C. M. *et al.* Domain movements of elongation factor eEF2 and the eukaryotic 80S ribosome facilitate tRNA translocation. *EMBO J.* **23,** 1008–1019 (2004).
16. Zhang, W., Dunkle, J. A. & Cate, J. H. Structures of the ribosome in intermediate states of ratcheting. *Science* **325,** 1014–1017 (2009).
17. Rodnina, M., Savelsbergh, A., Katunin, V. I. & Wintermeyer, W. Hydrolysis of GTP by elongation factor G drives tRNA movement on the ribosome. *Nature* **385,** 37–41 (1997).
18. Savelsbergh, A. *et al.* An elongation factor G-induced ribosome rearrangement precedes tRNA-mRNA translocation. *Mol. Cell* **11,** 1517–1523 (2003).
19. Gao, Y. G. *et al.* The structure of the ribosome with elongation factor G trapped in the posttranslocational state. *Science* **326,** 694–699 (2009).
20. Penczek, P. A., Frank, J. & Spahn, C. M. A method of focused classification, based on the bootstrap 3D variance analysis, and its application to EF-G-dependent translocation. *J. Struct. Biol.* **154,** 184–194 (2006).
21. Agrawal, R. K. *et al.* EF-G-dependent GTP hydrolysis induces translocation accompanied by large conformational changes in the 70S ribosome. *Nature Struct. Biol.* **6,** 643–647 (1999).
22. Scheres, S. H. *et al.* Disentangling conformational states of macromolecules in 3D-EM through likelihood optimization. *Nature Methods* **4,** 27–29 (2007).
23. Matassova, A. B., Rodnina, M. V. & Wintermeyer, W. Elongation factor G-induced structural change in helix 34 of 16S rRNA related to translocation on the ribosome. *RNA* **7,** 1879–1885 (2001).
24. Ticu, C. *et al.* Conformational changes in switch I of EF-G drive its directional cycling on and off the ribosome. *EMBO J.* **28,** 2053–2065 (2009).
25. Spirin, A. S. The ribosome as a conveying thermal ratchet machine. *J. Biol. Chem.* **284,** 21103–21119 (2009).
26. Schuette, J. C. *et al.* GTPase activation of elongation factor EF-Tu by the ribosome during decoding. *EMBO J.* **28,** 755–765 (2009).
27. Whitford, P. C. *et al.* Accommodation of aminoacyl-tRNA into the ribosome involves reversible excursions along multiple pathways. *RNA* **16,** 1196–1204 (2010).

Supplementary Information is linked to the online version of the paper at www.nature.com/nature.

Acknowledgements The present work was supported by grants from the Deutsche Forschungsgemeinschaft (DFG; SFB 740 TP A3 and TP Z1, SP 1130/2-1 to C.M.T.S., FU579 1-3 to P.F., HA 1672/7-5 to R.K.H. and WI3285/1-1 to D.N.W.), the European Union 3D-EM Network of Excellence (to C.M.T.S.), the European Union and Senatsverwaltung für Wissenschaft, Forschung und Kultur Berlin (UltraStructureNetwork, Anwenderzentrum) and US National Institutes of Health (NIH; grant GM 60635 to P.A.P.), the Cluster of Excellence 'Macromolecular complexes' at the Goethe University Frankfurt (DFG Project EXC 115 to P.F. and S.C.), and the Human Frontiers of Science Program Young Investigators Award HFSP67/07 (to P.F.). We thank the New Mexico Computing Application Center for generous time on the Encanto Supercomputer. P.C.W. is currently funded by a LANL Director's Fellowship. This work was also supported by the Center for Theoretical Biological Physics sponsored by the National Science Foundation (NSF; grant PHY-0822283) with additional support from NSF-MCB-0543906, the LANL LDRD program and NIH grant R01-GM072686.

Author Contributions A.M., A.L.S. and A.D. prepared the complexes. A.H.R. and T.M. collected the cryoelectron microscopy data. A.H.R, J.L., M.B., S.R.C. and C.M.T.S. did the image processing. P.C.W., Y.Y., J.O. and K.Y.S. developed and employed the MDFit method. P.W.H. participated in docking and analysed the FA-binding site. A.H.R., R.K.H., S.R.C., P.F., P.A.P., D.N.W. and C.M.T.S. discussed the results and wrote the paper.

Author Information The electron density maps and models of the TI^{PRE} and the TI^{POST} complexes have been deposited in the 3D-EM database with accession numbers EMD-1798 and EMD-1799, and in the Protein Data Bank database with PDB IDs 2xsy, 2xtg, 2xux and 2xuy. Reprints and permissions information is available at www.nature.com/reprints. The authors declare no competing financial interests. Readers are welcome to comment on the online version of this article at www.nature.com/nature. Correspondence and requests for materials should be addressed to C.M.T.S. (christian.spahn@charite.de) or D.N.W. (wilson@lmb.uni-muenchen.de).

©2010 Macmillan Publishers Limited. All rights reserved

METHODS

Formation of the EF-G–70S–GDP–FA complex. The *fusA* gene, encoding EF-G, was cloned from *Thermus thermophilus* HB8 genomic DNA into pET-46 Ek/LIC vector using primers (TthEFG_for, 5′-GCG CGC CCG GTG GTG ATG CAG CTC TTC CTG GGC TCC GCC CTG AAG AAC-3′; TthEFG_rev, 5′-GTT CTT CAG GGC GGA GCC CAG GAA GAG CTG CAT CAC CAC CGG GCG CGC-3′) in accordance with the manufacturer's instructions (Novagen) and expressed in BL21 (DE3) cells. Recombinant EF-G protein was then purified with a Ni^{2+}-nitrilotriacetate affinity column, followed by gel filtration in a buffer containing 10 mM Tris pH 7.8, 100 mM NaCl and 10 mM 2-mercaptoethanol. Tight-coupled 70S ribosomes were purified from exponential-phase *T. thermophilus* cells by using sucrose-density-gradient centrifugation, as described previously for 30S subunits[28]. As observed previously, the ribosomes contained a co-purified tRNA[14,29]. Binding of EF-G to 70S ribosomes was done by incubating 20 μM purified EF-G protein for 15 min with 5 μM *T. thermophilus* 70S ribosomes, 500 μM GTP and 500 μM FA at 65 °C, in a buffer containing 10 mM HEPES-KOH pH 7.8, 30 mM $MgCl_2$ and 75 mM NH_4Cl. The occupancy of EF-G in the complexes was about 60–70%, as judged by centrifugal binding assay[28].

Cryoelectron microscopy and image processing. Ribosomal complexes were diluted to a concentration of 30 nM and subsequently frozen onto Quantifoil grids using a Vitrobot (FEI) device. Micrographs where collected on a Tecnai G2 Polara (FEI) at 300 kV and a magnification of ×39,000 under low-dose conditions (19 e^- $Å^{-2}$) and scanned on a D8200 Primscan drum scanner (Heidelberger Druckmaschinen) with a step size of 4.758 μm, corresponding to 1.26 Å on the specimen scale.

The Contrast Transfer Function defocus values for the micrographs were determined with CTFind[30]. Ribosomal projection images were automatically identified with the program Signature[31] and were subsequently screened visually or automatically. From the selected projections, a reconstruction was generated by projection matching procedures and refined with the SPIDER software package[32]. The complete data set comprised 586,848 projection images collected from 677 micrographs at a defocus range of 1.3–4.8 μm. During the later refinement rounds, positivity of the reference volumes was enforced, the power spectrum of the cryoelectron microscopy map was scaled to the power spectrum of a model density derived from the atomic coordinates of the X-ray structure of the 70S ribosome[33], and the map was subsequently low-pass filtered according to the current resolution estimate.

After a first phase of multiparticle refinement[20,26,34,35], performed with three-times or two-times decimated pictures, we obtained a major subpopulation (52%; 303,665 particle images) that had strong EF-G density (Supplementary Fig. 1). However, as refinement progressed and the resolution reached the subnanometre range the data set was deemed heterogeneous. Parts of the 30S subunit, especially the head domain, became partly disordered. A second phase of multiparticle refinement was therefore employed, leading to the subdivision of the data into two further substates having EF-G (Supplementary Fig. 1). Both data subsets were further refined individually at full image size. The final reconstructions of substate I (113,214 particle images) and substate II (156,332 particle images) reached resolutions of 7.8 Å and 7.6 Å, respectively (Supplementary Fig. 2).

Using a similar strategy we revisited the previous data set (362,361 particle images; 371 micrographs) of the 70S–EF-G–GMPPNP complex[14]. In a first phase of multiparticle refinement a major population (118,991 particle images) was further sorted by a second phase of multiparticle refinement resulting in substate I (58,911 particle images) and substate II (38,055 particle images). The resolutions of the maps were 9.6 Å and 10.5 Å, respectively. As the resolution for the reconstructions of the 70S–EF-G–GMPPNP complex was significantly lower (as a result of the smaller size data set) than the resolutions obtained for the 70S–EF-G–GDP–FA complex, we restricted the comparison to a dissection of only the global conformational changes, such as ratcheting and head swivelling.

Nevertheless, this analysis suggests that the 70S–EF-G–GMPPNP complex coexists in two substates that resemble TI^{PRE} and TI^{POST} of the 70S–EF-G–GDP–FA complex (Supplementary Fig. 5 and Supplementary Table 1). The ratio of particles within each of the two substates of the 70S–EF-G–GMPPNP complex is inverted with respect to the 70S–EF-G–GDP–FA complex: in the 70S–EF-G–GMPPNP complex the particle ratio of TI^{PRE} and TI^{POST} is about 3:2 (58,911:38,055), whereas in the 70S–EF-G–GDP–FA complex the ratio is about 2:3 (113,214:156,332). This means that most of the ribosomes in the 70S–EF-G complex stalled with a non-hydrolysable GTP analogue are in TI^{PRE} (substate I), having a fully ratcheted 30S subunit but only a modest head swivel. However, in the 70S–EF-G complex stalled with GTP and FA, TI^{POST} dominates and here an intermediate inter-subunit rotation is coupled with a large head swivel instead (Supplementary Figs 4 and 5 and Supplementary Table 1).

Structure-based simulation fitting (MDFIT). To determine atomic models consistent with the cryoelectron microscopy densities, we employed structure-based molecular simulation[27,36,37] together with an energetic term developed in ref. 38, which incorporates the correlation between the simulated and experimental electron density throughout the simulation. Tama and co-workers[38] developed a similar method, which used a standard explicit solvent force field, as opposed to the structure-based force field. The advantage of the structure-based force field is that, because the potential energy function is defined by the X-ray structure, MDFIT retains tertiary contacts present in the X-ray structure without special constraints. Furthermore, because MDFIT explicitly includes all non-hydrogen atoms, there are no atomic clashes and proper stereochemistry is maintained in all fits.

We began the MDFIT procedure with a structure-based potential energy function defined by the classical unratcheted conformation. To induce hybrid-state formation and subunit pivoting we introduced the energetic term based on the correlation between the simulated cryoelectron microscopy map and the experimentally determined cryoelectron microscopy map. Specifically, the potential energy function is

$$V = V^{SB} + V^{map} = V^{SB} - W \sum_{ijk} \rho_{ijk}^{sim} \rho_{ijk}^{exp} \quad (1)$$

where W is the energetic weight of the map and ρ_{ijk}^{exp} and ρ_{ijk}^{sim} are the normalized experimental and simulated electron densities at voxel (i,j,k), respectively. The quantity V^{SB} is the structure-based potential energy function. To calculate the simulated map, each atom is described by a Gaussian function of width 5 Å with the tail truncated at 1% of the peak value. Here, because the structure-based forcefield has 1 unit (all calculations were in reduced units) of stabilizing energy per atom (by construction), we set W to a comparable value of 150,000. The contributions to the force due to V^{map} were updated every 200 time steps. Fitting simulations employed Langevin dynamics. All simulations were performed with code based on Gromacs version 4.0.5 (refs 39, 40). Calculations were performed on the Encanto Supercomputer. The structure-based force field is freely available online (http://smog.ucsd.edu).

Structural models. The crystallographic structure of the 70S ribosome in complex with EF-G[19] (PDB IDs 2WRI and 2WRJ) was used as an initial structure for MDFIT. Proteins without side chains in the X-ray structure were removed. The carboxy-terminal domain of ribosomal protein L7 from PDB entry 1RQU[41] was inserted by hand, before fitting. The E-site tRNA was also removed from the initial X-ray structure in accordance with the cryoelectron microscopy map. The P-site tRNA was included in the fitting process. To facilitate fitting of the tRNA molecule into a P/E conformation, stabilizing interactions between the tRNA and the ribosome were removed. Stabilizing interactions between EF-G and the ribosome (due to their proximity in the crystal structure) were also excluded from the calculations, as were stabilizing interactions between L7 and all other components in the system. Further, crystallographic interactions found between the 3′-CCA end of the E-site tRNA with the E site of the 50S subunit were reintroduced as short-range (of the type 6-12; see refs 27, 36, 37) attractive interactions between the 3′-CCA end of the fitted tRNA and the E site of the 50S subunit. Introducing these interactions ensured that the 3′-CCA end of the P/E tRNA was in a conformation identical to that of a classically bound E-site tRNA, although because these interactions were short-range they only affected the process once the major rearrangements in the tRNA had already been achieved. Codon–anti-codon interactions were restrained by harmonic interactions with minima corresponding to the classical configuration.

The tRNA–ribosome–EF-G crystal structure was first manually aligned in VMD[42], as a single rigid unit, to the map of TI^{PRE}. The first round of fitting was performed with the TI^{PRE} map after subjecting it to a 4-Å Gaussian low-pass filter. This filter decreased noise, effectively smoothing the energetic profile associated with V^{map}, which permitted more rapid fits. After 10^6 integration steps, the fit was continued for an additional 10^6 steps with V^{map} based on the TI^{PRE} map filtered at 2 Å. The TI^{POST} map, filtered at 2 Å, was then fitted, using the TI^{PRE} 4-Å fitted structure as the initial structure.

28. Sharma, M. R. *et al.* Interaction of Era with the 30S ribosomal subunit implications for 30S subunit assembly. *Mol. Cell* **18,** 319–329 (2005).
29. Yusupov, M. M. *et al.* Crystal structure of the ribosome at 5.5 Å resolution. *Science* **292,** 883–896 (2001).
30. Mindell, J. A. & Grigorieff, N. Accurate determination of local defocus and specimen tilt in electron microscopy. *J. Struct. Biol.* **142,** 334–347 (2003).
31. Chen, J. Z. & Grigorieff, N. SIGNATURE: a single-particle selection system for molecular electron microscopy. *J. Struct. Biol.* **157,** 168–173 (2006).
32. Frank, J. *et al.* SPIDER and WEB: processing and visualization of images in 3D electron microscopy and related fields. *J. Struct. Biol.* **116,** 190–199 (1996).
33. Selmer, M. *et al.* Structure of the 70S ribosome complexed with mRNA and tRNA. *Science* **313,** 1935–1942 (2006).
34. Spahn, C. M. & Penczek, P. A. Exploring conformational modes of macromolecular assemblies by multiparticle cryo-EM. *Curr. Opin. Struct. Biol.* **19,** 623–631 (2009).

©2010 Macmillan Publishers Limited. All rights reserved

35. Connell, S. R. *et al.* A new tRNA intermediate revealed on the ribosome during EF4-mediated back-translocation. *Nature Struct. Mol. Biol.* **15,** 910–915 (2008).
36. Whitford, P. C. *et al.* An all-atom structure-based potential for proteins: bridging minimal models with all-atom empirical forcefields. *Proteins* **75,** 430–441 (2009).
37. Whitford, P. C. *et al.* Nonlocal helix formation is key to understanding S-adenosylmethionine-1 riboswitch function. *Biophys. J.* **96,** L7–L9 (2009).
38. Orzechowski, M. & Tama, F. Flexible fitting of high-resolution x-ray structures into cryoelectron microscopy maps using biased molecular dynamics simulations. *Biophys. J.* **95,** 5692–5705 (2008).
39. Lindahl, E., Hess, B. & van der Spoel, D. J. GROMACS 3.0: a package for molecular simulation and trajectory analysis. *J. Mol. Model.* **7,** 306–317 (2001).
40. Berendsen, H. J. C., van der Spoel, D. & van Drunen, R. GROMACS: a message-passing parallel molecular dynamics implementation. *Comput. Phys. Commun.* **91,** 43–56 (1995).
41. Bocharov, E. V. *et al.* From structure and dynamics of protein L7/L12 to molecular switching in ribosome. *J. Biol. Chem.* **279,** 17697–17706 (2004).
42. Humphrey, W., Dalke, A. & Schulten, K. VMD: visual molecular dynamics. *J. Mol. Graph.* **14,** 33–38 (1996).

©2010 **Macmillan Publishers Limited. All rights reserved**

Paper 8

Formation of ε(R)-β-lysyl-hydroxylysine on translation elongation factor EF-P requires YjeK, YjeA and YfcM

Lauri Peil[1,4,5], Agata L. Starosta[2,4], Kai Virumäe[3], Gemma C. Atkinson[1], Tanel Tenson[1], Jaanus Remme[3,*], Daniel N. Wilson[2,*]

[1] Institute of Technology, University of Tartu, Tartu, Estonia

[2] Gene Center and Department for Biochemistry, University of Munich, Munich, Germany

[3] Institute of Molecular and Cell Biology, University of Tartu, Tartu, Estonia

[4] L.P. and A.L.S. contributed equally to this work.

[5] Present address: Wellcome Trust Centre for Cell Biology, University of Edinburgh, Edinburgh, United Kingdom.

[*] To whom correspondence should be addressed: Wilson@lmb.uni-muenchen.de or jremme@ebc.ee

Abstract

Elongation factor P (EF-P) is a highly conserved bacterial protein that interacts with the ribosome and stimulates peptide bond formation. Lysine 34 (K34) of *Escherichia coli* EF-P is lysinylated by YjeK and YjeA. Both EF-P and the modification are important for growth, drug resistance and virulence in pathogenic bacteria. Here we show that the currently accepted EF-P modification pathway is incomplete and that *in vivo* endogenous EF-P carries a unique ε(R)-β-lysyl-hydroxylysine modification. Firstly, we demonstrate that lysinylation of EF-P by YjeK and YjeA results in the addition of β-lysine to the ε-amino group of K34. Additionally, we have discovered a hydroxylase, YfcM, which subsequently modifies the C4/C5 position of K34 of lysinylated EF-P. YfcM is distinct from the deoxyhypusine hydroxylase involved in the maturation of eIF5A, the eukaryotic homolog of EF-P, indicating that bacteria and eukaryotes have evolved alternative pathways to maintain the fully modified state of these translation factors.

Introduction

Elongation factor P (EF-P) was originally identified as a soluble protein that binds to the ribosome and stimulates peptide bond formation[1-4]. Under some conditions EF-P has been shown to enhance the translation of natural and synthetic mRNAs *in vitro*[3]. EF-P is detected in the monosome and polysome fractions[5] suggesting that EF-P not only promotes formation of the first peptide bond, but may also be involved during translation elongation. Deletion of the *efp* gene leads to defects in (i) growth of *E. coli*[6] and *Acinetobacter baylyi*[7], (ii) swarming[8] and sporulation[9] of *Bacillus subtilis*, and (iii) virulence of *Agrobacterium tumefaciens*[10]. EF-P has a ubiquitous distribution, being conserved in all bacteria[11] and orthologous to archaeal and eukaryotic initiation factor 5A (a/eIF-5A)[12]. Similarly to EF-P, eIF-5A was also identified based on its ability to stimulate Met-puromycin formation (reviewed by [13]). Moreover, eIF-5A is essential in yeast and higher eukaryotes, and depletion studies in yeast indicate that loss of eIF-5A leads to a significant reduction in protein synthesis *in vivo*[13-16].

Crystal structures of bacterial EF-P reveal a three domain (I-III) architecture[6,17,18], whereas a/eIF-5A lack the C-terminal domain III of EF-P[19,20]. A strictly conserved lysine in domain I of eIF-5A is the site of a unique modification, called hypusine (reviewed by[13]). Co-sedimentation experiments indicate that eIF-5A binds to translating ribosomes in a hypusine-dependent manner[13]. The equivalent lysine 34 (K34) of endogenous *E. coli* EF-P has also been reported to carry a modification of ~144 Da[5]. Bound to the ribosome, K34 of EF-P, and by analogy the hypusine of eIF-5A, would interact with the CCA-end of the P-tRNA, suggesting that EF-P and eIF-5A stimulate peptide bond formation through stabilization and positioning of the acceptor end of the P-tRNA[18].

Hypusine is added post-translationally to eIF-5A in two enzymatic steps[13]; first, deoxyhypusine synthase (DHS) attaches the amino-butyl moiety of spermidine to the lysine of eIF-5A, and then the attached butyl moiety is hydroxylated by deoxyhypusine hydroxylase (DOHH). eIF-5A and DHS are essential in yeast, and while DOHH is dispensable in yeast, it is essential in higher eukaryotes[13]. Although the DHS and DOHH genes are absent from the *E. coli* genome, two unrelated enzymes, YjeK and YjeA (also termed PoxA/GenX), have been implicated in the EF-P modification pathway[6,11,21]. Deletion of *yjeA* or *yjeK* in *Salmonella typhimurium*

leads to growth defects, antibiotic sensitivity and attenuation of virulence[21-24], similar to that reported for Δ*efp* in *A. tumefaciens*[10]. YjeK is a lysine 2,3-aminomutase that converts (S)-α-lysine to (R)-β-lysine[25], whereas YjeA has homology to class II lysine-tRNA synthetases but lacks the tRNA anticodon recognition domain[11]. *In vitro* biochemical assays indicate that YjeA cannot aminoacylate $tRNA^{Lys}$,[26] but can activate lysine and transfer it to K34 of EF-P[6,21]. Recently, (R)-β-lysine was shown to be 100-fold more efficient as a substrate for lysinylation of EF-P by YjeA than either (S)-β-lysine or α-lysine[27]. Curiously, mass spectrometry analyses indicate that lysinylation of K34 of EF-P by YjeA results in an ~128 Da modification[6,21,27], leaving a difference of ~16 Da unexplained and unaccounted for when compared with the ~144 Da reported for endogenous EF-P[5].

We have used an *E. coli* lysate-based immuno-precipitation approach, coupled with high-resolution mass spectrometry (MS) and SILAC labeling, to characterize the chemical nature of the *E. coli* EF-P modification and delineate the modification pathway *in vivo*. Here we demonstrate that endogenous *E. coli* EF-P bears a +144.09 Da modification, resulting from the formation of ε(R)-β-lysyl-hydroxylysine of K34. The sequential action of YjeK and YjeA is responsible for the addition of 128.09 Da, with MS fragmentation data supporting the presence of β-lysine, rather than α-lysine, attached to the ε-amino group of K34 of EF-P. Additionally, we have discovered that the hypothetical protein YfcM is responsible for the discrepancy of 16 Da between the reported *in vitro* and *in vivo* results. Indeed, we can show that YfcM is involved in the modification of either the C4 (γ) or C5 (δ) position of K34 of EF-P. YfcM is unrelated in origin and mechanism to the eukaryotic DOHH and although lysyl-5-hydroxylases have been reported in eukaryotes, this would be the first report of C4/C5-hydroxylase activity in bacteria.

Results

Lysine 34 of endogenous *E. coli* EF-P is modified by 144.09 Da

Previous mass spectrometry (MS) analyses of tryptic fragments of *in vitro* modified EF-P reported mass increases of 127.7 Da[6] and 128 Da[21], compared with 143.77 ± 0.15 Da for endogenous EF-P[5]. Because of limited accuracy of the MS and the lack of supporting MS spectra in the latter publication, we decided to re-examine the modification state of endogenous *E. coli* EF-P. To do this, endogenous EF-P was

isolated from the S100 fraction of *E. coli* strain MRE600 using multi-step chromatography[28,29] and analyzed using high resolution and high mass accuracy nano-LC-MS/MS approach. MS of the full-length endogenous EF-P revealed a mass (mono-isotopic, unless otherwise stated) of 20,591.6 Da (**Fig. 1a**), which is 144.2 ± 0.1 Da larger than the expected mass of unmodified EF-P (20,477.4 Da, with N-terminal methionine cleaved off). To identify the site of modification, endogenous EF-P was immuno-precipitated from cell lysate using antibodies raised against recombinant *E. coli* EF-P and peptide fragments were generated by proteolysis using either chymotrypsin, which preferentially cleaves on the carboxyl side of Leu, Tyr, Trp and Phe, or the peptidase LysC, which preferentially cleaves on the carboxyl side of unmodified Lys. As expected, the chymotrypsin fragment containing K34 ($F_{.30}$VKPGK*GQAF_{38}.A) was the only peptide observed to have an increased mass, namely 1074.62 Da, which is 144.09 Da larger than the theoretical mass of 930.53 Da (**Fig. 1b**), and similar to that reported previously for endogenous EF-P[5]. Similarly, digestion of endogenous EF-P with LysC produced a peptide ($K_{.32}$PGK*GQAFARVK_{42}.L) with a mass of 1301.76 Da - again an increase of exactly 144.09 Da compared with the theoretical size of 1157.67 Da (**Fig. 1c**). Although the +144.09 Da modification state appears to be the predominant form of EF-P in the cell, peptides with masses corresponding to the partially modified (+128 Da) state were also detected, but only at ~1-2% of the level of the fully modified form (**Supplementary Fig. 1**).

Fragmentation of both the chymotrypsin peptide (F.VKPGK*GQAF.A) and the LysC peptide (K.PGK*GQAFARVK.L) revealed the modification site to be K34 (**Fig. 1b and 1c**), as expected from previous studies[5,6,11,21]. In the case of the LysC peptide, fragmentation of the doubly charged peptide precursor gave rise to four intense doubly charged peaks corresponding to the modified LysC peptide (K.PGK*GQAFARVK.L), but with nominal mass losses of 86 Da, 104 Da, 128 Da and 145 Da (peaks labeled X1-X4, respectively, in **Fig. 1c**). Similar peaks were also observed when a triply charged peptide precursor was fragmented in the MS (**Fig. 3c,d, Fig. 4a,b** and **Supplementary Table 1**). These mass peaks are consistent with the loss of a series of fragments from the modified K34, but not from C-terminal K42, as determined by [18]O-labeling (**Supplementary Table 1** and **Supplementary Fig. 2**): Peak X4 has a mass loss of 145 Da, which would result if the C6-N6 bond of the lysinylated K34 was fragmented (F4 in **Fig. 1d**), whereas the mass loss of 128 Da

(peak X3) is consistent with fragmentation at the amide bond between the ε-amino group of K34 and the carbonyl carbon of the added lysine (F3 in **Fig. 1d**). These fragmentation peaks therefore support the attachment of the activated lysine to the ε-amino group of K34 during lysinylation by YjeA, as assumed previously[6,11,21]. In contrast, mass losses of 86 Da and 104 Da (peaks X1 and X2) would arise when the linkage between the C2 (α) and C3 (β) positions of the added lysine are fragmented, with the additional loss of water (18 Da) from the peptide in peak X2 (F1 and F2 in **Fig. 1d**). Importantly, the loss of the 86 Da mass is explainable only if β-lysine, rather than α-lysine, is attached to K34. If α-lysine were present then fragmentation at the same bond would generate a mass loss of only 72 Da and such fragmentation event would be very rare and unexpected. Collectively, the fragmentation data suggest that modification of endogenous EF-P comprises β-lysine attached to ε-amino group of K34 accounting for 128 Da, and that the additional 16 Da modification is associated with K34 of endogenous EF-P, rather than the added lysine.

In vivo lysinylation of EF-P by YjeA requires YjeK

In order to demonstrate that YjeA and YjeK are responsible for the modification of K34 of EF-P *in vivo*, endogenous EF-P was immuno-precipitated from *E. coli* AT713 strains lacking the genes for *yjeA* (Δ*yjeA*) or *yjeK* (Δ*yjeK*), as performed above for the parental strain. In the case of Δ*yjeA*, only chymotrypsin could be used since LysC proteolysis resulted in digestion of unmodified K34-containing region into small peptides that were undetectable in our analysis. Chymotrypsin proteolysis of EF-P from the Δ*yjeA* strain produced a fragment containing K34 ($F_{.30}$VKPGKGQAF_{38}.A) that had a mass of 930.53 Da (**Fig. 2a**), corresponding exactly with the expected mass of 930.53 Da for the unmodified form. This is consistent with the finding that YjeA is the critical enzyme responsible for the *in vitro* modification of K34 of EF-P[6,21,27]. When YjeA was exogenously overexpressed from a plasmid (pYjeA) in the Δ*yjeA* strain, two LysC fragments containing modified K34 were detected: One fragment had a mass of 128.09 Da (data not shown) corresponding exactly with the predicted mass increase (+128.09 Da) when activated lysine is transferred to the ε-amino group of K34 of EF-P, as illustrated in **Fig. 1d**. The second fragment was 144.09 Da larger than the unmodified peptide (data not shown) and thus was identical to the mass detected in the endogenous EF-P from the parental wildtype strain, as illustrated in **Fig. 1c**).

Similarly, modified and unmodified chymotrypsin fragments were also detected upon proteolysis of EF-P isolated from the Δ*yjeK* strain (**Fig. 2b, c**). The modified form of the chymotrypsin fragment had a mass of 1058.62 Da (**Fig. 2c**), corresponding to a mass increase of +128.09 Da when compared with the expected mass (930.53 Da) of the unmodified form (note that the +144 Da-modified peptide was not detected). Quantification of the relative intensities of the peak areas for the modified (4.46×10^6) and unmodified fragments (2.18×10^8) reveals that the modified form is present at only ~2 % of the level of the unmodified form, assuming that these peptides ionize with similar efficiency (**Fig. 2d**). These observations indicate that while YjeA can perform the lysinylation of EF-P *in vivo* in the absence of YjeK (and therefore in the absence of (R)-β-lysine), the reaction appears to be extremely inefficient. Indeed, *in vitro* lysinylation of EF-P by YjeA performed in the absence of YjeK was also inefficient, requiring incubations of between 2-4 hours[6,21]. However, the reaction was 100-fold more efficient when (R)-β-lysine, rather than either (S)-β-lysine or α-lysine, was used as a substrate[27]. Similarly, efficient modification of exogenously overexpressed EF-P was only observed when EF-P was co-expressed with both YjeA and YjeK[6]. Nevertheless, it should be re-emphasized that in the reported *in vitro* lysinylation and co-expression experiments, the modification of K34 of EF-P was shown to be ~128 Da[6,21], rather than ~144 Da of endogenous EF-P, as shown here (**Fig. 1**) and reported previously[5].

Fully modified EF-P requires the presence of YfcM

Given the discrepancy of 16 Da between the modification mass of the endogenous EF-P (+144 Da; **Fig. 1**)[5] and *in vitro* lysinylated EF-P (+128 Da)[6,21], we reasoned that a third enzyme should exist that is also involved in the modification of K34 of EF-P *in vivo*. Moreover, the enzyme should be dependent on the action of YjeK and YjeA, since the absence of either of these genes leads to a predominance of completely unmodified EF-P *in vivo* (**Fig. 2**). We therefore used the STRING (Search Tool for the Retrieval of Interacting Genes/Proteins) database (http://string.embl.de) to search for proteins associated with YjeA, YjeK and EF-P. A query using *E. coli* PoxA (YjeA), for example, revealed an association (confidence value 0.6) with five proteins: EF-P, YjeK and three additional proteins YfcM, HflD and ECs0957. HflD is already reported to be involved in the λ lysis-lysogeny switch and ECs0957 has

homology with pyruvate dehydrogenases. In contrast, BLAST searches indicate that YfcM has no reasonable homology with any protein of known structure or function.

To investigate the potential involvement of YfcM in the modification of EF-P *in vivo*, we immuno-precipitated endogenous EF-P from the *E. coli* AT713 strain lacking the *yfcM* gene (Δ*yfcM*). Chymotrypsin proteolysis of EF-P from the Δ*yfcM* strain produced a fragment containing K34 ($F_{.30}$VKPGKGQAF_{38}.A) with a mass of 1058.62 Da (**Fig. 3a**) - a mass increase of 128.09 Da when compared with the expected mass of 930.53 Da for the unmodified fragment. When YfcM was exogenously overexpressed from a plasmid (pYfcM) in the Δ*yfcM* strain, the mass of the chymotrypsin fragment increased to 1074.62 Da (**Fig. 3b**), which is 144.09 Da larger than the unmodified fragment and identical to the mass increase observed for endogenous EF-P (see **Fig. 1b,c**). Similarly, the LysC fragment of EF-P containing K34 (K.$_{32}$PGK*GQAFARVK$_{42}$.L) isolated from the Δ*yfcM* strain had a mass of 1285.76 Da (**Fig. 3c**), exactly 128.09 Da larger than the unmodified fragment (1157.67 Da). The mass of the LysC fragment increased to 1301.76 Da with YfcM overexpression (**Fig. 3d**), indicating the YfcM is required for the addition of exactly 15.995 Da of the 144 Da that comprises the modification of K34 of endogenous EF-P. The precision of the mass difference, i.e. 15.995 Da, is indicative of one atom of molecular oxygen, which has a monoisotopic mass of 15.995 Da, thus revealing YfcM as a potential hydroxylase (mono-oxygenase) that modifies K34 of lysinylated EF-P.

The C4/C5 position of lysine 34 of EF-P is hydroxylated

Eukaryotic lysine hydroxylases modify the C5 position of lysine, which plays a critical role in the formation and stabilization of collagen, and loss of this activity leads to connective tissue disorders such as Ehlers–Danlos syndrome[30]. In contrast, to our knowledge, the only lysine hydroxylase activities reported in bacteria are the lysine N^6-hydroxylase involved in the synthesis of siderophores, such as aerobactin[31] and the lysine-2-mono-oxygenases involved in lysine degradation[32]. YfcM has no apparent homology with any of these enzyme families. Thus, in order to determine the site of hydroxylation by YfcM on K34 of EF-P, we utilized differentially deuterated lysine isoforms, namely 3,3,4,4,5,5,6,6-D8-L-lysine (D8-Lys) and 4,4,5,5-D4-L-lysine (D4-Lys) where the hydrogen atoms (1.008 Da) of the C3-C6 and C4-C5 positions of L-lysine, respectively, are substituted with deuterium (2.014 Da).

The lysine (and arginine) auxotrophic *E. coli* wildtype AT713 and AT713Δ*yfcM* strains were grown in minimal media supplemented with D4- or D8-lysine, rather than unlabelled D0-lysine. The endogenous EF-P was immuno-precipitated from the lysates as before and then digested with LysC. The masses of the K34 containing LysC fragment ($K._{32}$PGK*GQAFARVK$_{42}$.L) of EF-P isolated from the Δ*yfcM* strain were determined as 1297.84 Da when grown in D4- (**Fig. 4a**) and 1309.91 Da in D8-Lys (**Supplementary Fig. 3a**), i.e. mass increases of +12.07 Da or +24.15 Da, respectively when compared with the mass determined in D0-Lysine (1285.76 Da seen in **Fig. 3c**). Since the LysC fragment contains three lysines; K34, K42 and the lysine added to K34; the expected theoretical mass increases are calculated as [3 x 1.0063 Da x 4 (D4) =] +12.08 Da for D4-lysine and [3 x 1.0063 Da x 8 (D8) =] +24.15 Da for D8-lysine, which are in very good accordance with the experimental masses of +12.07 Da and +24.15 Da, respectively.

In contrast, the same LysC fragments isolated from the wildtype strain had masses of 1312.83 Da in D4-Lys (**Fig. 4b**) and 1324.90 Da in D8-Lys (**Supplementary Fig. 3b**), which are only +11.07 Da and +23.14 Da larger when compared with the mass determined in D0-Lys (1301.76 Da seen in **Fig. 1c**). When compared with the masses from LysC fragments isolated from the Δ*yfcM* strain, both LysC fragments from the wildtype YfcM-containing strain are 14.993 Da larger, instead of the expected 15.995 Da. This is consistent with 14.988 Da increase expected by the mass loss of a deuterium atom (-2.014 Da) and the addition of a hydroxyl OH group (+17.003 Da [= 15.995 Da + 1.008 Da]). Moreover, because the 1 Da loss is observed in both the D4- and D8-labelled fragments, this indicates that YfcM hydroxylates either the C4 (γ) or C5 (δ) position, but not the C3 (β) or C6 (ε) of K34 (**Fig. 4c** and **Supplementary Fig. 3c**).

Furthermore, data from the fragmented D8-labelled LysC peptide ($K._{32}$PGK*GQAFARVK$_{42}$.L) from both Δ*yfcM* and wildtype EF-P indicate that K34 is indeed β-lysinylated (**Supplementary Table 2**). It has previously been shown that the aminomutase YjeK transfers the α-amino group from C2 (α) to C3 (β), while one of the C3 (β) hydrogens is transferred back to C2 (α)[25], a reaction mechanism that is in very good accordance with our observations. Namely, the D8-labelled F1 and F2 fragments were ~1.006 Da smaller than anticipated (93.129 Da instead of 94.135 Da, and 111.140 Da instead of 112.145, respectively), which would correspond to a situation where one of the C3 (β) deuteriums has been transferred to the C2 (α),

thereby indicating that these fragments can only be derived from β-lysine (**Supplementary Table 1** and **Supplementary Fig. 2**). Both F3 and F4 fragments have a mass identical to that of theoretical lysine fragments containing eight deuteriums, confirming the conclusion that one deuterium is transferred from the C3 (β) to C2 (α) and not lost during the reaction (**Supplementary Fig. 2**).

In conclusion, fragmentation data using the D4- and D8-labelled LysC fragments, together with [18]O-labeling, is consistent with our previous suggestion that the additional 16 Da mass corresponding to lysine hydroxylation is associated with K34 of EF-P and not with the added β-lysine (**Supplementary Table 1**).

Substrate specificity of the YfcM hydroxylase

The eukaryotic lysine-5-hydroxylases utilize Fe^{2+}, O_2 and α-ketoglutarate to carry out oxidation, and then use ascorbic acid to return the iron to its oxidized state[30]. Similarly, human DOHH activity is also dependent on Fe^{2+} and O_2[33], but not α-ketoglutarate or ascorbic acid[34]. In contrast, the substrates for the bacterial lysine-N6-hydroxylases include NADPH, H^+, O_2 and the reaction requires FAD[31], whereas lysine-2-monoxygenases utilize O_2 and FAD but do not require metals[32]. To screen for potential substrates of YfcM, we utilized differential scanning fluorimetry (DSF), which monitors the increase in thermal stability of a protein due to the interaction with a ligand[35]. The thermal stability of recombinant YfcM protein was measured across a library of diverse ligands, including α-ketoglutarate, ascorbic acid, co-enzyme A (CoA), FAD, NAD, NADH, NADP, NADPH, ATP, ADP, PLP, L-lysine, thiamine, oxaloacetate, tetrahydrofolate, succinate as well as metals, such as Fe^{2+} and Mg^{2+} (**Supplementary Fig. 4**). The largest increases in thermal stability for YfcM were observed with nucleotide-based chemicals, for example, the maximum shift of ~5°C was observed in the presence of <600 μM NADP or CoA (**Fig. 5a**). In contrast, other ligands, such as Fe^{2+}, α-ketoglutarate or ascorbic acid did not stabilize YfcM (**Supplementary Fig. 4**), even at significantly higher concentrations (<10 mM). These findings suggest that YfcM is more likely to use a NAD- or FAD-based co-factor similar to other bacterial lysine hydroxylases, rather than Fe^{2+} or α-ketoglutarate/ascorbic acid co-factors as used by eukaryotic lysine hydroxylases.

The genomic distribution and context of yfcM

Previous bioinformatic analysis of 725 bacterial genomes revealed the presence of genes for *efp*, *yjeA* and *yjeK* in 200 genomes (28%)[11]. Here we have extended this analysis to include predicted proteomes of 1268 completely sequenced bacterial genomes and detect the presence of the YfcM protein in 179 species clustering within the γ-proteobacteria phyla (**Fig. 5b**, **Supplementary Table 2** and **Supplementary Fig. 5**). All bacterial species that contain the *yfcM* gene also have *efp*, *yjeA* and, with one exception (*Haemophilus influenzae* strain PittGG), *yjeK* (**Supplementary Table 2**). Moreover, we find that a lysine, equivalent to position 34 in *E. coli* EF-P, is strictly conserved (100%) in organisms that contain YfcM (**Supplementary Table 2**). However, unlike *yjeA* and *yjeK* that often cluster together in the same operon as *efp*[11], *yfcM* is always located in a distinct region of the chromosome. The six-gene operon structure of the *prmC-aroC-mepA-yfcA-**yfcM**-yfcL* operon is highly conserved within the *Enterobacteriaceae* family (**Fig. 5b**). *yfcA* and *yfcL* are hypothetical proteins of unknown function, whereas *aroC* and *mepA* are annotated as chorismate synthase and Murein DD-endopeptidase, respectively. Curiously, the *yfcM* gene often neighbors other modification enzymes, such as the methyltransferases *prmB* and *prmC*, which modify ribosomal protein L3 and release factor RF1/RF2, respectively, as well as *mnmC* and *yrdC* (*rimN*) that are involved in tRNA modification[36,37] (**Fig. 5b**).

Discussion

Here we have used high-resolution mass spectrometry to characterize the chemical composition of the lysinylation modification of EF-P as well as the enzymes of modification pathway. We demonstrate that the conserved K34 of endogenous *E. coli* EF-P bears a 144.09 Da modification, which results from two distinct reactions, namely a 128.09 Da lysinylation performed by YjeK and YjeA, followed by an additional 16 Da hydroxylation by YfcM (**Fig. 6a**). Our mass spectrometry fragmentation data support not only the attachment of the lysine to the ε-amino group of K34, but also indicate the presence of β-lysine, rather than α-lysine, as a product of the lysinylation reaction (**Fig. 1c,d, Supplementary Table 1,** and **Supplementary Fig. 3**). Moreover, the low level of modified peptide observed in the absence of *yjeK* (**Fig. 2b-d**), suggests that the conversion of (S)-α-lysine to (R)-β-lysine by YjeK

precedes the lysinylation of EF-P by YjeA (**Fig. 6a**). This is consistent with the observation that lysinylation of EF-P by YjeA is 100-fold more efficient using (R)-β-lysine instead of α-lysine[27] and that lysinylation of exogenously overexpressed EF-P requires co-expression of both YjeK and YjeA[6]. We believe that YfcM is the last enzyme in the EF-P modification pathway: The lack of +16 Da modified EF-P peptides in any of the Δ*yjeK* or Δ*yjeA* MS spectra suggests that YfcM cannot hydroxylate unmodified EF-P and therefore acts after YjeK and YjeA. Moreover, the +144 Da modified peptide was never detected in the Δ*yjeK* strain, which most likely indicates that α-lysinylated EF-P is a poor substrate for YfcM and that β-lysinylated EF-P is preferred. This is similar to the eukaryotic situation where deoxyhypusinylation of eIF-5A by DHS is a prerequisite for the subsequent hydroxylation by DOHH[13] (**Fig. 6b**). In contrast to eIF-5A where the added spermidine moiety is hydroxylated by DOHH, our fragmentation data support the hydroxylation by YfcM of the C4 or C5 position of K34 of EF-P, but not hydroxylation of the added β-lysine (**Fig. 1c,d, Supplementary Table 1,** and **Supplementary Fig. 3**).

The crystal structure of *T. thermophilus* EF-P bound to the 70S ribosome suggests that EF-P stimulates peptide bond formation by interacting with and stabilizing the tRNA at the P-site[18]. Modeling *E. coli* EF-P on the ribosome using the *T. thermophilus* structure, suggests that K34 and the lysinylation moiety would extend towards the peptidyl-transferase center and stabilize the CCA-end of the tRNA (**Fig. 6c**)[18]. Based on this model, hydroxylation of the C5 (δ), but not of the C4 (γ), position of K34 would allow additional potential stabilizing hydrogen bond interactions with the P-tRNA (**Fig. 6c**). EF-P and the lysinylation pathway are critical for attenuation of virulence in bacteria[10,21-24]. The taxonomic distribution reveals *yfcM* to be present with the *yjeK* and *yjeA* genes in most common Gram-negative pathogenic bacteria, such as *Acinetobacter baumannii, Escherichia coli O157:H7, Haemophilus influenzae, Klebsiella pneumoniae, Legionella pneumophila, Salmonella typhimurium, Vibrio cholerae* and *Yesinia pestis* (see **Fig. 5b** and **Supplementary Table 2**). Proteomics studies comparing wildtype *S. typhimurium* with Δ*yjeA* or Δ*yjeK* strains reveal large changes in the expression of proteins involved in virulence and metabolic adaption[21,24], suggesting that EF-P and the lysinylation modification are important for translational regulation of particular mRNAs. With a complete

description of the EF-P modification and pathway now in hand, this opens the way for future studies to address the mechanism of action of EF-P.

Methods

Strains. The parental strain *E. coli* K-12 BW25113 and the single gene deletion mutants Δ*efp* (JW4147), Δ*yjeK* (JW4106), Δ*yjeA* (JW4116) and Δ*yfcM* (JW5381) were obtained from the Keio collection (National BioResource Project (NBRP) at the National Institute of Genetics (NIG), Japan[38]). Note that the Δ*yjeK* strain was taken from plate 38, since the isolate on plate 37 is not a *bone fide yjeK* knock-out strain[39]. The *E. coli* strain AT713[40], which is auxotrophic for arginine and lysine, was kindly provided by Matthias Selbach (Max-Delbruch Zentrum, Buch-Berlin, Germany). P1 transduction from the Keio strains was used to generate the equivalent single gene deletions Δ*efp*, Δ*yjeK*, Δ*yjeA* and Δ*yfcM* in the AT713 background[40]. The deletions were confirmed using PCR and the strains were confirmed to be auxotrophic for arginine and lysine (data not shown).

Plasmids and protein expression. The *efp*, *yjeK*, *yjeA* and *yfcM* genes were PCR amplified from gDNA of *E. coli* K-12 strain MC4100 using the primers listed in Supplemental Table 3. For protein overexpression, the *efp* gene was cloned into pET14b (Novagen) using NdeI and BamHI restriction sites, whereas *yfcM* was cloned into pET21b (Novagen) using NdeI and SacI restriction sites. Both plasmids were transformed into BL21 (Novagen) and the overexpressed protein was purified using Ni-NTA (Novagen) chromatography according to manufacturers instructions, followed by gel filtration on a Superdex G75 column (GE Healthcare) in a buffer containing 100 mM Hepes-KOH pH 8.0, 125 mM NaCl, 25 mM KCl, 5 mM β-mercaptoethanol, 10% glycerol. Purified recombinant EF-P was used to generate rabbit polyclonal antibodies (Davids Biotechnologie, Regensburg, Germany). For the rescue experiments, the *yjeK*, *yjeA* and *yfcM* genes were cloned into pQE70 (Qiagen) and transformed into the appropriate AT713 deletion strain. Unfortunately, for technical reasons the rescue experiment expressing YjeA in the Δ*yjeA* AT713 strain was inconclusive.

Stable isotopic labeling and sample preparation. *E. coli* wildtype AT713 and deletion strains Δ*yjeA*, Δ*yjeK* and Δ*yfcM* in the AT713 background were grown in

50 ml MOPS minimal medium[41] supplemented with 0.2% glucose and 100 µg/ml of each amino acid[42]. For stable isotopic labeling, 'light' lysine was substituted with 'heavy' lysine: (4,4,5,5-D4)-lysine or (3,3,4,4,5,5,6,6-D8)-lysine (Cambridge Isotope Laboratories Inc., USA). Collected and PBS-washed cells were resuspended in 350 µl cold lysis buffer: 20 mM Tris-HCl pH 7.5, 100 mM NH_4Cl, 6 mM Mg-acetate, 2 mM PMSF). After 30 min incubation on ice, 1 mg/ml lysozyme, 20 U/ml DNase I, 0.5% DOC, 1% Brij were added. Cells were disrupted by sonication with multiple short bursts of maximum intensity, and the cell debris and aggregated proteins were collected by centrifugation at 13000 x g for 15 min at 4 °C. The supernatant was pre-cleared with 5 µl protein A bead suspension (Protein A Sepharose Fast Flow, GE Healthcare) for at least 30 min and then centrifuged. 30 µg of polyclonal antibody (1 mg/ml IgG was taken equal to 1.36 A_{280} units) was added to the pre-cleared lysate and incubated at 4 °C for 1 hour, followed by 40 µl of protein A beads and an additional incubation for 1 hour at 4 °C on rotator. The Sepharose beads were collected and washed several times with lysis buffer and the beads were resuspended in 1x SDS sample buffer, heated and EF-P protein was separated by SDS-PAGE. Proteins were in-gel digested with either LysC (Wako, Japan) or chymotrypsin (Promega, USA), according to standard procedures[43]. In case of [18]O-labeling, all steps were as before except for digestion which was carried out in [18]O-enriched water (Sigma, USA). Extracted peptides were purified on C18-StageTips[44] and analyzed via nano LC-MS/MS.

Nano-LC-MS/MS and direct infusion MS. Briefly, peptides were separated by reversed-phase chromatography using an Agilent 1200 series nanoflow system (Agilent Technologies) connected to a LTQ Orbitrap classic mass-spectrometer (Thermo Electron, Bremen, Germany) equipped with a nanoelectrospray ion source (Proxeon, Odense, Denmark). C18-StageTip purified peptides were dissolved in 0.1% trifluoroacetic acid, loaded on a fused silica emitter (75 µm × 150 mm, Proxeon) packed in-house with Reprosil-Pur C18-AQ 3 µm particles (Dr. Maisch, Germany) using a flow rate of 700 nl/min and separated with a 30 min 3-40% B gradient (A: 0.5% acetic acid, B: 0.5% acetic acid/80% acetonitrile) at a flow-rate of 200 nl/min. Eluted peptides were sprayed directly into LTQ Orbitrap mass-spectrometer operated at 180 °C capillary temperature and 2.0-2.2 kV spray voltage. The LTQ Orbitrap was operated in data-dependent mode with up to five MS/MS scans being recorded for

each precursor ion scan. Precursor ion spectra were recorded in profile in the Orbitrap (m/z 300-1900, R = 60 000); data-dependent MS/MS spectra were acquired in centroid either in the LTQ for low-resolution data (CID NCE 35%, wideband activation enabled) or in the Orbitrap for high-resolution data (CID NCE 35%, R = 7500). Mono-isotopic precursor selection was enabled, singly charged ions and ions with an unassigned charge state were rejected, each fragmented ion was dynamically excluded for 90 s. All measurements in the Orbitrap mass analyzer were performed with lock-mass option enabled (lockmasses m/z 445.12003 and 519.13882). Fragment MS/MS spectra from raw files were extracted as MSM files and then merged to peak lists using Raw2MSM version 1.11, selecting the top eight peaks for each 100 Da[45]. MSM files were searched with the Mascot 2.3 search engine (Matrix Science) against the protein sequence database composed of *E. coli* strain MG1655 sequences from UniprotKB and common contaminant proteins, such as trypsin, keratins etc. Search parameters were: 5 ppm for precursor mass tolerance, 0.6 Da for ion-trap MS/MS mass tolerance or 0.02 Da for Orbitrap MS/MS mass tolerance, up to three missed cleavages plus a number of variable modifications such as oxidation (M), lysinylation (K), and hydroxylation (K) plus their isotopically-labeled variants. Peptide hits returned by Mascot were manually validated and annotated when needed.

For full protein analysis, C8-StageTip purified sample was directly infused into the mass-spectrometer using borosilicate static nanospray emitters (Proxeon, Denmark) and positive ionization mode. Measurements were done with an ionization voltage of 1000 V, m/z range of 800-1500 and resolution of 60,000 @ m/z 400, 100 micro-scans were combined into one FT transient and external calibration was used.

Differential scanning fluorimetry. Thermal-dependent unfolding of YfcM was measured using differential scanning fluorimetry[35]. Purified YfcM (15 μM) was pre-mixed with SYPROrange dye according to manufacturers instructions (Invitrogen). YfcM stability was measured within a temperature range of 25-95°C using iCycler5 (Bio-Rad). Data points were measured every 0.3°C with 25s pre-incubation time. Concentration-dependent stability of YfcM in the presence of NADP, NADPH, NAD, NADH, FAD, ADP, ATP, GTP, coenzyme A, tetrahydrofolic acid, PLP, oxaloacetic acid and thiamine was tested at concentrations 0-600 μM, while higher concentrations (0-250 mM) of L-ascorbic acid and α-ketoglutarate were necessary. Stocks of each of

the ligands (Sigma Aldrich) were prepared in DMSO and diluted using YfcM buffer (100 mM Hepes-KOH pH 8.0, 125 mM NaCl, 25 mM KCl, 5 mM β-mercaptoethanol, 10% glycerol).

Phylogenetic analyses. Protein sequences were retrieved by BlastP searching against the NCBI RefSeq database and aligned using MAFFT version 6.626b[46]. Maximum likelihood phylogenetic analyses were carried out using RaxML version 7.0.4[47] run on the Cipres server (http://www.phylo.org/sub_sections/portal/) with the PROTCATWAG model and 100 bootstrap replicates. Ambiguously aligned regions of alignments were not included. To determine the presence and absence of *yfcM*, *yjeK* and *yjeA* genes across bacteria, hidden markov models (HMMs) were constructed from multiple sequence alignments of each family using HMMer 3.0b2[48], and searched against 1273 genomes across the bacterial tree of life. The genomic neighborhood was retrieved using Entrez Gene[49].

Acknowledgments

This research was supported by grants from the Deutsche Forschungsgemeinschaft WI3285/1-1 (to D.N.W.), Human Frontiers of Science Foundation (RGY88/2008), and the EMBO young investigator grant. L.P. and G.A. are supported by the European Social Fund program Mobilitas grant MJD144 and MJD99, respectively. Mass-spectrometric analyses were in part supported by the European Regional Development Fund through the Center of Excellence in Chemical Biology (Institute of Technology, University of Tartu).

Author contributions:

L.P., A.L.S., J.R., D.N.W designed research; L.P. performed and analyzed MS data, A.L.S. and K.V. performed biochemistry; G.A. performed bioinformatics; L.P., A.L.S., T.T., J.R. and D.N.W analyzed data and wrote the paper.

References

1. Glick, B. R. & Ganoza, M. C. Identification of a soluble protein that stimulates peptide bond synthesis. *Proc. Natl Acad. Sci. USA* **72**, 4257-4260. (1975).
2. Glick, B. R., Chladek, S. & Ganoza, M. C. Peptide bond formation stimulated by protein synthesis factor EF-P depends on the aminoacyl moiety of the acceptor. *Eur. J. Biochem.* **97**, 23-28. (1979).
3. Ganoza, M. C. & Aoki, H. Peptide bond synthesis: function of the efp gene product. *Biol. Chem.* **381**, 553-559 (2000).
4. Swaney, S. et al. Characterization of a high-throughput screening assay for inhibitors of elongation factor P and ribosomal peptidyltransferase activity. *J. Biochem. Screen.* **11**, 736-742 (2006).
5. Aoki, H. et al. Interactions of elongation factor EF-P with the Escherichia coli ribosome. *FEBS J.* **275**, 671-681 (2008).
6. Yanagisawa, T., Sumida, T., Ishii, R., Takemoto, C. & Yokoyama, S. A paralog of lysyl-tRNA synthetase aminoacylates a conserved lysine residue in translation elongation factor P. *Nat. Struct. Mol. Biol.* **17**, 1136-43 (2010).
7. de Crecy, E. et al. Development of a novel continuous culture device for experimental evolution of bacterial populations. *Appl. Microbiol. Biotechnol.* **77**, 489-496 (2007).
8. Kearns, D. B., Chu, F., Rudner, R. & Losick, R. Genes governing swarming in *Bacillus subtilis* and evidence for a phase variation mechanism controlling surface motility. *Mol. Microbiol.* **52**, 357-369 (2004).
9. Ohashi, Y. et al. Expression profiling of translation-associated genes in sporulating *Bacillus subtilis* and consequence of sporulation by gene inactivation. *Biosci. Biotechnol. Biochem.* **67**, 2245-2253 (2003).
10. Peng, W. T., Banta, L. M., Charles, T. C. & Nester, E. W. The chvH locus of *Agrobacterium* encodes a homologue of an elongation factor involved in protein synthesis. *J. Bacteriol.* **183**, 36-45 (2001).
11. Bailly, M. & de Crecy-Lagard, V. Predicting the pathway involved in post-translational modification of elongation factor P in a subset of bacterial species. *Biol. Direct* **5**, 3 (2010).
12. Kyrpides, N. C. & Woese, C. R. Universally conserved translation initiation factors. *Proc. Natl Acad. Sci. USA* **95**, 224-228 (1998).

13. Park, M. H., Nishimura, K., Zanelli, C. F. & Valentini, S. R. Functional significance of eIF5A and its hypusine modification in eukaryotes. *Amino Acids* **38**, 491-500 (2010).
14. Saini, P., Eyler, D. E., Green, R. & Dever, T. E. Hypusine-containing protein eIF5A promotes translation elongation. *Nature* **459**, 118-21 (2009).
15. Gregio, A. P., Cano, V. P., Avaca, J. S., Valentini, S. R. & Zanelli, C. F. eIF5A has a function in the elongation step of translation in yeast. *Biochem. Biophys. Res. Commun.* **380**, 785-790 (2009).
16. Henderson, A. & Hershey, J. W. Eukaryotic translation initiation factor (eIF) 5A stimulates protein synthesis in *Saccharomyces cerevisiae*. *Proc. Natl Acad. Sci. USA* **108**, 6415-6149 (2011).
17. Hanawa-Suetsugu, K. et al. Crystal structure of elongation factor P from *Thermus thermophilus* HB8. *Proc. Natl Acad. Sci. U S A* **101**, 9595-9600 (2004).
18. Blaha, G., Stanley, R. E. & Steitz, T. A. Formation of the first peptide bond: the structure of EF-P bound to the 70S ribosome. *Science* **325**, 966-70 (2009).
19. Kim, K. K., Hung, L. W., Yokota, H., Kim, R. & Kim, S. H. Crystal structures of eukaryotic translation initiation factor 5A from *Methanococcus jannaschii* at 1.8 Å resolution. *Proc. Natl Acad. Sci. USA* **95**, 10419-10424 (1998).
20. Peat, T. S., Newman, J., Waldo, G. S., Berendzen, J. & Terwilliger, T. C. Structure of translation initiation factor 5A from *Pyrobaculum aerophilum* at 1.75 Å resolution. *Structure* **6**, 1207-1214 (1998).
21. Navarre, W. W. et al. PoxA, yjeK, and elongation factor P coordinately modulate virulence and drug resistance in *Salmonella enterica*. *Mol. Cell* **39**, 209-221 (2010).
22. Kaniga, K., Compton, M. S., Curtiss, R., 3rd & Sundaram, P. Molecular and functional characterization of *Salmonella enterica serovar typhimurium poxA* gene: effect on attenuation of virulence and protection. *Infect. Immun.* **66**, 5599-5606 (1998).
23. Bearson, S. M., Bearson, B. L. & Rasmussen, M. A. Identification of *Salmonella enterica serovar Typhimurium* genes important for survival in the swine gastric environment. *Appl. Environ. Microbiol.* **72**, 2829-36 (2006).
24. Bearson, S. M., Bearson, B. L., Brunelle, B. W., Sharma, V. K. & Lee, I. S. A mutation in the *poxA* gene of *Salmonella enterica serovar typhimurium* alters

protein production, elevates susceptibility to environmental challenges, and decreases swine colonization. *Foodborne Pathog. Dis.* **8**, 725-732 (2011).

25. Behshad, E. et al. Enantiomeric free radicals and enzymatic control of stereochemistry in a radical mechanism: the case of lysine 2,3-aminomutases. *Biochemistry* **45**, 12639-46 (2006).
26. Ambrogelly, A., O'Donoghue, P., Soll, D. & Moses, S. A bacterial ortholog of class II lysyl-tRNA synthetase activates lysine. *FEBS Lett.* **584**, 3055-60 (2010).
27. Roy, H. et al. The tRNA synthetase paralog PoxA modifies elongation factor-P with (R)-beta-lysine. *Nat. Chem. Biol.*, epub (2011).
28. Glick, B. R. & Ganoza, M. C. Characterization and site of action of a soluble protein that stimulates peptide-bond synthesis. *Eur. J. Biochem.* **71**, 483-491 (1976).
29. Glick, B. R., Green, R. M. & Ganoza, M. C. Purification of factor EF-P, a protein that stimulates peptide bond synthesis with certain aminoacyl-tRNA analogues. *Can. J. Biochem.* **57**, 749-757. (1979).
30. Loenarz, C. & Schofield, C. J. Physiological and biochemical aspects of hydroxylations and demethylations catalyzed by human 2-oxoglutarate oxygenases. *Trends Biochem. Sci.* **36**, 7-18 (2011).
31. Plattner, H. J., Pfefferle, P., Romaguera, A., Waschutza, S. & Diekmann, H. Isolation and some properties of lysine N6-hydroxylase from *Escherichia coli strain EN222*. *Biol. Met.* **2**, 1-5 (1989).
32. Nakazawa, T., Hori, K. & Hayaishi, O. Studies on monooxygenases. V. Manifestation of amino acid oxidase activity by L-lysine monooxygenase. *J. Biol. Chem.* **247**, 3439-44 (1972).
33. Kim, Y. S. et al. Deoxyhypusine hydroxylase is a Fe(II)-dependent, HEAT-repeat enzyme. Identification of amino acid residues critical for Fe(II) binding and catalysis [corrected]. *J. Biol. Chem.* **281**, 13217-25 (2006).
34. Abbruzzese, A., Park, M. H. & Folk, J. E. Deoxyhypusine hydroxylase from rat testis. Partial purification and characterization. *J. Biol. Chem.* **261**, 3085-9 (1986).
35. Niesen, F. H., Berglund, H. & Vedadi, M. The use of differential scanning fluorimetry to detect ligand interactions that promote protein stability. *Nat. Protoc.* **2**, 2212-21 (2007).

36. Bujnicki, J. M. et al. Identification of a bifunctional enzyme MnmC involved in the biosynthesis of a hypermodified uridine in the wobble position of tRNA. *RNA* **10**, 1236-42 (2004).
37. Harris, K. A., Jones, V., Bilbille, Y., Swairjo, M. A. & Agris, P. F. YrdC exhibits properties expected of a subunit for a tRNA threonylcarbamoyl transferase. *RNA* **17**, 1678-87 (2011).
38. Baba, T. et al. Construction of *Escherichia coli K-12* in-frame, single-gene knockout mutants: the Keio collection. *Mol. Syst. Biol.* **2**, 2006 0008 (2006).
39. Yamamoto, N. et al. Update on the Keio collection of *Escherichia coli* single-gene deletion mutants. *Mol. Syst. Biol.* **5**, 335 (2009).
40. Taylor, A. L. & Trotter, C. D. Revised linkage map of Escherichia coli. *Bacteriol. Rev.* **31**, 332-353 (1967).
41. Neidhardt, F. C., Bloch, P. L. & Smith, D. F. Culture medium for enterobacteria. *J. Bacteriol.* **119**, 736-747 (1974).
42. Siibak, T. et al. Antibiotic-induced ribosomal assembly defects result from changes in the synthesis of ribosomal proteins. *Mol. Microbiol.* **80**, 54-67 (2010).
43. Shevchenko, A., Tomas, H., Havlis, J., Olsen, J. V. & Mann, M. In-gel digestion for mass spectrometric characterization of proteins and proteomes. *Nat. Protoc.* **1**, 2856-60 (2006).
44. Rappsilber, J., Mann, M. & Ishihama, Y. Protocol for micro-purification, enrichment, pre-fractionation and storage of peptides for proteomics using StageTips. *Nat. Protoc.* **2**, 1896-1906 (2007).
45. Olsen, J. V. et al. Parts per million mass accuracy on an Orbitrap mass spectrometer via lock mass injection into a C-trap. *Mol. Cell Proteomics* **4**, 2010-21 (2005).
46. Katoh, K., Kuma, K., Toh, H. & Miyata, T. MAFFT version 5: improvement in accuracy of multiple sequence alignment. *Nucleic Acids Res.* **33**, 511-8 (2005).
47. Stamatakis, A. RAxML-VI-HPC: maximum likelihood-based phylogenetic analyses with thousands of taxa and mixed models. *Bioinformatics* **22**, 2688-90 (2006).
48. Eddy, S. R. Profile hidden Markov models. *Bioinformatics* **14**, 755-63 (1998).
49. Maglott, D., Ostell, J., Pruitt, K. D. & Tatusova, T. Entrez Gene: gene-centered information at NCBI. *Nucleic Acids Res.* **35**, D26-31 (2007).

Figure Legends

Figure 1: Lysine 34 of endogenous EF-P is modified by 144.09 Da. (**a**) MS spectrum of full-length endogenous EF-P from wildtype *E. coli* strain MRE600. (**b**) MS/MS spectra of chymotrypsin fragment with mass of 1074.62 Da, mass increase of 144.09 Da compared to theoretical mass. (**c**) MS/MS spectra of LysC fragment with mass of 1301.76 Da, mass increase of 144.09 Da compared to theoretical mass. Fragmentation of LysC peptide with y and b peptides indicated as well as peaks F1-F4. The b and y ions correspond to N- and C-terminal charge-carrying fragments of peptide, respectively, where peptide backbone cleavage has taken place at CO-NH bonds. Under the conditions used, y ions are preferentially produced. (**d**) Chemical structures of lysinylated K34 with predicted chemical structures of mass loss fragments for peaks F1-F4, indicated with their respective molecular weights.

Figure 2: Lysinylation of EF-P *in vivo* requires YjeK and YjeA. (**a**) MS/MS spectra of chymotrypsin fragment of EF-P from AT713Δ*yjeA* with mass of 930.53 Da. (**b,c**) MS/MS spectra of chymotrypsin fragments of EF-P from AT713Δ*yjeK* with masses of (**b**) 930.53 Da and (**c**) 1058.62 Da. (**d**) Quantification of (b) and (c) reveals that modified fragment is present at 2% level of the unmodified.

Figure 3: Fully modified EF-P is dependent on the presence of YfcM. (**a,b**) MS/MS spectra of chymotrypsin fragment of EF-P from (**a**) AT713Δ*yfcM* with mass of 1058.62 Da, and (**b**) AT713Δ*yfcM*/pYfcM with mass of 1074.62 Da. (**c,d**) MS/MS spectra of LysC fragment of EF-P from (**c**) AT713Δ*yfcM* with mass of 1285.76 Da, and (**d**) AT713Δ*yfcM*/pYfcM with mass of 1301.76 Da.

Figure 4: YfcM hydroxylates the C4/C5 position of K34 of EF-P. (**a,b**) MS/MS spectra of LysC fragment of EF-P from (**a**) AT713Δ*yfcM* and (**b**) wildtype AT713 cells grown in D4-lysine, with masses of 1297.84 Da and 1312.83 Da, respectively. (**c**) Chemical structure of lysinylated K34 with potential hydroxyl positions indicated.

Figure 5: Characterization of the hydroxylase YfcM. (**a**) Differential scanning fluorimetry (DSF) of YfcM in the presence of indicated nucleotide analogues. Upper graph shows the relative fluorescence change as a function of temperature at 600μM

ligand concentration, whereas the lower panel shows the change (°C) in temperature stability maximum (ΔTm) as a function of ligand concentration (μM). (**b**) Phylogenetic tree (left) and genomic neighborhood (right) of representative YfcM proteins in bacteria (full tree in **Supplementary Fig. 5**). Only bootstrap support values >50% are shown.

Figure 6: Modification pathways of EF-P and eIF-5A. (**a**) The FeS protein YjeK converts (S)-α-lysine to (R)-β-lysine using S-adenosyl-l-methionine (SAM) and pyridoxal-5′-phosphate (PLP)[25]. YjeA uses ATP to lysinylate EF-P by the addition of β-lysine to the ε-amino group of K34[27]. YfcM uses molecular oxygen to hydroxylate the C4 (γ) or C5 (δ) position of K34 of EF-P. (**b**) Deoxyhypusine synthase (DHS) uses NAD to transfer the amino-butyl moiety from spermidine to the ε-amino group of K50 of human eIF5A, which is then hydroxylated by deoxyhypusine hydroxylase (DOHH)[13]. (**c**) Relative positions of K34 of EF-P (green) and the acceptor stem of the P-tRNA (blue) when bound on the ribosome. The γ, δ and ε carbon atoms of K34 and the C74, C75 and A76 positions of the tRNA are indicated. The model was built by mutation of Arg to Lys (equivalent to K34 in *E. coli*) in the *T. thermophilus* EF-P●70S structure[18].

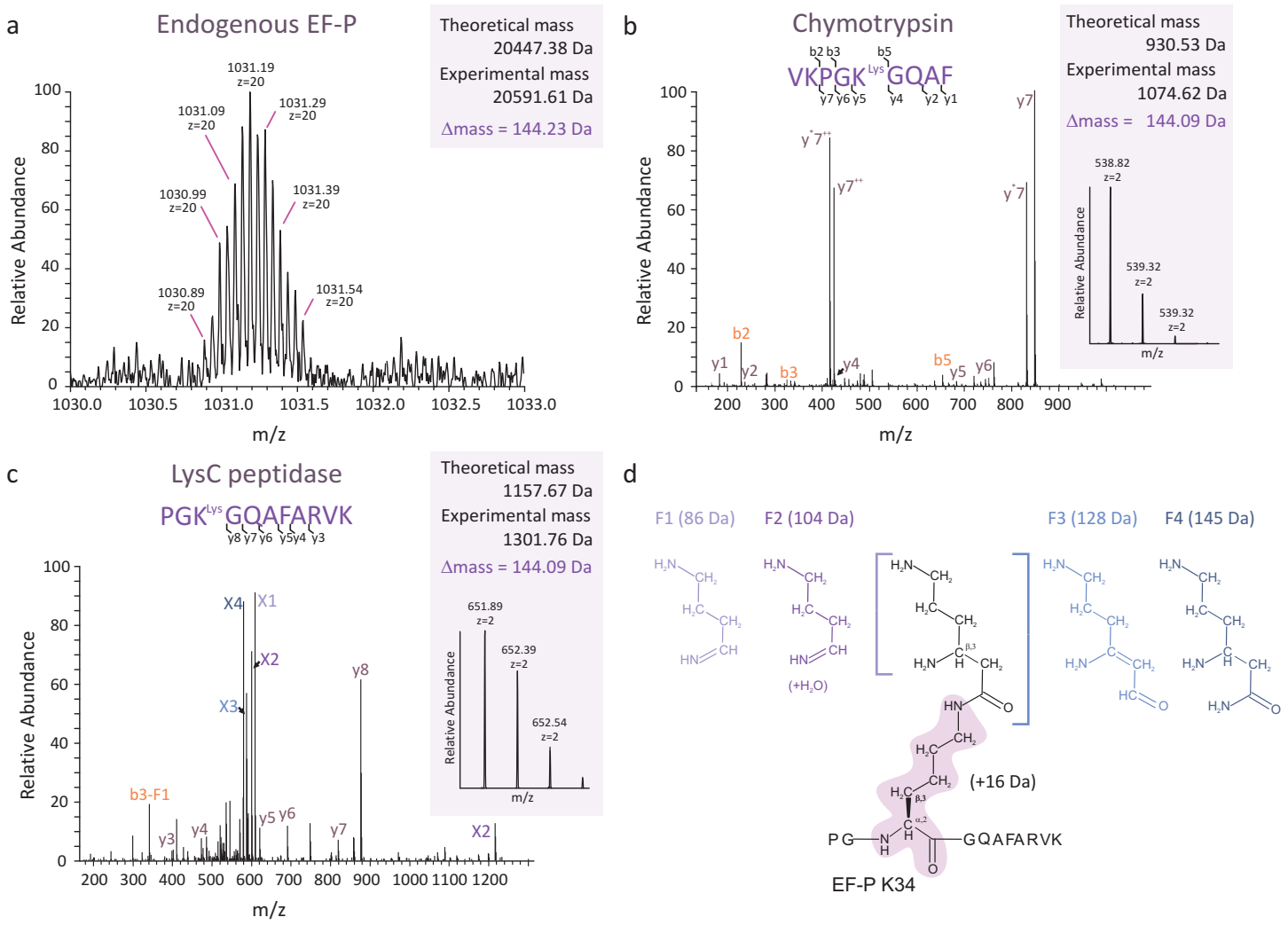

Peil et al
Figure 1

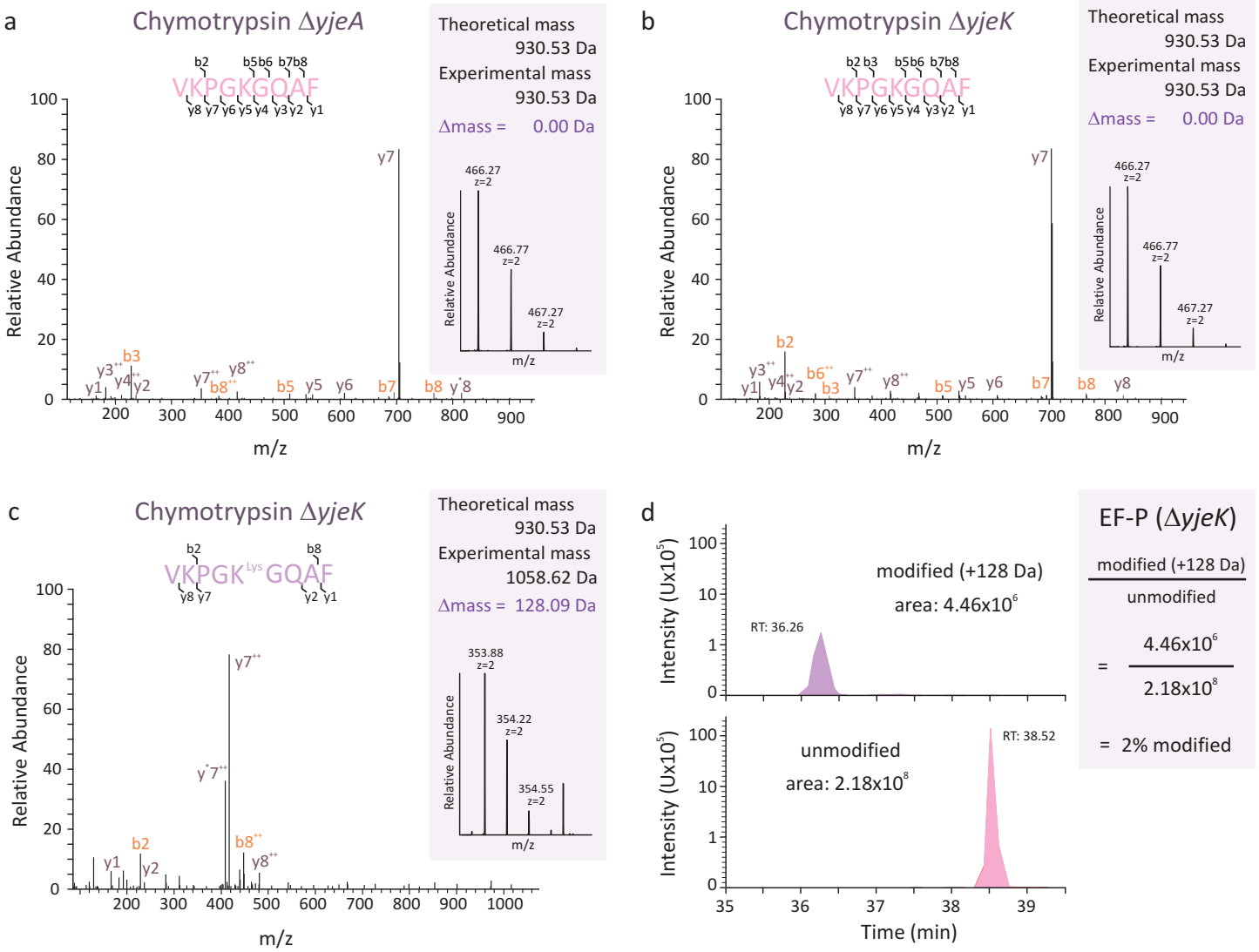

Peil et al
Figure 2

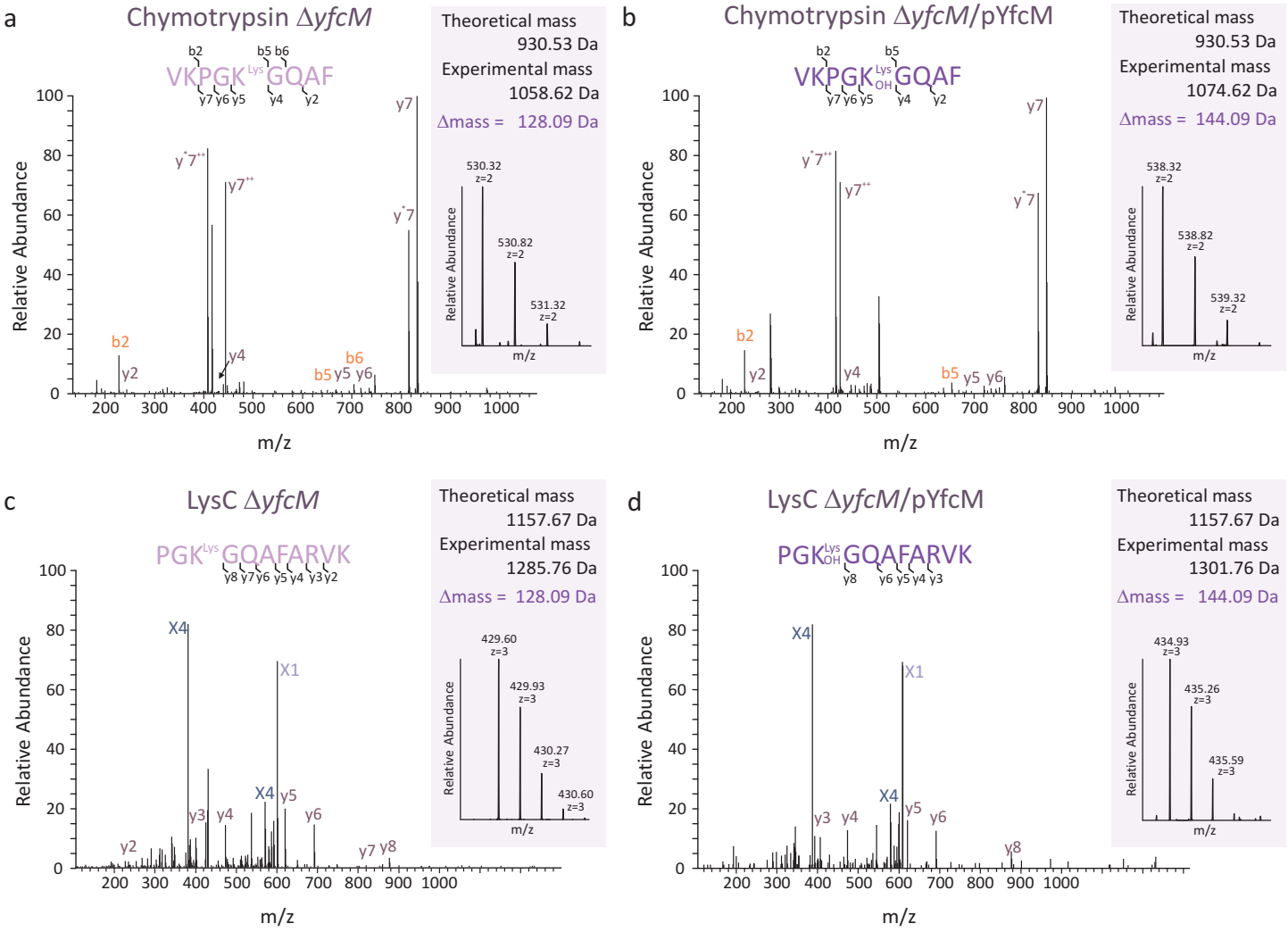

Peil et al
Figure 3

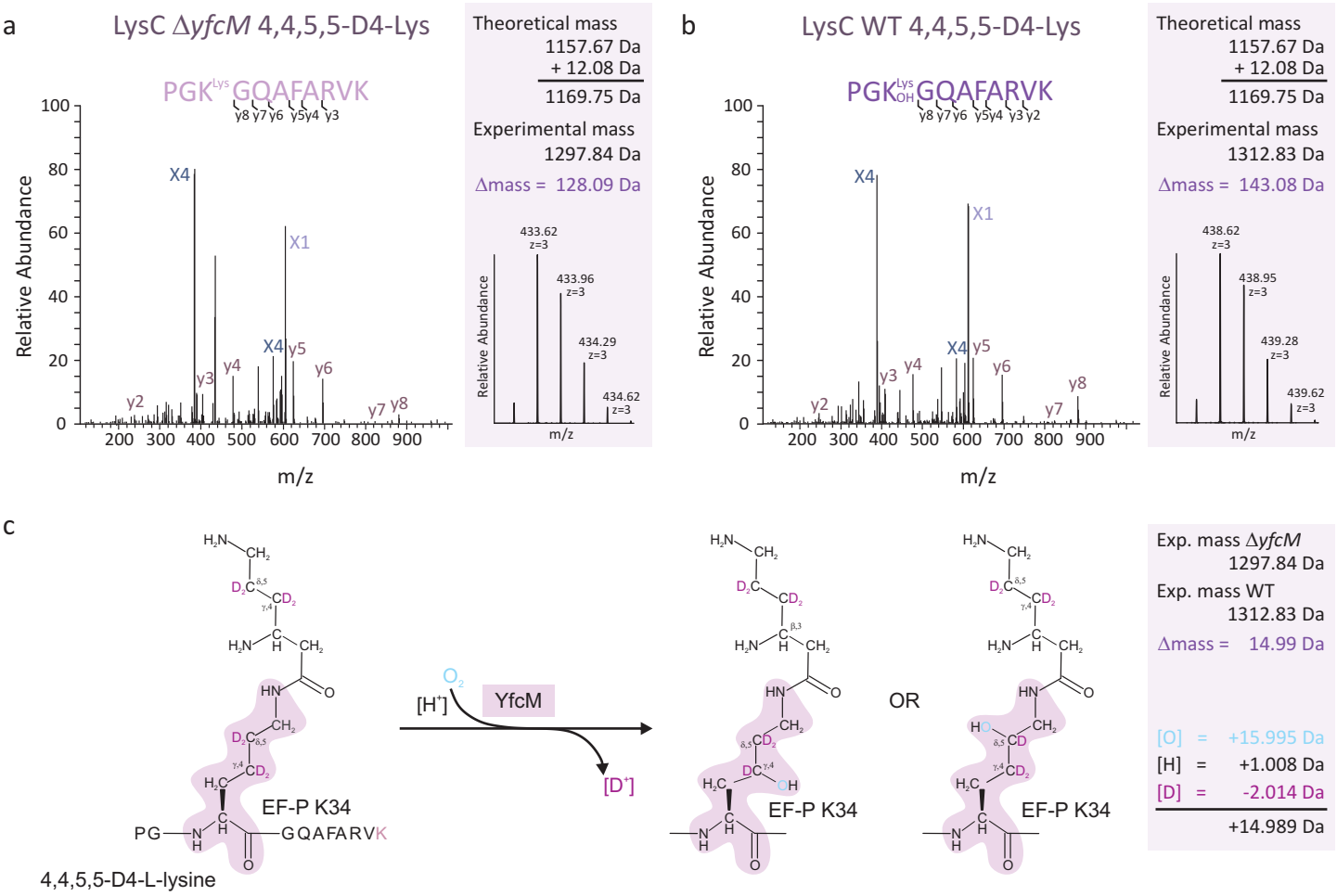

Peil et al
Figure 4

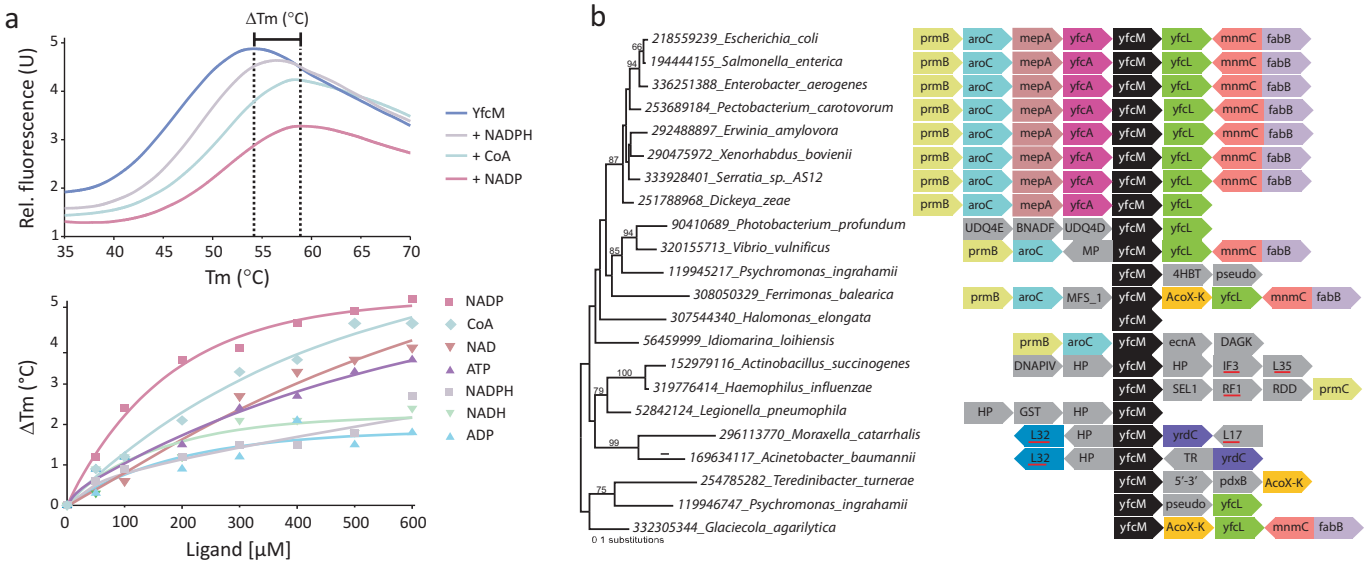

Peil et al
Figure 5

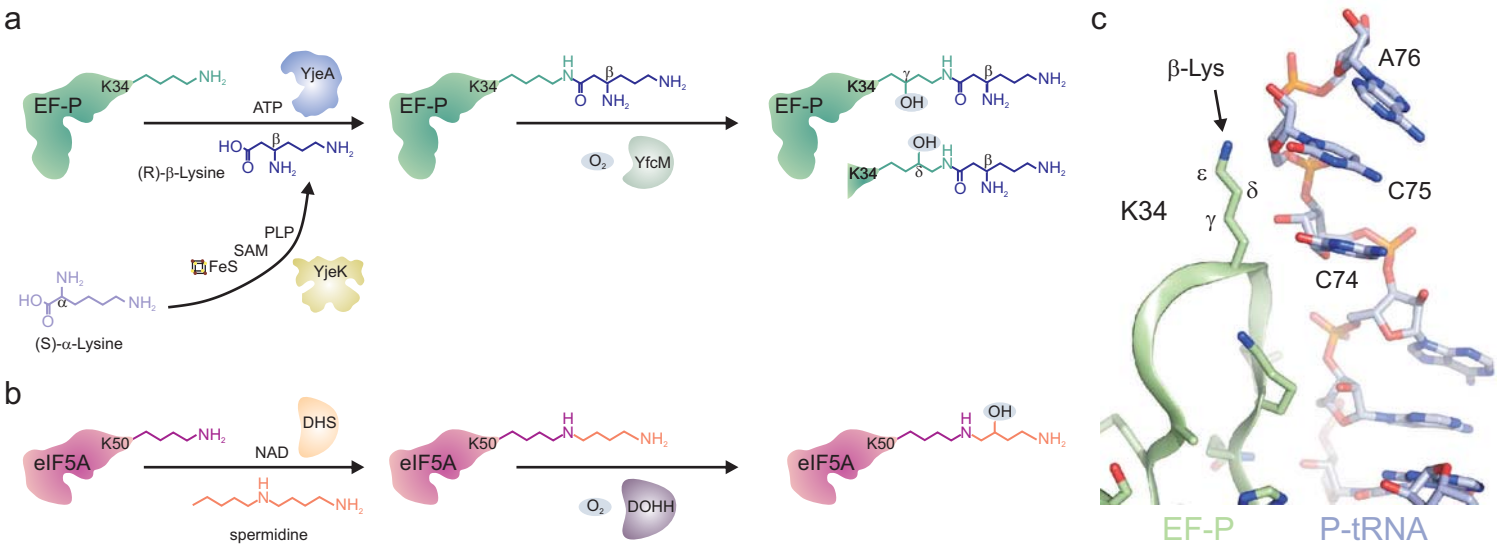

Peil et al
Figure 6

Agata Lucyna Starosta

Gene Center, LMU Munich
Nationality: Polish
Born on 03.09.1983 in Rzeszow, Poland
starosta@lmb.uni-muenchen.de

Scientific experience

10/2007 – 01/2012
PhD student In the laboratory of Dr. Daniel N. Wilson, Gene Center, Department of Biochemistry, University of Munich, Germany.
Topic: Antibiotics, Inhibition of Protein Synthesis

10/2002 – 06/2007
Master student In the laboratory of Prof. Dr. Andrzej Kozik, Analytical Biochemistry, Department of Biochemistry, Jagiellonian University, Crakow, Poland
Topic: Thiamin monophosphate synthase – dissecting enzyme's activity

Education

31.01.2012
PhD exam, grade: summa cum laude

10/2007 – 01/2012
PhD thesis in the group of Dr. Daniel N. Wilson, in Munich, Germany

27/06/2007
Master exam, grade: very good (A), MSc..
Master thesis: Thiamin monophosphate synthase – a key enzyme in thiamin biosynthesis pathway, Analytical Biochemistry. Supervisor Dr. M. Rapala-Kozik.

10/2002 – 06/2007
Master studies in biology, Faculty of Biology and Earth Science, Jagiellonian University, Cracow, Poland. Specialization: biochemistry, Faculty of Biochemistry, Biophysics, and Biotechnology, Jagiellonian University, Cracow, Poland.

Publications

Mikolajka, A., H. Liu, Y. Chen, **A.L. Starosta**, V. Márquez, M. Ivanova, B.S. Cooperman, and D.N. Wilson. 2011. Differential effects of thiopeptide and orthosomycin antibiotics on translational GTPases. *Chem Biol* 18 (5): 589-600.

Ratje, A. H., J. Loerke, A. Mikolajka, M. Brunner, P. W. Hildebrand**, A. L. Starosta**, A. Donhofer, S. R. Connell, P. Fucini, T. Mielke, P. C. Whitford, J. N. Onuchic, Y. Yu, K. Y. Sanbonmatsu, R. K. Hartmann, P. A. Penczek, D. N. Wilson, and C. M. Spahn. 2010. Head

swivel on the ribosome facilitates translocation by means of intra-subunit tRNA hybrid sites. *Nature* 468 (7324):713-716.

Starosta, A. L., V. V. Karpenko, A. V. Shishkina, A. Mikolajka, N. V. Sumbatyan, F. Schluenzen, G. A. Korshunova, A. A. Bogdanov, and D. N. Wilson. 2010. Interplay between the ribosomal tunnel, nascent chain, and macrolides influences drug inhibition. *Chem Biol* 17 (5):504-14.

Bhushan, S., H. Meyer, **A. L. Starosta**, T. Becker, T. Mielke, O. Berninghausen, M. Sattler, D. N. Wilson, and R. Beckmann. 2010. Structural basis for translational stalling by human cytomegalovirus and fungal arginine attenuator peptide. *Mol Cell* 40 (1):138-46.

Starosta, A. L., H. Qin, A. Mikolajka, G. Y. Leung, K. Schwinghammer, K. C. Nicolaou, D. Y. Chen, B. S. Cooperman, and D. N. Wilson. 2009. Identification of distinct thiopeptide-antibiotic precursor lead compounds using translation machinery assays. *Chem Biol* 16 (10):1087-96.

Petropoulos, A. D., E. C. Kouvela, **A. L. Starosta**, D. N. Wilson, G. P. Dinos, and D. L. Kalpaxis. 2009. Time-resolved binding of azithromycin to Escherichia coli ribosomes. *J Mol Biol* 385 (4):1179-92.

Palaniappan, N., V. Dhote, S. Ayers, **A. L. Starosta**, D. N. Wilson, and K. A. Reynolds. 2009. Biosynthesis of the aminocyclitol subunit of hygromycin A in Streptomyces hygroscopicus NRRL 2388. *Chem Biol* 16 (11):1180-9.

Dhote, V., **A. L. Starosta**, D. N. Wilson, and K. A. Reynolds. 2009. The final step of hygromycin A biosynthesis, oxidation of C-5"-dihydrohygromycin A, is linked to a putative proton gradient-dependent efflux. *Antimicrob Agents Chemother* 53 (12):5163-72.

Wilson, D. N., F. Schluenzen, J. M. Harms, **A. L. Starosta**, S. R. Connell, and P. Fucini. 2008. The oxazolidinone antibiotics perturb the ribosomal peptidyl-transferase center and effect tRNA positioning. *Proc Natl Acad Sci U S A* 105 (36):13339-44.

Ebbing, B., K. Mann, **A. Starosta**, J. Jaud, L. Schols, R. Schule, and G. Woehlke. 2008. Effect of spastic paraplegia mutations in KIF5A kinesin on transport activity. *Hum Mol Genet* 17 (9):1245-52.

Rapala-Kozik, M., M. Olczak, K. Ostrowska, **A. Starosta**, and A. Kozik. 2007. Molecular characterization of the thi3 gene involved in thiamine biosynthesis in Zea mays: cDNA sequence and enzymatic and structural properties of the recombinant bifunctional protein with 4-amino-5-hydroxymethyl-2-methylpyrimidine (phosphate) kinase and thiamine monophosphate synthase activities. *Biochem J* 408 (2):149-59.